



City Research Online

City, University of London Institutional Repository

Citation: Hadjisavvas, V. (2012). Treatment of brain cancer and ischaemic stroke utilising High Intensity Focus Ultrasound (HIFU) guide with MRI. (Unpublished Doctoral thesis, City University London)

This is the accepted version of the paper.

This version of the publication may differ from the final published version.

Permanent repository link: <https://openaccess.city.ac.uk/id/eprint/1399/>

Link to published version:

Copyright: City Research Online aims to make research outputs of City, University of London available to a wider audience. Copyright and Moral Rights remain with the author(s) and/or copyright holders. URLs from City Research Online may be freely distributed and linked to.

Reuse: Copies of full items can be used for personal research or study, educational, or not-for-profit purposes without prior permission or charge. Provided that the authors, title and full bibliographic details are credited, a hyperlink and/or URL is given for the original metadata page and the content is not changed in any way.

City Research Online:

<http://openaccess.city.ac.uk/>

publications@city.ac.uk



CITY UNIVERSITY
LONDON

Treatment of brain cancer and ischaemic stroke utilising High Intensity Focus Ultrasound (HIFU) guide with MRI

A thesis submitted to the graduate faculty in partial fulfilment of the requirements for the Degree of Doctor of Philosophy in Biomedical Engineering

Venediktos Hadjisavvas

School of Engineering and Mathematical Sciences
Electronic and Electrical Engineering

City University London
January 2012

TABLE OF CONTENTS

Table of Contents	ii
List of Figures	vi
List of Tables	x
List of Abbreviations	xi
Acknowledgements	xiii
Declaration	xiv
Abstract	xv
Chapter 1: Introduction	1
Chapter 2: The pathology and treatment of brain tumours and acute ischaemic stroke	5
2.1 Introduction	5
2.2 Physiology and anatomy of the human brain	5
2.2.1 Head Anatomy	5
2.2.2 Brain Regions and Functions	10
2.2.3 The cerebral circulatory system	12
2.2.4 Brain Cancer Statistics	13
2.3 Characterization and treatment of human brain tumours	14
2.3.1 The WHO brain tumour grading system	15
2.3.2 Types and sizes of brain tumours	19
2.3.3 Current state of the art in treating brain tumours	31
2.4 Thrombolysis for acute ischaemic stroke; characterization and treatment	34
2.4.1 Acute Ischaemic Stroke	34
2.4.2 Thrombolysis	35
2.4.3 Sonothrombolysis	38
Chapter 3: Overview of HIFU	41
3.1 Introduction	41

3.2 History of HIFU	42
3.3 Physical Principles of HIFU	45
3.4 Applications of HIFU in Medicine	47
3.5 Limitations and Future prospects of HIFU	49
3.6 Conclusion	51
Chapter 4: Physical aspects of ultrasounds	52
4.1 Introduction	52
4.2 Basic quantities in ultrasound	52
4.3 Power Field Calculations	57
4.4 Temperature simulations	60
4.5 Thermal dose calculations	63
Chapter 5: <i>In vitro</i> measurements of the attenuation and absorption of HIFU in animal brain tissues as a function of thermal dose.	67
5.1 Introduction	67
5.2 Materials and Methods	68
5.2.1 Sample Preparation	68
5.2.2 Attenuation Measurement System	69
5.2.3 Absorption Measurement	70
5.2.4 Acoustical Power Calibration	72
5.2.5 Intensity Field Measurement	73
5.2.6 Ultrasonic Transducer	73
5.3 Temperature Simulation	74
5.3.1 Temperature estimation	74
5.3.2 Thermal dose calculation	74
5.4 Results	74
5.5 Discussion	76
Chapter 6: Thermal simulation model for predicting lesion size during sonication using HIFU	79
6.1 Introduction	79
6.2 Transducer arrangement	79

6.3 Simulation methodology	80
6.4 Results	81
6.4.1 Simulation results for lesion size vs. time for different power and frequency	81
6.4.2 Simulation results for temperature vs. time for different power and frequency	86
6.5 Discussion	87
Chapter 7: <i>in vitro</i> and <i>in vivo</i> (rabbit brain) penetration of HIFU using MR imaging	90
7.1 Introduction	90
7.2 HIFU/MRI system	91
7.2.1 HIFU System	92
7.2.2 MRI Imaging	93
7.2.3 Positioning Device	93
7.2.4 Temperature Measurement	94
7.2.5 MRI Compatible Camera	94
7.3 <i>in vitro</i> and <i>in vivo</i> experiments	95
7.4 HIFU parameters	97
7.5 MRI processing and simulation	97
7.6 Results	98
7.7 Discussion	107
Chapter 8: A simulation model for predicting the temperature during the application of MR-guided pulsed focused ultrasound for stroke treatment	110
8.1 Introduction	110
8.2 Material and Methods	111
8.2.1 Temperature simulations	112
8.2.2 Temperature Measurements	112
8.2.3 <i>in vitro</i> experiments	113
8.3 Results	114
8.4 Discussion	123

Chapter 9: Application of MR-guided focused pulsed ultrasound for destroying clots <i>in vitro</i> using thrombolytic drugs	126
9.1 Introduction	126
9.2 HIFU system	129
9.2.1 Focused ultrasound system	129
9.2.2 Artery/tissue/clot model	129
9.2.3 Positioning device	130
9.2.4 Temperature measurements	131
9.3 <i>in vitro</i> experiments	132
9.4 Results	134
9.5 Discussion	140
Chapter 10: Application of MR-guided focused pulsed ultrasound for destroying clots <i>in vivo</i> using thrombolytic drugs	143
10.1 Introduction	143
10.2 Focused ultrasound system/Ultrasonic Doppler system	144
10.3 Artery/tissue/clot model	146
10.4 Testing the Thrombus functionality <i>in vivo</i>	146
10.5 Detection of thrombus using MRI	149
10.6 Thrombolysis <i>in vivo</i>	150
10.6.1 Coupling method	150
10.6.2 Thrombus model	151
10.7 Results	155
10.8 Discussion	159
Chapter 11: Conclusion and Future Work	161
11.1 Conclusion	161
11.2 Future Work	166

LIST OF FIGURES

Figure		Page
2.1	Skin and underlying subcutaneous tissue	6
2.2	The most important bones of the Skull	7
2.3	Various part of the brain	9
2.4	Cerebrospinal Fluid Circulation	10
2.5	Major Regions of the Brain	11
2.6	Major Regions of the cerebral hemispheres	11
2.7	Major cerebral arteries and the circle of Willis	13
4.1	Demonstration of wave reflection and transmission at a plane interface between two media	55
4.2	Geometry of spherically focused transducer	59
4.3	Flowchart of the simulation model to calculate temperature, thermal dose and to estimate lesion size	65
4.4	Demonstration of 2 min thermal dose at 43°C using an idealized temperature profile and a typical temperature profile created using high intensity ultrasound	66
5.1	Block diagram of the attenuation measurement system	70
5.2	Block diagram of the absorption measurement system	72
5.3	Attenuation vs. thermal dose referenced at 43 °C for lamb brain	75
5.4	Absorption vs. thermal dose referenced at 43 °C for lamb brain	76
5.5	Experimental and simulated temperature change vs. time (Power=15W, 4 sec pulse, F=4 MHz, R=100mm, d=40mm, depth in tissue=15mm).	76
6.1	Transducer arrangements	80
6.2	Lesion length/width distributions versus pulse duration at 0.5 MHz transducer (power= 50W, 60W, and 80W)	82
6.3	Lesion length/width distributions versus pulse duration at 1 MHz transducer (power= 20W, 30W, 40W, 50W, and 60W)	83
6.4	Lesion length/width distributions versus pulse duration at 1.5 MHz transducer (power= 20W, 30W, and 40W)	84

6.5	Lesion length/width distributions versus pulse duration at 1 MHz transducer (power= 20W, 30W, and 40W)	85
6.6	Temperature distributions versus pulse duration at 0.5, 1, 1.5 MHz transducers (power= 20W, 30W, 40W, 50W, 60W, and 80W)	87
7.1	Block diagram of the HIFU system under MRI guidance	92
7.2	The robot, the complete mechanical design, photo	93, 94
7.3	Coupling methods used for <i>in vitro</i> and <i>in vivo</i> experiments	95
7.4	Large lesions in a gel phantom	99
7.5	Single lesions under power of 70W, 42.5W and ultrasound exposure of 10s, 20s.	100
7.6	Single lesion using T1-W FSE TR=500 ms using 60W for 30 s, f=1 MHz and focal depth=1 cm	100
7.7	MRI images of three lesions in brain <i>in vitro</i> using T1-w FSE, f=2 MHz, d=5 cm and focal depth=1 cm	101
7.8	Images of large lesions monitored using a) T1-w FSE b) T2-w FSE and c) FLAIR	101
7.9	Contrast to noise ratio (CNR) vs. TR for T1-W FSE in excised lamb brain	102
7.10	Contrast to noise ratio (CNR) vs. TE for T2-W FSE in excised lamb brain	103
7.11	Large lesion in lamb brain <i>in vitro</i>	103
7.12	Lesion in rabbit <i>in vivo</i> , MRI using T1-W FSE (with TR=500 ms)	104
7.13	Injection of the trypan blue and lesion as seen after the injection of the trypan blue	104
7.14	Lesion-brain tissue interface	105
7.15	MRI image of a large thermal lesion in rabbit <i>in vivo</i> using T1-W FSE, f=2MHz and focal depth=1 cm	105
7.16	MRI image using T1-w FSE <i>in vitro</i>	106
7.17	MRI image using T1-w FSE <i>in vivo</i>	106
8.1	Timing diagram explaining PRP, DF, and total time	112
8.2	Schematic diagram of the MR-guided FUS system	113

8.3	Simulated and experimental Temperature vs. Time	114
8.4	Temperature vs. Duty Factor for different Power at FD=2.5 cm	116
8.5	Temperature vs. Duty Factor for different Power at FD=1 cm	117
8.6	Temperature vs. Duty Factor using using $f=0.5\text{MHz}$, 1MHz and FD=2.5cm, 1cm	119
8.7	Duty Factor that establishes safe temperature vs. Power, $f=0.5\text{MHz}$, Radius of Curvature=10 cm, Transducer Diameter=5 cm, Focal Depth=2.5 cm, PRP=1 s	119
8.8	Temperature vs. Duty Factor for different Power and $f=1\text{MHz}$	121
8.9	Temperature vs. Duty Factor for different Power and $f=0.5\text{MHz}$	123
9.1	HIFU system for <i>in vitro</i> sonothrombolysis	130
9.2	The positioning device	131
9.3	Photo of the temperature measurement system, the omega thermocouple-to-analogue connector, National Instruments data acquisition board, and the custom made software	131
9.4	Photo of the HIFU system setup in the Lab	133
9.5	Photo of the artery/clot system	134
9.6	Temperature change for different power, Duty Factor and Pulse Repetition Period	136
9.7	Temperature elevation vs power, duty factor, and Pulse Repetition Period	137
9.8	Silicone tube showing the clot (left), the rt-PA (right) and the dissolved clot in between	137
9.9	The effect of temporal average <i>in situ</i> intensity, the beam area, the frequency and the comparison between US+rt-PA and rt-PA on the volume of the dissolved clot with frequency of 1 MHz, duty factor of 10%, and PRF of 1 Hz	139
10.1	A top view of a rabbit brain after a craniotomy was performed	147
10.2	Axial and coronal MRI images in rabbit. Three-dimensional cranial CT of basilar and vertebral arteries in rabbit	147
10.3	MRA image of a rabbit MCA	148
10.4	Extracting the carotid	148
10.5	A. Ultrasonic imaging probe placed on top of the brain B.	149

	Ultrasonic imaging probe placed on the carotid	
10.6	The displacement of the catheter into the carotid	149
10.7	A. MRI compatible container. B. Artery / thrombus / brain tissue model	150
10.8	Long transducer holder	150
10.9	Transducer setup showing the two holes on top of the holder	151
10.10	Transducer localization	151
10.11	Shaving rabbit ears	151
10.12	injection of the thrombus	154
10.13	A. Creation of clot (thrombus) using a hammer; B. Clot formation	154
10.14	A. Thermocouple placements on clot for localization; B. Transducer target for quick localization	155
10.15	A. injection of rt-PA; B. Ultrasonic system setup	155
10.16	A. axial black-blood T2-weighted magnetic resonance images showing a 24-h old thrombus; B. the arrows indicate the thrombus in the injured right carotid artery, and the asterisk indicates the non injured left carotid artery; C. the appearance of the thrombus on the MRI correlates closely with the matched histologic section shown in C.	156
10.17	MRI images A. using T1 FSE; B. using T2 FSE	156
10.18	Blood flow using Doppler ultrasound; A. At the carotid; B. At the top of the brain	157
10.19	Blood flow after the injection of a thrombus using a Doppler ultrasound	158
10.20	Blood flow; A. before the thrombus injection; B. after thrombus injection	158
10.21	Blood flow; A. before thrombus creation; B. after artery occlusion; C. after sonothrombolysis	159

LIST OF TABLES

Table		Page
2.1	Incidence rate for brain tumour	14
2.2	Neuroepithelial tumours	20
2.3	Meningeal tumours	25
2.4	Germ cell tumours	26
2.5	Tumours of the sellar region	27
2.6	Tumours of uncertain histogenesis	28
2.7	Primary CNS lymphoma	28
2.8	Tumours of peripheral nerves that affect the CNS	28
2.9	Metastatic tumours	29
2.10	brain tumour: diameter or volume	30
2.11	Stroke statistics	34
3.1	HIFU Systems for Clinical Use	42
3.2	The development of HIFU technology throughout the century	43
4.1	Propagation velocities of some biological tissues	54
4.2	Acoustical impedances of soft tissues	55
4.3	Attenuation and absorption values for biological tissue	58
4.4	Parameters used for the temperature vs. time simulations	62
6.1	Summary of the recommended simulation results	89
7.1	Transducer parameters	92
7.2	Summary of the recommended HIFU system	109
8.1	Summary of the recommended HIFU system	125
9.1	Characteristics of Ultrasound and Thrombolysis (<i>in vitro</i>)	127
9.2	Various sonication parameters	134
9.3	Sonication parameters (without rt-PA)	135
9.4	Summary of the recommended HIFU system	142
10.1	Characteristics of Ultrasound and Thrombolysis (<i>in vivo</i>)	145
10.2	Thrombus model in animals	153
10.3	Summary of the recommended HIFU system	160

LIST OF ABBREVIATIONS

ABS	Acrylonitrile Butadiene Styrene
BBB	Blood-Brain Barrier
CNR	Contrast to noise ratio
CNS	central nervous system
CSF	cerebrospinal fluid
CT	Computed Tomography
CW	Continue Wave
DF	Duty Factor
FD	Focal Depth
FLAIR	fluid attenuated inversion recovery
FOV	Field of Interest
FSE	Fast Spin Echo
FSPGR	fast spoiled gradient
HIFU	High Intensity Focus Ultrasound
ICH	intracerebral-hemorrhage
MCA	Middle Cerebral Artery
MRA	Magnetic Resonance Angiography
MRgFUS	MRI-guided HIFU surgery
MRI	Magnetic Resonance Imaging
NEX	Number of Excitations
PNS	Peripheral Nervous System
PRF	Pulse Repetition Frequency
PRP	Pulse Repetition Period
PW	Pulse Wave
PZT	Piezoelectric Transducer
RF	Radio Frequency
ROI	Region of Interest

rt-PA	recombinant tissue-Plasminogen Activator
SATA	Spatial Average Temporal Average
SPTA	Spatial Peak Temporal Average
T1 & T2	MRI Basic Pulse Sequences
TE	Time to Echo
TR	Repetition Time
UET	Ultrasound-Enhanced Thrombolysis
US	Ultrasound
WHO	World Health organization

ACKNOWLEDGEMENTS

I would like to thank all the people who have helped and inspired me during my PhD thesis.

I especially want to thank my advisors, Prof. C. Damianou and Prof. P. Kyriacou, for their guidance during my research at City University London. Their everlasting energy and enthusiasm in research have motivated all their research students, including me. In addition, they were always accessible and willing to help their students. As a result, research life became smooth and rewarding for me.

Lastly, I would like to thank my fellow research students N. Mylonas and A. Couppis for their support and guidance.

ABSTRACT

In this thesis high intensity focused ultrasound (HIFU) is utilized for cancer treatment (thermal mode) and treatment of ischaemic stroke (mechanical mode). These two applications were investigated *in vitro* and *in vivo* models. MRI was utilized to monitor the lesions created by HIFU either in thermal or cavitation mode in freshly excised lamb brain tissue *in vitro*, and in rabbit brain *in vivo*. Additionally, MRI was used to monitor lesions deep in tissue for both *in vitro* and *in vivo* exposures. All three MRI sequences used (T1-W FSE, T2-W FSE and FLAIR) were able to detect lesions. Both thermal and bubbly lesions were best monitored using T1-W FSE with excellent contrast, proving the potential of HIFU to treat reliably tumours in the brain. A HIFU system was also used to assist thrombolysis in cooperation with a thrombolytic drug such as recombinant tissue plasminogen activator (rt-PA) *in vitro* and *in vivo*. It was shown that higher intensity results to higher volume of dissolved clot, but there is a limit of the intensity to be used in order to avoid heating of the clot and the surrounding tissue. The goal in this study was to achieve temperature elevation not exceeding 1°C (called safe temperature). It was found that the larger the beam area the larger the dissolved clot volume. Also, the lower the frequency, the larger the volume of the dissolved clot. The results reported herein point to the use of frequency around 0.5 MHz and pulsing to optimize thrombolysis and skull penetration and at the same time avoiding unwanted heating. Finally, an Acrylonitrile Butadiene Styrene (ABS) phantom skull model was developed in order to evaluate the propagation of ultrasound using a single element transducer. The skull model was appropriately designed so that it has the same attenuation as a human skull. It was demonstrated that using a frequency of 0.5 MHz versus 1 MHz, ultrasound propagation through the phantom skull was higher. Therefore, higher frequency has poor skull penetration and a small beam size at the focus, while low frequencies have better skull penetration but with the risk of reaching the unpredictable effect of cavitation. The developed system has proven to successfully create large lesions in the brain and at the same time, these lesions are successfully monitored with excellent contrast using MRI (T1-W FSE) enabling the accurate determination of the margins of these lesions. The results reported in this study point to the use of frequency around 0.5 MHz and pulsing to optimize thrombolysis and skull penetration and at the same time avoiding unwanted heating. For treating tumours located deep in the brain and for dissolving thrombus causing an acute ischaemic stroke, further extensive clinical studies will be needed before this technology is applied to humans.

CHAPTER 1: INTRODUCTION

Early studies on focused ultrasound treatment in the 1940s [1] and 1950s [2][3] have demonstrated the ability to perform precise lesioning in the human brain. However, the need for a craniotomy, as well as the lack of sophisticated imaging technology, resulted in limited growth of high-intensity focused ultrasound for neurosurgery. More recently, technological advances have permitted the combination of High Intensity Focused Ultrasound (HIFU) along with magnetic resonance imaging (MRI) guidance to provide an opportunity to effectively treat a variety of central nervous system disorders [4]-[5].

The purpose of this research is to develop an ultrasonic system that is guided with MRI imaging. The effect of temperature and of thermal dose on the attenuation and absorption of tissues namely lamb brain *in vitro* were investigated. The attenuation was measured using the transmission and reception method and the absorption was measured using the rate of heating method. The impact of variation of absorption due to tissue changes on the temperature elevation was demonstrated by temperature measurements and simulations.

Following the results of the attenuation and the absorption, a computer model was developed that estimates the lesion size based on the transducer characteristics (frequency, diameter, degree of focusing), treatment protocol (pulse duration, acoustical power), and anatomical site (size, depth, mode of operation). In addition, temperature elevation at the focal point inside the tissue was recorded. Temperature elevation had to be controlled in order to avoid heating of the brain during sonothrombolysis. Acoustic parameters (power, pulse duration, duty factor and pulse repetition frequency) were extracted to maintain a temperature increase of less than 1°C during the application of pulsed ultrasound. Based on the simulation results (for both cases), a transducer was designed that contains minimum amount of magnetic material so that it can function inside the MRI scanner without affecting the quality of the imaging.

MRI was utilized for the investigation and monitoring of small and large lesions created by HIFU under thermal and cavitation or bubbly lesions in freshly excised

lamb brain tissue *in vitro*, and in rabbit brain *in vivo*. In addition, MRI was used to monitor lesions deep in tissue for *in vitro* and *in vivo* exposures. MRI images were taken using T1-W fast spin echo (FSE), T2-W FSE and fluid attenuated inversion recovery (FLAIR) sequences.

A thrombus model was tested in the rabbit carotid and ear artery *in vivo* to investigate its functionality to block the artery. A HIFU system was used to assist thrombolysis in cooperation with a thrombolytic drug such as recombinant tissue plasminogen activator (rt-PA) *in vitro* and *in vivo*. An Ultrasonic Doppler system was also utilized to monitor the blood flow in the brain during sonothrombolysis. Various pulse protocols were investigated so that the temperature change at the clot does not exceed 1°C (called safe temperature).

An Acrylonitrile Butadiene Styrene (ABS) phantom skull model was developed in order to evaluate the propagation of ultrasound using a single element transducer. The skull model was appropriately designed so that it has the same attenuation as a human skull. Temperature was monitored at the focal point with and without the skull model.

A brief outline of the chapters to follow is given below.

Chapter 2 covers the basics of brain anatomy and physiology. It describes the cerebral circulatory system as well as some worldwide statistics on brain cancer. It also explains the different types of brain tumours and their different grading system based on the World Health Organization (WHO) classification. Current state of the art in treating brain tumours is also discussed. Finally, the basics of stroke characteristics are described with an emphasis on Acute Ischaemic Stroke. Methods of treatments with the help of thrombolytic drugs are also explained and the feasibility of ultrasound to enhance thrombolysis is accentuated.

Chapter 3 presents historically the technique of HIFU and explains its physical principles. The chapter also provides descriptions of HIFU applications in medicine and highlights the limitations of the technique and future prospects.

Chapter 4 describes the physical aspects of ultrasound such as basic quantities, power field calculations, temperature simulations, and thermal dose calculations.

Chapter 5 presents the results from the *in vitro* measurements of the attenuation and absorption in animal brain tissue as a function of thermal dose. Attenuation and absorption are the main physical parameters that affect the temperature rise in tissue. Due to high temperatures induced in tissue and due to sonication, it is important to know the variation of attenuation and absorption at this high level of temperature.

In chapter 6, the results derived from the simulation study are presented. Based on the optimized size and shape of lesions and temperature elevation derived from the simulation studies, the ultrasonic transducer was developed with the minimum amount of magnetic material. The transducer operated in thermal mode to produce tissue necrosis for the treatment of cancer.

Chapter 7 presents experimental results of HIFU *in vitro* (lamb brain) and *in vivo* (rabbit brain) using MR imaging. The creation of single, large and deep lesions was demonstrated and the effectiveness of MRI to monitor therapeutic protocols of HIFU in the brain was investigated.

In chapter 8 the simulations results are presented for the treatment of ischaemic stroke. The estimated temperature elevation derived from the simulation studies should not exceed 1°C, so that thermal effects are eliminated. Temperature elevation should be controlled in order to avoid heating of the brain during sonothrombolysis. The transducer operated in mechanical mode in order to partition the thrombus into small pieces.

Chapter 9 presents the results from the *in vitro* experiments in an effort to dissolve the clot using HIFU. At first, ultrasound alone (US) was used, then thrombolytic drug (rt-PA) alone was used and finally ultrasound combined with rt-PA (US + rt-PA) were used. The goal was to achieve temperature elevation not exceeding 1°C and at the same time to dissolve a large amount of clot.

Chapter 10 presents the results from the *in vivo* experiments. The ability to produce thrombus was tested *in vivo*. The ability to dissolve the thrombus created at the ear artery of a rabbit was presented using HIFU and rt-PA. A Doppler ultrasound was used to observe the blood flow in the brain and at the ear artery before and after the thrombus. Finally, chapter 11 presents conclusions and future work.

CHAPTER 2: THE PATHOLOGY AND TREATMENT OF BRAIN TUMOURS AND ACUTE ISCHAEMIC STROKE

2.1 INTRODUCTION

The human brain is the most important and the most complex organ in the human body. Brain cancer diseases or strokes are very difficult to treat even with the today's technology. Finding new methods of dealing with these kinds of diseases makes it very challenging. Therefore, in this thesis a HIFU system is utilized for cancer treatment and treatment of ischaemic stroke.

This chapter will discuss the main type of brain tumours and the various current state of the art treatment methodologies. Similarly, this chapter also covers the pathology and treatment of acute ischaemic stroke. Prior to the description of these, the basic anatomy and physiology of the anatomical parts related to these pathologies (i.e. brain) are also presented.

2.2 PHYSIOLOGY AND ANATOMY OF THE HUMAN BRAIN

2.2.1 HEAD ANATOMY

The human *nervous system* consists of the *central nervous system* (CNS) and *peripheral nervous system* (PNS). The CNS consists of the brain and spinal cord, while the PNS is composed of the nerves extending to and from the brain and spinal cord. The primary functions of the nervous system are to monitor, integrate (process) and respond to information inside and outside the body. The brain consists of soft, delicate, non-replaceable neural tissue. It is supported and protected by the surrounding skin, skull, meninges and cerebrospinal fluid [6].

SKIN

The skin constitutes a protective barrier against physical damage of underlying tissues, invasion of hazardous chemical and bacterial substances and it helps to maintain the body at a constant temperature. Together with the sweat and oil glands, hairs and nails it forms a set of organs called the *integumentary system*. Figure 2.1 shows a cross-section of the skin and underlying subcutaneous tissue.

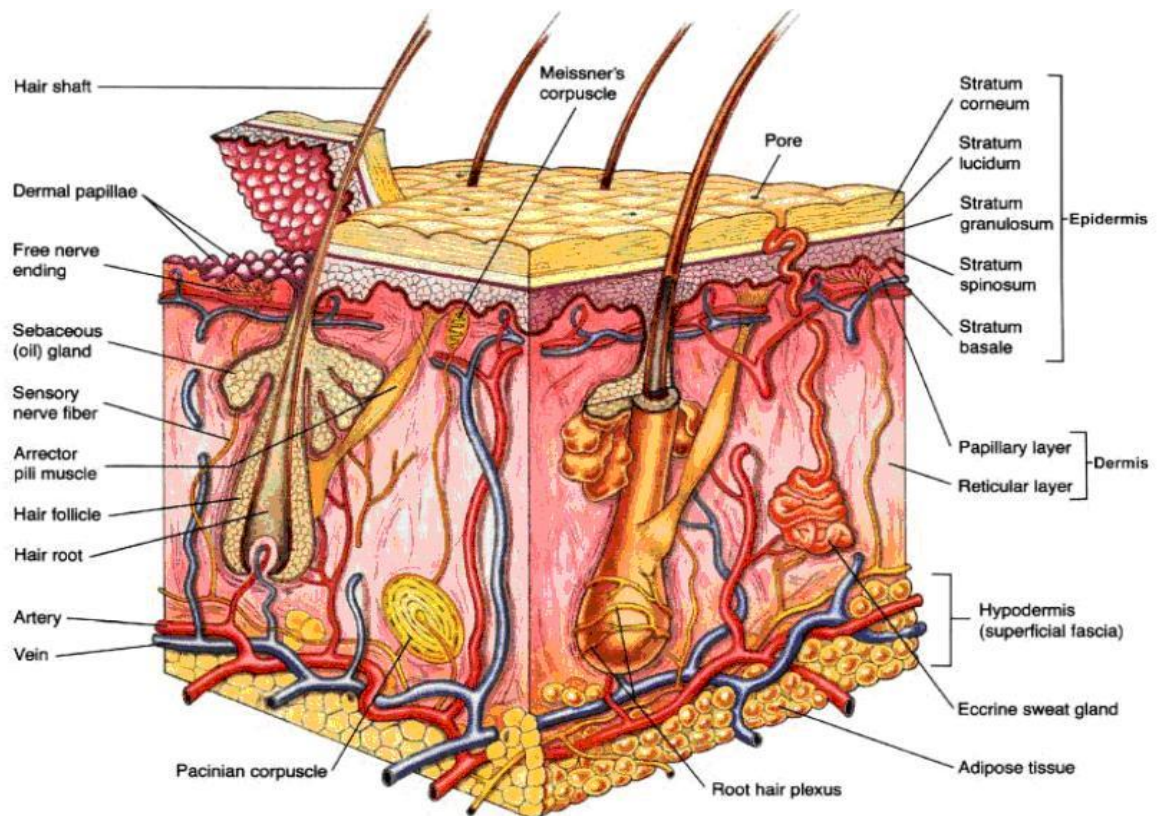


Figure 2.1 Skin and underlying subcutaneous tissue [6]

The skin consists of an outer, protective layer, the *epidermis* and an inner layer, the *dermis*. While the top layer of the epidermis, the *stratum corneum*, consists of dead cells, the dermis is composed of vascularised fibrous connective tissue. The *subcutaneous tissue*, located underneath the skin, is primarily composed of *adipose tissue* (fat) [6].

SKULL

Depending on their shape, bones are classified as long, short, flat or irregular. There are two types of bones: compact and spongy bone. Compact has a smooth structure, whilst the spongy bone is composed of small needle-like or flat pieces of bone called *trabeculae*, which form a network filled with red or yellow bone marrow. Most skull bones are flat and consist of two parallel compact bone surfaces, with a layer of spongy bone sandwiched between. The spongy bone layer of flat bones (the diploë) predominantly contains red bone marrow and hence has a high concentration of blood [6].

The skull is a highly complex structure consisting of 22 bones altogether. These can be divided into two sets, the *cranial bones* (or *cranium*) and the *facial bones*. The *facial bones* form the framework of the face, the cranial bones form the *cranial cavity* that encloses and protects the brain. All bones of the adult skull are firmly connected by *sutures*. Figure 2.2 shows the most important bones of the skull. The *frontal bone* forms the forehead and contains the *frontal sinuses*, which are air filled cells within the bone. Most superior and lateral aspects of the skull are formed by the *parietal bones* while the *occipital bone* forms the posterior aspects. The base of the occipital bone contains the *foramen magnum*, which is a large hole allowing the inferior part of the brain to connect to the spinal cord. The remaining bones of the cranium are the *temporal*, *sphenoid* and *ethmoid bones* [6].

MENINGES

The *meninges* (Figure 2.3) are three connective tissue membranes enclosing the brain and the spinal cord. Their functions are to protect the Central Nervous System (CNS) and blood vessels, enclose the *venous sinuses*, retain the *cerebrospinal fluid* (CSF), and form partitions within the skull. The outermost meninx is the *dura mater*, which encloses the *arachnoid mater* and the innermost *pia mater*. A brief description of the various parts of the brain are described at the next page [7];

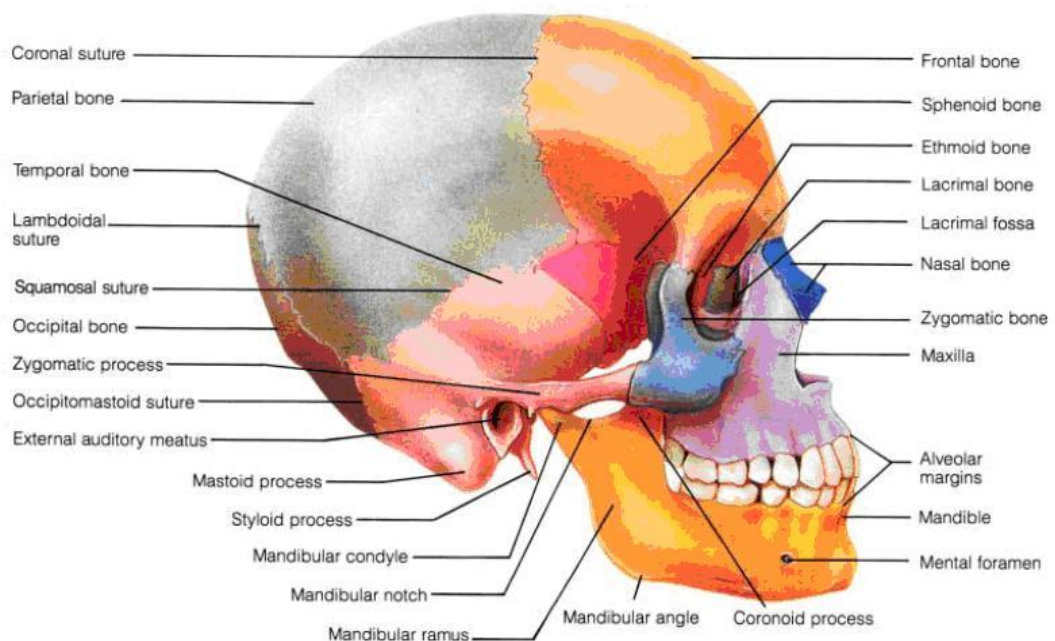


Figure 2.2 The most important bones of the Skull [6]

dura mater - The outermost and heaviest, most fibrous, layer of the meninges covering the brain and spinal cord, composed of dense irregular fibrous connective tissue, a structure which contains some of the larger blood vessels, particularly the venous sinuses; it forms a protective physical barrier for the CNS.

epidural space - The anatomical location external to the dura is merely a "potential" space in the cranium, since the dura is fused to the cranial periosteum, while, in contrast, in the vertebral canal, it generally contains adipose tissue.

subdural space - The anatomical location between the dura and the arachnoid is merely a "potential" space because under normal circumstances, the arachnoid is directly attached to the dura mater.

arachnoid - The middle layer of the meninges, a thin, spongy membranous covering of the brain and spinal cord with a spider-web-like appearance which does not conform to the irregularities of the surfaces of the brain and spinal cord. It is composed of a delicate loose fibrous connective tissue; the space under the arachnoid and above the pia mater, the subarachnoid space, contains cerebrospinal fluid.

pia mater -The inner layer of the meninges, a thin, membranous covering which adheres smoothly to the surface of the brain and spinal cord and conforms to all the irregularities of their surfaces. It is composed of a very thin layer of dense irregular fibrous connective tissue; the smaller surface blood vessels of the brain and spinal cord are contained within this layer; at spinal levels, the pia mater gathers laterally, pierces the arachnoid and attaches to the dura, forming the denticulate ligament. This stabilizes the spinal cord within the vertebral canal and decreases the likelihood of cord damage when physical trauma occurs.

subarachnoid space - The space under the arachnoid and above the pia mater which contains cerebrospinal fluid.

meningitis - Inflammation of the meninges of the brain and the spinal cord, most often caused by a bacterial or viral infection and characterized by fever, nausea and vomiting, intense headache, and stiff neck; bacterial forms tend to have more severe prognosis.

falx cerebri - The scythe-shaped mid-sagittal fold of the dura mater occupying the longitudinal fissure between the two cerebral hemispheres and which contains the sagittal venous sinuses.

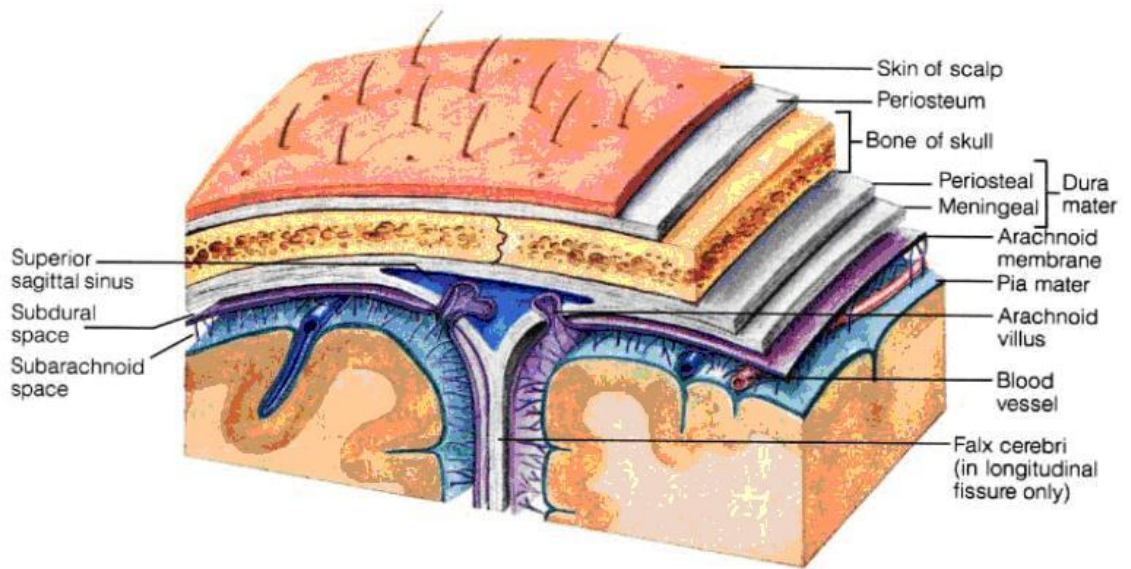


Figure 2.3 Various parts of the brain; meninges [7]

CEREBROSPINAL FLUID (CSF)

CSF is a watery liquid similar in composition to blood plasma. It is formed in the *choroid plexuses* and circulates through the ventricles into the *subarachnoid space*, where it is returned to the dural venous sinuses by the *arachnoid villi*. The prime purpose of the CSF is to support and cushion the brain and help nourish it. Figure 2.4 illustrates the flow of CSF through the central nervous system. CSF has several important functions. It cushions the brain within the skull, transports nutrients to brain tissue and carries waste away. CSF is produced at a site within the brain called the choroid plexus, which generates about 400-500 ml. (one pint) of the fluid each day or approximately 0.3 cc per minute. The total volume of CSF in the skull at any given time is around 140 ml. That means the body produces, absorbs and replenishes the total volume of CSF about 3-4 times daily [7].

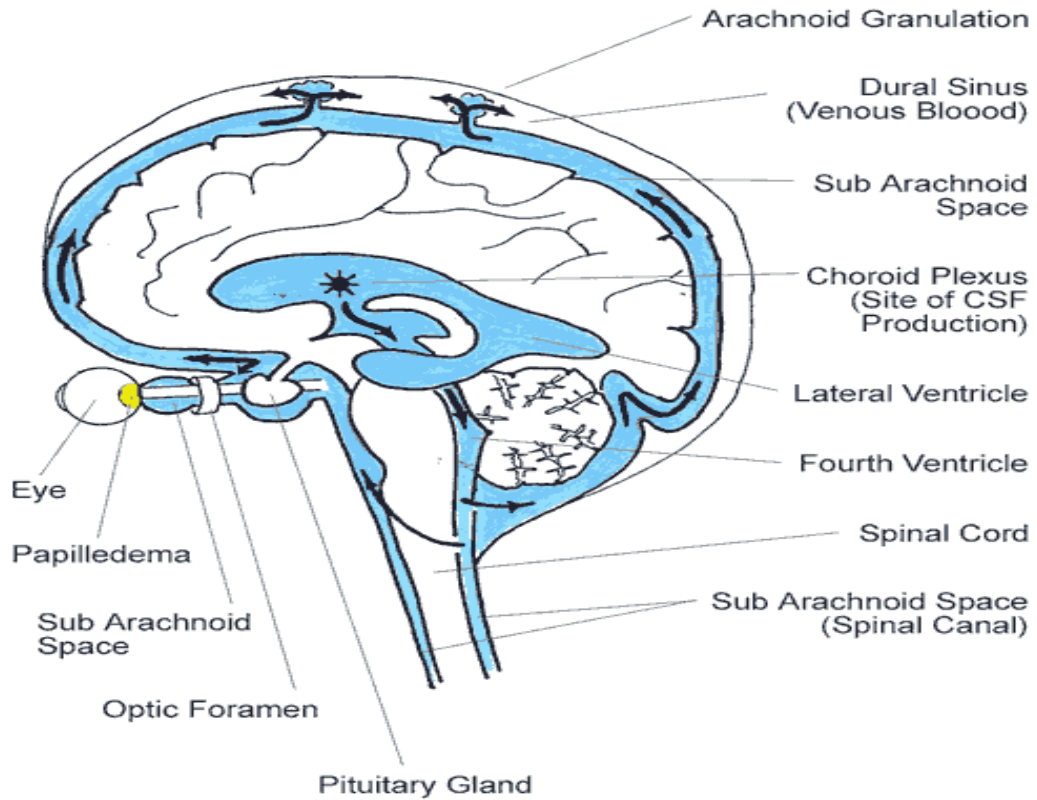


Figure 2.4 Cerebrospinal Fluid Circulation [7]

2.2.2 BRAIN REGIONS AND FUNCTIONS

The major regions of the brain (figure 2.5) are the *cerebral hemispheres*, *diencephalon*, *brain stem* and *cerebellum*.

CEREBRAL HEMISPHERES

The *cerebral* hemispheres (Figure 2.6), located on the most superior part of the brain, are separated by the *longitudinal fissure*. They make up approximately 83% of total brain mass, and are collectively referred to as the *cerebrum*. The *cerebral cortex* constitutes a 2-4 mm thick *grey matter* surface layer and, because of its many convolutions, accounts for about 40% of total brain mass. It is responsible for conscious behaviour and contains three different functional areas: the *motor areas*, *sensory areas* and *association areas*. Located internally are the *white matter*, responsible for communication between cerebral areas and between the cerebral cortex and lower regions of the CNS, as well as the *basal nuclei* (or *basal ganglia*), involved in controlling muscular movement [7].

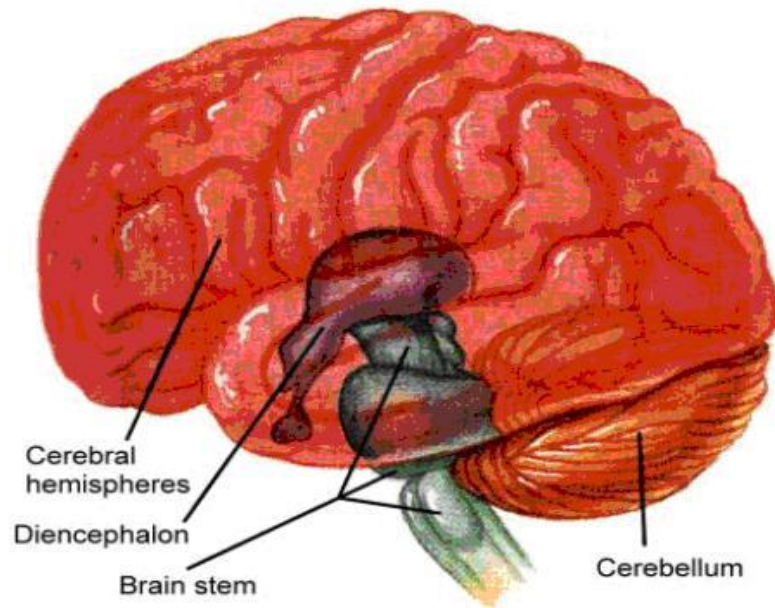


Figure 2.5 Major Regions of the Brain [7]

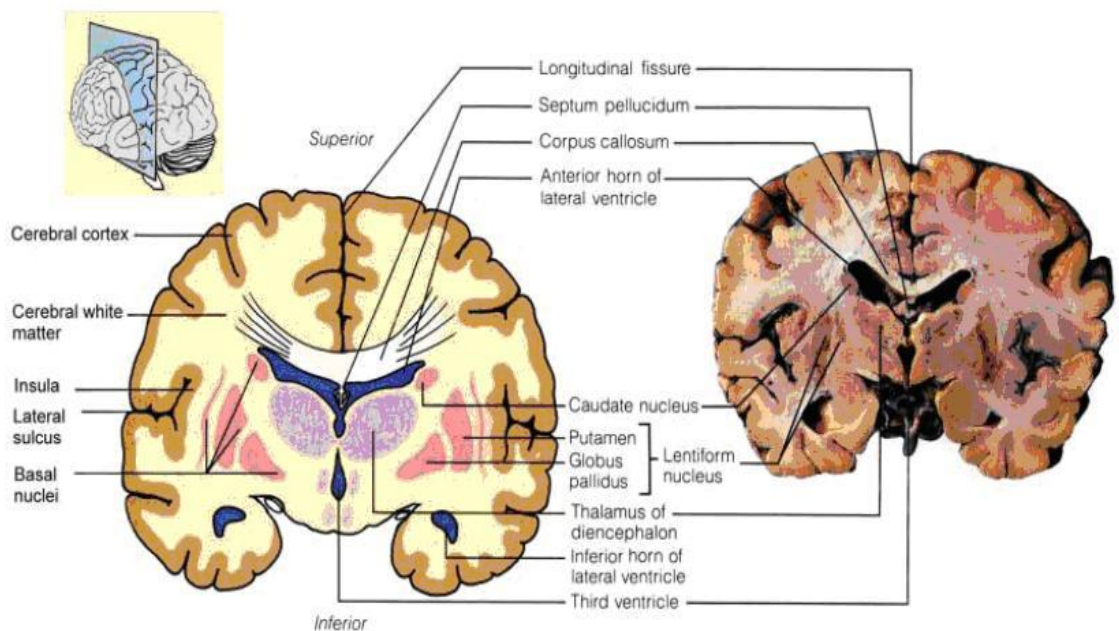


Figure 2.6 Major Regions of the cerebral hemispheres [7]

DIENCEPHALON

The *diencephalon* is located centrally within the forebrain. It consists of the *thalamus*, *hypothalamus* and *epithalamus*, which together enclose the third ventricle. The thalamus acts as a grouping and relay station for sensory inputs ascending to the sensory cortex and association areas. It also mediates motor activities, cortical arousal and memories. The hypothalamus, by controlling the

autonomic (involuntary) nervous system, is responsible for maintaining the body's homeostatic balance. Moreover, it forms a part of the *limbic system*, the 'emotional' brain. The epithalamus consists of the *pineal gland* and the CSF producing *choroid plexus* [7].

BRAIN STEM

The brain stem is similarly structured as the spinal cord: it consists of grey matter surrounded by white matter fibre tracts. Its major regions are the *midbrain*, *pons* and *medulla oblongata*. The midbrain, which surrounds the cerebral aqueduct, provides fibre pathways between higher and lower brain centres, contains visual and auditory reflex and subcortical motor centres. The pons is mainly a conduction region, but its nuclei also contribute to the regulation of respiration and cranial nerves. The medulla oblongata takes an important role as an autonomic reflex centre involved in maintaining body homeostasis. In particular, nuclei in the medulla regulate respiratory rhythm, heart rate, blood pressure and several cranial nerves. Moreover, it provides conduction pathways between the inferior spinal cord and higher brain centres [7].

CEREBELLUM

The *cerebellum*, which is located dorsal to the pons and medulla, accounts for about 11% of total brain mass. Like the cerebrum, it has a thin outer cortex of grey matter, internal white matter, and small, deeply situated, paired masses (nuclei) of grey matter. The cerebellum processes impulses received from the cerebral motor cortex, various brain stem nuclei and sensory receptors in order to appropriately control skeletal muscle contraction, thus giving smooth, coordinated movements.

2.2.3 THE CEREBRAL CIRCULATORY SYSTEM

Blood is transported through the body via a continuous system of *blood vessels*. *Arteries* carry oxygenated blood away from the heart into *capillaries* supplying tissue cells. *Veins* collect the blood from the capillary bed and carry it back to the heart. The main purpose of blood flow through body tissues is to deliver oxygen and nutrients to and waste from the cells, exchange gas in the lungs, absorb nutrients from the digestive tract, and help forming urine in the kidneys. All the

circulation besides the heart and the pulmonary circulation is called the *systemic circulation* [7].

BLOOD SUPPLY TO THE BRAIN

Figure 2.7 shows an overview of the arterial system supplying the brain. The major arteries are the *vertebral* and *internal carotid arteries*. The two *posterior* and single *anterior communicating arteries* form the *circle of Willis*, which equalises blood pressures in the brain's anterior and posterior regions, and protects the brain from damage if one of the arteries become occluded. However, there is little communication between smaller arteries on the brain's surface. Hence, occlusion of these arteries usually results in localized tissue damage [7].

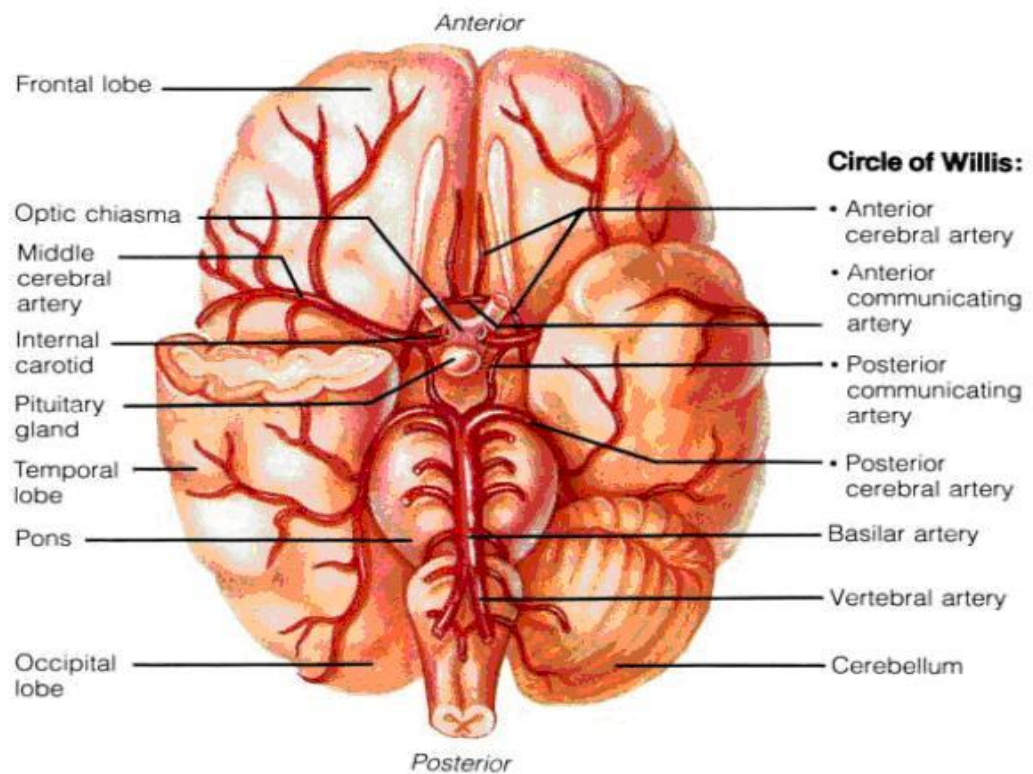


Figure 2.7 Major cerebral arteries and the circle of Willis [7]

2.2.4 BRAIN CANCER STATISTICS

Table 2.1 shows approximately the incidence rate for brain tumour in adults within the populations of various countries and regions for the year 2004 [8]. These incidences for brain tumour are only estimates and may have limited relevance to the actual incidence of brain tumours in adults in any region. The sources or statistics have only been taken from the population in the countries

listed and as such, therefore, this information may be inaccurate (especially for the developing or third world countries) and only give a general indications as to the actual prevalence or incidence of brain tumours of adults in that region.

Table 2.1 Incidence rate for brain tumour

Region (Approximate Statistics)- Brain Cancer	Approximate Incidence	Population Estimated
North America	32,492	432,994,000
South America	488,215	303,887,000
Northern Europe	1499	19,908,27736,881
Western Europe	16,200	215,014,622
Central Europe	11,710	164,423,520
Eastern Europe	15,769	209,272,527
South western Europe	2063,386	1348,32536
Southern Europe	5,177	2696,65072
South eastern Europe	3,853	51,188,794
Northern Asia	207	2,751,314
Central Asia	4342,802	5448,34844
Eastern Asia	8685,604	10896,69688
South western Asia	17371,208	21793,39376
South eastern Asia	34742,416	43586,78752
Middle East	69484,832	87173,57504
Northern Africa	138969,664	174347,15008
Western Africa	277939,328	348694,30016
Central Africa	555878,656	697388,60032
Eastern Africa	1111757,312	1394777,20064
Southern Africa	2223514,624	2789554,40128
Oceania	4447029,248	5579108,80256

2.3 CHARACTERIZATION AND TREATMENT OF HUMAN BRAIN TUMOURS

The human body has the ability to reproduce new cells only when old and damaged cells need to be replaced. A tumour will be formed when normal or abnormal cells keep multiplying when it is not needed. This unwanted growth or multiplication of these cells will result in a brain tumour.

There are two basic kinds of brain tumours: primary brain tumours and metastatic brain tumours. Primary brain tumours start, and tend to stay, in the brain. Metastatic brain tumours begin as cancer elsewhere in the body and spread to the brain. Depending of the malignancy or aggressiveness, tumours are called benign or malignant.

2.3.1 THE WHO BRAIN TUMOUR GRADING SYSTEM

PRIMARY BRAIN TUMOURS

A tumour that starts in the brain is a primary brain tumour. Glioblastoma multiforme, astrocytoma, medulloblastoma, and ependymoma are examples of primary brain tumours. The most common of these tumours are *gliomas*. They begin in glial cells. There are many types of gliomas [9]:

- ***Astrocytoma***—The tumour arises from star-shaped glial cells called *astrocytes*. In adults, astrocytomas most often arise in the cerebrum. In children, they occur in the brain stem, the cerebrum, and the cerebellum. A grade III astrocytoma is sometimes called an *anaplastic* astrocytoma. A grade IV astrocytoma is usually called a *glioblastoma multiforme*.
- ***Brain stem glioma***—The tumour occurs in the lowest part of the brain. Brain stem gliomas most often are diagnosed in young children and middle-aged adults.
- ***Ependymoma***—The tumour arises from cells that line the ventricles or the central canal of the spinal cord, and again they are most commonly found in children and young adults.
- ***Oligodendroglioma***—This rare tumour arises from cells that make the fatty substance that covers and protects nerves. These tumours usually occur in the cerebrum. They grow slowly and usually do not spread into surrounding brain tissue. They are most common in middle-aged adults.

Some types of brain tumours do not begin in glial cells. The most common of these are:

- ***Medulloblastoma***—This tumour usually arises in the cerebellum. It is the most common brain tumour in children. It is sometimes called a *primitive neuroectodermal tumour*.

- ***Meningioma***—This tumour arises in the meninges. It usually grows slowly.
- ***Schwannoma***—A tumour that arises from a *Schwann cell*. These cells line the nerve that controls balance and hearing. This nerve is in the inner ear. The tumour is also called an acoustic *neuroma*. It occurs most often in adults.
- ***Craniopharyngioma***—The tumour grows at the base of the brain, near the *pituitary gland*. This type of tumour most often occurs in children.
- ***Germ cell tumour*** of the brain—The tumour arises from a *germ cell*. Most germ cell tumours that arise in the brain occur in people younger than 30. The most common type of germ cell tumour of the brain is a *germinoma*.
- ***Pineal region tumour***—This rare brain tumour arises in or near the *pineal gland*. The pineal gland is located between the cerebrum and the cerebellum.

Primary brain tumours can be grouped into benign tumours and malignant tumours.

BENIGN BRAIN TUMOURS

A benign brain tumour consists of very slow growing cells, usually has distinct borders, and rarely spreads. When viewed under a microscope, the cells have an almost normal appearance. Surgery alone might be an effective treatment for this type of tumour. A brain tumour composed of benign cells, but located in a vital area, can be considered to be life-threatening — although the tumour and its cells would not be classified as malignant [9].

MALIGNANT BRAIN TUMOURS

A malignant brain tumour is usually rapid growing, invasive, and life-threatening. Malignant brain tumours are often called brain cancer [9]. However, since primary brain tumours rarely spread outside the brain and spinal cord, they do not exactly fit the general definition of cancer.

Cancer is a disease defined by:

- unregulated growth of abnormal cells
- abnormal cells that grow into/around parts of the body and interfere with their normal functioning
- spread to distant organs in the body

Brain tumours can be called malignant if they:

- have the characteristics of cancer cells or
- are located in a critical part of the brain or
- are causing life-threatening damage

Malignant brain tumours that are cancerous can spread within the brain and spine. They rarely spread to other parts of the body. They lack distinct borders due to their tendency to send “roots” into nearby normal tissue. They can also shed cells that travel to distant parts of the brain and spine by way of the cerebrospinal fluid. Some malignant tumours, however, do remain localized to a region of the brain or spinal cord.

METASTATIC BRAIN TUMOURS

Cancer cells that begin growing elsewhere in the body and then travel to the brain form metastatic brain tumours [9]. For example, cancers of the lung, breast, colon and skin (melanoma) frequently spread to the brain via the bloodstream or a magnetic-like attraction to other organs of the body. All metastatic brain tumours are, by definition, malignant.

TUMOUR GRADING

Tumours are diagnosed and then named based on a classification system. Most medical centres now use the World Health Organization (WHO) classification system for this purpose. Tumours are graded to facilitate communication, to plan treatment, and to predict outcome. The grade of a tumour indicates its degree of malignancy.

Grading is based on the tumour's microscopic appearance using some or all of the following criteria:

- similarity to normal cells (atypia)
- rate of growth (mitotic index)
- indications of uncontrolled growth
- dead tumour cells in the center of the tumour (necrosis)
- potential for invasion and/or spread (infiltration) based on whether or not it has a definitive margin (diffuse or focal)
- blood supply (vascularity)

Using the **WHO** grading system [9];

Grade I: are the least malignant tumours and are usually associated with long-term survival. The tumours grow slowly, and have an almost normal appearance when viewed through a microscope. Surgery alone might be an effective treatment for this grade of tumour. Pilocytic astrocytoma, craniopharyngioma, and many tumours of neurons - for example, gangliocytoma and ganglioglioma - are examples of grade I tumours.

Grade II: are relatively slow tumours growing and have a slightly abnormal microscopic appearance. Some can spread into nearby normal tissue and recur. Sometimes these tumours recur as a higher grade.

Grade III: are by definition, malignant tumours although there is not always a sharp distinction between a grade II and a grade III tumour. The cells of a grade III tumour are actively reproducing abnormal cells which grow into nearby normal brain tissue. These tumours tend to recur, often as a higher grade.

Grade IV: are the most malignant tumours. They reproduce rapidly, can have a bizarre appearance when viewed under the microscope, and easily grow into surrounding normal brain tissue. These tumours form new blood vessels so they can maintain their rapid growth. They also have areas of dead cells in their centre. The glioblastoma multiforme is the most common example of a grade IV tumour.

Tumours often contain several grades of cells. The highest or most malignant grade of cell determines the grade, even if most of the tumour is a lower grade. Some tumours undergo change. A benign growth might become malignant. In some tumours, a lower-grade tumour might recur as a higher-grade tumour [9].

2.3.2 TYPES AND SIZES OF BRAIN TUMOURS

BRAIN TUMOUR TYPE

A comprehensive review of the most common brain and spinal cord tumours, their typical symptoms and locations, and how they might be treated is presented in the tables shown below. The tumour names that have been used in this project are based on the WHO brain tumour classification system described above [9].

The following outline has been adapted from the WHO classification. Tumours of glial origin are grouped under a common heading, and tumours limited to the peripheral nervous system have been excluded.

- Neuroepithelial tumours (table 2.2)
- Meningeal tumours (table 2.3)
- Germ cell tumours (table 2.4)
- Tumours of the sellar region (table 2.5)
- Tumours of uncertain histogenesis (table 2.6)
- Primary CNS lymphoma (table 2.7)
- Tumours of peripheral nerves that affect the CNS (table 2.8)
- Metastatic tumours (table 2.9)

Table 2.2 Neuroepithelial tumours [9]

Neuroepithelial tumours:					
Type of Tumour	Description / Location	Grade	Treatment (Surgery/Radiation/Chemical/etc.)	Benign / Malignant	Comments
1. Glial tumours:					
Astrocytic tumours					
Pilocytic astrocytoma	Occurring throughout the neuraxis. the optic nerve, optic chiasm/hypothalamus, thalamus and basal ganglia, cerebral hemispheres, cerebellum, and brain stem	Grade I	Surgery, Surgery - Radiation	Benign	Typically affects children, cystic tumour, is often curable
Diffuse astrocytoma (including fibrillary, protoplasmic, and gemistocytic).	Are composed of well-differentiated fibrillary or gemistocytic neoplastic astrocytes May be located in any region of the CNS but most commonly develop in the cerebrum	Grade II	Surgery – Radiation, Surgery (age < 35)	Has a tendency for Malignant	Typically affects young adults
Anaplastic astrocytoma	Possess an intrinsic tendency to progress to glioblastoma. Affects the cerebral hemispheres	Grade III	Surgery – Radiation, Surgery – Radiation – Chemotherapy	Malignant	
Glioblastoma	Primarily affects the cerebral hemispheres	Grade IV	Surgery–Radiation, Radiotherapy plus continuous daily temozolomide.	Malignant	Is the most frequent brain tumour
Pleomorphic xanthoastrocytoma	Arise from a type of cell of the central nervous system known as a glial cell.	Grade II	Surgery, Radiation, Surgery- Radiation	Benign	Rarely do these tumours arise from the spinal column

Type of Tumour	Description / Location	Grade	Treatment (Surgery/Radiation/Chemical/etc.)	Benign / Malignant	Comments
Subependymal giant cell astrocytoma	Occurs almost exclusively in patients with tuberous sclerosis complex (TSC)	Grade I	Surgery	Benign	
Oligodendroglial tumours: Begin in the brain cells called oligodendrocytes, which support and nourish nerve cells					
Oligodendroglioma	Composed predominantly of cells morphologically resembling oligodendroglia, which grows diffusely in the cortex and white matter.[Grade II	Radiation, Chemotherapy	slow-growing	Most oligodendrogliomas occur in adults
Anaplastic oligodendroglioma	An oligodendroglial tumour with focal or diffuse histologic features of malignancy	Grade III	Surgery, Radiation, Chemotherapy	grow quickly	
Mixed gliomas: Brain tumours that contain more than one type of cell					
Oligoastrocytoma	Is composed of two distinct neoplastic cell types that morphologically resemble tumour cells in oligodendroglioma and diffuse astrocytoma	Grade II	Surgery – Radiation, Chemotherapy	slow-growing	
Anaplastic oligoastrocytoma	Anaplastic oligoastrocytomas are predominantly hemispheric tumours, and the frontal lobes are more commonly involved than the temporal lobes	Grade III	Surgery-Radiation, Surgery-Radiation-Chemotherapy		Mixed Gliomas
Ependymal tumours: Ependymal cells line the vertical of the brain and the center of the spinal cord.					
Myxopapillary ependymoma	Occur in the lower part of the spinal column.	Grade I	Surgery, Radiation		

Type of Tumour	Description / Location	Grade	Treatment (Surgery/Radiation/Chemical/etc.)	Benign / Malignant	Comments
Subependymoma	These tumours are usually located in the fourth and lateral ventricle, and sometimes in the spinal cord	Grade I	Microsurgical	Benign	
Ependymoma (including cellular, papillary, clear cell, and tanycytic)	These tumours occur at any site in the ventricular system and in the spinal canal.	Grade II	Surgery, Radiation-Surgery		
Anaplastic ependymoma	Commonly develop in the posterior fossa (the portion of the skull containing the cerebellum and brain stem).	Grade III, IV	Surgery-Radiation	Malignant	
Neuroepithelial tumours of uncertain origin					
Astroblastoma	The cerebral hemispheres are most affected; tumours may also develop in the corpus callosum, cerebellum, optic nerves, brain stem, and cauda equine	no WHO grade	Surgery, Radiation, Chemotherapy		This is a rare tumour for which no reliable epidemiological data exist.
Chordoid glioma of the third ventricle	low-grade tumour located in the third ventricle-hypothalamic region.	Grade II	Surgery		
Gliomatosis cerebri	Is characterized by a diffuse, or broad, spread of glial tumour cells in the brain.	Grade III	Radiation, Chemotherapy	Malignant	Widespread low-grade glioma

2. Neuronal and mixed neuronal-glia tumours (some glial component may be present)					
Type of Tumour	Description / Location	Grade	Treatment (Surgery/Radiation/Chemical/etc.)	Benign / Malignant	Comments
Gangliocytoma (ganglioneuromas)	Arise from ganglia-type cells, which are groups of nerve cells.	Grade I	Surgery	Benign	Locate in the temporal lobe of the cerebral hemispheres and the third ventricle, and also in the spine.
Ganglioglioma	Occur most commonly in the cerebrum (the largest and upper most section of the brain), but may occur in any part of the brain and spinal cord.	Grade I, II	Surgery, Radiation		May rarely undergo transformation into a higher grade, more malignant tumour.
Desmoplastic infantile astrocytoma/ganglioglioma	Located in the deep white matter, under the solid part of the tumour attached to the dura mater of the left frontal lobe	Grade I	Surgery		
Dysembryoplastic neuroepithelial tumour	a group of tumours that occur in the tissues that cover the brain and spinal cord.	Grade I	Surgery	Benign	
Central neurocytoma	Occur in the lateral ventricles with the foramina of Monro as the most common sites, and in the third ventricles.	Grade II	Surgery, Surgery-Radiation	Benign	
Cerebellar liponeurocytoma		Grade I, II	Surgery, Radiation	Benign	
Paraganglioma (Glomus fugulare)	Located in the lining of a large vein in the neck called the jugular vein.	Grade I	Surgery (neurosurgeon) – “Head and Neck” surgeon.	Benign	Can spread to the bone close to the inner and middle ear.

3. Nonglial tumours					
Type of Tumour	Description / Location	Grade	Treatment (Surgery/Radiation/Chemical/etc.)	Benign / Malignant	Comments
Embryonal tumours					
Ependymoblastoma	Brain tumour that consists of small round cells and is believed to originate from primitive nerve cells in the brain.	Grade IV	Chemotherapy, Radiation, Surgery	Malignant	
Medulloblastoma	Originate in the cerebellum are referred to as infratentorial because they occur below the tentorium,	Grade IV	Surgery, Radiation, Chemotherapy, Cerebrospinal fluid diversion	Malignant	Has a tendency to metastasize via CSF pathways
Supratentorial primitive neuroectodermal tumour (PNET)	Is an embryonal tumour in the cerebrum or suprasellar region that is composed of undifferentiated or poorly differentiated neuroepithelial cells.	Grade IV	Surgery-Craniospinal Radiation	Malignant	Considerable controversy exists regarding the histogenesis of these tumours.
Choroid plexus tumours					
Choroid plexus papilloma	Commonly invade or grow into nearby tissue and spread widely via the cerebrospinal fluid.	Grade I	Surgery, Chemotherapy, Radiation	Malignant	
Choroid plexus carcinoma	The choroids plexus papilloma grows slowly within the ventricles. It eventually blocks the flow of cerebrospinal fluid, causing hydrocephalus and increased intracranial pressure.	Grade III	Surgery, Shunt	Benign	

Type of Tumour	Description / Location	Grade	Treatment (Surgery/Radiation/Chemical/etc.)	Benign / Malignant	Comments
Pineal parenchymal tumours: Located at the rear of the third ventricle.					
Pineoblastoma	Rapidly growing and have worse prognoses.	Grade IV	Surgery-Radiation, Chemotherapy	Malignant	
Pineocytoma	Slow growing and carry variable prognoses for cure.	Grade II	Surgery-Radiation		

Table 2.3 Meningeal tumours [9]

Meningeal tumours					
Type of Tumour	Description	Grade	Treatment (Surgery/Radiation/Chemical/etc.)	Benign / Malignant	Comments
Meningioma	Attached to the dura mater and composed of neoplastic meningotheial (arachnoidal) cells.	Grade I-III	Conservative management, Surgery, Radiation (external beam RT, radiosurgery SRS, radiotherapy SRT).	I-II: Benign III: Malignant	The second most frequent primary brain tumours after gliomas.
Hemangiopericytoma	occurring in soft tissue and with a tendency to recur and to metastasize outside the CNS.	Grade II, III	Surgery, Radiation	Benign	
Melanocytic lesion	Located directly over fibrohistiocytic proliferations.		Surgery	Benign	

Table 2.4 Germ cell tumours [9]

Germ cell tumours: Arise in the pineal or suprasellar regions of the brain					
Type of Tumour	Description	Grade	Treatment (Surgery/Radiation/Chemical/etc.)	Benign / Malignant	Comments
Germinoma	Occurs in the pineal or suprasellar region of the brain and tends to spread via the cerebrospinal fluid.	No Grade	Surgery, Radiation, Chemotherapy		
Embryonal carcinoma	It grows with its cells dividing rapidly and indefinitely.			Malignant	The embryonal carcinoma is a reproductive cell gone out of control.
Yolk-sac tumour (endodermal-sinus tumour)	Often occurs as small "malignant foci" within a larger tumour, usually teratoma.		Surgery-Chemotherapy	Malignant	
Choriocarcinoma			Surgery, Chemotherapy	Malignant	
Teratoma	Teratomas derived from embryonal cells usually occur on the body midline: in the brain, elsewhere inside the skull, in the nose, in the tongue, under the tongue, and in the neck.		Surgery, Chemotherapy	Benign	

Table 2.5 Tumours of the sellar region [9]

Tumours of the sellar region					
Type of Tumour	Description	Grade	Treatment (Surgery/Radiation/Chemical/etc.)	Benign / Malignant	Comments
Pituitary adenoma,	<p>Found in the pituitary gland, a small organ about the size of a pea in the center of the brain just above the back of the nose.</p> <p>The radiographical classification:</p> <ul style="list-style-type: none"> • 0: Normal pituitary appearance. • I: Enclosed within the sella turcica, microadenoma, smaller than 10 mm. • II: Enclosed within the sella turcica, macroadenoma, 10 mm or larger . • III: Invasive, locally, into the sella. • IV: Invasive, diffusely, into the sella. 		Surgery, Radiation, Medication	Benign	Grow very slowly and do not spread from the pituitary gland to other parts of the body.
Pituitary carcinoma				Malignant	Spread in the central nervous system (brain and spinal cord) or outside of the central nervous system.
Craniopharyngioma	Occur in the sellar region, near the pituitary gland. They often involve the third ventricle, optic nerve, and pituitary gland.	Grade I	Surgery, Shunt, Radiation (Radio-Surgery, Conformal Radiation, radioactive Phosphorous)	Benign	These localized tumours grow by expansion and may reach a large size before they are diagnosed.

Table 2.6 Tumours of uncertain histogenesis [9]

Tumours of uncertain histogenesis					
Type of Tumour	Description / Location	Grade	Treatment (Surgery/Radiation/Chemical/etc.)	Benign / Malignant	Comments
Capillary hemangioblastoma	May occur in any part of the CNS, sporadic tumours occur primarily in the cerebellum.	Grade I	Microsurgical techniques	Benign	

Table 2.7 Primary CNS lymphoma [9]

Primary CNS lymphoma					
Type of Tumour	Description / Location	Grade	Treatment (Surgery/Radiation/Chemical/etc.)	Benign / Malignant	Comments
	Is defined as lymphoma limited to the cranial-spinal axis without systemic disease. It is usually confined to the CNS and/or the eye.		Preradiotherapy (RT), Methotrexate (MTX), barrier-dependent chemotherapy.	Malignant	

Table 2.8 Tumours of peripheral nerves that affect the CNS [9]

Tumours of peripheral nerves that affect the CNS					
Type of Tumour	Description / Location	Grade	Treatment (Surgery/Radiation/Chemical/etc.)	Benign / Malignant	Comments
Schwannoma	Is a benign (noncancerous) tumour on the 8th cranial nerve. This nerve leads from the brainstem to the ear and is involved in hearing and maintaining balance.	Grade I	Observation, microsurgical removal, Radiation	Benign	Peripheral nerves that accounts for an estimated 8% of brain tumours and 29% of primary spinal tumours

Table 2.9 Metastatic tumours [9]

Metastatic tumours					
Type of Tumour	Description / Location	Grade	Treatment (Surgery/Radiation/Chemical/etc.)	Benign / Malignant	Comments
	<p>SPINAL FLUID METASTASES METASTATIC SPINAL TUMOURS The types of cancer that commonly spread to the brain are melanoma and cancers of the lung, breast, unknown primary site, and colon.</p>		<p>Surgery, Radiation, Ambulation after treatment.</p>		<p>The most common primary cancers metastasizing to the brain are lung cancer (50%), breast cancer (15%–20%), cancer of unknown primary site (10%–15%), melanoma (10%), and colon cancer (5%)</p>

BRAIN TUMOUR SIZE

The following literature summarizes brain tumour size (table 2.10). Either the diameter or volume is given. The literature covers most of the popular tumour types in the brain including metastasis. The information regarding tumour size is very critical for determining the range of motion of the 3D robotic system used in this project. It is concluded that by selecting a range of motion of 10 cm is more than enough to cover all tumour types in the brain. Basically a 5 cm range will cover most of the tumour types except high grade gliomas, Boisserie G. et al [12]. The mean average brain lesion type according to, Gralla J. et al [14] and Paleologos T. et al [16] was found to be between 3.3-3.6 cm. The average depth from skin based on Paleologos T. et al [16] is around 3.6 cm.

Table 2.10 brain tumour: diameter or volume

Type of tumour	Diameter (cm)	Volume (cm ³)	Reference	No. of Subjects
Intracerebral cavernous hemangiomas.	0.7-4.5		Woydt M et al [10]	35
Glioma		12.7	Julow J et al [11]	19
High grade gliomas	2.1-10.1 (median: 6.4 cm)	2-122 cm ³ (median: 22 cm ³).	Boisserie G et al [12]	20
Pituitary adenomas	1.92 (mean)	5.4 (mean)	Kobayashi T et al [13]	67
Brain lesions	3.3 (mean)		Gralla J et al [14]	57
Brain metastasis	2.1	0.06-4.58 Median 0.67	Chang EL et al [15]	135
Brain lesions	3.6 (mean) Distance from skin 3.6 (mean)		Paleologos TS et al [16]	125
Brain metastasis	MRI: 1.28+/- 0.91 CT 2.03+/-0.7		Yokoi K et al [17]	332
Ependymomas Subependymomas	4 (mean) 2.6 (mean)		Furie DM et al [18]	14
Glioblastoma multiforme Anaplastic astrocytoma	Equivalent diameter= 3.5	22.5	Buatti JM et al [19]	11
Malignant skull base tumours	3.35 (mean)		Tanaka T et al [20]	19
Malignant intracranial tumours.		17.1	Hou Y et al [21]	281
Recurrent glioblastomas	1.2-10.1 median: 5.7	1.6-122 median: 23	Simon JM et al [22]	42
Astrocytomas Grade I Astrocytomas Grade II	2.54 (mean) 2.37 (mean)		Kida Y et al [23]	51
Gliomas	3-7		Landy HJ et al [24]	18
Meningocerebral astrocytomas	6-12		Taratuto AL et al [25]	6

2.3.3 CURRENT STATE OF THE ART IN TREATING BRAIN TUMOURS

Treatment depends on a number of factors, including the type, location, size, and grade of the tumour. For some types of brain cancer, the clinician also needs to know whether cancer cells were found in the cerebrospinal fluid. Depending on the tumour type and stage, there are several treatment options such as [26]:

- Surgery Neurosurgery,
- radiation therapy,
- chemotherapy,
- hyperthermia

These types of treatment have been mentioned above in the various tables. This section gives a brief description of each treatment type.

SURGERY

Surgery is the usual treatment for most brain tumours. Surgery to open the skull is called a craniotomy. It is performed under general anesthesia. Before surgery begins, the scalp is shaved. The surgeon then makes an incision in the scalp and uses a special type of saw to remove a piece of bone from the skull. After removing part or all of the tumour, the surgeon covers the opening in the skull with that piece of bone or with a piece of metal or fabric. The surgeon then closes the incision in the scalp. Sometimes surgery is not possible. If the tumour is in the brain stem or other areas, the surgeon may not be able to remove the tumour without damaging normal brain tissue. Patients who cannot have surgery may receive radiation or other treatment [26].

NEUROSURGERY

When treating brain tumours, tumour resection (tumour removal by operation) is still a common treatment. Until recently, open neurosurgery meant a fairly high risk for patients in terms of damaging important structures of the brain. Today, computer-based image-guided surgery assists the surgeon during all phases of the operation. This allows the surgeon to keep the operation minimally invasive and to avoid critical structures of the brain, reducing risks and hospital time while at the same time improving the success rate [26].

RADIATION THERAPY

Radiation therapy (also called radiotherapy) uses high-energy rays to kill tumour cells. The radiation may come from *x-rays*, *gamma rays*, or *protons*. A large machine aims radiation at the tumour and the tissue close to it. Sometimes the radiation may be directed to the entire brain or to the spinal cord. Radiation therapy usually follows surgery. The radiation kills tumour cells that may remain in the area. Sometimes, patients who cannot have surgery, have radiation therapy instead. The treatment schedule depends on the type and size of the tumour and the age of the patient. Each treatment lasts only a few minutes [26].

Necessary steps to protect the healthy tissue around the brain tumour:

- ***Fractionation***—Radiation therapy usually is given five days a week for several weeks. Giving the total dose of radiation over an extended period helps to protect healthy tissue in the area of the tumour.
- ***Hyperfractionation***—The patient gets smaller doses of radiation two or three times a day instead of a larger amount once a day.
- ***Stereotactic radiation therapy***—Narrow beams of radiation are directed at the tumour from different angles. For this procedure, the patient wears a rigid head frame. An MRI or CT scan creates pictures of the tumour's exact location. The doctor uses a computer to decide on the dose of radiation needed, as well as the sizes and angles of the radiation beams. The therapy may be given during a single visit or over several visits.
- ***3-dimensional conformal radiation therapy***—A computer creates a 3-dimensional image of the tumour and nearby brain tissue. Multiple radiation beams aim to the exact shape of the tumour. The precise focus of the radiation beams protects normal brain tissue.
- ***Proton beam radiation therapy***—The source of radiation is protons rather than x-rays. The proton beams are aimed at the tumour. Protons can pass through healthy tissue without damaging it.

CHEMOTHERAPY

Chemotherapy is a well-known treatment and it uses chemotherapeutic substances to either inhibit the division of tumour cells or kill tumorous cells. They are given to the patient intravenously or taken orally over an extended period of time. Many

chemotherapeutic drugs are less suitable for the treatment of brain tumours as they often cannot pass the blood-brain barrier [26].

HYPERTHERMIA

Hyperthermia therapy is a type of treatment in which body tissue is exposed to high temperatures (up to 106°F), to damage and kill cancer cells, or to make cancer cells more sensitive to the effects of radiation and certain anticancer drugs. Local hyperthermia treatment is when heat is applied to a very small area (such as a tumour). This is a well-established cancer treatment method that when temperature rise to 106°F and last for one hour within a cancer tumour then the cancer cells will be destroyed.

Hyperthermia therapy is usually used with other forms of therapy (radiation therapy, chemotherapy, and biological therapy) to increase their effectiveness. With hyperthermia therapy the area may be heated externally with high-frequency waves aimed at a tumour from a device outside the body. To achieve internal heating, one of several types of sterile probes may be used, including thin, heated wires or hollow tubes filled with warm water; implanted microwave antennae; and radiofrequency electrodes.

High intensity focus ultrasound can be used to produce heat within the tumour. Ultrasound is more easily focused than other energy modalities, and can be applied to tumours located from the skin to 10 cm within your body. This allows the treatment of tumours unreachable by other external modalities [26].

2.4 THROMBOLYSIS FOR ACUTE ISCHAEMIC STROKE; CHARACTERIZATION AND TREATMENT

2.4.1 Acute Ischaemic Stroke

Acute Ischaemic Stroke is considered to be the third most common cause of death in the United States, Europe, and in many other countries from the rest of the world. A large number of new cases are reported every year, and approximately 20% out of these new cases died [8]. Table 2.11 shows statistically the percentage of stroke incidence worldwide and the rate of survival [9].

Table 2.11 Stroke statistics

Consequences of Stroke
<ul style="list-style-type: none"> Worldwide, stroke is the second leading cause of death, responsible for 4.4 million (9 percent) of the total 50.5 million deaths each year.
<ul style="list-style-type: none"> Stroke is the No. 3 cause of death in the U.S., behind heart disease (with which it is closely linked) and cancer.
<ul style="list-style-type: none"> Stroke affects more than 700,000 individuals annually in the United States (approximately one person every 45 seconds). About 500,000 of these are first attacks, and 200,000 are recurrent attacks.
<ul style="list-style-type: none"> Someone in the U.S. dies every 3.3 minutes from stroke
<ul style="list-style-type: none"> Stroke is the leading cause of disability among adults in the U.S.
<ul style="list-style-type: none"> More than 4 million people in the United States have survived a stroke or brain attack and are living with the after-effects.
<ul style="list-style-type: none"> Four out of five families will be somehow affected by stroke over the course of a lifetime.
Survival rates
<ul style="list-style-type: none"> 10 percent of stroke victims recover almost completely.
<ul style="list-style-type: none"> 25 percent of stroke victims recover with minor impairments.
<ul style="list-style-type: none"> 40 percent of stroke victims experience moderate to severe impairments requiring special care.
<ul style="list-style-type: none"> 10 percent of stroke victims require care in a nursing home or other long-term care facility.
<ul style="list-style-type: none"> 15 percent die shortly after the stroke.
<ul style="list-style-type: none"> 7.6 percent of ischaemic strokes and 37.5 percent of hemorrhagic strokes result in death within 30 days.
<ul style="list-style-type: none"> While subarachnoid hemorrhage (SAH) represents only about 7 percent of all strokes, it is the most deadly
<ul style="list-style-type: none"> With more than a 50 percent fatality rate. Of the survivors, approximately half will suffer permanent disability.
<ul style="list-style-type: none"> 22 percent of men and 25 percent of women die within a year of their first stroke.
<ul style="list-style-type: none"> 14 percent of people who have a stroke or TIA will have another within a year.
<ul style="list-style-type: none"> About 25 percent of stroke victims will have another within five years.

Stroke is the leading cause of serious, long-term disability in the United States. Each year, about 795,000 people suffer a stroke. About 600,000 of these are first attacks, and 185,000 are recurrent attacks. Among adults age 20 and older, the prevalence of stroke in 2005 was 6,500,000 (about 2,600,000 males and 3,900,000 females). On average, every 40 seconds someone in the United States has a stroke [27]. Each year, about 55,000 more women than men have a stroke. Men's stroke

incidence rates are greater than women's at younger ages but not at older ages. The male/female incidence ratio is 1.25 at ages 55–64; 1.50 for ages 65–74; 1.07 at 75–84 and 0.76 at 85 and older [27]. Stroke accounted for about one of every 17 deaths in the United States in 2005. Stroke mortality for 2005 was 143,579 (56,586 males, 86,993 females). From 1995–2005, the stroke death rate fell 29.7 percent and the actual number of stroke deaths declined 13.5 percent. For the rest of the world, according to the World Health Organization, 15 million people suffer stroke worldwide each year. Of these, 5 million die and another 5 million are permanently disabled. Europe averages approximately 650,000 stroke deaths each year [27].

Stroke is caused when the blood flow to the brain is interrupted (an ischaemic stroke) causing brain cells in the affected area to die, or when there is rupture of blood vessels in the brain (a hemorrhagic stroke), which in turn causes moderate to severe damage to the brain. The majority of strokes are ischaemic due to the occlusion of arteries that deliver essential nutrients and oxygen to the brain. Seventy seven percent of strokes are ischaemic and twenty-three percent are hemorrhagic (17% intracerebral and 6% subarachnoid hemorrhage) [28][29].

So far, the only pharmacologic treatments proven effective following ischaemic stroke are administration of aspirin and acute thrombolysis using tissue-Plasminogen Activator (t-PA). Since the study of intravenous (i.v.) rt-PA in acute ischaemic stroke in 1995 by the National Institute of Neurological Disorders and Stroke [31], many clinical trials have tried to define the ideal patient population for this therapeutic strategy and to extend the therapeutic time window through a more detailed understanding of the pathophysiology of ischaemic stroke.

2.4.2 Thrombolysis

Many studies since the late 1950s have used pharmacologic thrombolysis in the treatment of patients following acute ischaemic stroke [30]. However, these studies showed that the potential benefits of re-establishing circulation to an ischaemic area must be weighed against an increased risk of hemorrhagic complications [32]. Orso et al [30] in 1995, in a Phase III trial, successfully identified a population of stroke patients who significantly benefited from

thrombolysis. At that time, interest in thrombolysis was at its peak following the earlier success of thrombolytic strategies in the treatment of acute myocardial infarction [33]. This had enthused similar investigations of thrombolysis in the setting of ischaemic stroke such as Streptokinase and rt-PA.

Streptokinase: The first of the tested thrombolytic compounds, streptokinase, is a direct plasminogen activator produced by β -hemolytic streptococcus. Streptokinase was investigated in three large multi-center trials of acute stroke: the Multicentre Acute Stroke Trial – Italy (MAST-I) [34], Multicenter Acute Stroke Trial – Europe (MAST-E) [35] and the Australian Streptokinase Trial [36]. The experimental designs of these trials varied significantly; nevertheless, all three attempted to select their patients to minimize hemorrhagic sequel and maximize the possibility of clinical benefit. As a result an increase rate of mortality caused by symptomatic intracranial haemorrhage made the two of the three trials (MAST-E and MAST-I) to prematurely terminated and further investigation of streptokinase in the treatment of ischaemic stroke ceased.

rt-PA: Clinical trials of rt-PA showed success, beginning with the National Institute of Neurological Disorders and Stroke (NINDS) rt-PA Stroke Study, a randomized, placebo-controlled trial in which patients were randomized to receive intravenous i.v. rt-PA (0.9 mg/kg) or placebo in < 3 h of symptom onset. This study clearly excluded patients with a certain level of hypertension, low levels of platelets, hypoglycaemia, or recent history of certain haemorrhages or invasive procedures. There was an increase in symptomatic intracranial haemorrhages (ICH) in the patients receiving rt-PA but this did not lead to a statistical difference in 90-day mortality. The Safe Implementation of Thrombolysis in Stroke-Monitoring Study (SITS-MOST) by Wahlgren et al [37] have shown that this course of therapy is safe and effective even in centres with little previous experience with thrombolytic stroke therapy.

Much of the more recent work has focused on broadening the patient population that can safely receive rt-PA thrombolysis. Despite these efforts, treatment of patients is still limited, particularly by advanced age (greater than 80 years). Thus, research has involved expanding the therapeutic time window in which patients

can receive the drug as well as the setting in which the patient can receive treatment. Thus, while it seems safe and effective to administer rt-PA in any setting in which pre-treatment radiological evaluation can be made, it seems that the maximal benefit for patients with acute ischaemic stroke derives from treatment in a specialized stroke unit.

Several clinical trials have examined the use of rt-PA beyond the 3-h treatment window. The European Cooperative Aneurysm Acute Stroke Study (ECASS) [38] examined administration of 1.1 mg/kg of rt-PA in 6 h of onset of stroke in a randomized, double-blind, placebo-controlled trial. The treated patients exhibited improved 90 day neurological recovery, no difference in mortality or ICH, but larger ICH. However, ECASS-II, a larger placebo-controlled trial that followed by Hacke et al [39], did not achieve the same positive results. In that study, i.v. rt-PA (0.9 mg/kg) was administered in the 6 h post-ictus period to patients with no or minor early signs of infarction on initial CT scan and < 33% swelling in the middle cerebral artery (MCA) territory. There was a significantly greater incidence of large ICH in the rt-PA group.

ATLANTIS, the Alteplase ThromboLysis for Acute Non-interventional Therapy in Stroke randomized, double-blinded study, examined patients who were treated with i.v. rt-PA (0.9 mg/kg) in a 3 – 5 h window [40]. This study revealed no significant difference in 90 day recovery between groups, but again showed significantly more ICH, symptomatic ICH and fatal ICH in the rt-PA cohort.

However, pooled analysis of the NINDS stroke study, ECASS, ECASS II, ATLANTIS and the Part A of ATLANTIS revealed that treatment of acute stroke even between 3 and 4.5 h imparts a significantly favourable 90-day outcome and improved mortality [41]. ECASS III then sought to clarify this point through a randomized, placebo-controlled trial by enrolling patients treated with i.v. rt-PA between 3 and 4.5 h after the onset of stroke symptoms [42]. This trial revealed improved outcome at 90 days, however, also a higher rate of ICH without a difference in mortality in the rt-PA cohort. Thus, in an appropriately selected patient population, the window of treatment of acute stroke with i.v. rt-PA may now be extended to 4.5 h post-ictus. This important finding has subsequently led to the change in treatment protocols in many parts of Europe and North America.

There remains the possibility that administering rt-PA up to 6 h after onset of stroke is beneficial. The Third International Stroke Trial (IST III), a large, open-label study, is currently enrolling patients receiving i.v. rt-PA up to 6 h after stroke beginning to determine if there is, in fact, a small benefit of treating patients with this extended window and to identify factors that may be associated with a better outcome in this group [43].

2.4.3 Sonothrombolysis

The feasibility of ultrasound to enhance thrombolysis was reported in the mid 70s by Trubestein et al [44] and Tachibana et al [45]. Clinical application of this new therapeutic ultrasound method for producing thrombolysis has already started since 2001. Clinical trials in Europe and in the USA have been reported using miniature ultrasound transducers at the tip of catheters that approach the clots via arterial vessels (MicroLysUS infusion catheter, EKOS Corp, USA). Mahon [46] presented early experience with the MicroLysUS infusion catheter for acute embolic stroke treatment in North America. This study was designed to demonstrate the safety of the device and to determine if ultrasound accelerates thrombolysis and improves clinical outcomes. The EKOS catheter for leg peripheral arterial thrombolysis was approved by the FDA in 2004 and was probably the first drug/ultrasound combination product to be marketed in the cardiovascular field.

Alexandrov et al. [48] reported findings from a large phase II clinical trial entitled “Combined Lysis of Thrombus in Brain Ischemia using Transcranial Ultrasound and Systemic tPA” (CLOTBUST). In this trial involving 126 patients, evidence was obtained for the existence of ultrasound-enhanced thrombolysis in the middle cerebral artery thrombus. The CLOTBUST aims were: (1) To compare recanalization and recovery in patients with standard IV tPA therapy and those receiving additional continuous targeted ultrasound monitoring. (2) Compare safety in the two groups. This large clinical trial concluded that continuous transcranial Doppler augmented t-PA-induced arterial recanalization, with a non significant trend toward an increased rate of recovery from stroke, as compared with placebo. More evaluation is needed to see if diagnostic level ultrasound intensity can truly penetrate the skull and accelerate thrombolysis.

Kimura et al [49] and Akiyama et al [50] have shown that therapeutic low-frequency ultrasound in experimental models, using lower frequencies (20 kHz to 1 MHz), tPA-mediated clot degradation was more efficient when ultrasound was added. Consequently, it has been postulated by Behrens et al [52] and Daffertshofer et al [51] [53][54] that the use of therapeutic low frequency ultrasound, in combination with rt-PA might be a efficient and safe for the treatment of acute stroke. This hypothesis was tested in the transcranial low-frequency ultrasound-mediated thrombolysis in brain ischemia (TRUMBI) trial, a single-centre randomized-controlled trial by Daffertshofer et al [55]. The investigators used low-frequency ultrasound (300 kHz in order to avoid standing waves) with a Spatial Peak Temporal Average (SPTA) intensity of 700 mW/cm². Ultrasound was applied simultaneously with intravenous administration of tPA.

Currently, a phase I–II randomized placebo-controlled, international multi-centre study (TUCSON trial) using perfultren-lipid microspheres (MRX 801, Imarx Therapeutics, Inc., Tuscon, AZ) is underway [56]. A total of 72 patients with acute intracranial arterial occlusion will be randomized to microspheres-potentiated ultrasound-enhanced thrombolysis (4 groups with increasing doses of perfultren-lipid microspheres) versus tPA alone.

Ishibashi et al. [47] have accepted the challenge of sonicating transcranially to accelerate thrombolysis. A noninvasive method was tested in an occlusion model of rabbit femoral artery, produced with thrombin after constriction of the artery led to stenotic flow and endothelial damage. After stable occlusion was confirmed, alteplase (t-PA) was administered intravenously, and ultrasound (490 kHz, 0.13W/cm²) was applied (TUS group). The recanalization ratio in the TUS group was higher than that in the t-PA group.

Shaw et. al [167] has shown that using 120 KHz unfocused ultrasound exposure in an *in vitro* environment that the lytic efficacy of the of rt-PA is increased. The ultrasound-enhanced thrombolysis (UET) group was greater than that of rt-PA

group at all rt-PA concentrations with the maximum results over the concentration values of 1-3 $\mu\text{g/mL}$.

Eggers et. al. [166] conducted experiments *in vitro* using 1.8-MHz PW US. Blood clots from 0.5-mL venous blood samples were insonated for 1 h. The experiments were performed with or without recombinant tissue-type plasminogen activator (rt-PA) at a concentration of 10 $\mu\text{g/mL}$. Thrombolysis was measured by means of clot weight loss after 1 h of insonation. A higher reduction in thrombus occurred when both US and rt-PA were combined together were thrombus reduction reach almost 79%. Eggers et. al. [57] has also demonstrated in an *in vivo* experiments using the same parameters as described above (frequency of 1.8 MHz, diagnostic US) and with rt-PA concentration of 0.9 mg/kg. Recanalization of almost 60% occurred when US and rt-PA were combined. When only rt-PA was used, recanalization was only at 22.2%.

To improve the efficacy of this thrombolytic therapy, Holland et. al. [173] have used the effect of rt-PA and 120 kHz or 1.0 MHz ultrasound in an *in vitro* porcine clot model. They have shown that for rt-PA alone, the mass loss increased slowly as a function of rt-PA concentration up to approximately 0.050 mg/ml. With ultrasound and rt-PA exposure, clot mass loss increased by as much as 104% over rt-PA alone. Ultrasound without the presence of rt-PA did not significantly enhance thrombolysis.

Daffertshofe et. al. [54] has shown that Ultrasound bio-effects can facilitate rt- PA mediated thrombolysis in peripheral arteries. They have used an embolic stroke model in the rat. In all rats, they have induced an ischaemic stroke by a selective occlusion of the middle cerebral artery with whole blood clots. Four different groups have been investigated. First group took no treatment, second group took full dose of rt-PA, third group took half dose of rt-PA and US, and the last group took full dose of rt-PA and US. Only the fourth group had significant reduction infarct volume and safe with regard to bleeding.

CHAPTER 3: OVERVIEW OF HIFU

3.1 INTRODUCTION

The use of therapeutic ultrasound in medicine has a very promising prospect. At present medical devices are being developed that use high intensity focus ultrasound to treat tumours and to stop bleeding [58],[59][60]]. The ability of therapeutic ultrasound to penetrate deep into the body and deliver a beam of thermal or mechanical energy to a specific part of the body with sub millimeter accuracy eliminates the need of invasive surgery. However, realizing the full potential of acoustic therapy requires precise targeting and monitoring. Fortunately, several imaging devices can be used for this purpose thus leading to the concept of image-guided acoustic therapy.

The field of medicine is undergoing a remarkable change towards minimally invasive and noninvasive therapy. Compared with open surgeries, these minimally invasive approaches offer the advantages of reducing surgery time, tissue damage associated with surgery, and transfusion requirements and their associated infection risks.

The result is a shorter recovery time and hospital stay, a reduction in cost of health care, and a generally superior therapeutic outcome. However, not all brain tumours can be treated with this technology. Brain tumours located close to sensitive nerves, or they have unbalanced shape are very difficult or impossible to treat. Many researchers and industries such as Jolesz et al [5], Kinoshita et al [61] and Hynynen et al [62] are engaged in the research and development of noninvasive, image-guided therapy systems.

Such systems will increase the trend toward noninvasive surgery by enabling therapy to be delivered from outside of the body. It is envisioned that devices that can stop the internal bleeding of a trauma victim using a HIFU beam will be used without surgery. HIFU can generate a lot of heat quickly causing biological tissues where the ultrasound is focused to shrink and fuse together, stopping bleeding. Noninvasive, bloodless surgery is close to realization. Versions of this

technology are already in clinical application for the treatment of both malignant and benign tumours and a variety of other efforts are in various stages of scientific and clinical development [63]. Table 3.1 list several HIFU clinical systems that are used today for different clinical applications.

Table 3.1 HIFU Systems for Clinical Use

HIFU System	Frequency (MHz)	Focal Length (mm) / Focusing Method	Clinical Applications	No. of Patients Treated
Sonablate 500 (Focus Surgery Inc. USA)	4	34, 40 2 elements, back to back	Prostate Cancer	241
Ablatherm (Edap-Technomed, France)	3	45 Single Concave Element	Prostate Cancer	1414
ExAblate 2000 (InSightec Ltd, Israel)	0.9, 1.3	150 Phased Array	Breast Tunour, Liver Cancer, Bone Metastic, Prostate Cancer	290
Model-JC (Chongqing Inc. China)	0.8, 1.6, 3.2	90, 130, 160 Flat Ceramic	Liver, Kidney, Breast, Pancreatic, and Uterine Fibroid	192
FEP-BY02 (Beijing Yuande Inc. China)	1	255 Phased Array	Liver, Kidney, Breast, Pancreatic, and Uterine Fibroid	251

3.2 HISTORY OF HIFU

The era of modern ultrasonic began in the early 20th century. Table 3.2 shows the development of high intensity focused ultrasound technology throughout the century.

The first time that high intensity focus ultrasound (HIFU) was used to cause tissue destruction was reported by Lynn in 1942 [76]. However, the Fry brother's [2] in 1950 found that the lesion induced with HIFU was well bounded without any damage to the overlying and surrounding tissues. In addition, William Fry and his team [3][77], have used HIFU to successfully produced lesions in the brain of animals such as cats and monkeys. Consequently, Fry [2] developed techniques to treat patients with Parkinson's disease and other neurological conditions after removing a piece of skull for creating an "acoustic window".

Table 3.2 The development of HIFU technology throughout the century

Date	Event
1880	Piezoelectric effect, Jacques and Pierre [64]
1907	Electronic vacuum tube, Lee De Forest [65]
1918	Sonar (Langevin), Paul Langevin [66]
1927	Effects on biological tissues, Ronald et al [67]
1942	HIFU effects, Lynn et al [1]
1950 – 1969	Molecular studies on HIFU effects, Fry and Fry et al [2][3][68]
1951 – 1960	Radiofrequency generator and electrode development, Cosman [69]
1951 – 1967	Radiosurgery and gamma knife development, Leksell [70]
1960 – 1980	Clinical studies on HIFU surgery with open cranium, Fry et al [71][72], Heimburger [73]
1980 – present	MRI technology
Early 1990s	Ultrasound phased arrays, Hynynen et al [62]
Mid – 1990s	MRI thermometry, Jolesz et al [74]
2001	First integrated MRgFUS machine, Insightec [75]
2006	Report on MRgFUS for treatment of glioblastoma multiforme (GBM) after craniotomy, Ram et al [58]
Present	Trial on MRgFUS with cranium intact, Jolesz et al [4][5]

Fred Lizzi's group [79][80], in the 1970s, spent significant time and effort into the use of HIFU in the field of ophthalmology. They investigated the possibility of using HIFU to treat glaucoma, choroidal melanomas and capsular tears, and clinical results looked very exciting [78]. The introduction of medical lasers used in ophthalmology, which occurred at the same time and because of its ease of use, outdated HIFU in most ophthalmological applications.

The developments of medical imaging modalities, such as computed tomography (CT), B-mode ultrasonography, and magnetic resonance imaging (MRI), have led to recent advances in HIFU technology in the past two decades, see table 3.1. Based on their experience with extracorporeal shock-wave lithotripsy, which was used for destroying calculi of the kidney, uterine and bladder by physical forces in clinical practice, Guy Vallancien and his colleagues constructed an extracorporeal focused ultrasound device with Dr Dory's help in the 1990s. His team used this pyrotherapy device to treat superficial bladder tumours under ultrasound imaging guidance. The disappearance of the tumour in two cases and coagulation necrosis in the remaining patients were noted by Vallancien et. al. 1993 [81], and 1996 [82].

Gail Ter Haar and her colleagues [83] developed a HIFU prototype in the 1990s. This device employed a spherical ceramic transducer of 10 cm diameter and 15 cm focal length. It was driven at a frequency of 1.7 MHz and operated at free field spatial intensities between $1000\text{W}\cdot\text{cm}^{-2}$ and $4660\text{W}\cdot\text{cm}^{-2}$ [83]. In phase I trials, the results that Visioli [84] demonstrated using HIFU treatment of liver cancer were well tolerated.

An initiation of HIFU research began in 1988 at the Chinese Institute of Ultrasonic Engineering in Medicine and the Clinical Centre for Tumour Therapy of Chongqing Medical University in Chongqing,. Laboratory and animal studies were carried out from 1988 to 1997. After finishing studies in animals, they designed and constructed an extracorporeal HIFU prototype for clinical trials. Until October 2001, a total of 1038 patients with solid tumours received extracorporeal HIFU (Model-JC HIFU system, Chongqing HAIFU, China) in 10 Chinese hospitals [85]. From November 2001 to March 2004, approximately 2500 patients underwent HIFU treatment in 20 Chinese hospitals. The same device (Model-JC HIFU system, Chongqing HAIFU, China) has been introduced into the UK by Kennedy and Roberts, and Kennedy and Phillips, 2004 [87][88] and in Japan by Okuno [89].

Ultrasound imaging was used in all the HIFU devices mentioned above to guide and monitor therapeutic procedure. However, Kullervo Hynynen's group [90] at the Brigham and Women's Hospital in Boston, USA incorporated HIFU into an MRI system, and constructed an MRI-guided HIFU device in 1993. With MRI thermometry techniques, the device can record focal temperature rises on the anatomical images during treatment procedure. This MRI-guided HIFU has been used clinically to ablate breast neoplasm and uterine fibroids, and the results shown by Hynynen et al [91] and Tempany et al [92], indicate successful ablation of targeted tumours.

Besides extracorporeal HIFU treatment, the technique was also used to treat patients with prostate cancer using a transrectal HIFU device. Two commercially available devices are reported to treat prostate cancer in clinical practice. One transrectal device (Sonablate, Focused Surgery, USA) uses a 4 MHz PZT

transducer for both imaging and treatment [93], and another (Ablatherm, EDAP, France) uses a 2.25-3.0 MHz rectangular transducer for treatment and a retractable 7.5 MHz probe for imaging guidance [94]. These devices have been widely used in the treatment of patients with prostate cancer, and clinical results are enthralling [95].

3.3 PHYSICAL PRINCIPLES OF HIFU

Human tissue at a specific depth can be reformed with the use of a High Intensity Focus Ultrasound beam. Various mechanisms which can be produced by HIFU have an effect on tissue, such as *heating*, *cavitation* and *mechanical* forces.

Heat is created by absorption of the ultrasonic energy going through the human tissue. The ultrasonic energy is continuously absorbed and produces a temperature elevation within the medium. The temperature elevation is dependent on the intensity of the ultrasonic energy and the acoustic absorption coefficient of the tissue. Using HIFU, the intensity at the focus is much higher than outside the focus. If the temperature elevation is large enough and is maintained for a period of time (seconds), the exposure will result in tissue damage [96]. When ultrasonic energy passes through a viscous medium, such as human soft tissue, the intensity of the beam is attenuated. This attenuation depends on both the energy that is absorbed by the medium and the energy that is scattered from interfaces or inhomogeneities within the tissue. Because most of the attenuation is related to tissue absorption, it can be assumed that almost all of the energy from the primary ultrasound beam results in tissue heating [97].

At high intensity levels, the biological effects are sometimes associated with the formation of small gas bubbles or the oscillation of those small bubbles already present. This type of interaction is called *cavitation*, and it can cause complete destruction of the tissue located next to the gas bubble. Cavitation occurs when the negative component of the acoustic wave causes liquid components to fail under tension, resulting in the formation of gas or bubbles. These bubbles will oscillate at large displacement amplitudes if the acoustic field is continued. The mechanically driven bubbles cause damage to their surroundings, particularly if they oscillate near tissue interfaces. Cell death may occur owing to acoustic

cavitation if the oscillating bubble disrupts the cell membrane. Cavitation damage tends to be more random than thermally mediated cell death because cavitation requires the existence of a nucleation site.

When a bubble is sonicated at its resonance frequency it may intercept and radiate energy, thereby absorbing much more acoustic power than would pass through normal tissue of its geometrical cross-section. This type of bubble oscillation is called stable cavitation and can cause microstreaming of the fluids around the bubble. When stable cavitation occurs, it can significantly increase the power attenuation and thus cause unexpected temperature elevations in tissue layers through which the tumour is sonicated. Cavitation in tissues depends largely on ultrasound intensity and the frequency used by the device. The higher the frequency, the higher the intensity required to initiate cavitation. For example, cavitation thresholds have been measured to be 1000 W/cm^2 for 1-MHz frequencies and 2800 W/cm^2 for 3-MHz frequencies in dog thigh muscle, shown by Hynynen K [98]. Thus, by operating at a higher frequency cavitation may be avoided.

Stable oscillations of bubbles induce fluid velocities and exert shear forces on the surrounding tissues. Collapse cavitation bubbles generate shock waves with amplitudes exceeding 10,000 atmospheres depending on the bubble size. Although cavitation induce shock waves persist for a very short period of time, the large spatio-temporal pressure gradients associated with shock waves can disrupt tissues. During the collapse, the temperature of the bubble core can increase by more than 1,000 K and induce chemical changes in the medium. Acoustic cavitation has the main role in sonophoresis, particularly under low-frequency conditions. Experimental and theoretical studies have led to a mechanistic picture, which suggests that the shock waves generated after the collapse of cavitation bubbles microscopically disrupts the topmost layer of the skin, the stratum corneum, and thereby enhances skin permeability. The skin eventually recovers, possibly through natural barrier-recovery mechanisms [99].

Miller and Song [100] have shown that Pulsed-HIFU exposures, using low duty cycles (i.e. the relative time 'ON' during each pulse, or duty factor can be 10%),

generate energy deposition rates low enough that temperature elevations are well below the threshold for thermal damage in the tissues. The effects of pulsed-HIFU are more *mechanical* in nature, such as the creation of acoustic radiation forces. These forces, shown by Nightingale et al [101] and Lizzi et al [102], if high enough, can produce local displacements on the order of cellular dimensions. It has been suggested that repetitive displacements are capable of inducing structural alterations in the tissue, through the creation of locally induced strain. The strain results from shear forces produced between adjacent regions of tissue experiencing non-uniform displacement, and the alterations (i.e. widening of intercellular spaces between both endothelial and parenchymal cells) may increase the tissue's permeability [103].

3.4 APPLICATIONS OF HIFU IN MEDICINE

The main goal of HIFU surgery is to destroy pathological tissue without affecting the surrounding normal tissue. Focused ultrasound promises multiple therapeutic functions in the field of neurological diseases through both ablative tissue disruption and nonablative effects (e.g., delivery of therapeutic agents to a targeted volume by temporary opening of the Blood-Brain Barrier (BBB), enhanced immune response, or reversible blocking of neuronal functions).

Tissue Ablation; The success of the Fry brothers' experiments as discussed in section 3.1, demonstrates that successful tissue targeting is possible using HIFU treatment [2]. Cohen et al. [104] using a HIFU system (ExAblate 2000, Insightec Inc., Tirat Carmel, Israel) on a swine model showed that the HIFU-induced thermal lesions were sharply demarcated from the surrounding brain with no anatomic or histological abnormalities outside the target. A current study at the Brigham and Women's Hospital in USA is examining the effectiveness of Magnetic Resonance Imaging-Guided High Intensity Focused Ultrasound (MRgHIFU) treatment for glioma patients without a craniotomy. Regions of the brain close to the cranium remain a limitation of MRgHIFU because of cranial heating. This limitation may be partially circumvented by inserting ultrasound contrast agents (preformed microbubbles) into the bloodstream. These agents have been known to enhance focal heating during sonication and may reduce the time-averaged power needed during transcranial focused ultrasound ablation.

Targeted Drug Delivery; The BBB (Blood-Brain Barrier) is a persistent obstacle for the delivery of macromolecular therapeutic agents to the central nervous system, even though many drugs have proven their potential for treating central nervous system diseases. It has been recognized that ultrasound can disrupt the BBB; the prospect of creating a controlled reversible process introduces significant promise for delivering agents that cannot currently be delivered into the brain. Hynynen et al. [105] first described a controlled, reversible, and reproducible manner of opening the BBB; MRI can monitor the process. The study by Kinoshita et al [61] and Treat et al [106] have demonstrated the potential use of focused ultrasound to deliver chemotherapeutic agents, antibodies, growth factors, or genes to the desired area of brain.

Clot Lysis; Ischaemic and hemorrhagic strokes are the third most common cause of death in the United States. Recent studies have demonstrated the potential of ultrasound and microbubbles in thrombolysis. The effect can be increased through the administration of microbubbles. Enhanced effects of thrombolytic agents such as urokinase and tissue plasminogen activator with acoustic energy have been demonstrated. Recent clinical studies have demonstrated improved thrombolysis with the concomitant use of focused ultrasound and a thrombolytic agent for ischaemic stroke. Ultrasound enhanced the binding of tissue plasminogen activator to fibrin and also increased the activity of tissue plasminogen activator through hyperthermia. Clot Lysis followed by stereotactic needle aspiration might also be feasible for hemorrhagic stroke in the future [107][108].

Coagulation; Focused ultrasound has been demonstrated by Zderic et al [59] to provide an effective method for haemorrhage control of blood vessels in acute animal studies. The changes in the adventitia and tunica media recovered to normal appearance within 28 days. These results show that focused ultrasound can produce effective haemostasis while preserving normal blood flow and vessel wall structure. Post treatment histological observations of the ultrasound-treated arteries showed disorganization of adventitia and coagulation and thinning of the tunica media. It remains to be shown whether a higher acoustic intensity can cause endothelial proliferation and, thus, be used for the treatment of vascular anomalies.

3.5 LIMITATIONS AND FUTURE PROSPECTS OF HIFU:

In 1954, Lindstrom [109] studied the effects of HIFU mediated lesioning as an alternative to a lobotomy procedure and reported on the pathological effects of ultrasound on human brain tissue in 25 patients with carcinomatosis and cancer-related pain. In this study, autopsies on 14 of the 15 patients who had died of cancer indicated a satisfactory lobotomy procedure, with minimal disruption to the brain outside of the targeted region. Following Lindstrom, Leksell [70] designed a specially adapted frame and ultrasound transducer for the purpose of HIFU lesioning, and he used it successfully on patients for periventricular lesioning. The major limitations for Leksell, however, in treating human patients were the accuracy in targeting deep-seated structures and the need for a craniotomy, because ultrasound could not permit visualization through the intact cranium. These limitations were compounded by the lack of reliable imaging tools to plan HIFU treatments.

During the 1950s and 1960s, although progress had been achieved in selecting the most desirable acoustic parameters for ultrasound, it was difficult to focus the ultrasound to a precise location, thus limiting the efficacy of the procedure. Lele's insights [110][111] offered promise, as he had conducted a number of experiments using implanted thermocouples and had established that ultrasound could cause tissue damage by a temperature elevation at the beam's focus. Other limitations of focused ultrasound existed as well. These included the lack of real-time imaging during the procedure and the need for a craniectomy operation because of beam distortion caused by an intact cranium. When the cranium distorts the ultrasound field, it absorbs energy, resulting in heating of the cranium and attenuation of the ultrasound beam. Attempts to address this problem were investigated in the 1970s by Fry and Goss [71] and Fry et al. [72], as they began experimenting on the use of HIFU without a craniectomy.

The craniectomy problem was solved in the 1990s with the development of phased arrays of ultrasound transducers, which permitted the focusing of the ultrasound beams, with the use of a hemispheric transducer design, by correcting the phase aberrations induced by the different pathways. The early designs required an implantable hydrophone to determine these aberrations, but

technology that is more modern uses a preoperative computed tomographic scan to measure the thickness of the cranium along the various acoustic pathways, Hynynen et al [62]. These measurements then permit individual transducers to emit a specific phase and amplitude to reduce phase aberration induced by the variable cranial thickness. The other major revolution in the development of modern HIFU surgery came with improvements in MRI. Because the concept of an “ideal surgery” requires that, only the targeted tumour tissue is removed or destroyed without associated injury to the adjacent normal tissue, imaging verification of the target is vital.

The first, and most obvious, method used for guiding focused ultrasound treatment was diagnostic ultrasound. However, ultrasound had two limitations: 1) less resolution than computed tomography or MRI in accurately detecting the location of the lesions, and 2) its inability to detect real-time temperature changes and confirm thermally induced tissue changes (although modern ultrasound technology may permit this). MRI, with its excellent sensitivity for imaging soft tissue tumours, was found to be preferable over other imaging modalities for localizing 3-dimensional tumour margins and targeting tumour volumes. In addition, MRI is capable of measuring temperature changes inside the body with accuracy in the range of $\pm 3^{\circ}\text{C}$ at 1.5-T field strengths, and with even greater accuracy at higher field strengths. Because of its excellent temperature sensitivity, the HIFU focal volume can be imaged and localized well before irreversible tissue damage is induced. Moreover, the ability of MRI to capture the temperature change enables the physician to delineate temperature maps and tumour volume during the procedure [5][62].

Thus, the development of the modern HIFU surgical device combined three technological advances into a single unit: 1) thermal ablation with HIFU, 2) intraoperative guidance by MRI and temperature-sensitive MRI, and 3) the use of ultrasound phased arrays to correct for cranial distortion. Two commercially available MRI-guided HIFU surgery (MRgFUS) units are currently being marketed by Insightec (Haifa, Israel). Another model has been developed by Supersonic Imagine (Aix-en-Provence, France).

3.6 CONCLUSION

In practice, cancer therapy usually needs to have multiple treatment methods for long-term survival benefit in addition to local therapy such as surgery. For instance, in the treatment of patients with breast cancer, surgery, chemotherapy, radiotherapy and endocrine therapy must be provided in tandem, because many clinical results indicate that the combination of these modalities can provide better survival benefit than one in isolation. HIFU is a local therapy for non-invasive destruction of the tumour, and it is imperative that it is combined it with other therapies in clinical applications. There are two goals of HIFU in the treatment of patients with solid malignancy. The first goal is the ablation of the tumour in patients with early-stage cancer in order to affect a cure [85]. In order to achieve this, HIFU can be used as a local treatment to induce complete necrosis of the targeted tumour. Additional treatments such as chemotherapy, radiotherapy and endocrine therapy are essential to patients with breast cancer for conservation of the diseased breast, if HIFU is used locally in patients with early-stage breast cancer. In surgical oncology, it is necessary to resect the entire tumour along with an adequate tumour-free margin, to prevent local recurrence. In the same way, HIFU treatment should adopt a similar principle and aim to kill the entire malignant focus along with tumour-free margin of healthy tissue. The other goal of HIFU treatment is palliative for patients with advanced-stage cancer [86]. They are usually those who have an unresectable tumour and for whom conventional tumour therapies, including chemotherapy and radiotherapy, have failed to control tumour growth. HIFU can be clinically used to impede tumour growth and to improve the quality of life for such patients. Symptoms such as pain caused by tumour disappear after HIFU, and survival time can be extended.

The following chapter describes the physical aspects of ultrasound. The basic principles of ultrasound such as basic quantities, power field calculations, temperature simulations, and thermal dose calculations will be discussed.

CHAPTER 4: PHYSICAL ASPECTS OF ULTRASOUND

4.1 INTRODUCTION

This chapter describes the physical aspects of ultrasound waves and how temperature and thermal dose is calculated. Ultrasound is an essential tool for diagnostic and therapeutic cancer diseases such as brain tumours. The following section will describe the principles of ultrasound such as basic quantities, power field calculations, temperature simulations, and thermal dose calculations.

4.2 BASIC QUANTITIES IN ULTRASOUND.

The displacement amplitude u of a particle in simple harmonic motion from its rest position is given by;

$$u = u_0 \sin(\omega t - \varphi) \quad (1)$$

where u_0 is the peak displacement, ω is the angular velocity, t is the time and φ is the phase.

The particle displacement repeats itself with certain time interval - the so called period of motion (τ) where τ is the reciprocal of the frequency f

$$\tau = \frac{1}{f} \quad (2)$$

The particle velocity v which is the rate of change of displacement is given by

$$v = \frac{du}{dt} = u_0 \omega \cos(\omega t - \varphi) \quad (3)$$

Similarly the particle acceleration a is the rate of change of velocity and is given by

$$a = \frac{dv}{dt} = -u_0 \omega^2 \sin(\omega t - \varphi) = -\omega^2 u \quad (4)$$

which means that the acceleration is proportional, but in opposite direction to the particle displacement.

The wavelength λ is the minimum distance between points with the same particle displacement. The wavelength is related with frequency by

$$c = \lambda f \quad (5)$$

where c is the propagation velocity within a medium. The propagation velocity relates the second spatial derivative of particle displacement with the second time derivative of the displacement through the well known wave equation:

$$\frac{\partial^2 u}{\partial t^2} = \frac{1}{c^2} \frac{\partial^2 u}{\partial x^2} \quad (6)$$

The solution of the above equation gives the particle displacement with respect to time and the distance x by:

$$u(x, t) = u_0 \sin \omega \left(t - \frac{x}{c} \right) \quad (7)$$

The propagation velocity is given in terms of physical parameters by

$$c = \left(\frac{K}{\rho} \right)^{\frac{1}{2}} \quad (8)$$

where K is the bulk modulus of medium and ρ is the density of the medium. Thus, the propagation velocity is strictly dependent on the medium. Knowing the frequency and the propagation velocity of the medium the wavelength can be found. The wavelength is a very important parameter because it determines the shape of the power field. Air has the lowest propagation velocity because the bulk modulus is the lowest. Aluminium which is an example of solid has the highest propagation velocity (higher bulk modulus). Water has an intermediate value. Soft tissues have values similar to water, except for lung which has the lowest (due to air spaces) and bone which has the highest (highest bulk modulus). Table 4.1 gives some typical values of propagation velocities of biological tissues.

The compressive force at distance x is given by Hooke's law

$$F_x = -KA \frac{du}{dx} \quad (9)$$

where A is the cross-sectional area and $\frac{du}{dx}$ is the longitudinal strain.

The pressure then is given by

$$p = \frac{F_x}{A} = -K \frac{du}{dx} = \rho c^2 \frac{du}{dx} = \rho c u_0 \omega \cos \left(\omega t - \omega \frac{x}{c} \right) = |\rho c v| \quad (10)$$

Table 4.1 Propagation velocities of some biological tissues [112], [113]

Tissue type	Propagation velocity c (m/s)
Bone	1500-3700
Tendon	1750
Kidney	1564-1640
Liver	1540-1640
Muscle	1508-1630
Testis	1595
Brain	1516-1575
Skin	1498
Fat	1400-1490
Lung	470-658

A very important quantity in ultrasound is the acoustic impedance. The acoustic impedance is defined as the ratio of pressure and particle velocity.

$$Z = \frac{p}{v} = \frac{\rho cv}{v} = \rho c \quad (11)$$

Thus, the acoustic impedance depends on the medium. The concept of impedance is better understood by considering analogous quantities from electricity. The pressure is equivalent to the voltage, the particle velocity is analogous to the current and the acoustic impedance is analogous to the electrical impedance. Table 4.2 shows typical values of impedances in tissue. Most soft tissues have value similar to the water except lung which has the lowest value (lowest propagation velocity) and bone which has the highest (highest propagation velocity).

Acoustic impedance is very important because its value determines the amount of reflection in the interface of two medium of different acoustic properties. Figure 4.1 shows that the incident wave is reflected and partially transmitted at the interface.

Table 4.2: Acoustical impedances of soft tissues [112], [113]

Tissue type	Acoustic impedance Z ($10^6 \text{ kgm}^{-2}\text{s}^{-1}$)
Bone	3.75-7.38
Tendon	-
Kidney	1.62-1.71
Liver	1.7-1.74
Muscle	1.61-2.07
Testis	-
Brain	1.56-1.62
Skin	1.8
Fat	1.29-1.37
Lung	0.188-0.263

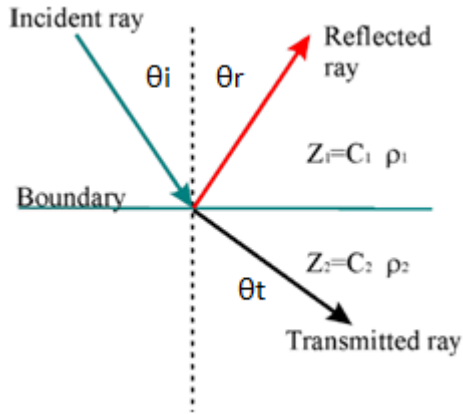


Figure 4.1 Demonstration of wave reflection and transmission at a plane interface between two media.

By using the fact that the pressure is continuous the following expression is derived relating the ratio of incident and reflected pressure with respect to the acoustic impedances.

$$\frac{p_r}{p_i} = \frac{Z_2 \cos \theta_i - Z_1 \cos \theta_t}{Z_2 \cos \theta_i + Z_1 \cos \theta_t} \quad (12)$$

where the subscript r denotes reflection and the subscript i denotes incidence.

Now, considering normal incident ($\theta_i = \theta_r = 0^\circ$) then the expression is simplified to

$$\frac{p_r}{p_i} = \frac{Z_2 - Z_1}{Z_2 + Z_1} \quad (13)$$

Let's consider two important cases

a) $Z_1 \approx Z_2$ then $\frac{p_r}{p_i} \rightarrow 0$ This means that the reflected pressure tends to zero.

This happen when the wave goes from soft tissue to soft tissue.

b) When $Z_2 \gg Z_1$ then $\frac{p_r}{p_i} \rightarrow 1$ Therefore, all the pressure is reflected. This is seen when ultrasound travels from soft tissue to bone interface.

The total energy of a particle is the sum of the kinetic energy (K.E.) and the potential energy (P.E.). At the rest position the particle has only K.E., therefore, the energy is given by

$$e = \frac{1}{2} m v_0^2 \quad (14)$$

where v_0 is the particle velocity amplitude at rest.

The total energy is the sum of the energies of all the particles. The energy per volume is given by

$$E = \frac{1}{2} \rho v_0^2 \quad (15)$$

The intensity I is the power per unit area and is defined as the product of the wave propagation velocity and the total energy.

$$I = cE = \frac{c\rho v_0^2}{2} = \frac{(c\rho v_0)^2}{2\rho c} = \frac{p^2}{2Z} \quad (16)$$

Thus, the intensity depends on the square of pressure and it is inversely proportional to the impedance. In a real medium the ultrasound is attenuated according to an exponential law. For the plane wave case the intensity as a function of depth in tissue is given by;

$$I(x) = I(0)e^{-2\mu x} \quad (17)$$

where $I(x)$ is the intensity at depth x , $I(0)$ is the intensity at the tissue interface, μ is the attenuation coefficient per unit length, and x is the depth.

Now, for a continuous, single frequency, plane ultrasound wave, and neglecting the shear viscosity the temporal average absorbed power density $\langle q \rangle$ is given by

$$\langle q \rangle = 2\alpha I \quad (18)$$

where a is the absorption coefficient (Np/m/MHz). The above relationship is valid also at the focal point of a focused transducer. The absorbed power intensity is very important quantity because it is the primary factor determining the temperature elevation in tissue.

Two terms that are often confused is attenuation and absorption. Attenuation is due to absorption (energy loss due to heat conversion), scattering and reflection. Therefore, absorption is a subcategory of attenuation. There are two theories to explain absorption. The first one is the classical, which is based on viscosity. Due to shear forces in the medium there is lag between the pressure amplitude and the particle velocity which results to energy loss for every cycle. However, this theory predicts quadratic relationship of the absorption coefficient with frequency which was not seen in tissues (at low frequencies). The alternative theory of relaxation was proposed which explains the linear dependence of absorption coefficient with frequency. During the compressive part of the cycle the acoustical energy is converted to kinetic energy (carried by the molecules). This energy is redistributed in the system in the form of lattice vibrational energy, translational energy, and molecular vibrational energy. If there was no coupling, between these types of energy all the energy would have been sent back during the expansion cycle and the absorption would be zero. However, due to coupling between the energy compartments there is a finite time associated with the redistribution of energy. Thus, the returned energy is in phase with the transmitted energy and this will result to absorption. Table 4.3 shows values of attenuation and absorption for some biological tissues. The absorption values are smaller than the attenuation values.

4.3 POWER FIELD CALCULATIONS

The numerical calculation of the power field is based on the solution of the Rayleigh-Sommerfield diffraction integral [114], which relates the velocity potential Ψ with the normal velocity, by the following equation:

$$\Psi = \iint_A \frac{u_a}{2\pi s} e^{-jks} dA \quad (19)$$

where k is the wave number ($2\pi/\lambda$), u is the normal velocity and s is the distance from a source point in the surface element ds on the transducer to a field point where Ψ is to be evaluated.

The assumptions governing the solution of the above integral are:

- a) The amplitude is assumed small so that non-linear effects do not play any role
- b) The surface S should be slightly curved so that secondary diffraction due to the radiation of waves of the various transducer elements is neglected.

Table 4.3 Attenuation and absorption values for biological tissue [112], [113]

Tissue type	Attenuation μ (Np/m/MHz)	Absorption α (Np/m/MHz)
Brain	4-29	1.2-6.4
Kidney	3-10	3.3
Liver	3.2-18	2.3-3.2
Lung	4.3-480	7
Muscle	4.4-15	2-11
Bone	150-350	-

The normal velocity is represented by

$$u = U_0 e^{i\omega t} \quad (20)$$

where ω is the angular velocity and U_0 is a constant.

The acoustic pressure is represented by

$$p = \rho \frac{\partial \Psi}{\partial t} = i\omega \Psi = ikc\Psi \quad (21)$$

where ρ is the density of the medium and c is the propagation velocity.

Figure 4.2 shows the geometrical arrangement of the transducer illustrating the various distances. z is the distance in the axial direction from the origin to the field point Q, r is the distance from the central axis to point Q in the radial direction, R is the radius of curvature, d is the diameter of the transducer, h is the depth of the concave surface, α is the angle between the line connecting the focus and the

transducer boundary and the line of the central axis. These, quantities are related by the following expressions:

$$\frac{d}{2} = R \sin \alpha \quad (22)$$

$$h = R - R \cos \alpha \quad (23)$$

$$S = 2\pi Rh \quad (24)$$

The emittance e (W/cm^2) of the transducer is given by

$$e = \frac{P}{S} \quad (25)$$

where P is the acoustic power.

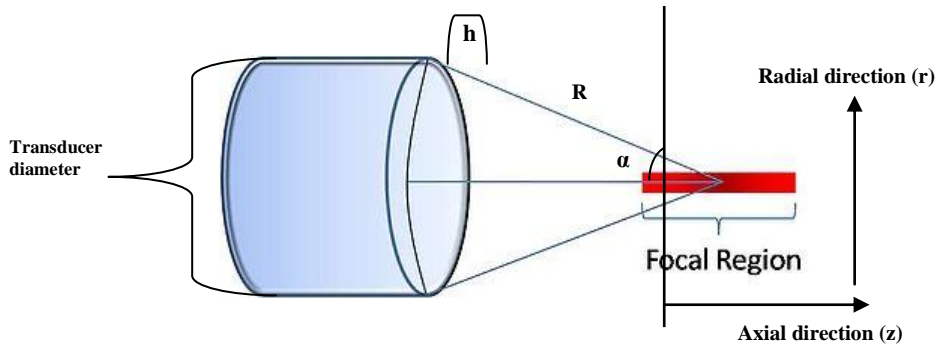


Figure 4.2 Geometry of spherically focused transducer.

SIMPLIFIED MODEL TO ESTIMATE POWER

In this project in order to simplify calculations, only those elements of area on the transducer over which s is constant are considered. This reduces the integral to a one-dimensional integral [115]. Another simplification used is associated with the effective attenuation distance s' . In a weakly attenuating medium, the effect of attenuation is approximated using eq. (17). In this model s' is assumed as the distance from the water-tissue interface to the point of interest. (This is true for a planar transducer, good approximation for high F-number transducers and weaker approximation for low F-number transducers). Because of the above simplifications the integral is reduced to

$$\Psi(s) = \frac{u}{2\pi} e^{-\mu s'} \left(e^{-ik_{sm} \frac{A_m}{S_m}} \right) \quad (26)$$

where A_m is the area of the m^{th} annular strip and M is the number of strips in which the transducer is divided into.

A program was written in MatLab to calculate the power field. The program requires information such as the frequency, radius of curvature, diameter of the transducer, acoustic power, attenuation coefficient, distance of transducer from the skin (controls depth of focus in the tissue). The dimensions of the field size can also be inputted by the user as well as the spatial step. Numerical calculations of the temperature requires equal spatial step in the radial and axial direction.

PARALLEL FLAT PLANE INTERFACE MODEL

It was stated in section 4.2 that when sound waves cross the interface between two mediums of different acoustical properties, refraction and reflection takes place. The angle of the transmitted wave depends on the angle of incidence and propagation velocities of sound in the media as described by Snell's law. A model was developed by Fan and Hynynen [116] which incorporates the refraction of the wave in the interface. The model calculates the acoustic pressure in the second medium due to a point source located in the first medium. The problem was simplified by assuming a plane interface between the media. After a rigorous analysis the pressure in the second medium is calculated as a function of pressure transmission coefficient, amplitude diminution factor, ray length (proportional to medium thickness) and propagation velocities of the media. The ray path length, transmission coefficient, and amplitude factor are determined from the angle of incident. The model calculates the acoustic pressure in a given medium for the general case of n media and $n-1$ interfaces. The above idea was applied for the case of a transducer by dividing the transducer into small elements (point sources). The contribution of each element was added by using Huygen's principle.

4.4 TEMPERATURE SIMULATIONS

The temperature vs time history was obtained by solving numerically the bio-heat equation proposed by Pennes (1948) [117]. The explicit form of this equation is given by

$$\rho_t c_t \frac{\partial T}{\partial t} = k \nabla^2 T + w_b c_b (T - T_a) + Q_p + Q_m \quad (27)$$

where ρ_t is the density of the tissue, c_t is the specific heat of the tissue, T is the temperature of the tissue, t is the time, w_b is the blood perfusion rate, c_b is the specific heat of the blood, T_a is the arterial blood temperature, k is the thermal conductivity of the tissue, Q_p is the ultrasonic power deposition rate, and Q_m is the local metabolic rate which was neglected in the computer simulations. The first term in the above equation represents the temperature rise with respect to time, the second term represents the conduction effect which tends to decrease the temperature, the third term represents the convection effect due to blood which decreases the temperature, and the fourth term represents the power absorbed due to the ultrasonic source which increases the temperature. The blood perfusion is modelled as a uniform heat-sink with blood supplied by vessels into the tissue volume at body temperature T_a and exiting at tissue temperature T . All units and values of the above parameters are given in Table 4.4.

Tissue metabolic rate determines the precision of local blood flow. According to metabolic feedback theories of exercise hyperemia, the vasodilatation of muscle exercise results from an increase in tissue fluid concentration of vasodilators produced during muscle contraction. On the other hand, the fall in resting blood flow that accompanied depression of tissue oxygen consumption by cold suggests that reduced tissue metabolism causes a decrease in the tissue fluid concentration of vasodilator metabolites normally produced at rest [118]. For the experiments in vitro there is no blood flow and therefore metabolic rate was assumed to be zero. Since there is blood flow during the experiments in vivo, normally a small value of metabolic rate should be considered depending of the treatment location in the body. Including metabolic rate values into simulation program lower values of temperature should be encountered during an ultrasound exposure.

The bioheat transfer equation was solved by using the finite difference method. In order to demonstrate how the temperature is evaluated at a certain time the following subscripts are used:

- z: variable representing distance in the axial direction.
- r: variable representing distance in the radial direction.
- t: Time
- l: adjacent spatial step (in positive direction) in distance if used in conjunction with z or r, otherwise new time step.
- l: adjacent spatial step (in negative direction) in distance if used in conjunction with z or r.

Table 4.4: Parameters used for the temperature vs. time simulations [121]

Symbol	Definition	Value	Units
ρ_t	Density of tissue	998	kg/m ³
C_t	Specific heat of tissue	3770	J/kg°C
t	Time	Variable	s
T	Temperature	Calculated	°C
W_b	Blood perfusion	0.5, 5, 10	kg/m ³ s
c_b	Specific heat of blood	3770	J/kg°C
T_a	Arterial Temperature	37	°C
K	Thermal conductivity of tissue	0.5	W/m°C
Q_p	Power deposition rate	Variable	W/m ³
Q_m	Local metabolic rate	0	W/m ³

The time derivative of the temperature is given by a two point finite difference

$$\frac{\partial T}{\partial t} = \frac{(T_{zrt+l} - T_{zrt})}{\Delta t} \quad (28)$$

The Laplacian term of eq. (27) in cylindrical coordinates is given by

$$\nabla^2 T = \frac{\partial^2 T}{\partial z^2} + \frac{1}{r} \frac{\partial^2 T}{\partial r^2} + \frac{\partial^2 T}{\partial r^2} + \frac{\partial^2 T}{\partial \theta^2} \quad (29)$$

Now since it is assumed that there is no variation of T with θ the last term in the Laplacian drops out.

The first term in the Laplacian is approximated by using a three point finite difference

$$\frac{\partial^2 T}{\partial r^2} = \frac{(T_{z+1rt} - 2T_{zrt} + T_{z-1rt})}{(\Delta z)^2} \quad (30)$$

similarly the second term is given by

$$\frac{\partial^2 T}{\partial r^2} = \frac{(T_{zr+1t} - 2T_{zrt} + T_{zr-1t})}{(\Delta r)^2} \quad (31)$$

The bioheat equation is now written as;

$$\rho_t c_t \frac{(T_{zrt+1} - T_{zrt})}{\Delta t} = k \left[\frac{(T_{zr+1t} - 2T_{zrt} + T_{zr-1t})}{(\Delta r)^2} + \frac{1}{r} \frac{(T_{zr+1t} - 2T_{zrt} + T_{zr-1t})}{(\Delta r)^2} + \frac{(T_{z+1rt} - 2T_{zrt} + T_{z-1rt})}{(\Delta z)^2} \right] + w_b c_b (T_{zrt} - T_a) + Q_{zrt} \quad (32)$$

Thus, the temperature at the new time step is given by

$$T_{zrt+1} = T_{zrt} + \frac{k \Delta t}{\rho_t c_t} \left[\frac{(T_{zr+1t} - 2T_{zrt} + T_{zr-1t})}{(\Delta r)^2} + \frac{1}{r} \frac{(T_{zr+1t} - 2T_{zrt} + T_{zr-1t})}{(\Delta r)^2} + \frac{(T_{z+1rt} - 2T_{zrt} + T_{z-1rt})}{(\Delta z)^2} \right] + w_b c_b \frac{\Delta t}{\rho_t c_t} (T_{zrt} - T_a) + \frac{\Delta t}{\rho_t c_t} Q_{zrt} \quad (33)$$

4.5 THERMAL DOSE CALCULATIONS

The effect of hyperthermia depends on the temperature and the duration of the heating, if a constant temperature could be maintain then the duration of heating would be a reasonable way of expressing thermal dose, with units of time. In reality, however a constant temperature is not maintained, so it is necessary to find a method of relating a treatment to an equivalent time at a specified reference temperature. A mathematical relation between time and temperature is described by Dewey [119].

$$t_1 = t_2 R^{(T_1 - T_2)} \quad (34)$$

where T_1 , T_2 are temperatures at times t_1 and t_2 respectively, and R is a constant given by

$$R = e^{\frac{-\Delta H}{2T(T+1)}} \quad (35)$$

where ΔH is the activation energy (cal/mol), T is the absolute temperature ($^{\circ}\text{K}$) and the number 2 is the approximation to the universal constant (1.98 cal/ $^{\circ}\text{K}$ -mol)

The calculation of the thermal dose for changing temperature exposure that cannot be described analytically was done by using the technique suggested by Separeto and Dewey [120]. The technique uses numerical integration to calculate the accumulated dose at a reference temperature under different temperature profiles. The reference temperature of 43 °C has been chosen. For small Δt the dose can be found by

$$t_{43} = \sum_{t=0}^{t=final} R^{(43-T_t)} \Delta t \quad (36)$$

where t_{43} is the equivalent time at 43 °C, T is the average temperature during Δt . The value of R equal to 0.25 was chosen for temperatures smaller than 43 °C and 0.5 for temperatures higher than 43 °C [120]. Figure 4.3 shows the flowchart of the simulation model to calculate temperature, thermal dose and to estimate lesion size. In the flow chart, z denotes axial distance, r radial distance and t time.

The concept and unit of thermal dose referenced to a certain temperature is best illustrated by means of Figure 4.4. It is assumed that an idealized constant temperature of 43°C is maintained for 120 s. Then the thermal dose is 2 min. Now, a high intensity ultrasound pulse of 5 s duration is applied. This will cause temperatures elevations higher than 43°C. By using the function of eq. (36), the thermal dose referenced at 43°C is 2 min (established by adjusting the power). Thus, the same thermal dose of 2 min (as in the case of low power and long duration) can be induced with high intensity and short durations.

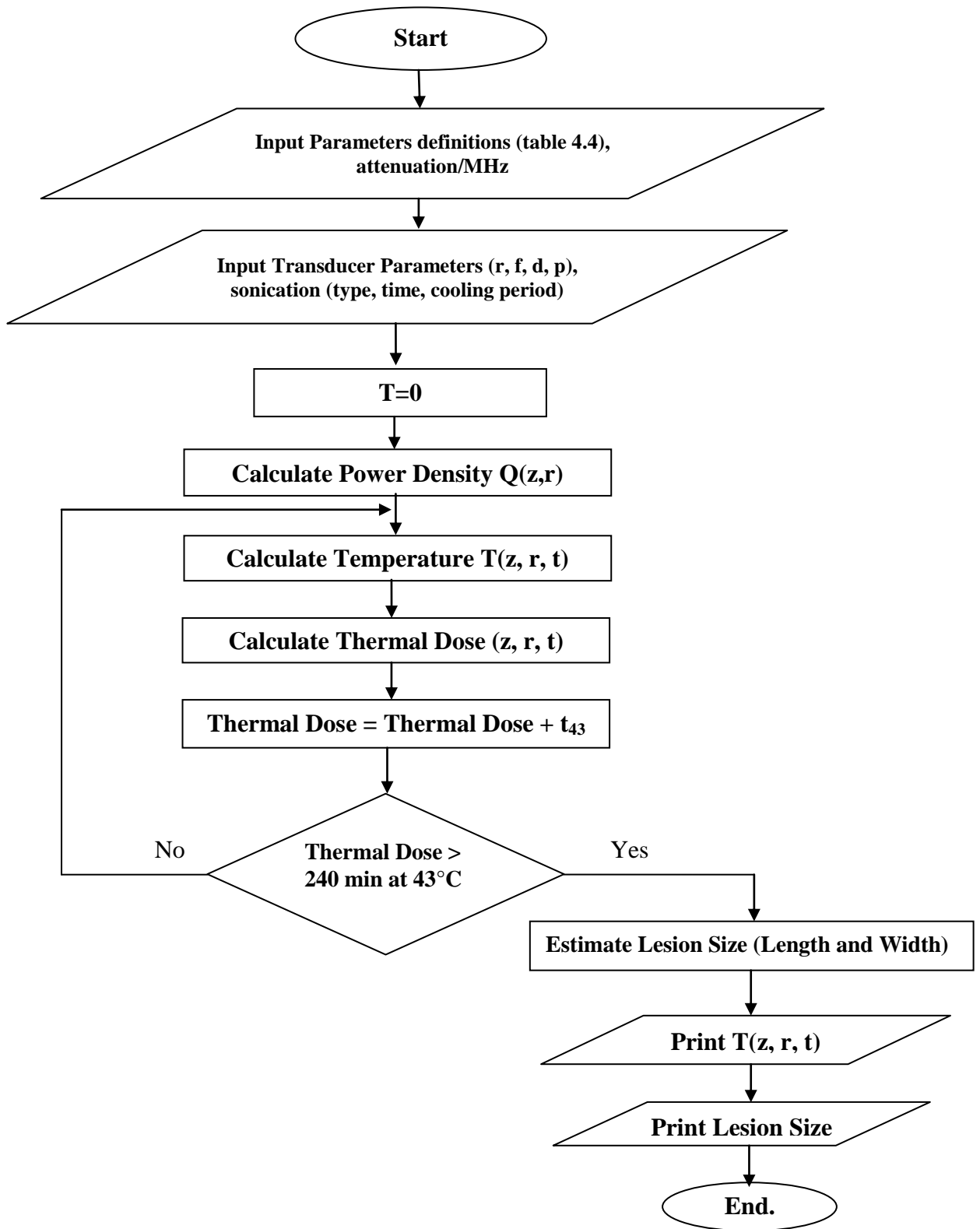


Figure 4.3 Flowchart of the simulation model to calculate temperature, thermal dose and to estimate lesion size

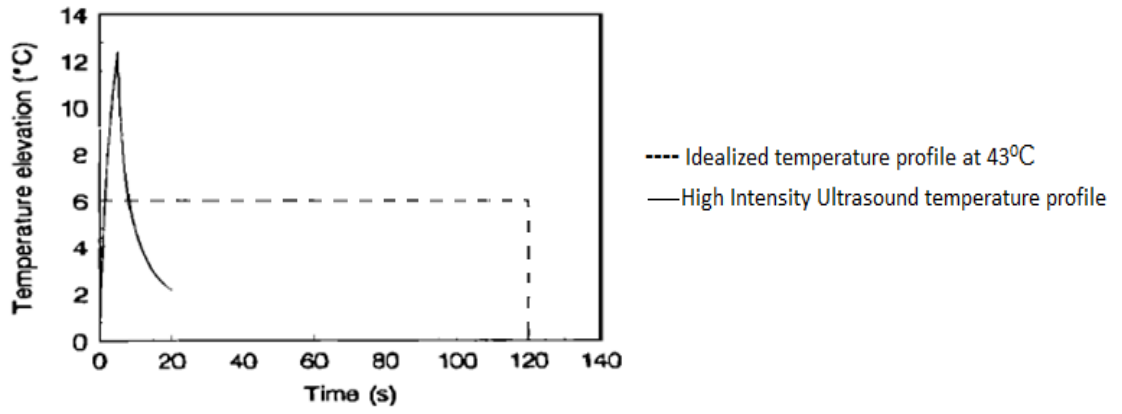


Figure 4.4 Demonstration of 2 min thermal dose at 43 °C using an idealized temperature profile and a typical temperature profile created using high intensity ultrasound.

CHAPTER 5: *IN VITRO* MEASUREMENTS OF THE ATTENUATION AND ABSORPTION OF HIFU IN ANIMAL BRAIN TISSUES AS A FUNCTION OF THERMAL DOSE

5.1 INTRODUCTION

One of the most important issues for HIFU surgery is the understanding and control of thermal exposure in tissue. It was shown by Damianou et al [121][122][123] that when tissue temperature is maintained between 50-100°C for a few seconds (<5 s), tissue necrosis occurs, and thermal lesions are created. There is now a very good understanding how thermal lesions vary with the amount of acoustical power applied and the pulse duration for some tissues (for example brain and liver), demonstrated by Kennedy et al [88], Daum et al [96] and Vykhodtseva et al [124]. However, there is not enough information about the effect of heating on absorption (tissue variable) which also affects the size, shape and placement of the thermal lesions. Absorption is an acoustical property of tissue with wide variation from tissue to tissue, and represents the rate at which energy in tissue is converted to heat. For short pulses (<5 s) it is one of the primary factors contributing to the temperature elevation in tissue since the effect of blood flow is minimized. Attenuation includes absorption, scattering and reflection but when minimizing scattering and reflection, attenuation will reflect mostly losses due to absorption.

There are a number of studies on the effect of temperature on tissue attenuation or absorption. Dunn [125] studied the effect of absorption with temperature (up to 30 °C) in the spinal cord of mice, where an increase of absorption with temperature was reported. Dunn and Brady [126] studied the absorption as a function of temperature in mammalian central nervous tissue at different frequencies and it was shown that the absorption decreased for frequencies lower than 1 MHz and increased for frequencies higher than 1 MHz. Gammel et al. [127] studied the effect of attenuation with temperature for excised porcine liver, kidney, backfat and spleen and for human liver. The frequency was varied from 1.5-10 MHz and three different temperatures were studied (4, 20, 37 °C). It was found that basically above 5 MHz the attenuation decreased with temperature for

all tissues including the human liver. The pressure absorption was studied by Fry et al. [128] on rat liver, where for the temperatures studied (30, 37, and 41 °C), there was no statistically significant differences in absorption in this temperature range.

However, for tissue ablation the attenuation at higher temperatures (50-100°C) is required. Robinson and Lele [129] studied the changes in attenuation (from 30°C to 90 °C) in cat brain and showed that the attenuation stays essentially constant up to 50°C, and then increases rapidly. Bamber and Hill [130] studied the effect of temperature on attenuation in the range of 5-65°C on excised liver tissues. Many trends were observed, for example the attenuation of bovine liver decreased and then increased until it reached 65°C where it stayed constant. In human liver the attenuation dropped with temperature and for frequencies lower than 2 MHz, the change was insignificant.

Basically in the past years, some studies examined attenuation or absorption as a function of temperature (up to 37°C) and some at higher temperatures. However, there is no study that examined both attenuation and absorption (at least for one tissue) as a function of temperature (with maximum temperature reached close to temperatures seen in HIFU surgery) or as a function of thermal dose.

This Chapter reports on the effect of temperature and of thermal dose on the attenuation and absorption of tissues namely lamb brain *in vitro* for temperatures from 23°C up to 70°C. The attenuation was measured using the transmission and reception method (Kossoff et al. [131]), and the absorption was measured using the rate of heating method (Fry and Fry [132]). The impact of variation of absorption due to tissue changes on the temperature elevation was demonstrated by temperature measurements and simulations.

5.2 MATERIALS AND METHODS

5.2.1 SAMPLE PREPARATION

For all the animal experiments protocol, approval was taken by the national body in Cyprus responsible for animal studies (Ministry of Agriculture, Animal

Services). Tissue samples extracted from lamb brain, immediately after euthanasia, were immersed in 0.9 % saline at room temperature. Twenty lamb brain were used weighting approximately 140 g. The samples were placed in a small custom-made vacuum chamber until all the bubbles were removed (determined by visual inspection). It was proven by Bamber and Nassiri [133], that this method is very successful in removing air inclusions from the tissue, especially in liver tissue. After this procedure, the attenuation or absorption measurement was taken immediately because some reports indicated change in attenuation with time after excision [134]. When moving the tissue samples from the vacuum chamber to the water bath, they were submerged to minimize air exposure.

5.2.2 ATTENUATION MEASUREMENT SYSTEM

The attenuation coefficient was measured based on the transmission and reception method described by Kossoff et al. [131]. Initially, the signal through the water V_w was measured. Then, the signal V_s was measured with the presence of a tissue sample. The following equation gives the value of attenuation in dB/cm:

$$\alpha(f_o) = \left[20 \log \left(\frac{V_w}{V_s} \right) \right] / 2d$$

Where d is the sample thickness measured in cm.

Two unfocussed circular transducers of 8 mm diameter (T1 and T2; see Figure 5.1) and frequency of 4.32 MHz were connected. The transducer system with the sample in between was immersed in a degassed saline bath (Figure 5.1). A controlled heat exchanger with adjustable temperature (HAAKE, model D1) was immersed in the bath to vary the tissue temperature and the thermal dose. A needle type thermocouple (Physitemp Instruments, NJ, USA) was placed inside the tissue and the temperature was measured using an HP 7500 series B system and an HP 1326B multimeter. The transmission transducer was driven by a signal generator (Textronix, Model TM 5003). The applied voltage was typically (between 10-20 V) and the burst mode was used. The resonant frequency of the transducer was 4.32 MHz. Both the applied and received signals were monitored using a 150 MHz oscilloscope. The received signal was sent from a pulse/receiver (Panametrics 5050 PR) through a signal amplifier (Panametrics

Model 5601) to a digitizer (Tektronix RTD 710). The data was stored in a Dell PC. The signal without and with the sample was measured and based on the decrease of the signal strength, the sample thickness and the frequency, the attenuation in Np/m-MHz was measured.

One useful hint when measuring attenuation is that, the lower the value, the more reliable is the data. High attenuation coefficients imply air inclusions or reflections in some interfaces, which should not be included in the ultrasonic path when measuring a specific type of tissue.

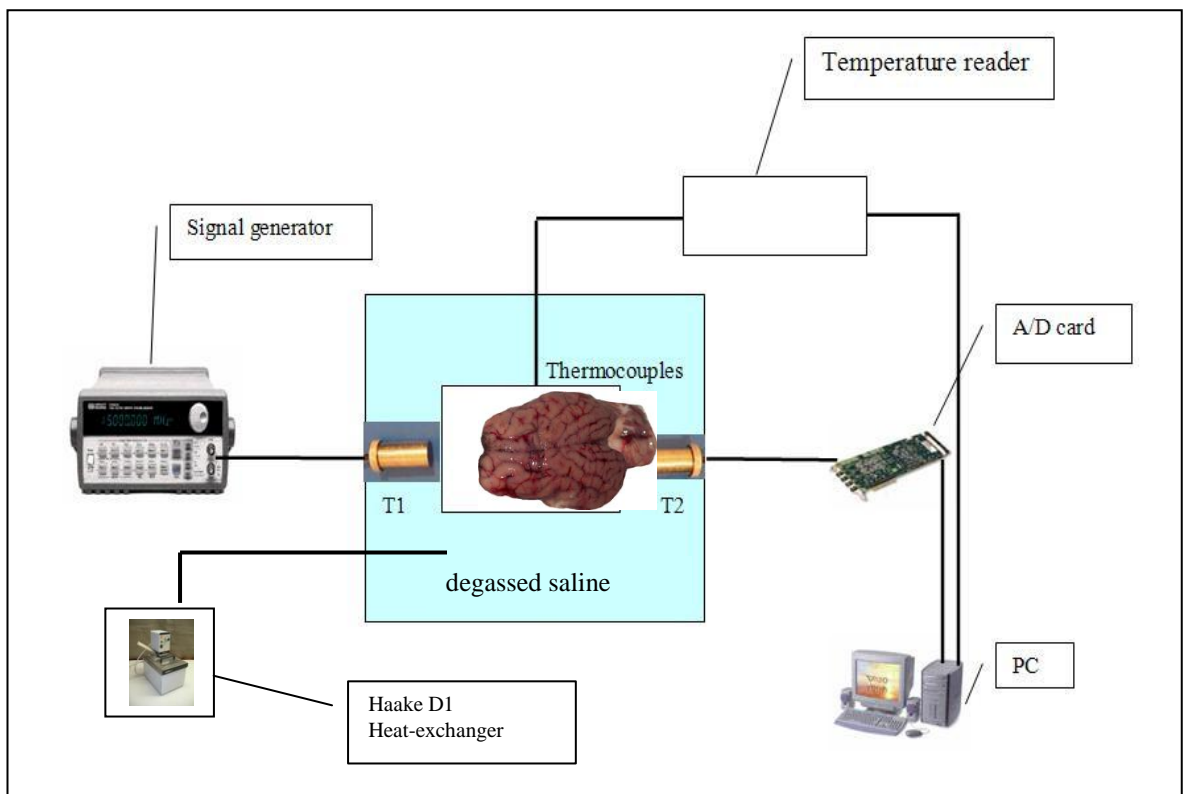


Figure 5.1 Block diagram of the attenuation measurement system

5.2.3 ABSORPTION MEASUREMENT

The absorption was measured using the widely used rate of heating method (Fry and Fry [132]). The principle of this method is based on relating temperature change with the absorption of ultrasound by the following equation:

$$\alpha = \frac{\rho_t c_t \frac{\partial T}{\partial t}}{2I_0}$$

where α is the absorption coefficient (Np/m-MHz), ρ_t is the density of the tissue, c_t is the specific heat of the tissue, T is the temperature of the tissue, t is the time, and I_0 is the focal intensity in tissue which varies exponentially with depth in tissue. By measuring the temperature close to the surface of the tissue the exponential term is dropped. The above equation is derived based on negligible thermal conduction. Therefore, to measure the absorption one needs to measure the rate of temperature rise in the focal spot of short pulse of known intensity, provided that the focal spot is placed at few mm depths in the tissue. A spherically focused transducer of 20 mm was used to produce temperature elevation in the tissue for measuring absorption using a wide beam and thus, minimizing the conduction effect. The pulse applied was in the continuous mode with pulse duration of 1 s. The power chosen was such that the temperature elevation was about 1-2 °C, thereby, reducing the conduction effect. The rate of temperature change was measured using finite differences. The value used for density was 1100 kg/m³, and the value for specific heat was 3770 J/kg- °C (Dumm [125], Gammel et al [127], Fry and Fry [132] and Frizzell et al [134]).

The temperature was measured using a 50 μ m, T-type, copper-constantan thermocouple (Physitemp). The accuracy of the thermocouple was checked by using a mercury thermometer of 0.1 °C resolution. The thermocouple was placed a few millimeters beneath the surface of the tissue and the temperature was measured every 0.1 s using an HP 7500 series B system and an HP 1326B multimeter. In order to eliminate viscous heating, the rate of temperature change was measured 0.3 s after the ultrasound was turned on. At that interval, the rate of temperature change was linear. The tissue was submerged in saline when the thermocouple was placed. Figure 5.2 shows the block diagram of the absorption measurement system. It consists of a signal generator (Tektronix, Model TM 5003) and an amplifier system (ENI, model 240L) for driving the transducer thereby elevating the temperature in the tissue, and the thermometry system described above for measuring the temperature.

The accuracy of measuring absorption depends on three factors: a) correct measurement of the peak intensity at the thermocouple site, b) correct measurement of the temperature derivative with respect to time and c) eliminating the effect of conduction which affects factor b). The effect of conduction spatially was minimized by using a sufficiently wide beam. The pulse duration and applied power were chosen such as small temperature elevations were induced, thus eliminating the effect of conduction. Thus, we believe that the technique used for measuring the absorption was very accurate. The higher the absorption measured, the more reliable the data. Lower values indicate that the measurement is affected by conduction and this would lower the temperature gradient or the focus is not placed close enough to the the thermocouple.

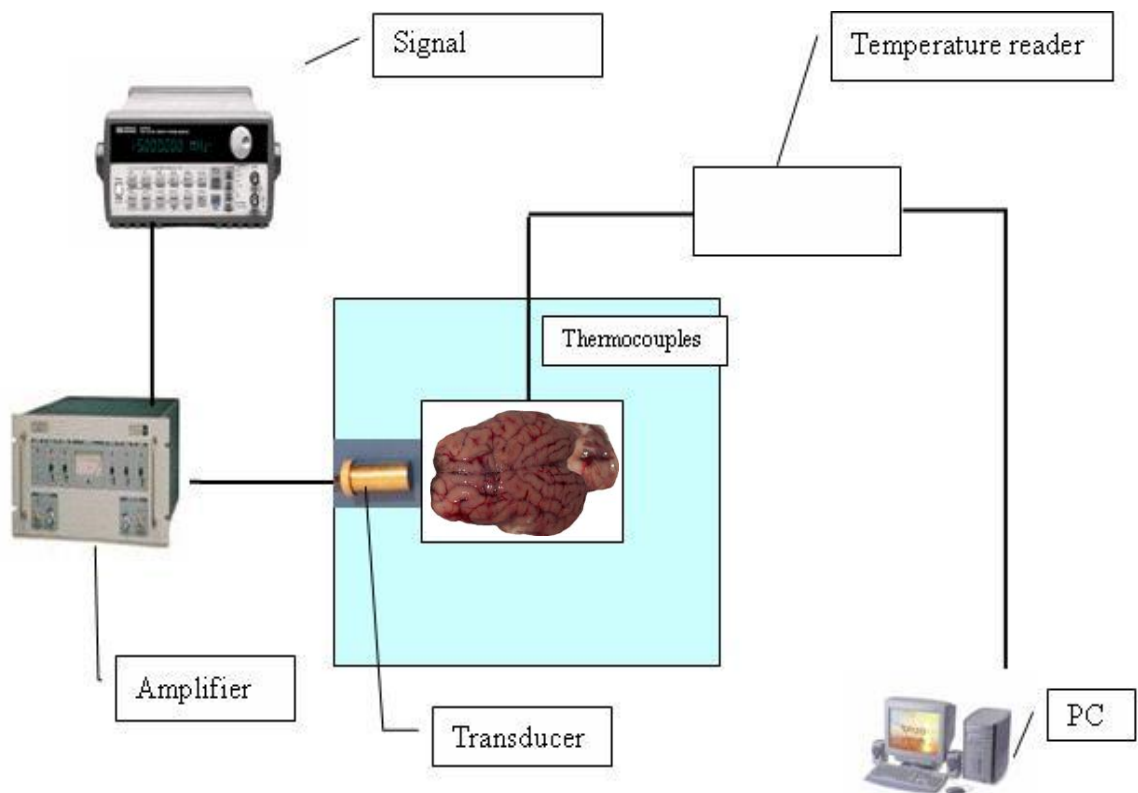


Figure 5.2 Block diagram of the absorption measurement system

5.2.4 ACOUSTICAL POWER CALIBRATION

In order to measure the absorption, the peak intensity at the focus is required. This can be found by measuring the total acoustical power delivered and the half-intensity beam width of the focused transducer. In this experiment, the acoustical

power delivered by the transducer was measured using the ultrasound power meter (Precision Advanced, Model UPM-DT-10). The transducer was driven by a signal generator (Tektronix, Model TM 5003) through an RF-power amplifier (Kalmus, 50W1000A, 1 MHz - 1000 MHz, Advanced Test Equipment Corp, CA, USA). The transducer was immersed in the bath of the power meter's tank containing a force balance and an ultrasonic absorber, which is placed 1-2 cm from the transducer surface. The measurement was taken a few seconds after the power was applied to the transducer, until measurement stabilization was established. The acoustical power was measured as a function of signal generator voltage. Power was measured by converting the force applied to the balance into acoustical power.

5.2.5 INTENSITY FIELD MEASUREMENT

The intensity beam of a transducer was estimated using a needle hydrophone of active element diameter of 0.5 mm (Specially Engineering Associate, San Jose, CA). The transducer under test was connected to the transmitter of a high frequency pulser-receiver (Panametrics 5050PR) which sends an echo-pulse to the hydrophone. The hydrophone was connected to the receiver input of the pulse-receiver, and then its signal was amplified by another pulser-receiver (Panametrics Model 5601) and digitized using an A/D card (Gage, IL, USA) at the rate of 50 MHz. The three dimensional intensity profile was obtained by moving the hydrophone laterally and axially, using stepper motors (Velmex, Inc, NY, USA) through a stepper driver (Velmex). The average intensity at the focus was estimated from the ratio of power and the area of the lateral half-intensity beam. For this transducer, the peak intensity was twice the average intensity (proved analytically and experimentally). The peak intensity was also measured directly using a calibrated ultrasonic Hydrophone (Specialty Engineering Associate, San Jose, CA), and both methods measured the same peak intensity (difference was about 1%).

5.2.6 ULTRASONIC TRANSDUCER

A spherically focused transducer of 40 mm was also used to elevate the tissue temperature using a sharply focused beam in order to compare experimental and simulated temperature during typical ultrasonic surgery protocols. The transducer

used was made out of Piezoelectric material (Etalon Inc., Lebanon, IN). The driving frequency was 4 MHz with a focal length of 100 mm.

5.3 TEMPERATURE SIMULATION

In this section, thermal dose and bioheat equations were used to calculate the thermal dose and the temperature versus time respectively (see sections 4.4 and 4.5).

5.3.1 TEMPERATURE ESTIMATION

Experimental temperature vs. time profiles were obtained in lamb brain *in vitro* as described in section 5.1.3 and then compared to the corresponding simulated profiles described in section 4.4. The temperature was estimated from the bioheat equation by using finite difference techniques described in detail in chapter 4, section 4.4. The estimation of the temperature requires the power density profile for a specific transducer, power, and absorption. The power density was calculated by using a computer program, which is described in chapter 4, section 4.3.

5.3.2 THERMAL DOSE CALCULATION

Before the attenuation or absorption measurement was taken, the tissue temperature and the total applied thermal dose (referenced at 43 °C) were measured, see section 4.5. Since the rate at which the temperature increased was low, the thermal dose was measured every 1 s. The thermal dose was measured only at one location since a homogeneous tissue sample was always chosen in the experiments. The thermal dose equation was also used to estimate the simulated thermal dose based on the temperature history.

5.4 RESULTS

For the figure 5.3 and figure 5.4, the absorption and attenuation formulas together with the thermal dose equation (36) were used. Using a thermocouple, temperature was calculated and utilized to derive thermal dose. Figure 5.3 shows the attenuation vs. thermal dose referenced at 43°C. A significant increase in

attenuation was seen for thermal dose higher than 1-1000 min, and the maximum attenuation was reached at 10^3 min when using tissue of lamb brain.

Figure 5.4 shows the effect of thermal dose on absorption in lamb brain. Differences in absorption at each temperature were less than 0.2 Np/m-MHz. The trend of absorption observed was similar to the trend seen for attenuation. Significant absorption changes occurred at 50°C and at a thermal dose of 100 min. Maximum absorption was established at 65°C and at a dose higher than 10^3 mins. The absorption at 65°C was 1.7 times the absorption at 37°C.

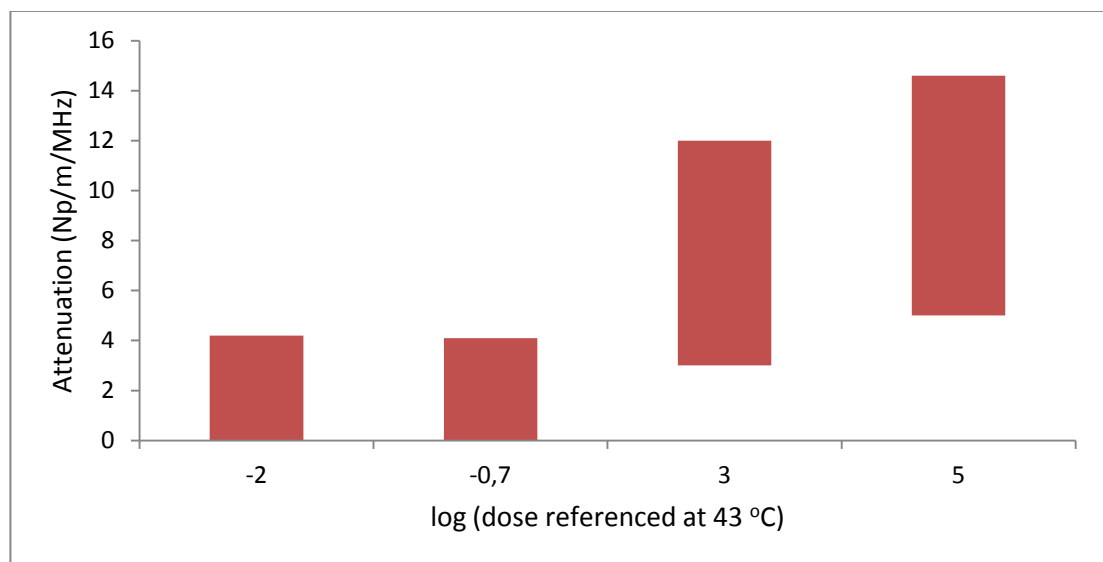


Figure 5.3 Attenuation vs. thermal dose referenced at 43 °C for lamb brain

Figure 5.5 shows experimental and simulated temperature profiles for a 4 s pulse and applied power of 15 W using a dose dependent absorption based on the results of Figure 5.4. This clearly shows the effect of dose dependence of absorption on the tissue temperature estimation, which resulted to a few degrees of difference between simulated and experimental temperature profiles.

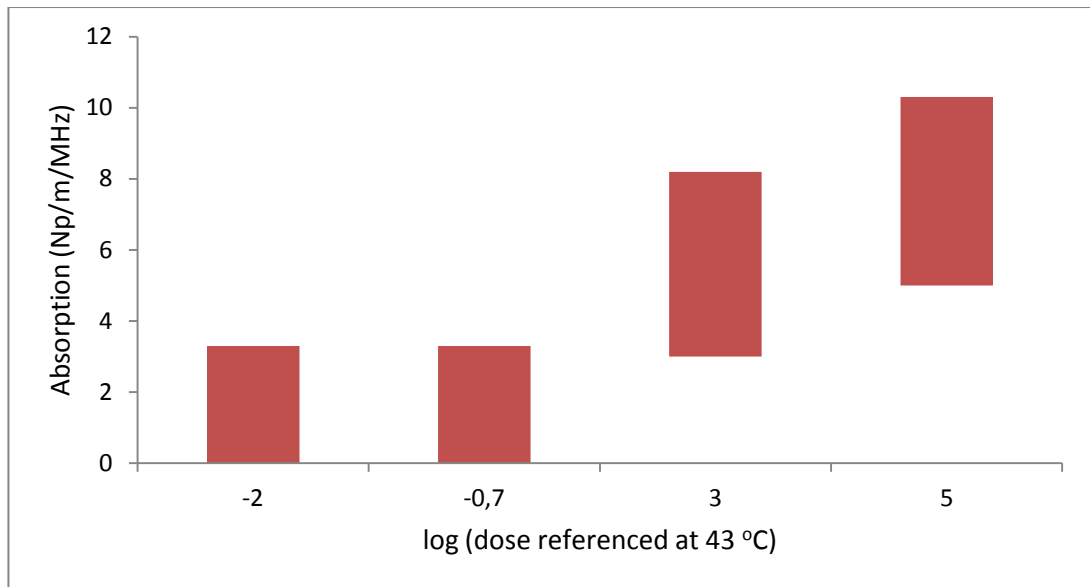


Figure 5.4 Absorption vs. thermal dose referenced at 43 °C for lamb brain

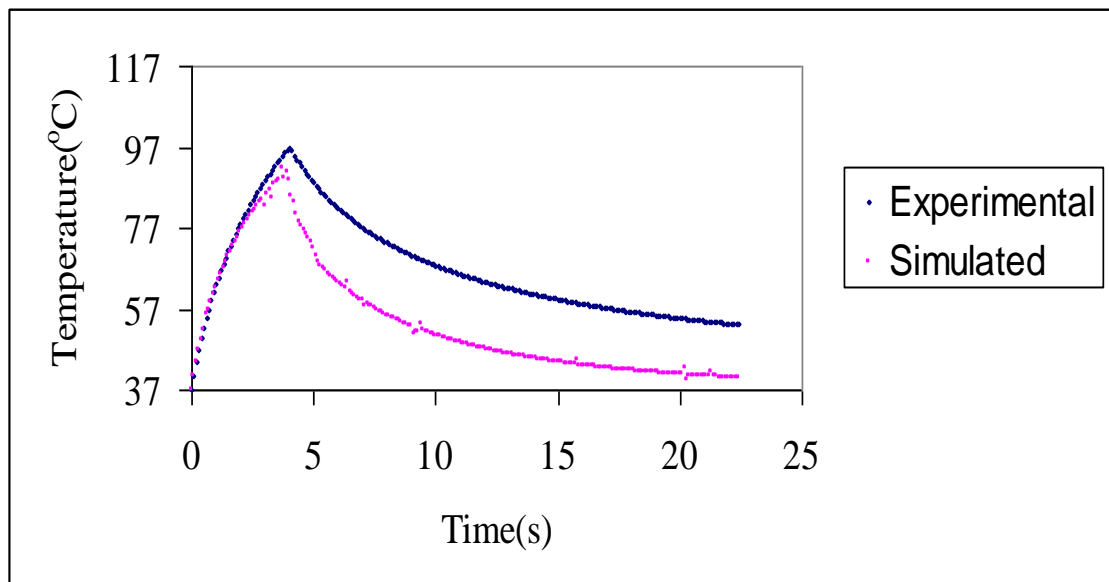


Figure 5.5 Experimental and simulated temperature change vs. time (Power=15W, 4 sec pulse, F=4 MHz, R=100mm, d=40mm, depth in tissue=15mm).

5.5 DISCUSSION

The lamb brain attenuation, measured in this study, of about 4.2 Np/m-MHz at 37 °C, is comparable to absorption or attenuation values appeared in the papers by Fry et al [128] and Frizzell et al [134].

For low dose, it was seen that the change in attenuation is insignificant. This information is important for hyperthermia applications, because it reveals that any variation in the temperature should not be attributed to variation in attenuation. The attenuation of soft tissues shows increase with temperature for all three types studied above 50 °C. The increase above this temperature is monotonic and eventually at some temperatures (about 65 °C) a maximum attenuation is reached. This maximum attenuation is almost twice the value at physiological temperatures (37 °C). The same trend of increasing absorption with temperature was reported by Dunn and Brady [126] for frequencies higher than 1 MHz with the result of this study (at 4 MHz). The attenuation vs. temperature study alone does not give a sound physical explanation of the effect of heating. The time the temperature is maintained (estimated using the thermal dose) gives more information on the physical changes in tissue. The attenuation vs. thermal dose trend shows that the attenuation starts to increase in soft tissues for doses in the range of 100-1000 min (thermal dose referenced to 43 °C). This proves that when the thermal dose threshold of necrosis is reached the tissue attenuation starts to increase. Depending on the tissue type, there is literature that reports the thermal threshold of necrosis in minutes at different temperatures. Damianou et al. [121] summarizes the thresholds in equivalent minutes referenced at 43 °C for various tissues. Typically, the threshold for all important tissue types varies from 50-240 min. Eventually, when high dose is applied (typically 10^7 min) the tissue reaches a state where no more damage is caused (total necrosis), and thus the attenuation does not change.

The trend of absorption in lamb brain with temperature and thermal dose showed similar behaviour with those seen in the attenuation study. The attenuation changed from 4.2 Np/m-MHz at 37 °C to about 9.6 Np/m-MHz at 65 °C. The corresponding change in absorption was from 3.3 Np/m-MHz to 5.3 Np/m-MHz. Thus, the change of attenuation with temperature was dominated primarily by the absorption. The value of absorption at 37 °C (3.3 Np/m-MHz) was about 78.6 % of the attenuation at 37 °C (4.2 Np/m-MHz). The corresponding contribution of absorption at 65 °C is 55.2 %. The rest of the attenuation is contributed mainly by

scattering and then reflection. Thus, the lower contribution of absorption in the attenuation at high temperatures is attributed partly to increases in reflection.

The effect of temperature dependence on absorption has a tremendous impact on the tissue temperature elevation. During the application of short pulse ultrasound the temperature elevation depends primarily on the ultrasonic source parameters (intensity *and* pulse duration), and on the absorption of the tissue. The ultrasonic source parameters are accurately determined and controlled. Thus, the tissue absorption remains the key factor for determining the tissue temperature. Moreover, for high intensity applications where the tissue temperature is typically 50-100 °C, the change in absorption with temperature can be the dominant factor for understanding temperature trends. In thermal modelling, the change of absorption used was chosen from the high rate (applied dose/per min) curve. The simulated temperature was in good agreement with the experimental during HIFU exposures only when the effect of temperature was accounted for. During the decaying part, the experimental temperature was higher than the simulated. When the power is off, conduction is the dominant factor for the temperature change, therefore the difference between the experimental and simulated temperature is attributed to uncertainty in conductivity. Therefore, to achieve an identical simulated and experimental values and especially during the decaying part of figure 5.5, more accurate values for conductivity must be used, or a smaller Δr , or Δt in the simulation program.

By calculating attenuation and absorption, we are now able to calculate the temperature elevation at the focal point inside the tissue. The prediction of lesion size requires the knowledge of the thermal dose that causes necrosis. The aim is to predict the lesion size based on the intensity used or the resulting tissue temperature at the focal point. This quantity allows us to execute a theoretical study to investigate the effect of various physical parameters on the size and shape of the lesions. At the next chapter, we can observe this temperature elevation as well as the lesion size (length and width).

CHAPTER 6: THERMAL SIMULATION MODEL FOR PREDICTING LESION SIZE DURING SONICATION USING HIFU.

6.1 INTRODUCTION

Once attenuation and absorption are known (chapter 5) a computer model was developed that estimates the lesion size based on the transducer characteristics (frequency, diameter, degree of focusing), treatment protocol (pulse duration, acoustical power), and anatomical site (size, depth, mode of operation).

The cranium presents a particularly difficult challenge because of both high attenuation and uneven thickness and density over its extent. The main problems in transmitting ultrasound through the skull are HIFU defocusing and lesion formation unpredictability. To avoid creating an acoustic window by removing a piece of the skull we have used low frequencies. Low frequencies are proven by Hynynen et al [62] to penetrate the skull and easily create a focal point. This chapter describes the results regarding lesion size and temperature elevation at the focal point in brain tissue.

6.2 TRANSDUCER ARRANGEMENT

Transducer diameter of 5 cm was assumed in this simulation program in order for the whole system to fit in the MRI scanner using our MR compatible positioning device (Daminanou et al [145]). Two different focal points were used; 5 cm deep in the tissue to simulate a human brain, and 1 cm deep in the tissue, to simulate a rabbits brain.

The modelling parameters are: transducer frequencies are 0.5 MHz, 1 MHz, and 1.5 MHz, the radius of curvature is 10 cm, the diameter of the transducer is 5 cm, and the transducer is located:

- (i) 5 cm from the water-tissue interface (simulate human brain) and
- (ii) 9 cm from the water-tissue interface (simulate rabbit brain).

The geometrical arrangement of the transducer is illustrated in Figure 6.1.

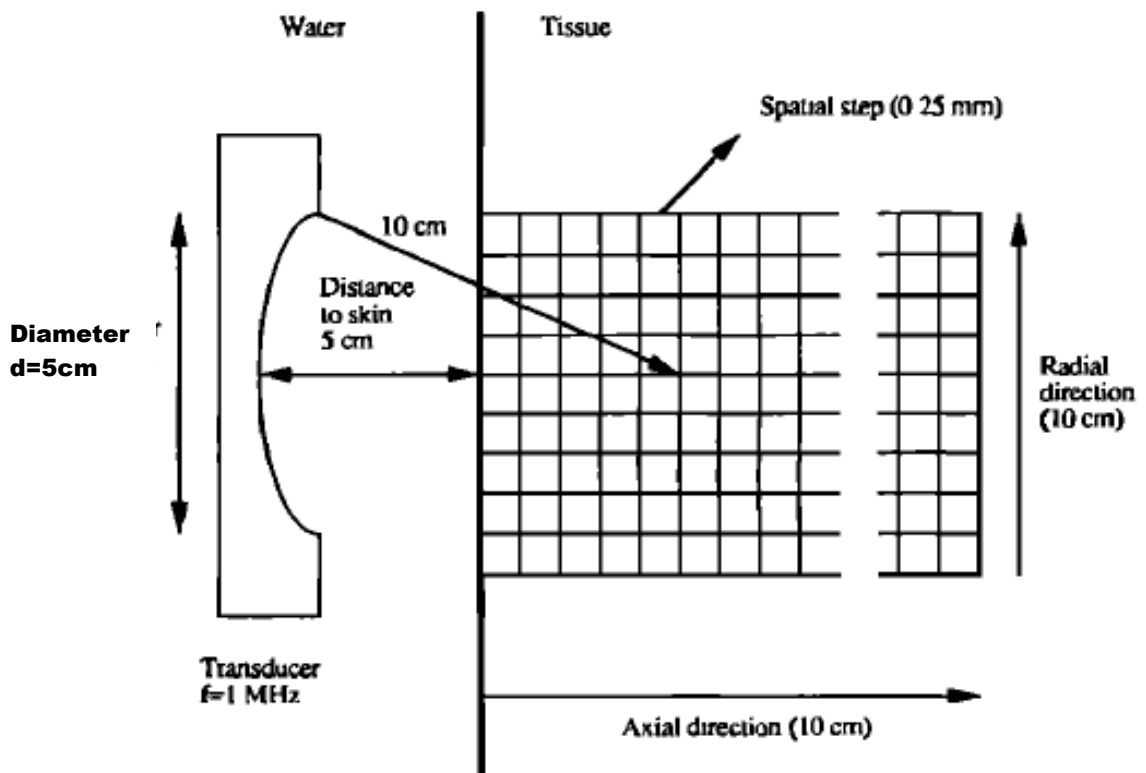


Figure 6.1 Transducer arrangements

6.3 SIMULATION METHODOLOGY

Using frequency of 0.5 MHz, 1 MHz and 1.5 MHz we have examined the lesion length and lesion width at depth of 5 cm and 1 cm deep in the brain tissue. Longer pulse durations will assume larger lesions. Therefore, different pulse duration will be investigated for different power and for different frequency in order to evaluate the size (length and width) of the lesion (figure 6.2 – figure 6.5).

Temperature distribution at the focal point should be observed in order to avoid boiling the tissue in the case that is exceeded 100°C. Therefore, to investigate temperature elevation, the properties of the transducer such as frequency, radius of curvature, diameter, and acoustical power were varied. The ultrasound field distribution was calculated from the water-tissue interface up to a distance which was at least 5 cm beyond the focus in a direction parallel to the beam propagation and 5 cm radially. Different properties used in the simulations such as tissue velocity and brain impedance were given in table 4.1 and table 4.2. Parameters used for temperature calculation were given in Table 4.4. Attenuation and

absorption were calculated in chapter 5 and their values were used in the simulation program.

A program was written in MatLab to calculate the power field, temperature at the focal point, thermal dose and lesion size (length and width). The program requires information such as the frequency, radius of curvature, diameter of the transducer, acoustic power, attenuation coefficient, distance of transducer from the skin (controls depth of focus in the tissue). The dimensions of the field size can also be inputted by the user as well as the spatial step. Numerical calculations of the temperature requires equal spatial step in the radial and axial direction.

6.4 RESULTS

The effect of applied acoustic power on the lesion size (length and width) under different frequencies was investigated. The lesion length and width increases as a function of applied power with the rate of increase dependent upon the pulse duration.

The lesion length and width were simulated for different power and pulse duration. In addition, the temperature distribution was measured for different power and pulse duration.

6.4.1 SIMULATION RESULTS FOR LESION SIZE VS. TIME FOR DIFFERENT POWER AND FREQUENCY.

Figure 6.2 shows results from the simulation for the lesion length and lesion width distribution when using 0.5 MHz transducer. The transducer diameter (D) is 5cm with a 10cm radius of curvature (R). The focus is at approximately 10cm, 5cm deep in the tissue. The effect of pulse duration on the lesion size was investigated using power of 50W, 60W, and 80W. The lesion length and width are increased with increased pulse duration.

Figure 6.3 shows the lesion length and lesion width distribution for the 1 MHz transducer. The transducer diameter (D) is 5cm with a 10cm radius of curvature (R). The focus is at approximately 10 cm, 5 cm deep in the tissue. The effect of pulse duration on the lesion size was investigated using power of 20W, 30W, 40W, 50W, and 60W. The lesion length and width are increased with increased pulse duration.

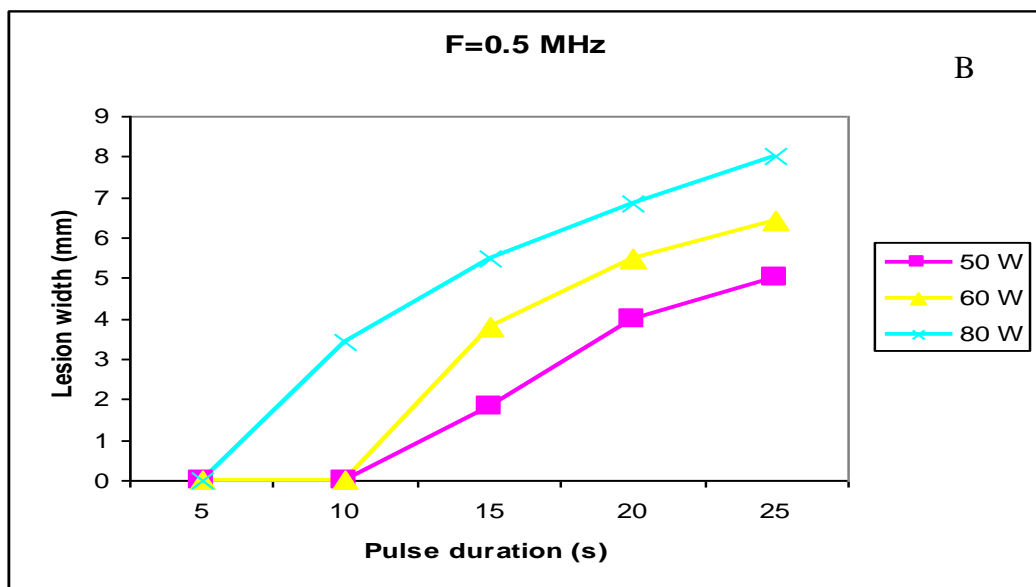
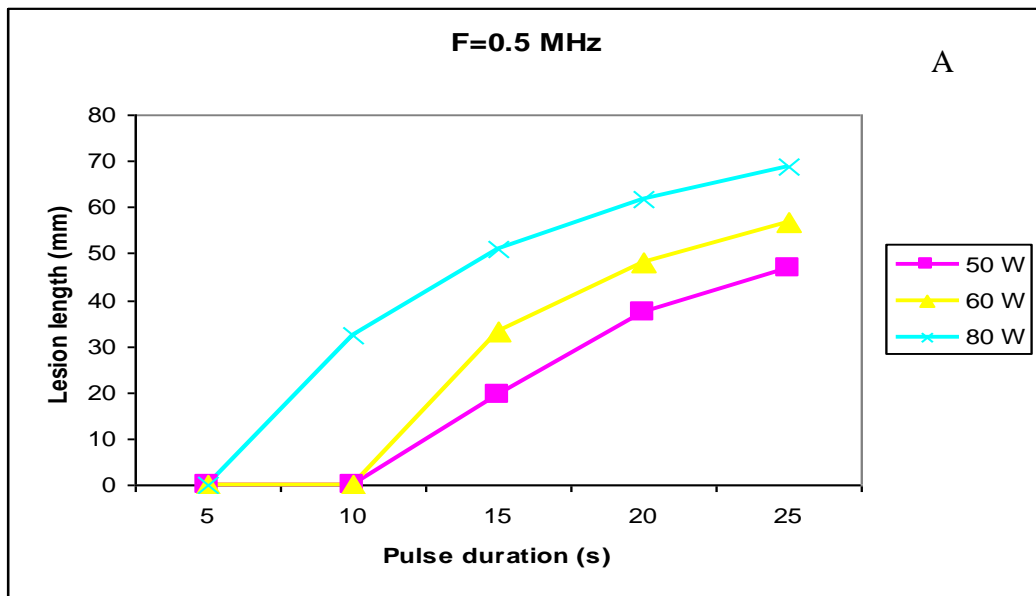


Figure 6.2 A. Lesion length distribution versus pulse duration for the 0.5 MHz transducer (power= 50W, 60W, and 80W, D=5 cm and Focal Depth=5 cm); B. Lesion width distribution versus pulse duration for the 0.5 MHz transducer (power= 50W, 60W, and 80W, D=5 cm and Focal Depth=5 cm).

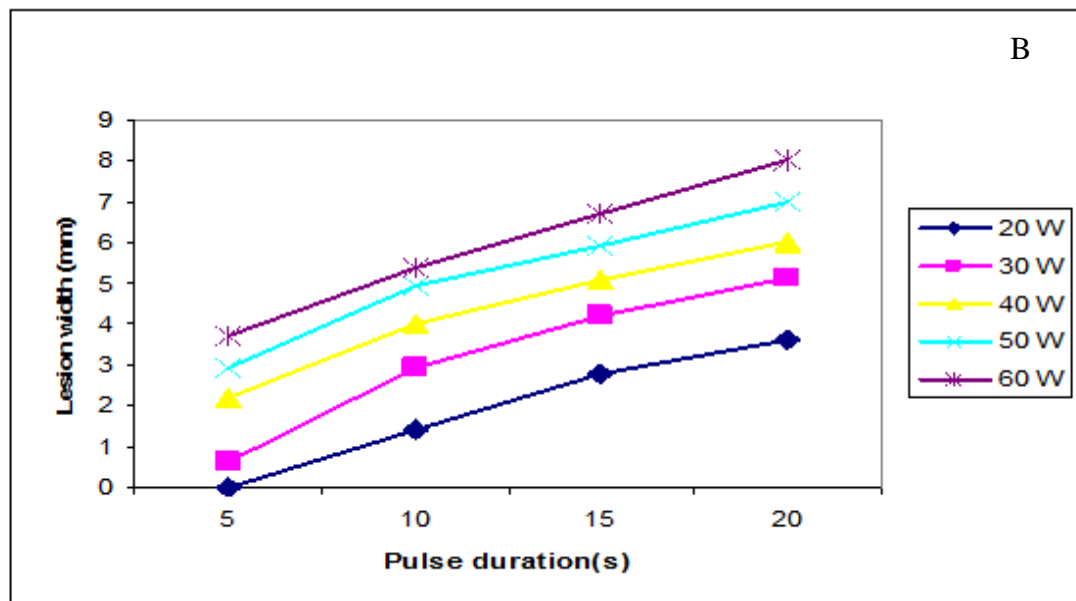
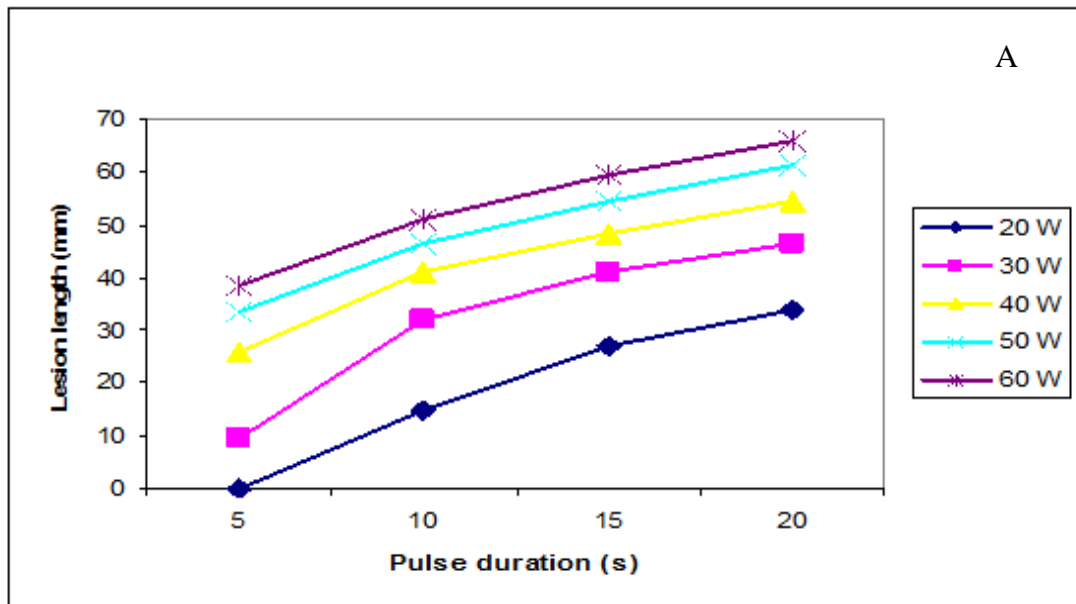


Figure 6.3 A. Lesion length distributions versus pulse duration for the 1 MHz transducer (power= 20W, 30W, 40W, 50W, and 60W, D=5 cm and Focal Depth=5 cm); B. Lesion width distributions versus pulse duration for the 1 MHz transducer (power= 20W, 30W, 40W, 50W, and 60W, D=5 cm and Focal Depth=5 cm).

Figure 6.4 shows the lesion length and lesion width distribution for the 1.5 MHz transducer. The transducer diameter (D) is 5 cm with a 10 cm radius of curvature (R). The focus is at approximately 10 cm, 5 cm deep in the tissue. The effect of pulse duration on the lesion size was investigated using power of 20W, 30W, and 40W. The lesion length and width are increased with increased pulse duration.

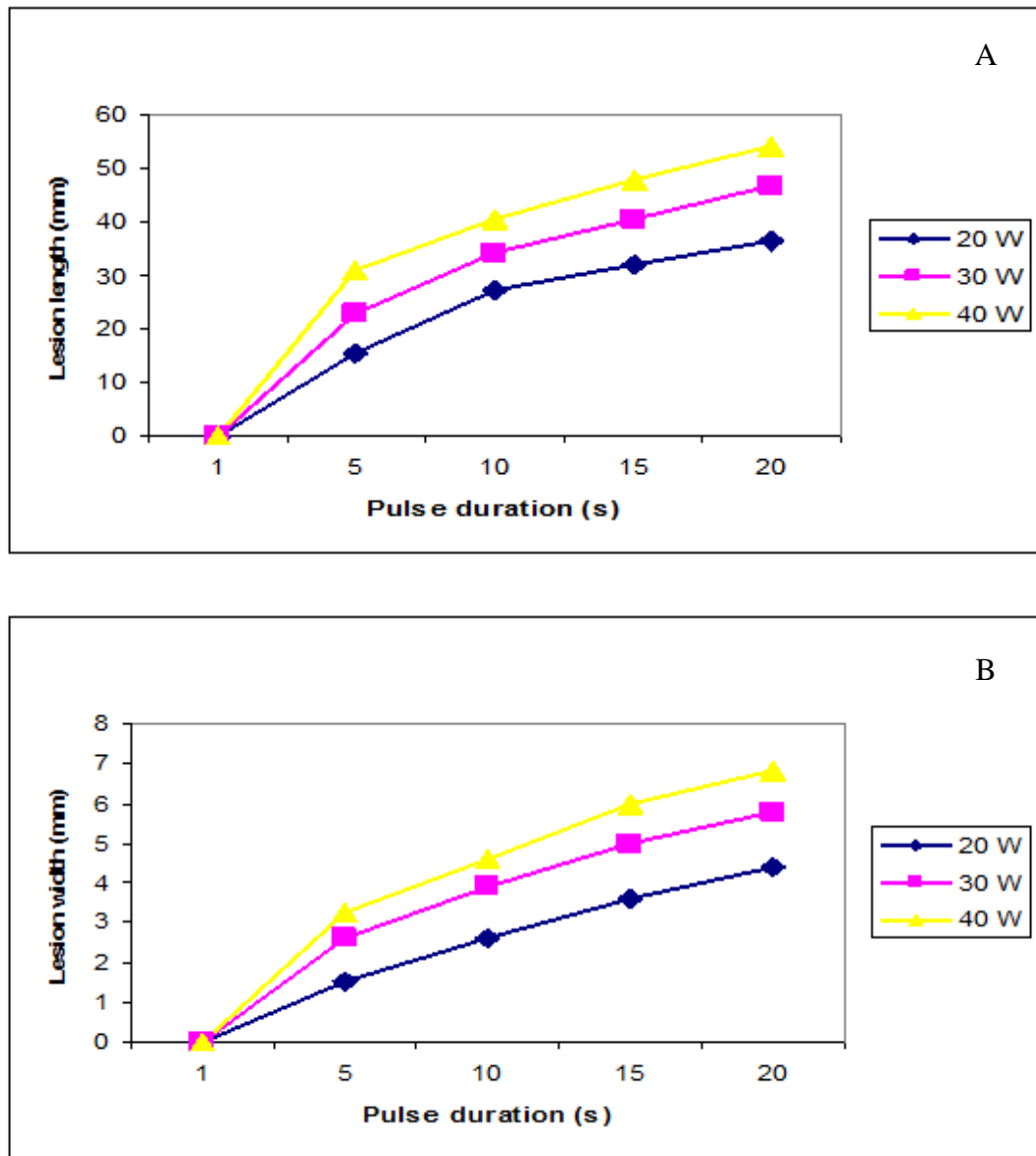


Figure 6.4 A. Lesion length distributions versus pulse duration for the 1.5 MHz transducer (power= 20W, 30W, and 40W, D=5 cm and Focal Depth=5 cm); B. Lesion width distributions versus pulse duration for the 1.5 MHz transducer (power= 20W, 30W, and 40W, D=5 cm and Focal Depth=5 cm).

Figure 6.5 shows the lesion length and lesion width distribution at 1 MHz transducer. The transducer diameter (D) is 5 cm with a 10 cm radius of curvature (R). The focus is at approximately 10 cm, 1 cm deep in the tissue. The effect of pulse duration on the lesion size was investigated using power of 20W, 30W, and 40W. The lesion length and width are increased with increased pulse duration.

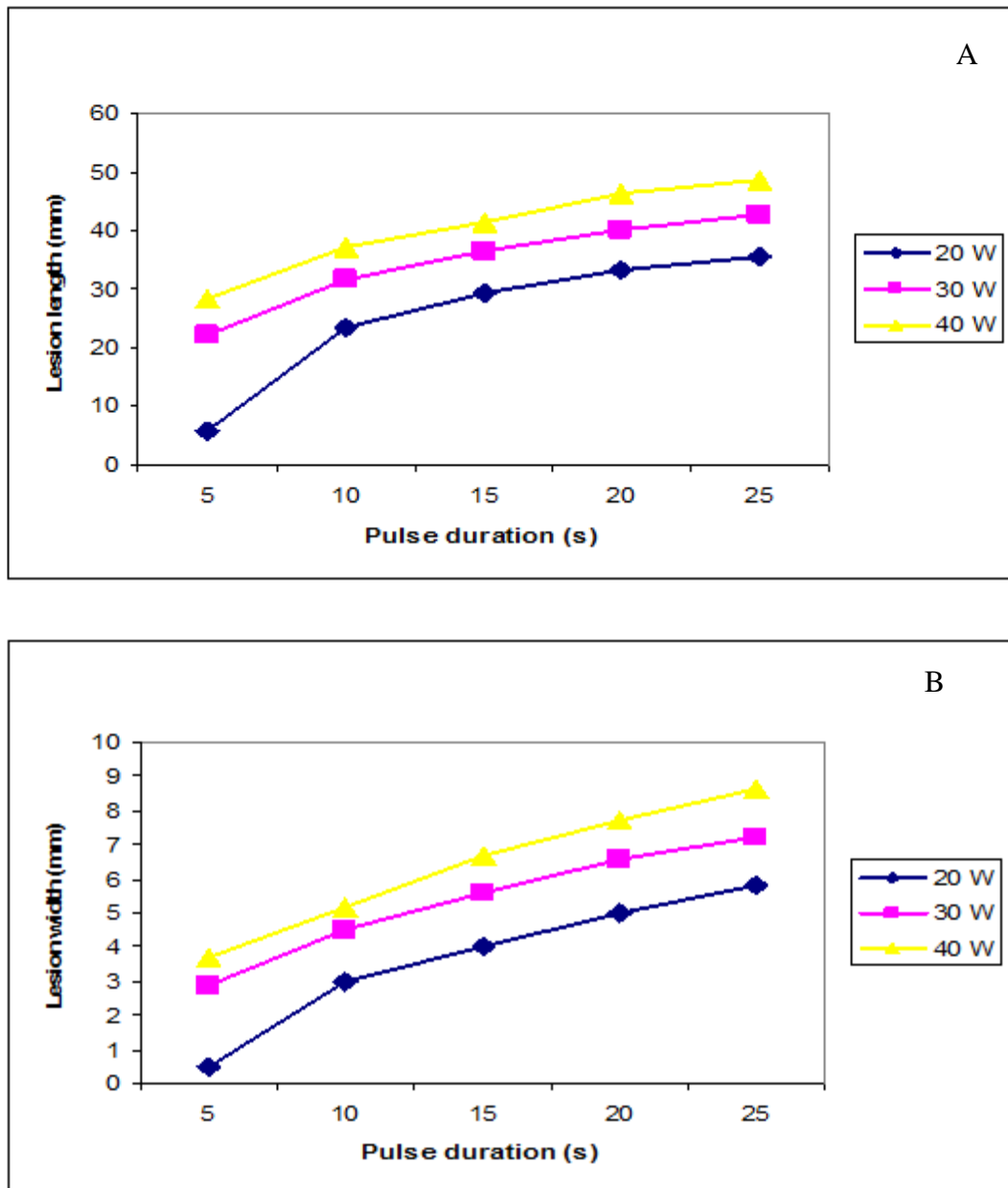
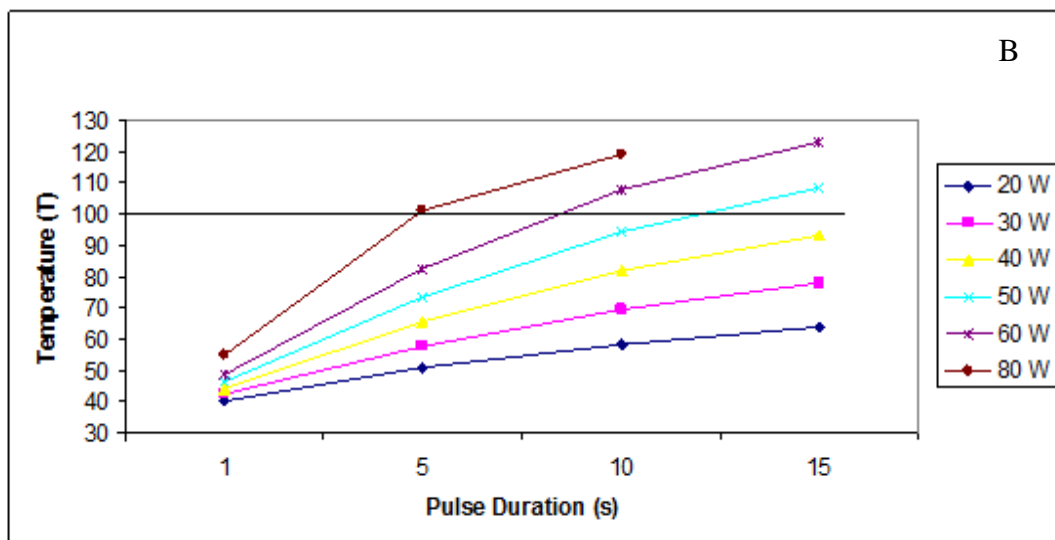
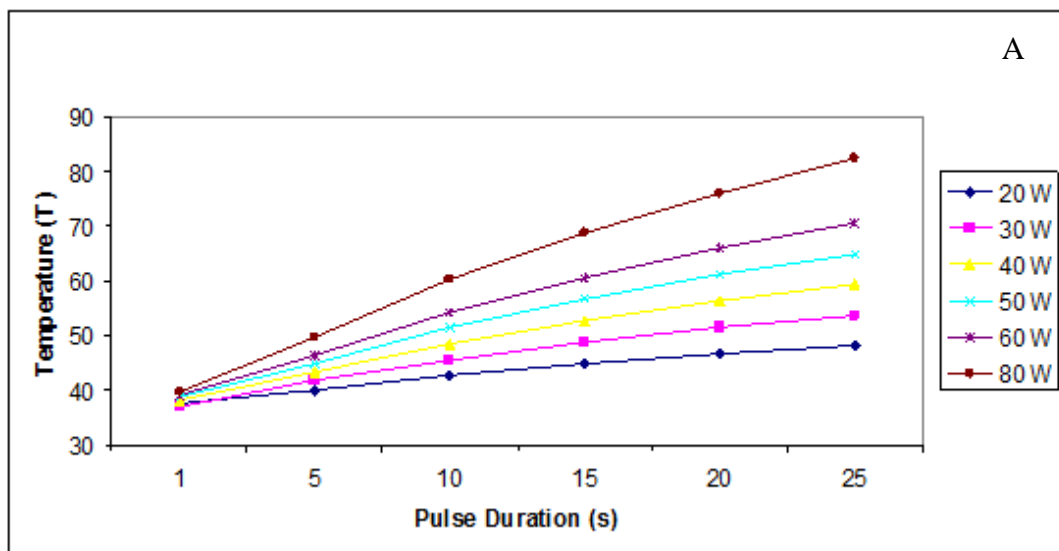


Figure 6.5 A. Lesion length distributions versus pulse duration for the 1 MHz transducer (power= 20W, 30W, and 40W, D=5 cm and Focal Depth=1 cm); B. Lesion width versus pulse duration for the 1 MHz transducer (power= 20W, 30W, and 40W, D=5 cm and Focal Depth=1 cm).

6.4.2 SIMULATION RESULTS FOR TEMPERATURE VS. TIME FOR DIFFERENT POWER AND FREQUENCY.

Figure 6.6 shows the temperature at the focal point for the 0.5 MHz, 1 MHz, and 1.5 MHz transducers. The transducers diameter (D) is 5 cm with a 10 cm radius of curvature (R). The focus in tissue at approximately 5 cm deep in the tissue, except figure 6.6d were the focus is at 1 cm deep in the tissue. The effect of temperature elevation is investigated using power of 20W, 30W, 40W, 50W, 60W, and 80W. The temperature is increased with increased pulse duration and eventually a saturation point is reached.



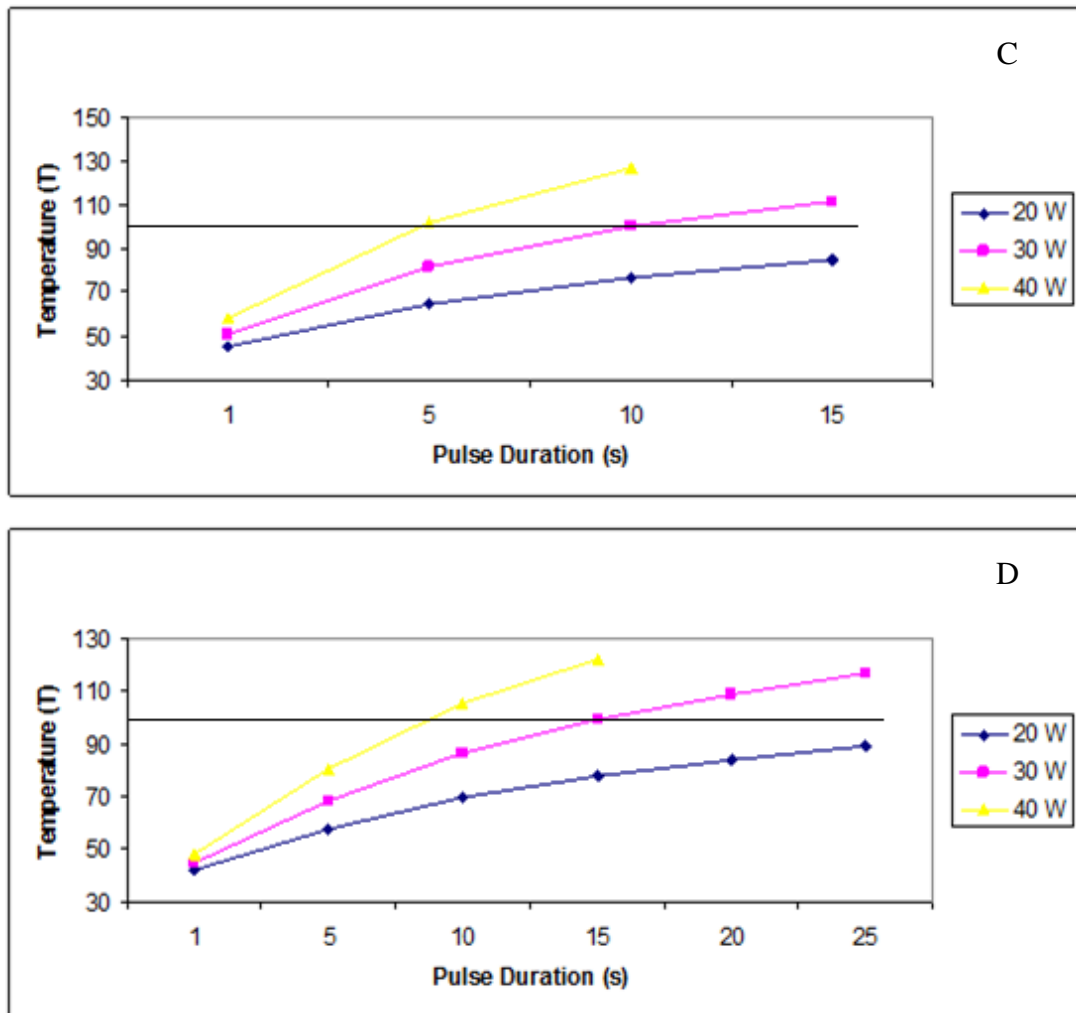


Figure 6.6 Temperature at the focus versus pulse duration for the A. 0.5 MHz transducer (power= 20W, 30W, 40W, 50W, 60W, and 80W, D=5 cm and Focal Depth=5 cm); B. 1 MHz transducer (power= 20W, 30W, 40W, 50W, 60W, and 80W, D=5 cm and Focal Depth=5 cm); C. 1.5 MHz transducer (power= 20W, 30W, and 40W, D=5 cm and Focal Depth=5 cm); D. 1 MHz transducer (power= 20W, 30W, and 40W, D=5 cm and focal depth=1 cm).

6.4 DISCUSSION

The simulation results can give us a good indication regarding lesion size (length and width) and temperature elevation at the focal point. Also, the simulation results can have a significant contribution in the development of the transducers. These results will guide us towards the best sonication system in a faster and more appropriated way than using extensive animal experiments.

The simulation results suggest that the lesion size can be controlled by adjusting the duration of the sonication and by adjusting the amount of the acoustical

power. Figure 6.2, 6.3, 6.4, and 6.5 shows that the lesion size increases with the pulse duration because the longer the duration, the higher the temperature elevation and the larger the heated volume at the focal point. The size of the lesions can be changed by varying the focal shape and size, which are controlled by the operating frequency and transducer geometry.

Figure 6.2 shows the lesion length and lesion width for 0.5 MHz frequency. Lesion size may approach saturation point at higher power but with the risk of reaching the boiling point. For example, with pulse duration of 20 s and power of 50 W, lesion length is 37 mm long and lesion width is 4 mm (adequate lesion). With the same pulse duration (20 s) but with power of 80 W the lesion length is 60 mm and the lesion width is 7 mm which is very large lesion but you may reach the boiling point.

Using frequency of 1 MHz, power of 20 W, pulse duration of 20 s and with focal depth of 1 cm we have noticed that the lesion length was 32 mm and the lesion width was 4.5 mm (figure 6.5). When the focal depth was changed to 5 cm, lesion length was increased to 35 mm but lesion width was decreased to 3.8 mm (figure 6.3). Therefore, the deeper as we go into the tissue, the lesion length is increased but the lesion width is decreased. The system behaves the same way for different pulse duration and for different power.

Comparing figures 6.5 with 6.3 we can observe that if the focal depth is closed to the skin (1 cm deep), then the lesion width is increased and the lesion length is decreased (compared to 5 cm depth). In addition, comparing figures 6.6B with 6.6D we can observe that the temperature is higher when the focal depth is closed to the skin (1 cm). This is happening because intensity drops less at points closer to the transducer surface and decreases deeper into the tissue due to the attenuation and absorption. Also, when the focus is closed to the surface, lesion length is limited due to the skin boundaries while the lesion width is not. As the frequency increases from 1 MHz to 1.5 MHz (figure 6.4 and 6.5) and using the same power, it was observed that lesion size remains the same.

When frequency of 0.5 MHz is used, with focal depth of 5 cm and with any power, boiling point is never reached. When higher frequency (1 MHz and 1.5 MHz) is used with high power, boiling point may be reached. For example, with frequency of 1 MHz or 1.5 MHz, pulse duration of 10 s and focal depth of 5 cm, any power above 50 W or 30 W respectively will reach the boiling point. Table 6.1 presents a summary of the simulation results showing the recommended parameters that can be used for an ideal HIFU system.

Table 6.1 Summary of the recommended simulation results

F = 0.5 MHz (Focal Depth = 5 cm)			
Power (W)	Pulse Duration (s)	Temperature (°C)	Lesion: Length/Width (mm)
30 - 80	10 - 50	60.3 – 68.8	19.6 – 51 / 1.85 - 5.5
F = 1 MHz (Focal Depth = 5 cm)			
Power (W)	Pulse Duration (s)	Temperature (°C)	Lesion: Length/Width (mm)
20 - 50	4 - 20	64 – 73.7	25.7 – 33.6 / 2.2 – 3.6
F = 1 MHz (Focal Depth = 1 cm)			
Power (W)	Pulse Duration (s)	Temperature (°C)	Lesion: Length/Width (mm)
20 – 40	5 – 20	69 – 86.7	23.6 – 31.6 / 2.9 – 4.5
F = 1.5 MHz (Focal Depth = 5 cm)			
Power (W)	Pulse Duration (s)	Temperature (°C)	Lesion: Length/Width (mm)
20 - 50	1 - 5	64.6 – 81.5	15 – 27.1 / 1.2 – 2.6

The following chapter presents experiments in phantoms and excised brain tissue in animals *in vitro* and *in vivo*. The creation of large and deep lesions is demonstrated. Also, the effectiveness of MRI to monitor therapeutic protocols of HIFU in the brain is investigated.

CHAPTER 7: *IN VITRO* AND *IN VIVO* (RABBIT BRAIN) PENETRATION OF HIFU USING MR IMAGING.

7.1 INTRODUCTION

Thermal ablation of brain in animals with high intensity focused ultrasound (HIFU) was very popular in the 50's and 60's [3][135]. HIFU was used in the clinical setting by Fry and Johnson [136] and showed that HIFU had the potential to treat brain cancer. Several groups such as Britt et al [137] and Guthkelch et al [138] have used hyperthermia (heating of several minutes at 43°C) to treat brain tumours. The clinical trials were abandoned probably due to the inexistence of effective imaging modality to guide the therapy. Especially for the case of brain, it is extremely important to have absolute control of the ablation in order to avoid vital brain tissue damage such as the neurons. Now with the advancement of HIFU technology guided by magnetic resonance imaging (MRI), it will be possible to conduct clinical studies for brain cancer. Today, there is only one clinical study using the ExAblate (MRgFUS Surgery Treatment of Brain Tumors) system and is started on November 2011 by InSightec to treat Glioma and Metastatic Brain Cancer [139].

Since 1994 several studies by the group of Dr. Hynynen [124], [140], [141], [142], [143], [144] demonstrated the creation of lesions in animal brain and the use of MRI for monitoring. However, in these studies only pure thermal lesions were shown. Also, in the above studies the production of well-controlled large lesions was never demonstrated. Currently there is a HIFU system, which is guided by MRI developed by Insightech, which treats fibroids [60]. This system which is already FDA approved has been deployed in 30 locations worldwide. Therefore, HIFU guided by MRI, opens the possibility for treating tumours in other organs.

In this chapter, we have explored extensively the use of MRI to image both lesions created under thermal and cavitation or boiling mechanisms. Also in this work, it was demonstrated the creation of well-controlled large thermal and bubbly lesions. Another issue that was never demonstrated in previous studies is

the lesion penetration deep in tissue, an issue which is explored in this chapter for *in vitro* and *in vivo* exposures.

Single element spherically focused transducers of different diameter; different focusing and operating frequency (table 7.1) were used in this study. The transducer was scanned in a 3-d grid using an MRI compatible mechanical positioning device designed and developed by Damianou et al. [145]. The positioning device designed is simple, cost effective, portable and universal. By universal, we mean that it can be used in any MRI scanner available, since it is placed on the table of the MRI scanner and therefore integration with all MRI scanners is possible. Also, the current device includes a flexible coupling system, and thus it can be used in all the anatomies accessible by HIFU (liver, kidney, breast, brain and pancreas). For the experiments *in vitro*, non-degassed freshly excised lamb brain tissue it was used. Lamb brain is a good experimental model for easily initiating cavitation, due to the trapped bubbles in the brain vasculature. For the *in vivo* experiments, New Zealand adult rabbits were used.

The main goal of this chapter is to investigate the effectiveness of MRI to monitor therapeutic protocols of HIFU in the brain. Thus, we have used the basic pulse sequences T1-w and T2-w fast spin echo (FSE). These MRI pulse sequences have been successful in other organs regarding their ability to identify thermal lesions. For example in muscle the contrast of lesions was investigated by Hynynen et al. [146], in kidney by Hynynen et al. and Damianou et al. [147][148], in liver by Rowland et al. [149], and in prostate by Rouviere et al. and by Pisani et al. [150][151]. We have also use FLAIR since this is the predominant pulse sequence used in brain in the clinical setting.

7.2 HIFU/ MRI SYSTEM

Figure 7.1 shows the block diagram of the HIFU/MRI system which includes the following subsystems: 1) HIFU system, 2) MR imaging, 3) Positioning device (robot), 4) Temperature measurement, and 5) MRI compatible camera. All subsystems are described below.

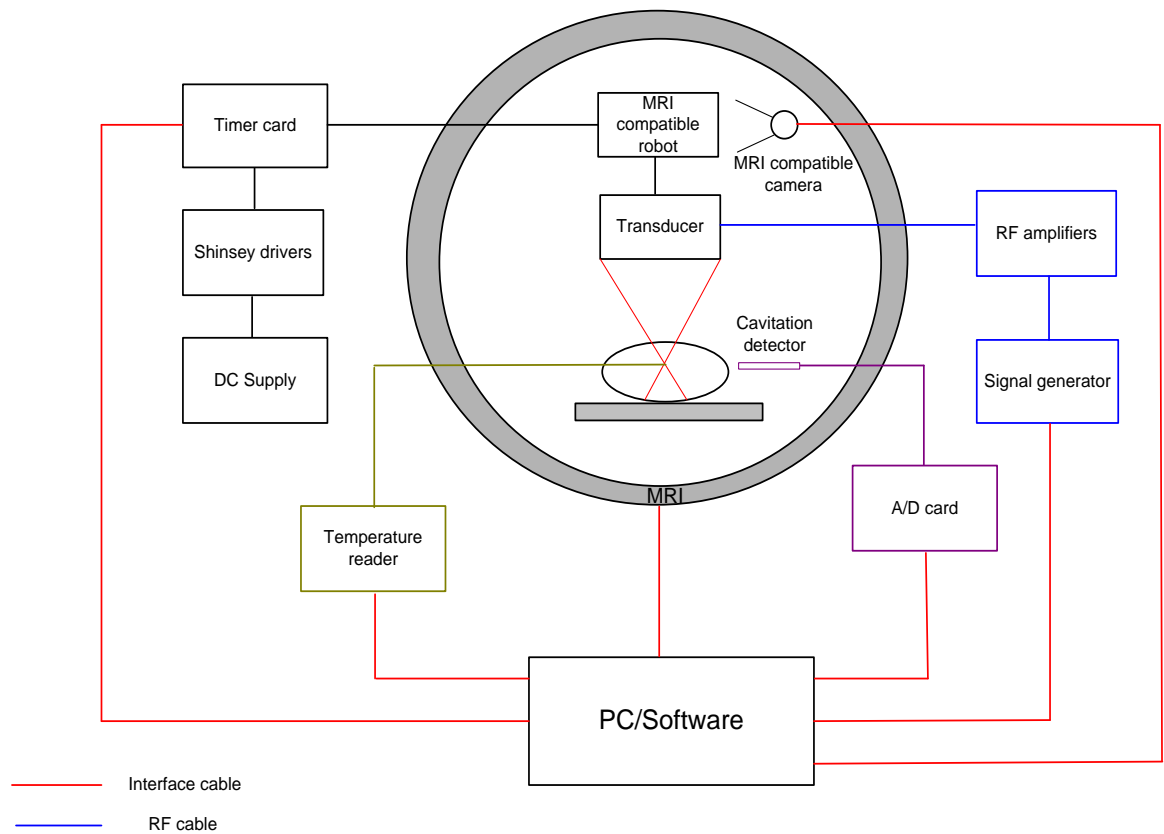


Figure 7.1. Block diagram of the HIFU system under MRI guidance.

7.2.1 HIFU SYSTEM

The HIFU system consists of a signal generator (HP 33120A, Agilent technologies, Englewood, CO, USA), a RF amplifier (250 W, AR, Souderton, PA, USA), and a spherically shaped bowl transducer made from piezoelectric ceramic of low magnetic susceptibility (Etalon, Lebanon, IN, USA). Two transducers were used to create single or large lesion either *in vitro* or *in vivo* experiments. For the *in vitro* experiments freshly lamb brains were used and for *in vivo* experiments rabbits were used. Table 7.1 list both transducers used in the experiments and their parameters. The transducer was rigidly mounted on the MRI-compatible positioning system (MEDSONIC LTD, Limassol, Cyprus) which is described at the next page.

Table 7.1 transducer parameters

	Transducer	Focal Depth	Diameter	Animal / Method
1.	1 MHz	10 cm	5 cm	Lamb Brain / <i>in vitro</i> Rabbit Brain / <i>in vivo</i>
2.	2 MHz	10 cm	5 cm	Lamb Brain / <i>in vitro</i> Rabbit Brain / <i>in vivo</i>

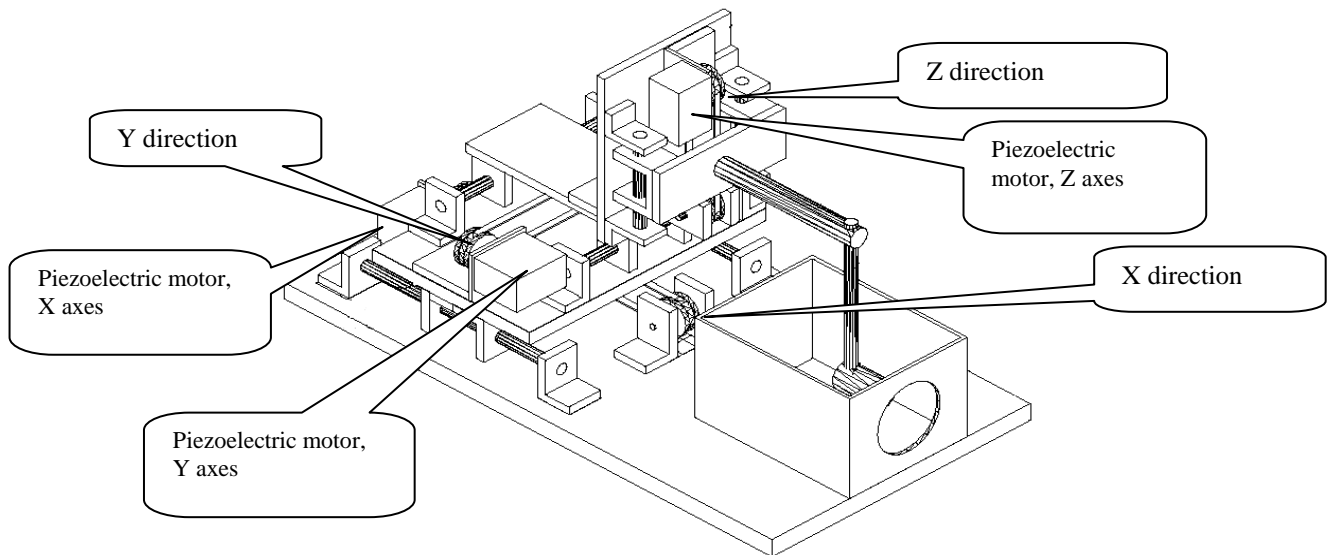
7.2.2 MRI IMAGING

The 3-d positioning device and the transducer were placed inside a MRI scanner (Signa 1.5 T, by General Electric, Fairfield, CT, USA). A brain coil (USA instruments, Cleveland, OH, USA) was used to acquire the MRI signal.

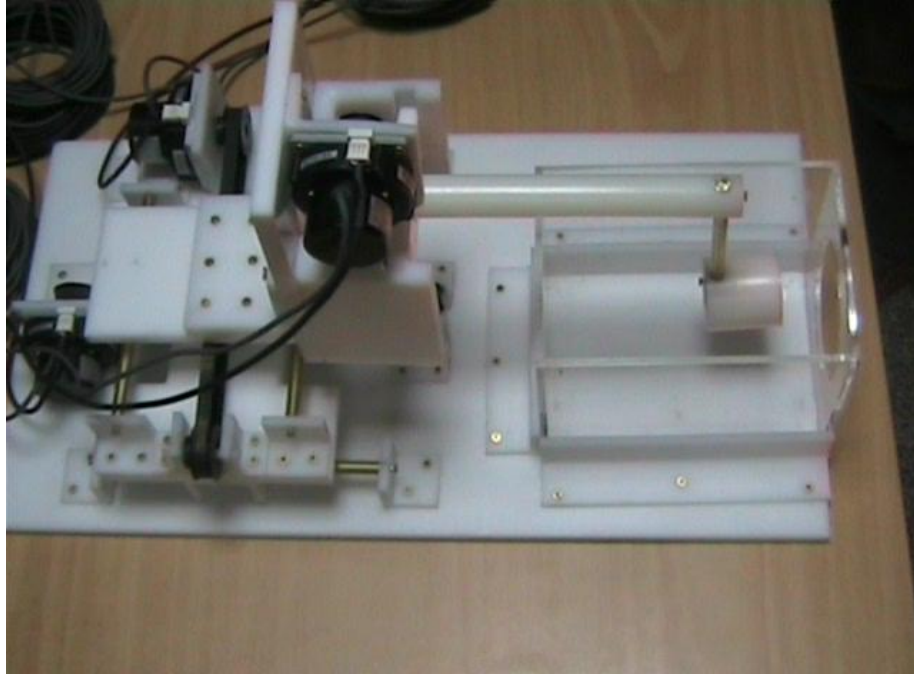
7.2.3. POSITIONING DEVICE

The robot has been developed by Damianou et al. [145] initially for three degrees-of-freedom (X, Y, Z direction), but it can be easily developed for 5 degrees of motion. Since the positioning device is placed on the table of the MRI scanner its height should be around 55 cm (bore diameter of the MRI scanner). The length of the positioning device is 45 cm and its width 30 cm. The weight of the positioning device is only 6 kg and therefore it can be considered portable. Figure 7.2A shows the complete mechanical design of the robot and figure 7.2B shows a photo of the robot made out of polyethylene.

The container was filled with degassed water. A plastic membrane was attached in the front hole of the container where the skull will be placed in order to avoid any air gaps. The transducer is immersed in the water container which is filled with degassed water or saline. The water is poured in a mylar bag. The mylar bag is made thin enough to conform to the contours of the target. A circular window is opened in the water container in order to allow ultrasound energy to be applied through the body.



A



B

Figure 7.2 A. The robot, the complete mechanical design; B. Photo of the robot.

7.2.4 TEMPERATURE MEASUREMENT

Temperature of brain tissue at the focal point is measured using a data acquisition system (HP 34970A, Agilent technologies, Englewood, CO, USA). Temperature is sensed using a 50- μm diameter T-type copper-constantan thermocouple (Physitemp Instruments, Inc. New Jersey, USA) which is MRI compatible. The thermocouple is placed in the tissue by means of a catheter. The thermocouple measures the temperature at the focus. This is achieved by applying low-intensity (low enough not to cause tissue damage) and during the application of ultrasound; the transducer is scanned accordingly in order to detect the maximum temperature. This establishes positioning of the thermocouple in the focus of the transducer. The temperature error of the thermocouple is in the order of 0.1°C.

7.2.5 MRI COMPATIBLE CAMERA

In order to monitor the condition of the animal or humans (future use), a MRI compatible camera (MRC Systems GmbH, Heidelberg, Germany) was mounted on the system. The camera was interfaced by means of a video card. With the aid of the MRI compatible camera the researcher can monitor the welfare of the animal.

7.3 IN VITRO AND IN VIVO EXPERIMENTS

Various *in vitro* experiments were carried out to image (using MRI) the lesions created in brain tissue using HIFU. The acoustical coupling of Figure 7.3 was used for the *in vitro* and *in vivo* experiments. With this method, the tissue is placed outside the water container, which is filled with degassed water. Due to the weight of the water container, the coupling with this method is excellent. This method can be described as a superior to inferior approach, meaning that the transducer is on top of the tissue. In commercial systems the approach used is inferior to superior, meaning that the transducer is below the tissue.

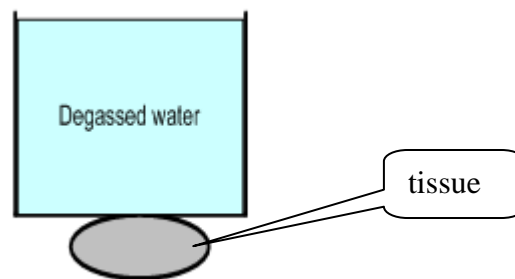


Figure 7.3 Coupling method used for *in vitro* and *in vivo* experiments.

The tissue was placed on top of an absorbing material in order to shield adjacent tissue from stray radiation from the bottom. The transducer was placed on the arm of the positioning device and was immersed in the water tank, thus providing good acoustical coupling between tissue and transducer. Any bubbles that may have collected under the face of the transducer were removed in order to eliminate any reflections. In all experiments, the tissues used were extracted from non-degassed freshly killed lamb, and the experiment was conducted in the same day. Totally 22 lamb brains were ablated for investigating various issues.

For the *in vivo* experiments, New Zealand adult rabbits were used weighting approximately 3.5-4 kg. Totally 8 rabbits were used in the experiments. The rabbits were anaesthetized using a mixture of 500 mg of ketamine (100 mg/mL, Aveco, Ford Dodge, IA), 160 mg of xylazine (20 mg/mL, Loyd Laboratories, Shenandoah, IA), and 20 mg of acepromazine (10 mg/mL, Aveco, Ford Dodge, IA) at a dose of 1 mL/kg. The animal experiments protocol was approved by the

national body in Cyprus responsible for animal studies (Ministry of Agriculture, Animal Services).

Using a single element transducer it was very difficult to penetrate through the skull and it was also very difficult to locate the focus since the signal was shifted. In addition, the presence of the skull in the ultrasonic path not only distorts the field by reflection, but may also destroy the underlying tissue in contact with it by absorbing ultrasonic energy and dissipating it as heat. A craniotomy adequate in extent to permit unimpeded passage of the cone of sound was imperative. The extent of the craniotomy depends on the solid angle of radiation and the depth of the target from the cranial surface. The larger the angle and the deeper the target, the larger the size of craniotomy needed. For the transducer used and a target depth of 1 cm, a circular craniotomy of 3 cm in diameter was adequate.

To perform histology on the rabbit brain after a lesion was created and to observe under the microscope (Olympus, BX51TF, Tokyo, Japan) how dead cells versus live cells appear, a trypan blue was used. Trypan blue is a mark that can be applied on living cells without killing them. It can selectively colour dead tissues. Live tissues are not coloured. However, it traverses the membrane in a dead cell or tissue. The dead cells are shown as a distinctive blue colour under the microscope. Using frequency of 1 MHz at the same target of 1 cm, lesion in the brain was created. As soon as the lesion was created a trypan blue (0.5 ml/Kg) was injected through the ear artery.

To process histology the brain tissues were sliced into very thin sections for observation on the light microscope, after they were first processed to prevent cell damage. The processing involved a series of steps:

- Fixation: Chemical fixatives are used to preserve tissue from degradation and to maintain the structure of the cell and of sub-cellular components.
- Dehydration: Water has to be removed from tissues and replace with a medium that solidifies to allow thin sections to be cut.
- Embedment: The tissue samples are placed into molds along with liquid embedding material (such as wax) which is then hardened.

- Sectioning: A steel knife mounted in a microtome is used to cut 4-10 micrometer-thick tissue sections which are mounted on a glass microscope slide.
- Staining: Staining is employed to give both contrast to the tissue as well as highlighting particular features of interest.
- Mounting: To preserve and support a stained section for light microscopy, it is mounted on a clear glass slide, and covered with a thin glass cover slip. The slide and coverslip must be free of optical distortions, to avoid viewing artifacts.
- Observation: Light microscope to make observations on the cellular structure of the slices.

7.4 HIFU PARAMETERS

The *in situ* spatial average intensity was estimated based on the applied power and the half-power width of the beam of the transducer. The details of the intensity estimation can be found in Damianou [152]. To create lesions in lamb or rabbit brain two transducers (table 7.1) operating at 1 MHz and 2 MHz were used. The ultrasound exposure used was 10 s, 20 s, and 30 s with 10 s delay between successive firings. In order to create large lesions, a square grid pattern of 4x4 overlapping lesions was used. The spacing between successive transducer movements was 2 mm, which creates overlapping lesions for the intensity and pulse duration used. In all experiments, the focal point was at 1 cm inside the tissue.

7.5 MRI PROCESSING AND SIMULATION

The parameters used for the MRI processing were:

T1-W FSE: TR=500 ms, TE=9 ms, slice thickness=3 mm (gap 0.3 mm), matrix=256x256, FOV=16 cm, NEX=1, and ETL=8.

T2-W FSE: TR=2500 ms, TE=60 ms, slice thickness=3 mm (gap 0.3 mm), matrix=256x256, FOV=16 cm, NEX=1, and ETL=8.

FLAIR: TR=8000 ms, TE=80 ms, slice thickness=3 mm (gap 0.3 mm), matrix=256x256, FOV=16 cm, NEX=1, ELT=8, and inversion time=1200-2200ms. The Region of Interest (ROI) was circular with diameter of nearly 2 mm.

The simulated signal intensity for the FSE MRI sequence was estimated based on the following Equation:

$$S = N \left(1 - e^{-\frac{t}{T_1}} \right) e^{-\frac{t}{T_2}}$$

Where S is the MRI signal, N is the proton density, t is time, T_1 is the spin-lattice relaxation time, and T_2 is the spin-spin relaxation time. The figure of noise was taken from values measured during the experiments. The Contrast to noise ratio (CNR) was obtained by dividing the difference in the signal intensity of lesion and normal tissue by the standard deviation of the noise.

7.6 RESULTS

The results demonstrates that with this system we were able to create single lesions, large lesions (by producing overlapping lesions), lesions deep in the brain and it was possible to monitor these lesions using MRI with excellent contrast. In addition, we have used trypan blue in order to perform histology on the rabbit brain after the creation of lesion. The experimental and simulated results (chapter 6) are comparable, indicating that the simulation model can be used for guidelines to various thermal protocols. Continues ultrasound was applied with pulse duration of 20 s using 1 MHz and 2 MHz transducer. In most cases, the lesion size (length and width) derived from the simulation results was bigger than the experimental.

Before creating large lesions in the brain (protocol to be used for treating tumours), we have tested the system in a gel phantom (SEA, Sunnyvale, CA, USA). Figure 7.4A shows a photograph of the large lesion created in the phantom at a plane perpendicular to the transducer beam. Figure 7.4B shows the corresponding photograph in a parallel plane. Figure 7.4C shows the MRI image of the result of figure 7.4A using T1-W FSE and figure 7.4D shows the same result using T2-W FSE. Figure 7.4E shows the MRI image of figure 7.4B using T2-W FSE. With T1-W FSE, we noticed that the contrast is poor because T_1 value of gel and lesion is very similar. With T2-W FSE, we noticed that the contrast is satisfactory because T_2 value of gel and lesion are sufficiently different. In addition, we can observe few small cavitations (the small black spots) within the lesion (figure 7.4D).

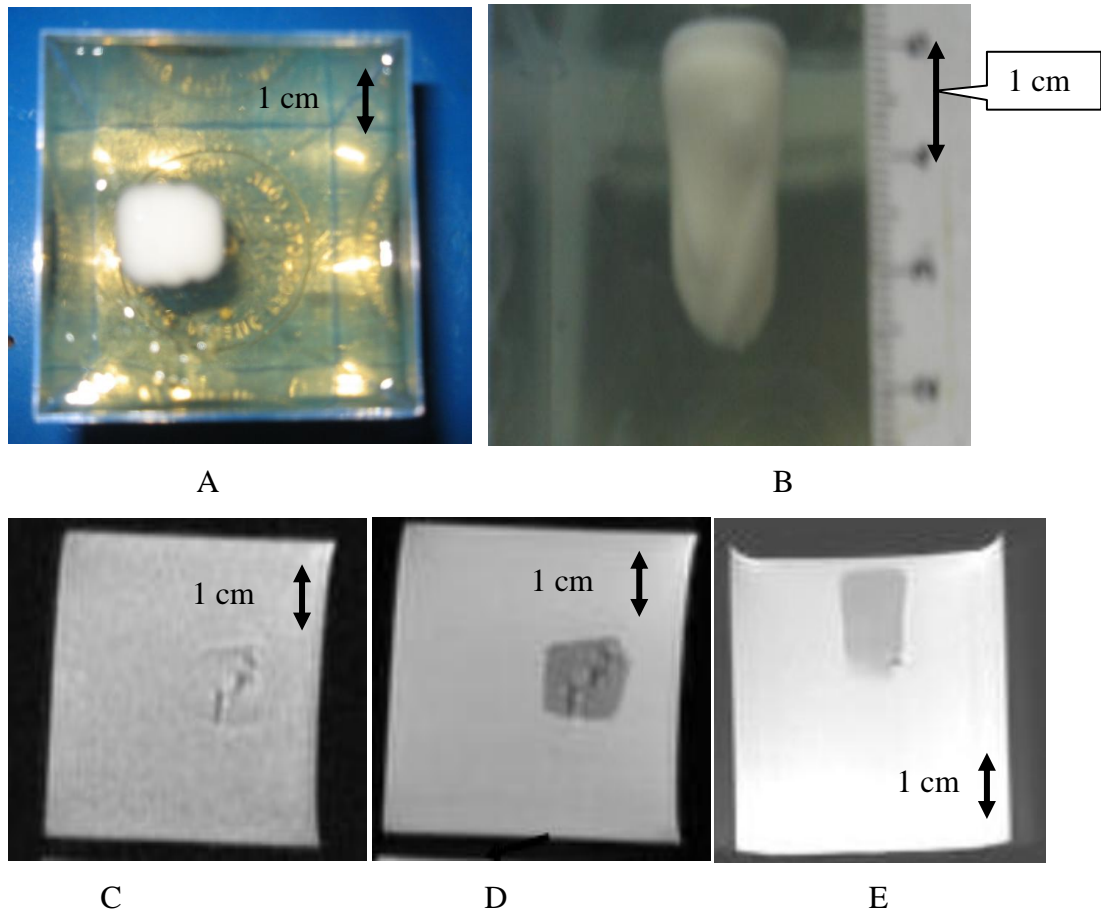
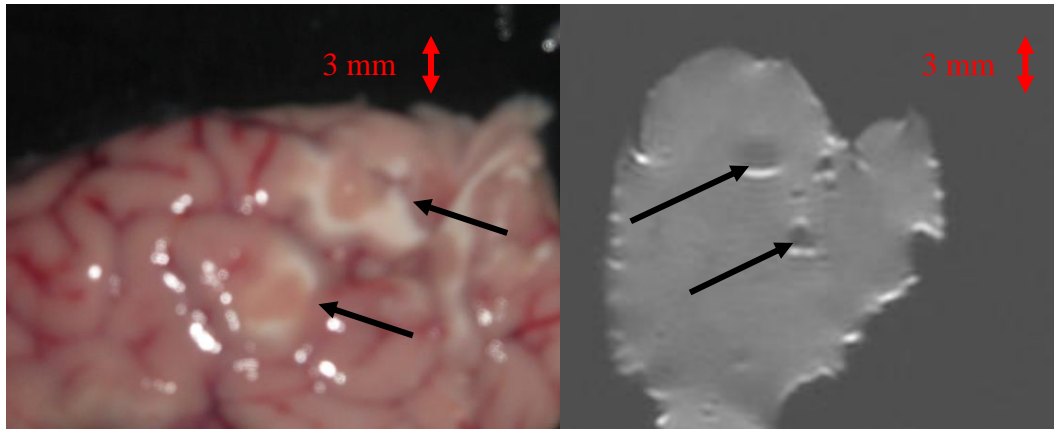


Figure 7.4 Large lesion in a gel phantom; A. photo of a large lesion at a plane perpendicular to the transducer beam; B. photo of a large lesion in a parallel plane; C. MRI image of figure 7.4A using T1-W FSE; D. MRI image of figure 7.4A using T2-W FSE; E. MRI image of figure 7.4B using T2-W FSE.

Using transducer with frequency of 1 MHz, single lesions were created in the lamb brain. The focal depth insight the tissue was at 1 cm. Single lesions were created using acoustic power of 70 W and 42.5 W, with ultrasound exposure of 10 s and 20 s respectively. Figure 7.5A shows a picture of the lesions created and figure 7.5B shows an MRI image of the same lesions. Figure 7.6 shows a lesion created using acoustic power of 60 W and with ultrasound exposure of 30 s.



A

B

Figure 7.5 Single lesions; A. picture of the lesions; B. MRI image (T1 FSE TR=500 ms).

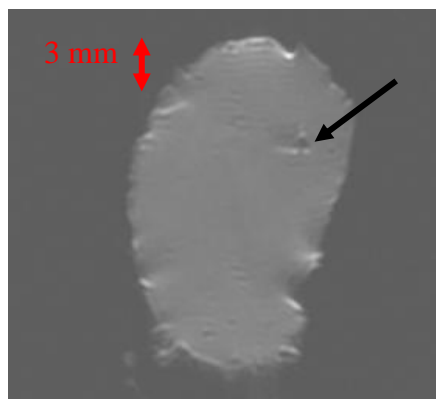


Figure 7.6 Single lesion (T1-w FSE TR=500 ms using 60W for 30 s, $f=1$ MHz and focal depth=1 cm)

Figure 7.7 shows 3 single lesions in brain *in vitro* using T1-w FSE. The lesion on the left was created using in situ spatial intensity of 1000 W/cm^2 for 20 s. The other two lesions were created using in situ spatial intensity of 2000 W/cm^2 for 20s. The two lesions in the left were created using thermal mechanisms (no acoustic emission was detected). The thermal lesions appear bright and the contrast with brain tissue is excellent. The lesion in the right was created under cavitation (acoustic emission detected) or due to boiling, and results to a cavity within the lesion. Therefore, the lesion appears dark, with bright margin (possibly in the early stage of the lesion development thermal mechanism existed). Although, two lesions were created with the same intensity (2000 W/cm^2), one of the lesions was created under thermal mechanisms, and the other one probably under cavitation mechanisms or possibly boiling. Although the intensity used would not result to temperatures above boiling, the high temperatures (caused possibly by cavitation) resulted possibly to tissue boiling. The presence of bubbles

in the vasculature is leading to the conclusion that the cavities formed are attributed most likely to cavitation.

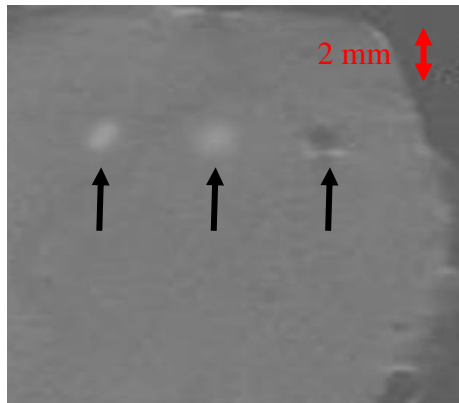


Figure 7.7 MRI images of three lesions in brain *in vitro* using T1-w FSE, $f=2$ MHz, $d=5$ cm and focal depth=1 cm.

Figure 7.8 shows MRI images of lesions created in lamb brain *in vitro* using in situ spatial intensity of 2000 W/cm^2 for 20 s and monitored using T1-w FSE (Figure 7.8A), T2-w FSE (Figure 7.8B), and FLAIR (Figure 7.8C). The parameters of these three sequences are described in section 7.5. With T1-w FSE the signal of the brain tissue is homogeneous, thus by using T1-w to monitor HIFU, the contrast between lesions and brain proves to be the best. T2-w FSE and FLAIR provides better anatomical information within the brain (gray and white matter are easily distinguished), however the contrast between lesion and brain is not of high quality. The reason is that if a lesion of low signal (such as a bubbly lesion) falls inside a region of the brain with low signal, then it is difficult to separate this type of lesion from brain tissue. The lesions in brain were visible approximately 10 minutes after the ablation.

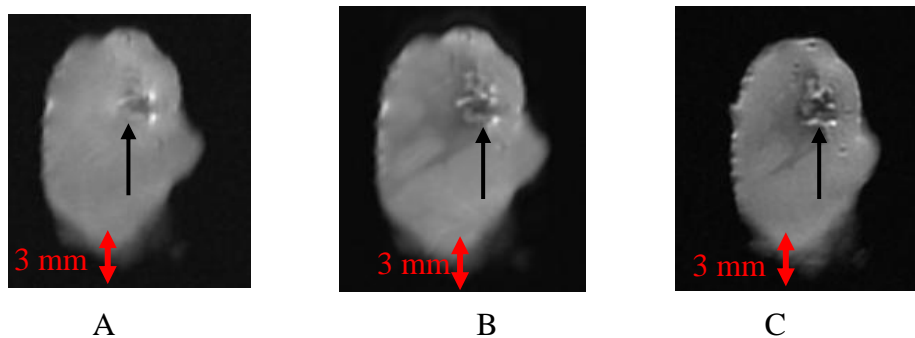


Figure 7.8 Images of large lesions monitored using MRI; A. T1-W FSE; B. T2-W FSE and C. FLAIR

The effect of TR on the CNR was evaluated using T1-W FSE at different TR (from 100 to 1000 ms). Figure 7.8A shows a lesion in brain *in vitro* using T1-W FSE (TR = 500 ms). Figure 7.9 shows the contrast to noise ratio (CNR) between lesion and brain plotted against TR for the MRI image of Figure 7.8A. Small percentage of experimental error is shown on the CNR vs TR and CNR vs TE graphs.

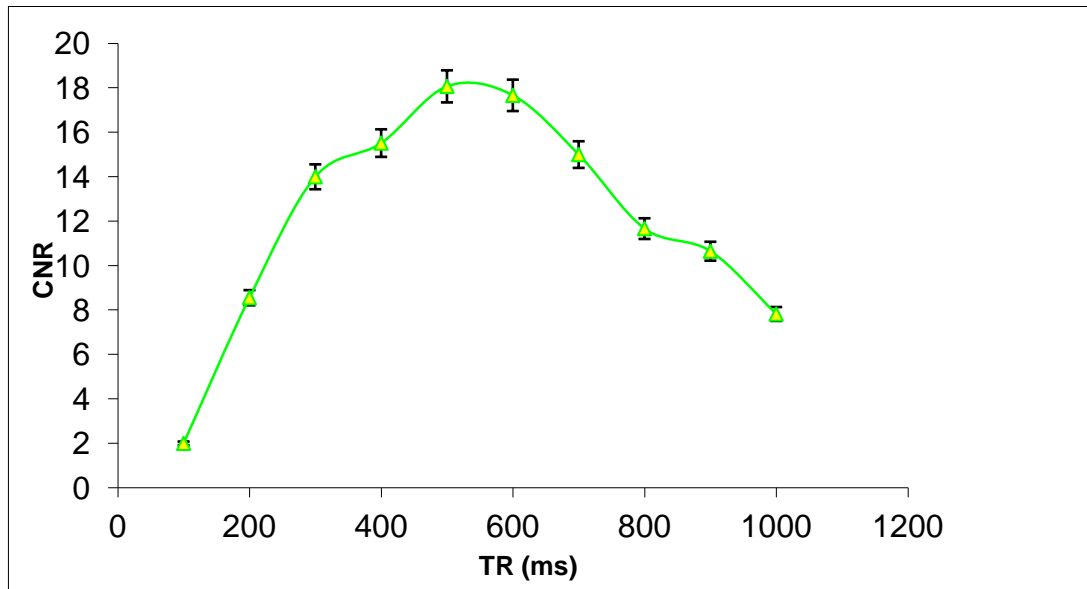


Figure 7.9 Contrast to noise ratio (CNR) vs. TR for T1-W FSE in excised lamb brain.

The effect of TE on the CNR was evaluated using T2-W FSE at different TE (from 10 to 140 ms). Figure 7.8B shows the MRI images of the same lesion as in Figure 7.8A using T2W FSE (TE = 60 ms). Figure 7.10 shows the CNR between lesion and brain plotted against TE for the brain and lesion of the MRI image of Figure 7.8B.

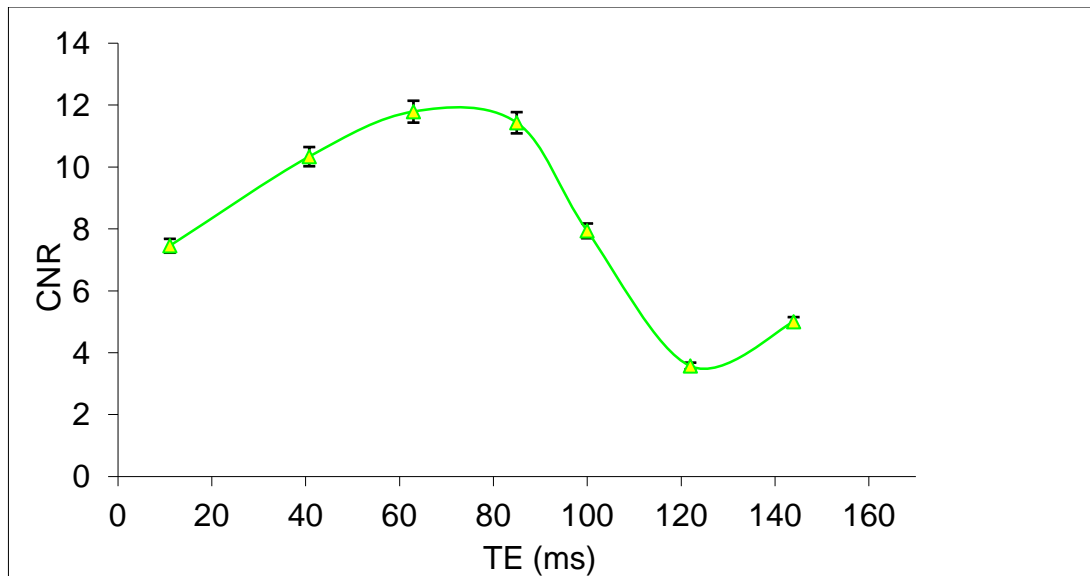


Figure 7.10 Contrast to noise ratio (CNR) vs. TE for T2-W FSE in excised lamb brain.

Figure 7.11 shows the MRI image of a large lesion in lamb brain *in vitro* created by scanning the transducer on a 4x4 grid using 2000 W/cm^2 and T1-W FSE resulting to a large bubbly lesion. Note that in some location no lesion was created due to poor ultrasound penetration and possibly due to the air bubbles trapped in the blood vessels. This image shows once more the excellent contrast between normal brain and lesions (in this case bubbly lesions).

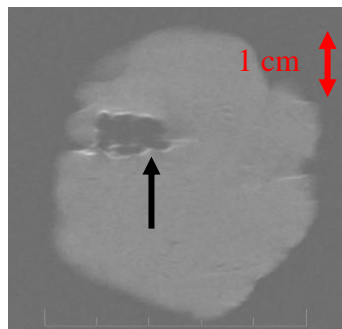


Figure 7.11 Image of a large lesion in lamb brain *in vitro* using T1-W FSE with $f=2 \text{ MHz}$, $d=5 \text{ cm}$ and focal length= 10 cm .

Figure 7.12 shows a lesion in rabbit brain *in vivo*. Focal depth for all lesions was at 1 cm. Single lesion was created using acoustic power of 36 W at exposure time of 20 s. Lesion created in the brain was confirmed by MRI. Transducer frequency of 1 MHz was used.

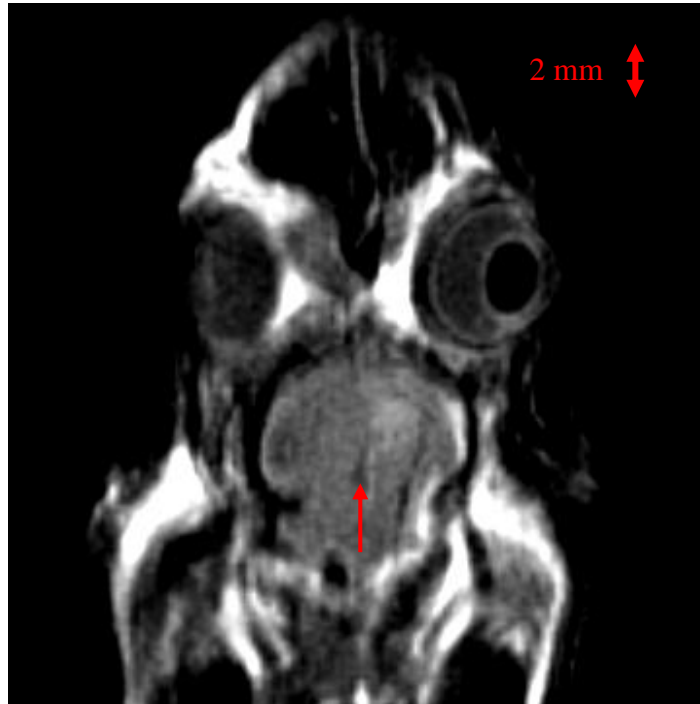


Figure 7.12 MRI image using T1-W FSE (with TR=500 ms) showing lesion width using $f=1$ MHz, $d=5$ cm and focal point=10 cm.

Using frequency of 1MHz, focusing at 1 cm deep in the brain and with intensity of 1000 W/cm^2 , lesion was created in rabbit brain in *in vivo*. As soon as the lesion was created, a trypan blue was injected through the ear artery. Figure 7.13A shows the injection of the trypan blue through the ear artery. After 20 min the rabbit was put into sleep and the brain was removed. Figure 7.13B demonstrates a picture of the brain showing how the brain appears with the trypan blue. Lesion was visible with gross anatomy using trypan blue. Figure 7.14 clearly shows the interface between lesion and brain tissue.



A

B

Figure 7.13 A. injection of the trypan blue; B. lesion as seen with the trypan blue.

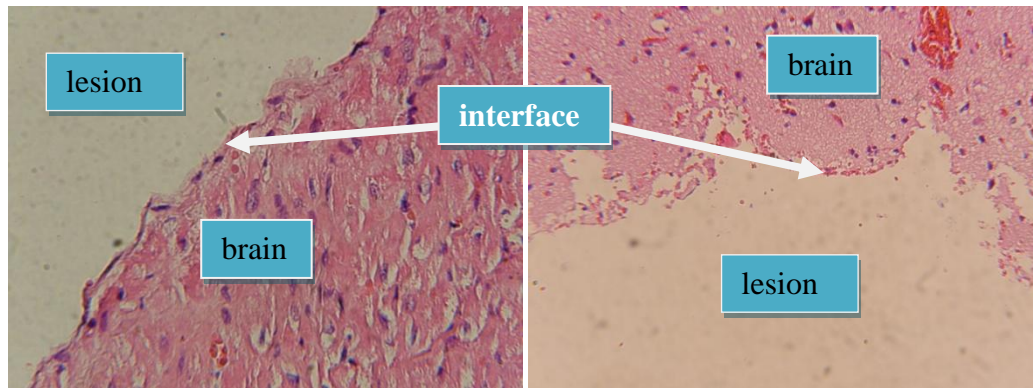


Figure 7.14 Lesion-brain tissue interface

Figure 7.15 shows ablation in rabbit *in vivo* using a 4x4 grid with intensity of 2000 W/cm^2 for 20 s and $f=2 \text{ MHz}$. This large lesion was created using thermal mechanisms and therefore the lesion appears bright. With T1, the signal in the brain is homogeneous (gray colour) and therefore the contrast with thermal lesion is excellent. The contrast of thermal lesions is definitely much better than the case of bubbly lesions. Unlike the *in vitro* case of Figure 7.11 where with this level of intensity bubbly lesions were created, in this *in vivo* example in none of the 16 lesions a bubbly lesion was produced. This proves our speculation that *in vitro* brain includes bubbles, which are responsible for producing bubbly lesions possibly due to cavitation.

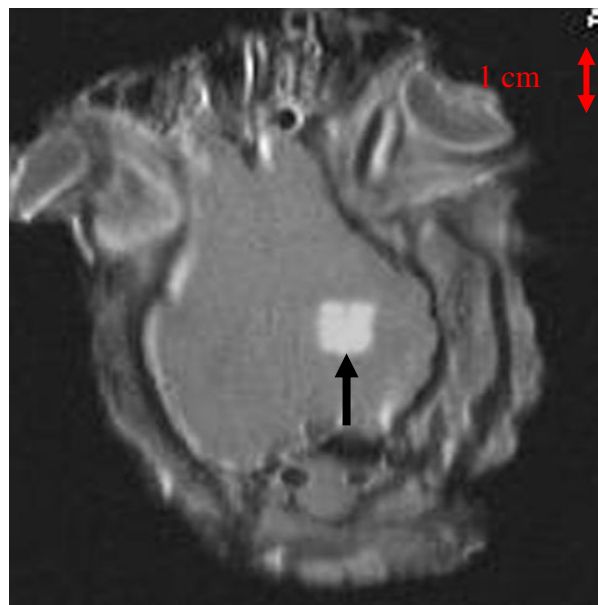


Figure 7.15 MRI image of a large thermal lesion in rabbit *in vivo* using T1-W FSE, $f=2\text{MHz}$ and focal depth=1 cm.

Figure 7.16 shows MRI images using T1-w FSE of a lesion deep in the lamb brain (*in vitro*) using in situ spatial average intensity of 1000 W/cm² for 20 s. The length of the lesions is smaller than expected, only 12 mm, possibly due to the reflection caused by the trapped bubbles. Figure 7.17 shows a lesion deep in brain *in vivo* under the same exposure conditions and transducer, and demonstrates that good penetration of HIFU in brain can be achieved if no bubbles are present. The lesion propagates all the way through the brain and is 20mm long.

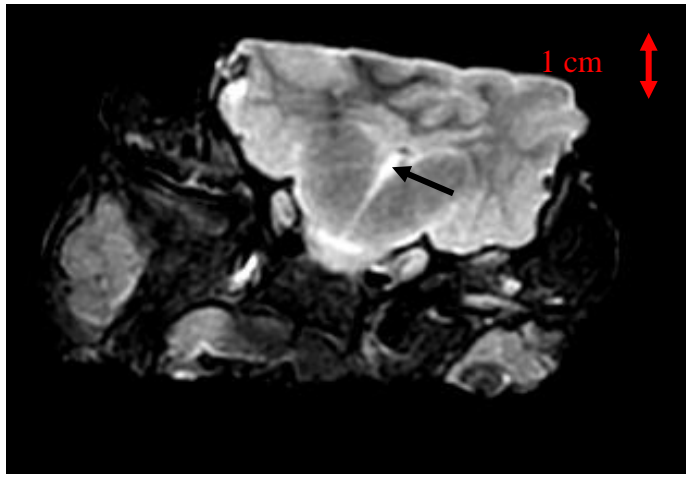


Figure 7.16 MRI image using T1-W FSE *in vitro*.

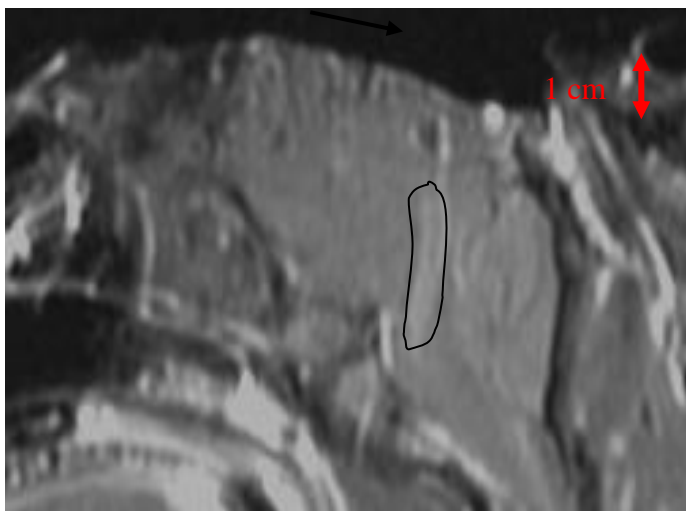


Figure 7.17 MRI image using T1-W FSE *in vivo*.

7.7 DISCUSSION

The procedure of creating lesions in a gel phantom was always used, before animal experiments, for quality assurance of the HIFU transducer. It was found that the relaxation time T1 of the lesion and gel used are similar and therefore the contrast of T1-W FSE is poor, whereas the relaxation time T2 of the lesion and gel is sufficiently different resulting to a good contrast using T2-W FSE.

Previous literature [142][143] demonstrated that lesions can be monitored with excellent contrast in rabbit brain (*in vivo*) using T1-W FSE with TR=500 ms. The lesions imaged in the previous studies and also in this study appeared bright with T1-W FSE, whereas brain tissue appeared gray. However, in the previous studies only thermal lesions were shown. In this chapter, we have explored extensively the use of MRI to image both lesions created under thermal mechanisms and mechanisms that create bubbly lesions (cavitation or boiling). MRI could detect the lesion approximately 10 mins after the ablation. In the study by Chen et al. [153], the lesions in the brain appeared in MRI in 15 mins using T2-weighted FSE, which is very close to what we found in this study (10 mins).

The contrast between lesion and brain tissue out of the 3 pulse sequences used it was found to be best with T1-w FSE. The signal intensity of the brain tissue is homogeneous when using this method, and therefore the contrast with thermal lesions or with bubbly lesions is excellent. Best contrast is observed for TR above 500 ms. This was proved by plotting the CNR vs. TR. The relaxation time T1 of thermal lesions increases, and therefore lesions appear brighter than brain tissue. The trend of increasing of T1 due to heating was also reported by Dickinson et al [154].

The three pulse sequences T1-W FSE, T2-W FSE and FLAIR were all able to detect lesions. This advantage is attributed to the significant difference in signal intensity between the thermal or bubbly lesions and brain tissue. It was observed that bubbly lesions appear darker than thermal lesions. Bubbly lesions appear dark, due to the air spaces resulting from cavities. This chapter demonstrates that non-degassed excised tissue is a good model for easily initiating cavitation. This model of cavitation might not be of any significant for clinical use since the

cavitation threshold in live tissue is very different from the threshold in the *in vitro* tissue. However, this model of initiating cavitation is very useful for the purpose of studying the MRI appearance of bubbly lesions. Cavitation is initiated if a blood vessel (which might include trapped bubbles) is targeted. Thus, the nature of lesion (thermal or cavitation) in brain *in vitro* primarily strongly depends on the nature of the target and secondarily to the level of intensity.

This is the first study demonstrating creation of large lesions in brain formed by scanning the transducer in grid formation. Both thermal and bubbly lesions were monitored successfully using T1-W FSE with excellent contrast, proving the potential of HIFU to treat reliably tumours in the brain in the future. The proposed system effectively creates large lesions in brain and at the same time, these lesions are effectively monitored using MRI enabling the accurate determination of the margins of these lesions, especially when using T1-W FSE.

The length of the lesions *in vivo* measured parallel to the ultrasonic beam (i.e. deep in the brain) were much higher than the length in *in vitro*, proving that the penetration in the *in vitro* brain is limited by reflection due to trapped bubbles in the blood vessels.

Previous clinical studies [147] proved the feasibility of HIFU to ablate brain tissue. Recently, studies have shown the effectiveness of MRI to monitor HIFU in the brain of animals [151][152]. Moreover, in the area of the brain ablation several studies have shown that the blood brain barrier in the brain can be opened using ultrasound [153], which means that HIFU can be combined with drugs in order to increase the therapeutic effect. Moreover, it has been shown that transcranial transmission is possible by using phased arrays [155][63]. Therefore, in conclusion, it has been demonstrated that (a) tumours can respond to HIFU, (b) MRI can monitor these changes, (c) drugs can be delivered locally to the brain, and (d) transcranial transmission of ultrasound is possible. Therefore, we believe that the prospect of treating patients with brain diseases in the clinical setting using HIFU is very promising.

Table 7.2 presents a summary of the parameters used for the recommended HIFU system.

Table 7.2 Summary of the recommended HIFU system

Parameters	Values
Frequency (f)	1 MHz
Intensity (I)	1000-2000 W/cm ²
Pulse Duration (PD)	20 – 30 s
MRI Sequence	T1 W FSE

At the next chapter a computer model was used with the main aim to extract the acoustic parameters (power, pulse duration, duty factor and pulse repetition frequency) that maintains a temperature increase of less than 1°C during the application of pulsed ultrasound.

CHAPTER 8: A SIMULATION MODEL FOR PREDICTING THE TEMPERATURE DURING THE APPLICATION OF MR-GUIDED PULSED FOCUSED ULTRASOUND FOR STROKE TREATMENT.

8.1 INTRODUCTION

Ultrasound can be used for noninvasive treatment in combination with the administration of thrombolytic drug in order to dissolve clots located deep in the brain without destroying the surrounding tissue [48][156], [157], [158], [159]. High intensity focused ultrasound (HIFU) is being used today primarily to thermally destroy tissue [160][161]. Heat produced at the focal point is very high in a very short period of time. As a result, temperature elevations in the exposed area can ablate the tissue [162][163].

During the past few years, treatment of ischaemic stroke using ultrasound has received great attention. Most previous studies have used unfocused ultrasound at very low intensities. Several experimental studies have been performed by Alexandrov et al. [48], Zenitani et al. [164], Soltani et al. [165], Eggers et al. [166], [169], Shaw et al. [167] and Saguchi et al. [168] to investigate the effectiveness of sonothrombolysis with, and without, thrombolytic drugs such as rt-PA.

Recently, experiments have demonstrated the ability of HIFU to be used for noninvasive procedures to dissolve thrombus [108], [156], [157], [170], [171]. Maxwell et al. [156][157] reported that Histotripsy therapy using short, high-intensity, focused ultrasound pulses can cause mechanical breakdown of targeted soft tissue by acoustic cavitation, which is guided by real-time ultrasound imaging.

The mode of action of ultrasound during sonothrombolys is mechanical. Therefore, temperature elevation is the key safety issue in treating patients with ischaemic stroke. It was shown that when the temperature rises to 43°C and above, enough thermal dose is produced to destroy human tissue [120]]. In order

to avoid any unwanted effects on human tissue caused by temperature rise, in this simulation study a maximum temperature limit was set to 1°C.

The aim of this study was to control temperature elevation in order to avoid heating of the brain during sonothrombolysis. A computer model was used to estimate the temperature elevation, based on the transducer characteristics (frequency, diameter, degree of focusing), treatment protocol (pulse duration, duty factor, acoustical power), and the anatomical site (depth). A single element spherically focused transducer of 5 cm diameter, focusing at 10 cm and operating at either 0.5 MHz or 1 MHz was considered. For all simulations, the focus was set at either 1cm or 2.5cm deep into the tissue. The goal was to extract the acoustic parameters (power, pulse duration, duty factor and pulse repetition frequency) that maintains a temperature increase of less than 1°C during the application of pulsed ultrasound.

8.2 MATERIAL AND METHODS

To avoid overheating of the brain tissue, the values of the following parameters such as pulse duration, pulse repetition period (PRP), and duty factor were investigated. Pulse duration is the amount of time from the beginning to the end of a single pulse of ultrasound. PRP is the amount of time from the start of one pulse to the start of the next pulse. It includes both the sound “ON” time and “OFF” time. PRP of 1 ms and 1 s are used. Figure 8.1 shows a diagram explaining PRP. Duty factor (DF) is the proportion of time that the ultrasound transducer is actually producing sound energy. It is the ratio between pulse duration (sound ON time) and PRP (sound ON plus sound OFF time). The DF ranges from 2% to 100%. The sonication period used in all simulations and experiments are 60 s and 120 s.

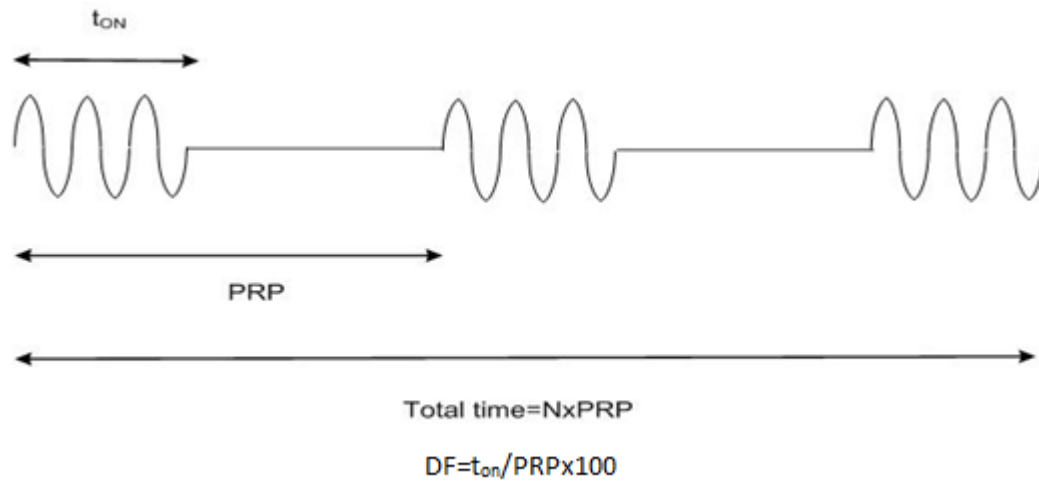


Figure 8.1 Timing diagram explaining PRP, DF, and total time.

8.2.1 TEMPERATURE SIMULATIONS

The power field was calculated by using a computer program, which is described in chapter 4, section 4.3. The temperature vs. time history was obtained by solving the bio-heat equation proposed by Pennes (1948) numerically [117]. The explicit form of this equation is given by:

$$\rho_i c_i \frac{\partial T}{\partial t} = k \nabla^2 T + w_b c_b (T - T_a) + Q_p + Q_m$$

The temperature distribution at a given time was observed by solving the bio-heat differential equation using a finite difference technique (see section 4.3).

8.2.2 TEMPERATURE MEASUREMENT

A data acquisition board (6251 DAQ, National Instruments, Texas, USA) was used to measure the temperature. An analogue input of the board was used to capture the temperature. An Omega M2813-1205 (OMEGA Engineering, INC. Stamford, Connecticut, USA) thermocouple-to-analogue connector was used to give analogue output (1mv per degree). This was entered in to the data acquisition card and read by custom-made software written in MatLab (The Mathworks Inc., Natick, MA). A thermocouple (Omega engineering INC, Connecticut, USA) was placed in the thrombus in order to measure temperature elevation at the focal point (clot).

8.2.3 IN VITRO EXPERIMENTS

Experiments were carried out to investigate the accuracy of the simulation model. Figure 8.2 shows the HIFU system, which consists of a signal generator and RF amplifier (100 W, JJ&A Instruments, USA), and a spherically shaped transducer made from piezoelectric ceramic of low magnetic susceptibility (Piezotechnologies, USA). The transducer operates at 1 MHz and has a focal length of 10 cm and diameter of 5 cm. The transducer is mounted on the 3D positioning device (MEDSONIC, Cyprus). Blood clots were obtained by natural coagulation of animal blood samples from healthy cows. Blood was drawn into small containers and placed in a 37°C water bath for 3 h and storing the clots in a 5°C refrigerator for at least 72 h before use in the experiments to allow complete clot retraction [173]. The blood clot was placed inside the silicon tube (figure 8.2). A thermocouple was inserted in the middle of the clot to monitor temperature elevation. During the experiments, temperature was recorded every 0.2s.

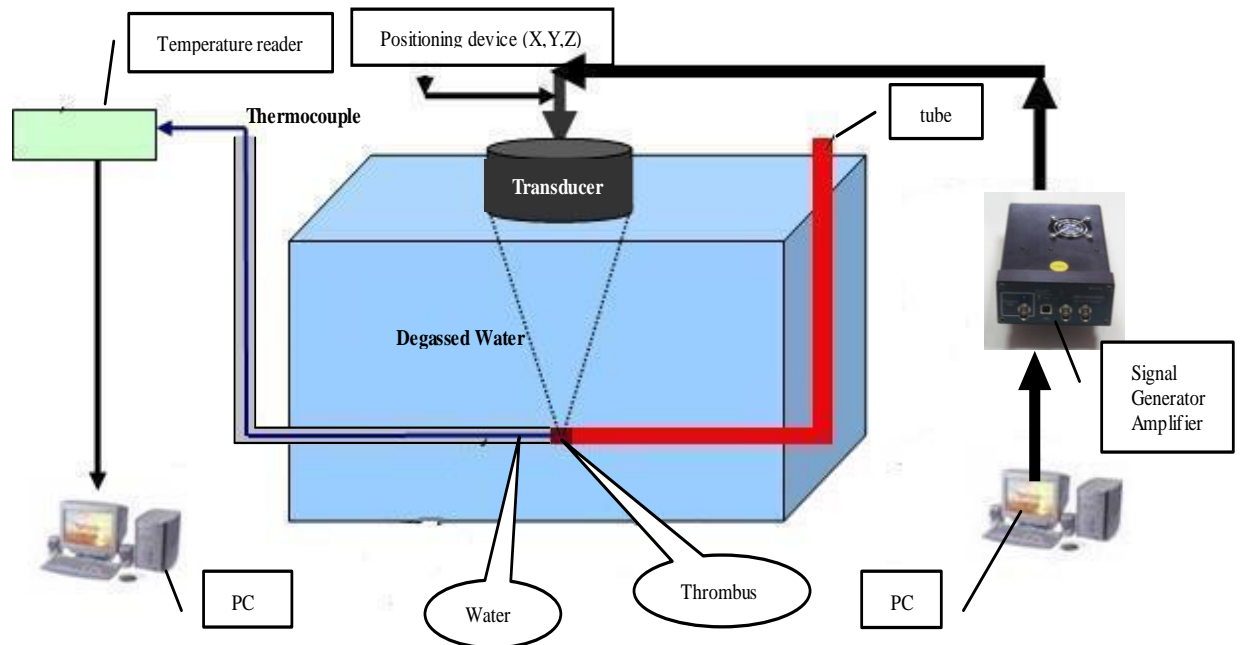


Figure 8.2 Schematic diagram of the MR-guided FUS system.

8.3 RESULTS

The simulation model was tested on thrombi immersed in a water bath. Pulsed ultrasound was applied with pulse repetition period of 1 s using a 1 MHz transducer. Figure 8.3 compares simulated and experimental temperatures. The experimental and simulated results agree well, indicating that the simulation model can be used to give guidelines for various sonothrombolysis protocols.

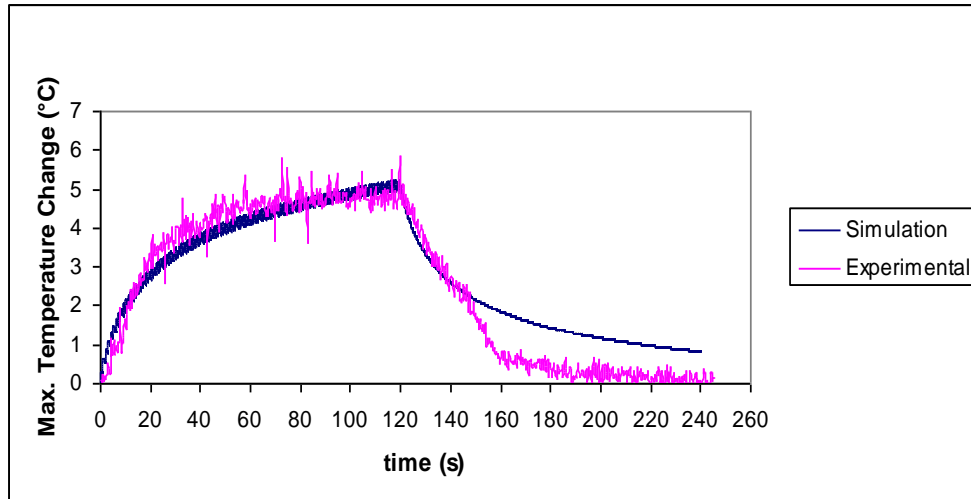
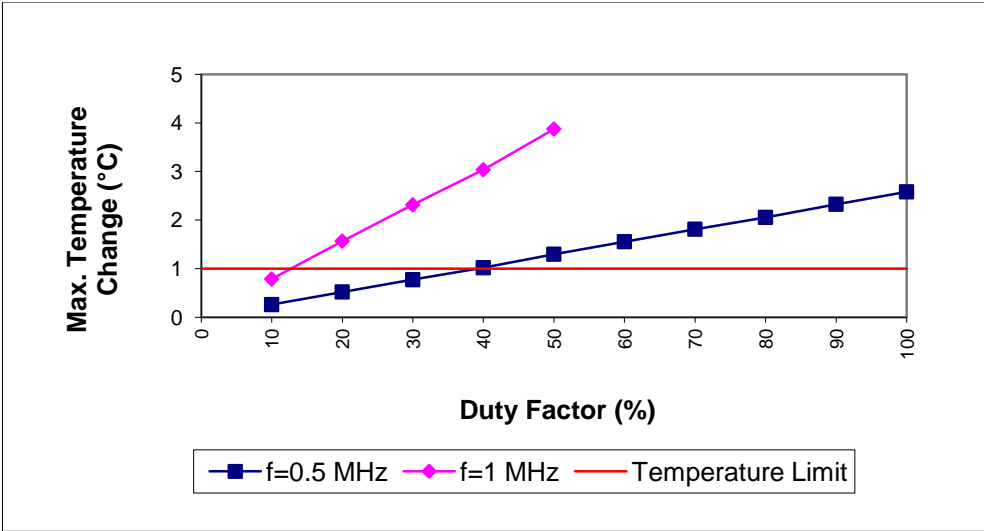


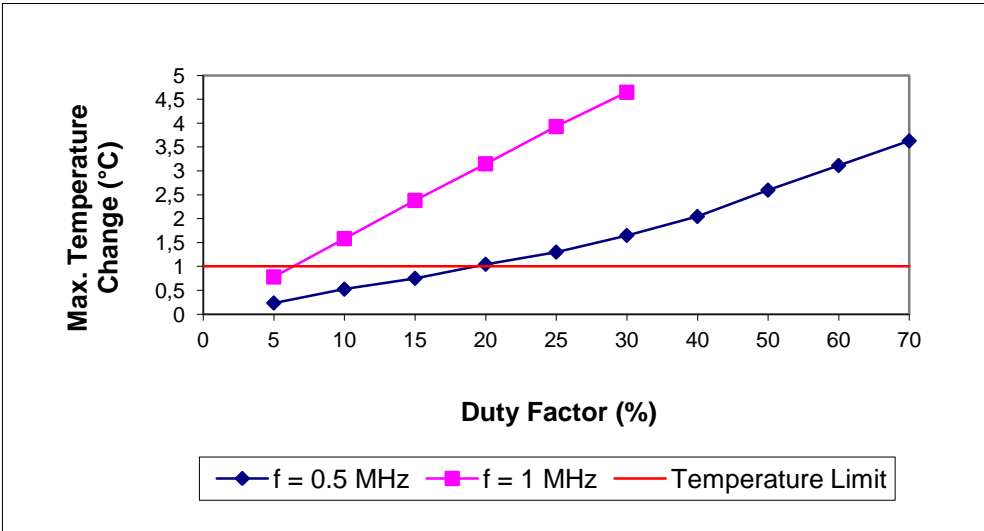
Figure 8.3 Simulated and experimental Temperature vs. Time with Duty Factor=5%, Power=20W, $f=1\text{MHz}$, Radius of Curvature=10cm, Transducer Diameter=5cm, Focal Depth=1cm, PRP=1s

Figure 8.4 shows the simulated temperature elevation at frequencies of 0.5 MHz and 1 MHz with a focal depth (FD) of 2.5 cm. The effect of duty factor on temperature elevation was investigated using power of 2.5 W, 5 W, 10 W, and 20 W. The maximum temperature at steady state increased linearly with duty factor. When higher frequency is used, the duty factor needed to maintain safe temperature is lower for the same power.

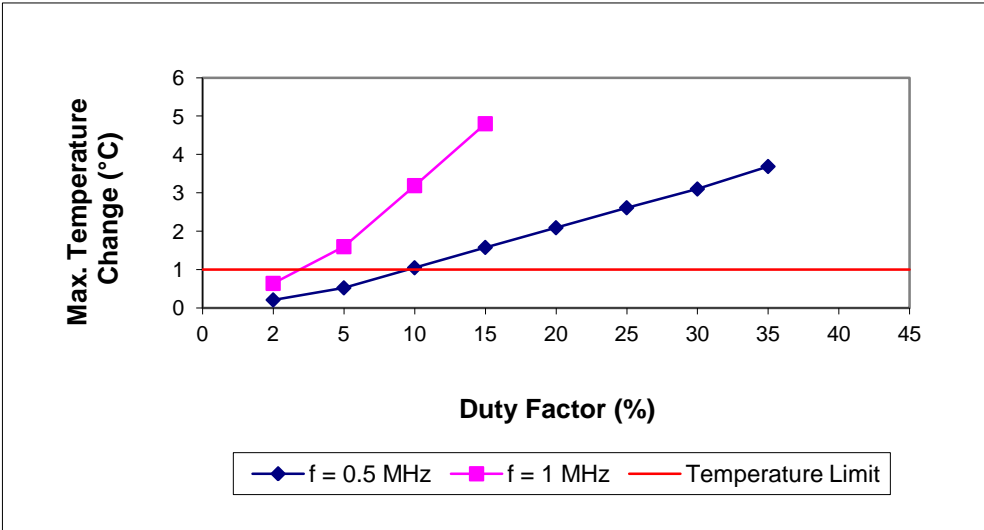
Figure 8.5 shows also the simulated temperature elevation at frequency of 0.5 MHz and 1 MHz using the same parameters as in figure 8.4 but with a focal depth of 1 cm. The trend of temperature is similar as with the focal depth of 2.5 cm. With focal depth of 1 cm, temperature rise faster and therefore less duty factor required to maintain safe temperature.



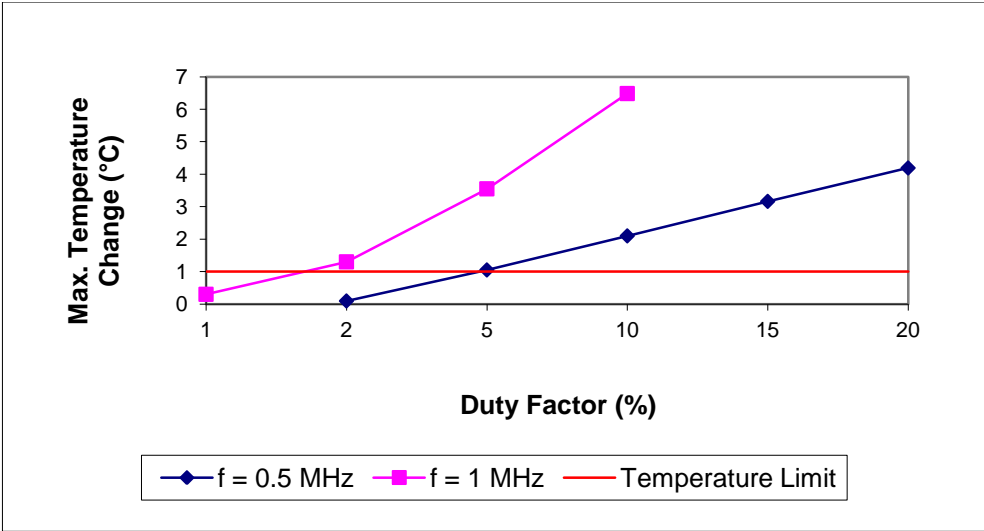
A



B

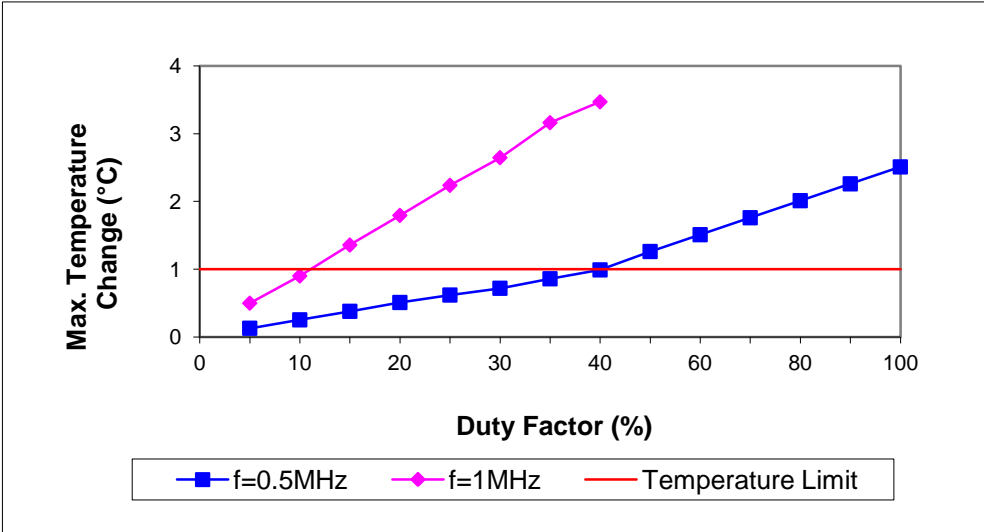


C

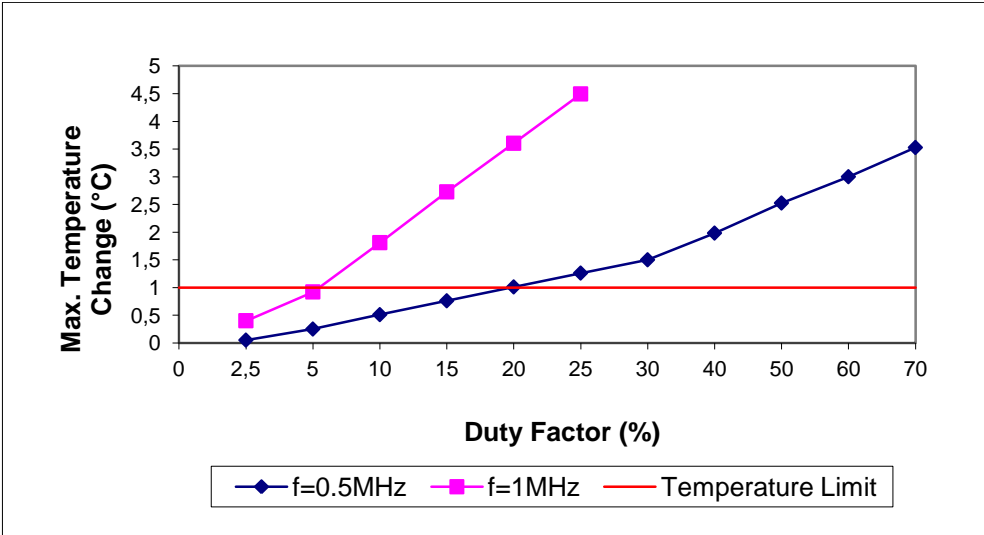


D

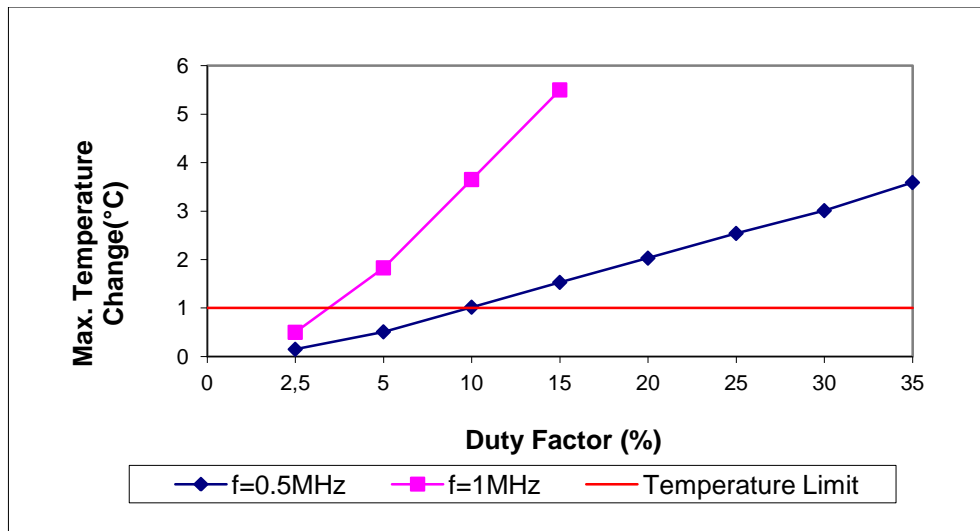
Figure 8.4 Temperature vs. Duty Factor for different Power at FD=2.5 cm; A. 2.5 W; B. 5 W; C. 10 W; D. 20 W



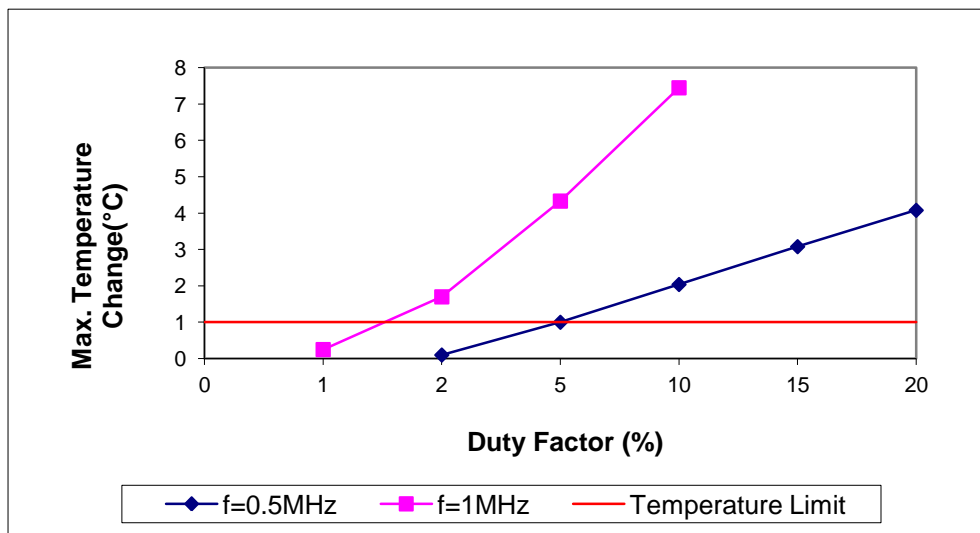
A



B



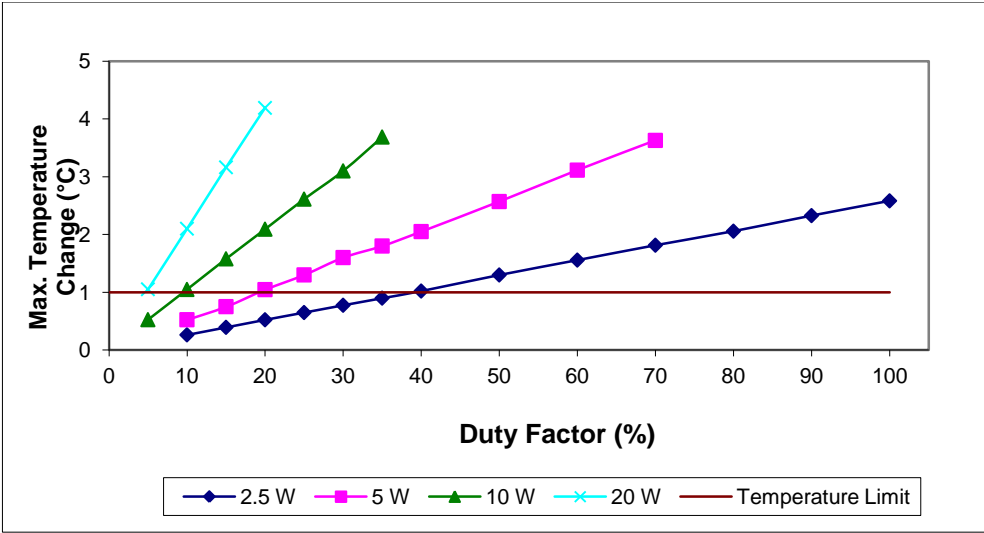
C



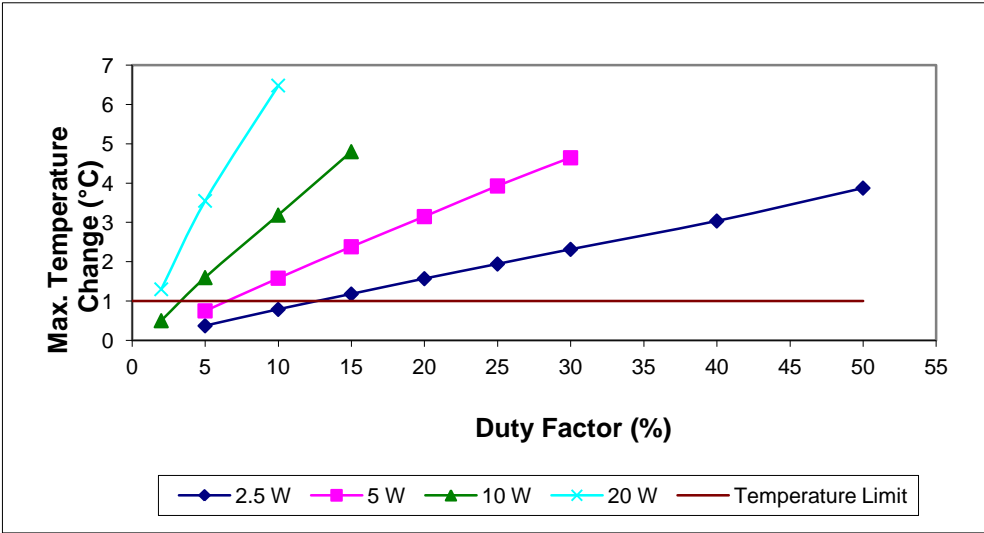
D

Figure 8.5 Temperature vs. Duty Factor for different Power at FD=1 cm; A. 2.5 W; B. 5 W; C. 10 W; D. 20 W

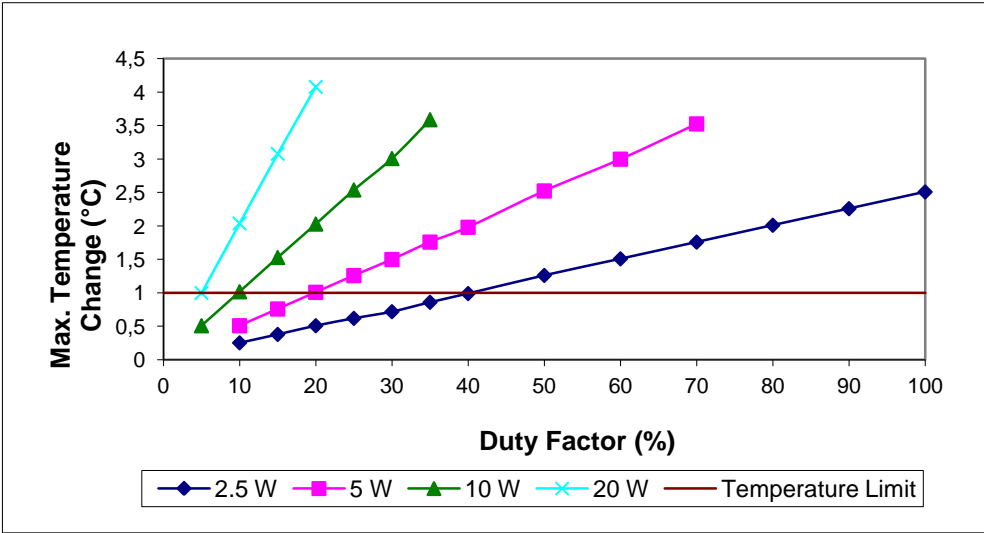
The effect of the applied acoustical power on the temperature elevation is shown in figure 8.6, with focal depth of 1 cm and 2.5 cm, PRP=1s, and frequencies of 0.5 MHz and 1 MHz. With a lower frequency such as 0.5 MHz the duty factor needed for different power is almost the same regardless the focal depth, either for 1 cm or for 2.5 cm. When the frequency is increased to 1 MHz, safe temperature cannot be achieved at any power (5 W, 10 W, and 20 W) except when 2.5 W is used. Temperature limit was reached at 10% for 2.5 W and at focal depth of 1cm where 14% is needed at focal depth of 2.5 cm. Finally, the duty factor allowed maintaining safe temperature is higher for lower power.



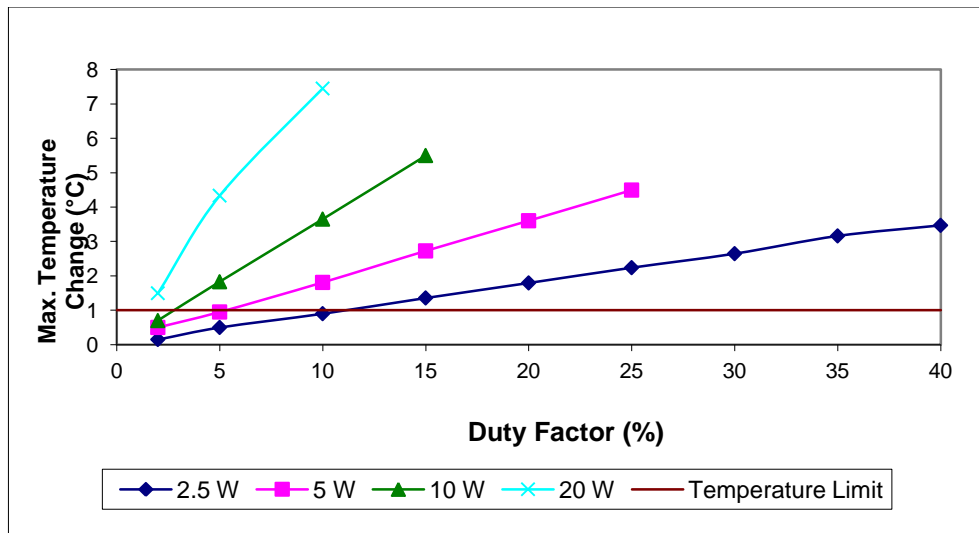
A



B



C



D

Figure 8.6 Temperature vs. Duty Factor; A. $f=0.5$ MHz, $FD=2.5$ cm; B. $f=1$ MHz, $FD=2.5$ cm; C. $f=0.5$ MHz, $FD=1$ cm; D. $f=1$ MHz, $FD=1$ cm.

Figure 8.7 summarizes the effect of applied acoustic power on the duty factor which establish safe temperature at frequency of 0.5 MHz. Acoustical power is inversely related to duty factor, the higher the power the lower the duty factor.

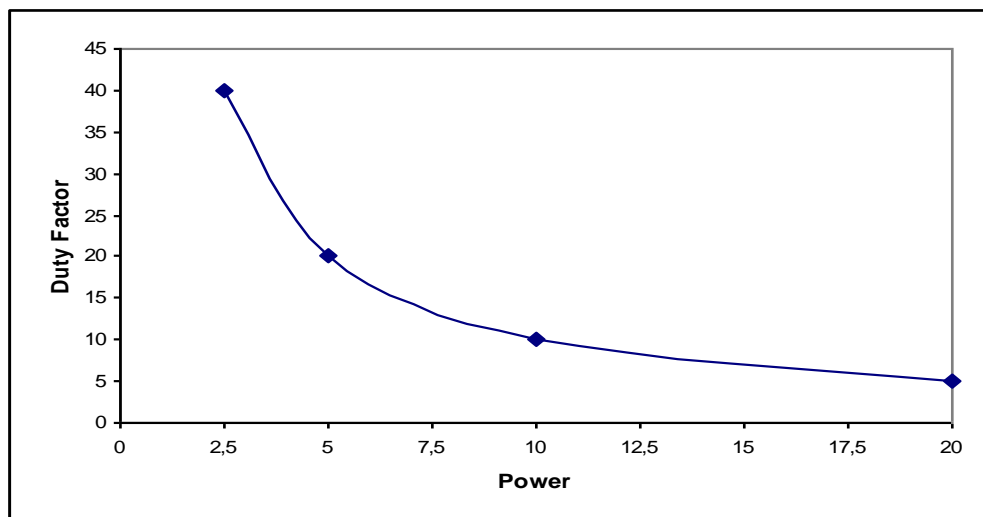
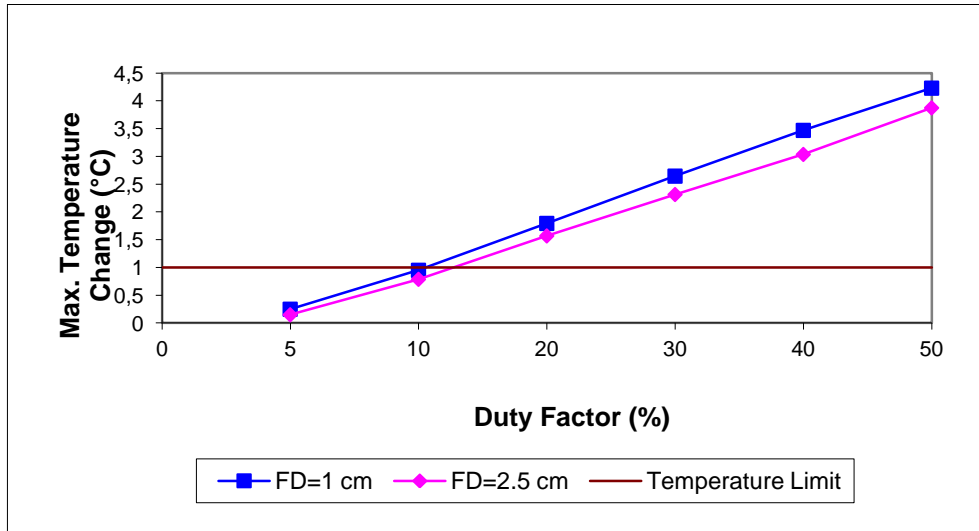


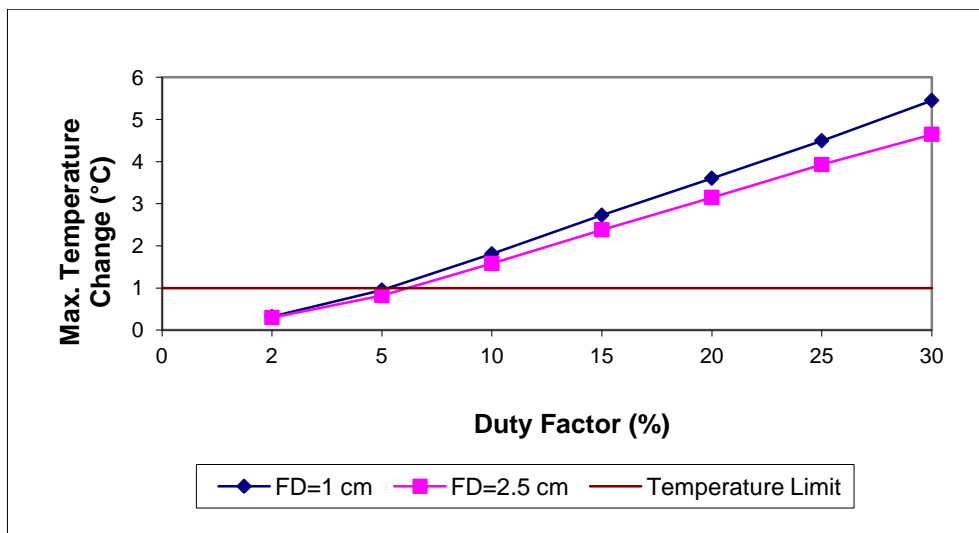
Figure 8.7 Duty Factor that establishes safe temperature vs. Power, $f=0.5$ MHz, Radius of Curvature=10 cm, Transducer Diameter=5 cm, Focal Depth=2.5 cm, PRP=1 s

Figure 8.8 shows simulation results for the safe temperature using a 1 MHz transducer. Two different focal depths were used: 1cm and 2.5cm. The effect of duty factor (DF) on the safe temperature was investigated using power of a) 2.5 W, b) 5 W, c) 10 W, and d) 20 W. When FD is close to the surface (1 cm deep)

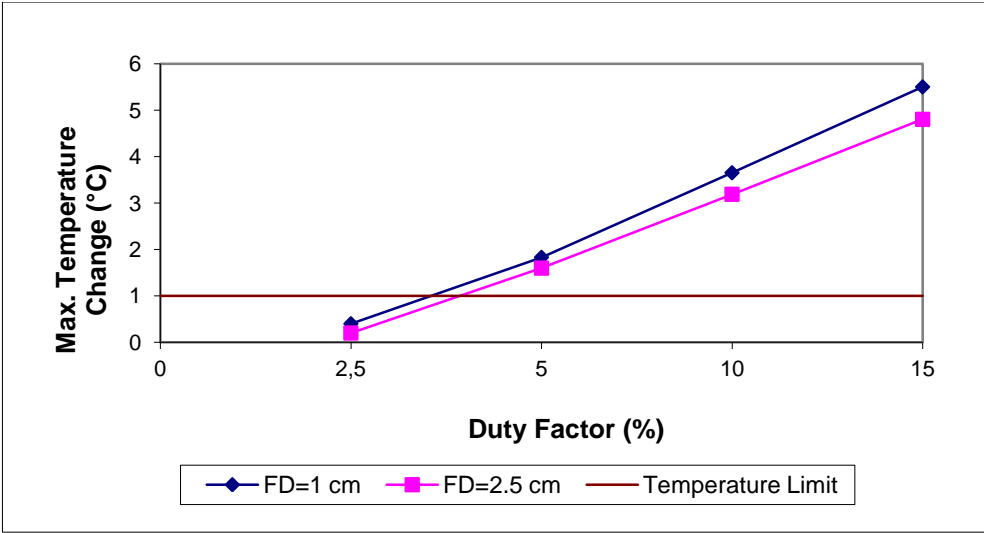
the intensity is higher compared to that at 2.5cm and therefore a lower DF needed to reach the temperature limit. Figure 8.9 shows the same results as in figure 8.8 but at a frequency of 0.5 MHz. Using a frequency of 0.5 MHz, the temperature limit was reached at DF=40%, 20%, 10%, and 5% for power of 2.5W, 5W, 10W, and 20W respectively for both focal depth (1 cm or 2.5 cm).



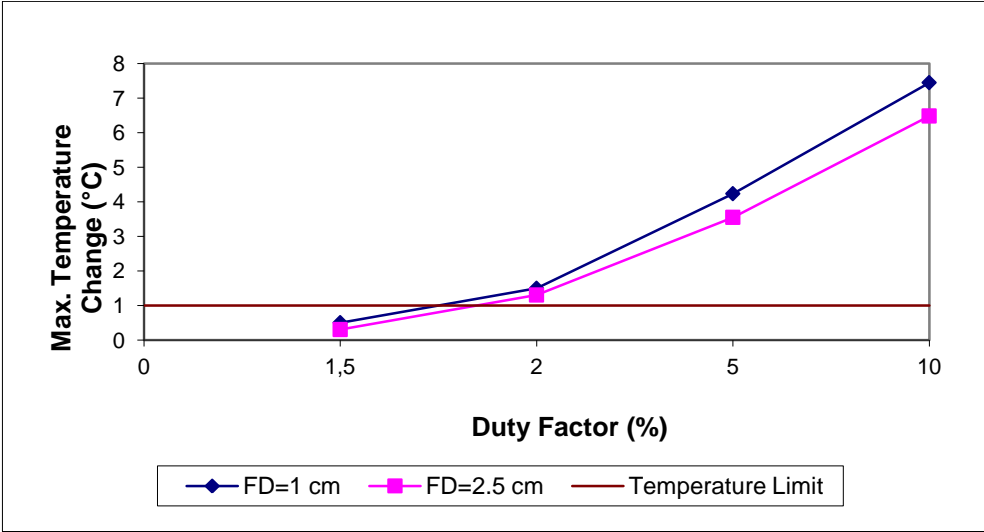
A



B

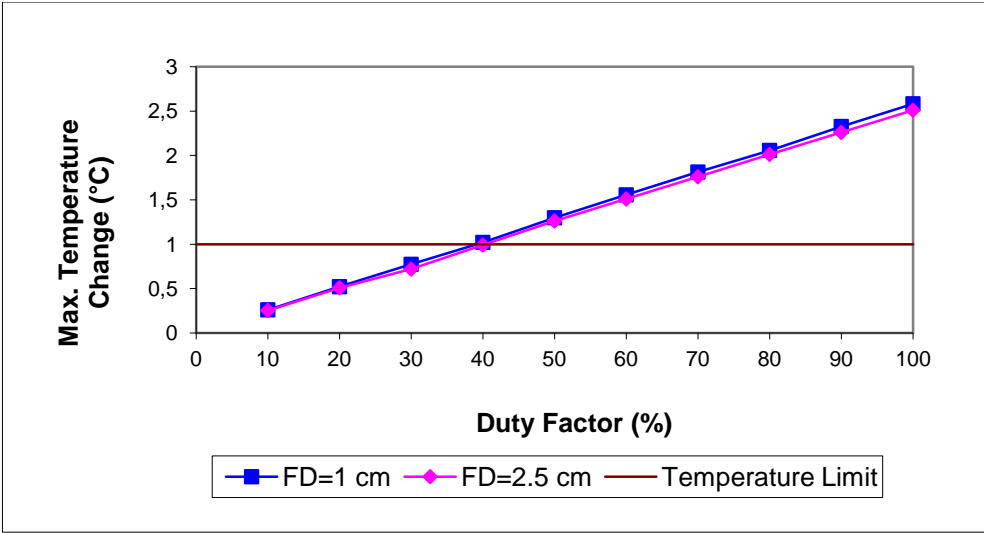


C

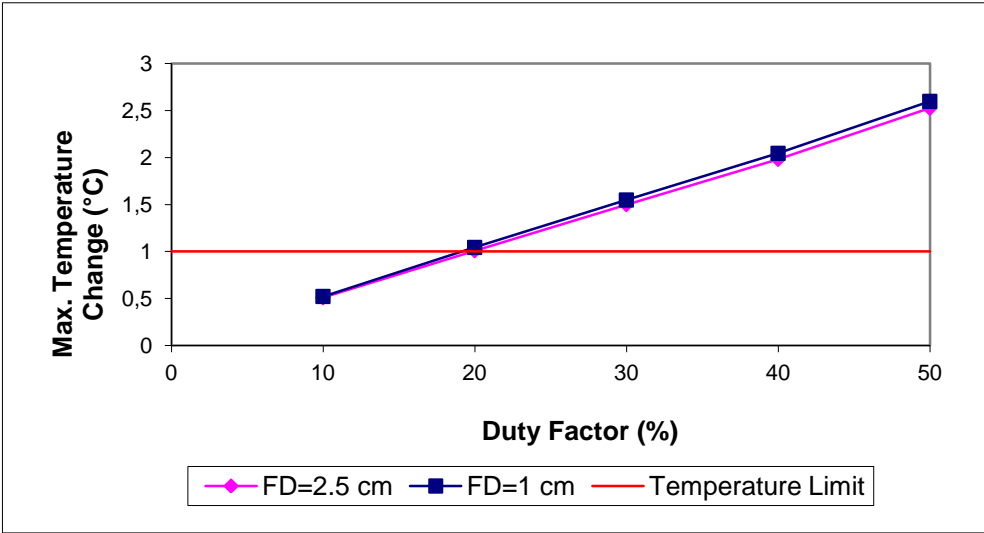


D

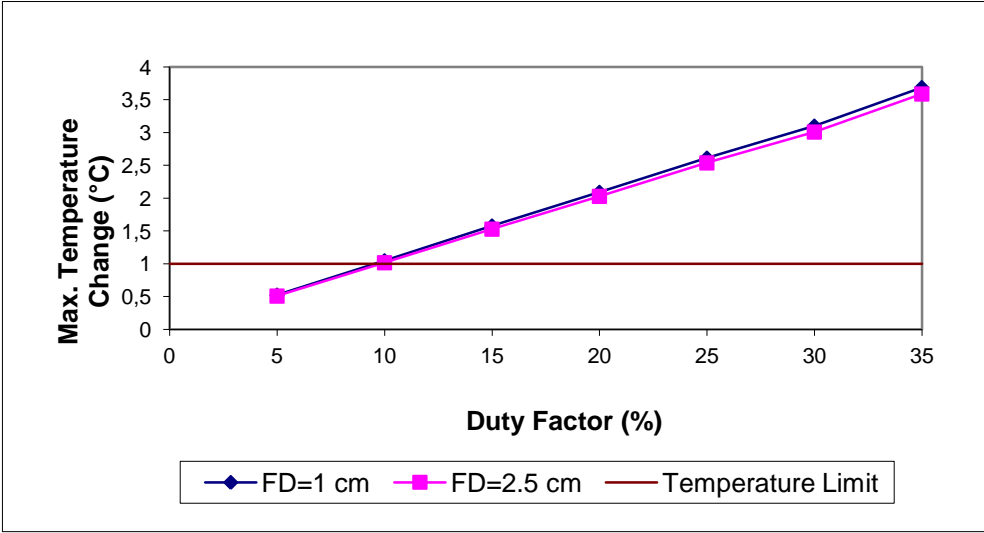
Figure 8.8 Temperature vs. Duty Factor for different Power and $f=1$ MHz; A. 2.5W; B. 5W; C. 10W; D. 20W



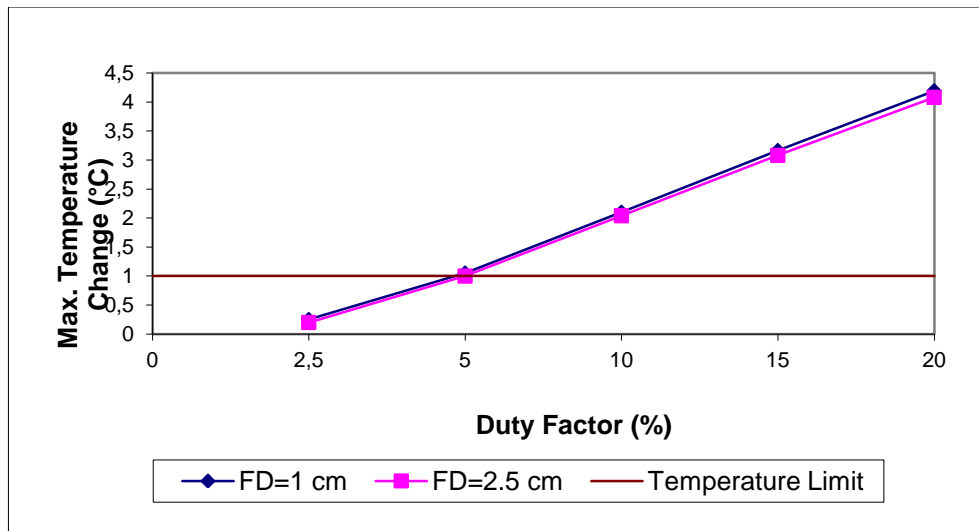
A



B



C



D

Figure 8.9 Temperature vs. Duty Factor for different Power and $f=0.5$ MHz; A. 2.5W; B. 5W; C. 10W; D. 20W

8.4 DISCUSSION

It was found that the temperature increases linearly with duty factor. The higher the power the lower the duty factor needed to keep the temperature change within the safe limit of 1°C . Also, the higher the frequency the lower the duty factor needed to keep the temperature change to the safe limit of 1°C . Finally, the deeper the target, the higher the duty factor needed to keep the temperature changes to the safe limit of 1°C .

The simulation results provide a good indicator of temperature elevation at the focal point. The temperature increases as a function of applied power with the rate of increase dependent upon the duty factor and frequency. The temperature elevation was simulated for different power and duty factor. These results will guide us towards the best sonication system in a faster and more appropriate way than using extensive animal experiments.

The simulation results agree well with the experimental results. However, further experiments either *in vitro* or *in vivo* will require, verifying the current simulation results. Various pulse protocols will be investigated based on the parameters derived from the simulation, to verify that temperature change at the focal point will not exceed 1°C , which is called “safe temperature”. In addition, the

experimental results (*in vitro* and *in vivo*) will guide us towards the best possible protocol to be used in collaboration with thrombolytic drug and MRI. Most of the previous experimental studies have demonstrated temperature elevation above 3°C [174][175]. If this temperature elevation cannot be controlled will cause unwanted tissue damage during sonication [90]. There are also cases shown by Ishibashi et al. [47] and Nedelmann et al. [175] when either low intensities or low frequencies are applied and temperature elevation drops below the 3°C. We have shown that temperature elevation can be controlled and kept within the safe region by adjusting various parameters such as the duty factor, the operating frequency, and the amount of acoustic power.

The simulation results prove that longer duty factors will increase the temperature elevation. Figure 8.6 shows that the temperature increases with increasing duty factor. This happens because greater duty factors allow less time for the tissue to cool off, causing the temperature to rise higher than the allowed maximum limit of 1°C.

Temperatures also increase faster when the focal depth is 1cm deep in the tissue, or more slowly when it is 2.5 cm deep in the tissue. A comparison of the effect of frequency in figures 8.4 & 8.5 indicate that if the focal depth is close to the skin (1 cm), then the temperature rises faster than when the focal depth is deeper below the skin (2.5 cm). This happens because the intensity drops less at points closer to the surface and decreases as we go deeper into the tissue due to the attenuation and absorption coefficients. In addition, when using 1 MHz frequency, the beam at the focal point is narrower and very sharp compared to frequency of 0.5 MHz. Figure 8.9 shows that when 0.5 MHz frequency is used, the difference in temperature elevation at the focal point of 1 cm and 2.5 cm is very small indicating that at lower frequencies the effect of focal depth is smaller compared to higher frequencies. Also, as the frequency increases from 0.5 MHz to 1 MHz (figures 8.2 to 8.5) under the same power, the temperature elevation is raised faster and therefore we need to use much lower duty factors to prevent the temperature exceeding the maximum limit.

Finally, this simulation model is considered as a very useful tool for providing acoustic parameters (frequency, power, duty factor, pulse repetition frequency) during the application of pulse ultrasound at various depths in tissue so that safe temperature is maintained during the treatment. Table 8.1 presents a summary of the parameters used for the recommended HIFU system

Table 8.1 Summary of the recommended HIFU system

Focal Depth (FD) = 2.5 cm			
Frequency (MHz)	Power (W)	Duty Factor (%)	ΔT ($^{\circ}C$)
0.5	5 - 20	5 - 40	≤ 1
1	2.5 - 10	2 - 10	≤ 1
Focal Depth (FD) = 1 cm			
Frequency (MHz)	Power (W)	Duty Factor (%)	ΔT ($^{\circ}C$)
0.5	2.5 - 10	10 - 35	1
1	2.5 - 5	2 - 5	≤ 1

The following chapter presents experiments *in vitro* where the ability of MRgFUS system to dissolve clots in combination with rt-PA is demonstrated. The evaluation on the effect of intensity, beam area and frequency on the volume of the dissolved clot is evaluated, while temperature change maintain below $1^{\circ}C$ at the centre of the clot.

CHAPTER 9: APPLICATION OF MR-GUIDED FOCUSED PULSED ULTRASOUND FOR DESTROYING CLOTS *IN VITRO* USING THROMBOLYTIC DRUGS.

9.1 INTRODUCTION

The feasibility of ultrasound to enhance thrombolysis was reported in the mid-70s by Trubestein et al. [44] and Tachibana [45]. In the following years, several *in vitro* studies by Kimura et al. [49] and Spengos et al. [158] have confirmed the above results. In the former studies, the range of intensity ranged from 0.2–2.0 W/cm² (spatial peak temporal average intensities) and the frequency ranged from 20 kHz to 2 MHz using unfocused ultrasound. Table 9.1 summarizes some of the characteristics of ultrasound and thrombolysis derived from experiments *in vitro*.

It is speculated that ultrasound accelerates enzymatic fibrinolysis primarily through mechanical mechanisms, by enhancing transport of thrombolytic drugs into the clot shown by Francis et al. [176]. Other mechanical effects of ultrasound such as cavitation and radiation force are possibly influencing drug transport [177][178]. Acoustic cavitation plays a very significant role in ultrasound-accelerated fibrinolysis [177]. Other theories revolve around the fact that ultrasound promotes motion of fluid around the clot, an effect called microstreaming [178].

These preliminary findings are promising, and provide insight into understanding the potential of ultrasound in dissolving blood clots during ultrasound-assisted thrombolysis, which is an important first step in improving thrombolytic efficacy, while minimizing unwanted thermal bioeffects.

Birnbaum et al. [179] reported that *in vivo* arterial clot dissolution can be achieved with intravenous microbubbles and transcutaneous ultrasound delivery alone. Moreover, a study by Culp et al. [180] has shown the effectiveness of transcutaneous ultrasound and intravascular microbubbles in lysing intracranial clot in pigs.

Table 9.1: Characteristics of Ultrasound and Thrombolysis (Protocol: *in vitro*)

Subject	Frequency	Intensity	Mode	Duty Factor	Sonication Time (min)	Focused / Unfocused	rt-PA Dose	Results	First Author
Human skull, tube	a) 33 KHz b) 71 KHz	a) 0.5 W/cm ² b) 3.4 W/cm ²	CW		a) 60 b) 180	unfocused	1 mL/100 µg/mL	Thrombus weight reduction at: a) 33 KHz: 51% b) 71 KHz: 46%	Behrens et al. 1998 [216]
	1 MHz	524 mW/cm ²	PW	PRF: 16KHz	30	Diagnostic ultrasound	1mL/100mg /mL	Recanalization 90% - 100%	Spengos et al. 2000 [158]
	120 KHz	Pressure:0.35 MPa	PW	50% PRF= 1667 Hz	30	unfocused	0-10 µg/mL	120 KHz UET maximizes lytic efficacy while minimize rt-PA exposure.	Shaw et al. 2008 [167]
Thrombus in Eppendorf pipette tip + human temporal bone tube	1.8 MHz	179 mW/cm ²	PW	transcranial pulsed wave	60	diagnostic ultrasound	10 µg/mL	thrombus reduction=78.7%	Eggers et al. 2009 [166]
tube	40 KHz	0.25 W/cm ²	CW		60	unfocused	1.0 mg/mL	Fibrolysis: 60m: 39% 120m: 93%	Suchkova et al. 1998 [187]
	490.6 KHz	0.13 W/cm ²	CW		60	unfocused	1.2 mg	Recanalization ratio: 66.7%	Ishibashi et al. 2002 [47]
	500 KHz	0.7 W/cm ²	CW		1	unfocused	0.5 mg/mL (rt_PA + BL)	Clot reduction: 29%	Zenitanni et al. 2008 [164]
	2 MHz TCD	Negative Acoustic Pressure: 0.5, 1.7, 3.5 MPa	PW	10000-cycles (5ms) burst	60	unfocused	522,000 IU/mL: 0.9 mL t_PA 0.1 mL: PBS OR 0.1 mL optison	The presence of stable cavitation was verified and did not impact the stability of alteplase.	Soltani et al. 2008 [165]
	1 MHz	2.8 W/cm ² and 36.8 W/cm ²	PW	10%	60	HIFU	1.0 mg/mL	volume of the dissolved clot: 95.3 mm ³	Hadjisavvas et al. 2012

Administration of gaseous microspheres dramatically lowers the threshold for cavitation and increases the lytic activity of ultrasound [181]. Because the bubbles are destroyed in the process, they must be constantly injected for complete clot dissolution. Recent studies have demonstrated that microbubbles can be concentrated at the surface of clot by attaching a glycoprotein 2b/3a receptor antagonist, which increases their adherence to acute clot, to the bubbles [182].

Currently there are few but significant clinical trials: a) The CLOTBUST (Combined Lysis of Thrombus in Brain ischemia using transcranial Ultrasound and Systemic Recombinant Tissue-Type Plasminogen Activator (rt-PA)) is a phase II randomized multi-center international clinical trial [48]. b) The EKOS study [183] which involves the insertion of a catheter is now being tested in phase II–III Interventional Management of Stroke (IMS) trials. c). The TRUMBI trial [55], using transcranial low-frequency ultrasound-mediated thrombolysis in brain ischemia in combination with intravenous administration of tPA, and 4). The TUCSON trial [56], a phase I–II randomized placebo-controlled, international multi-center study, using perflutren-lipid microspheres (MRX 801, Imarx Therapeutics, Inc., Tuscon, AZ) which is underway.

In this chapter the effect of therapeutic ultrasound was examined using the synergy of rt-PA to dissolve clot which is placed in a silicone tube model *in vitro*. In the current study higher intensities were used than what was proposed in the study by Alexandrov [184]. It was predicted that by using higher intensities, the rate of clot destruction would be accelerated. The previous studies mostly make use of unfocused ultrasound [168][169][173], thus the intensity levels that could be used were limited. In this study, focused ultrasound was investigated and therefore higher intensities can be easily applied provided that thermal effects are avoided. Therefore, a parametric study was presented which evaluates the effect of ultrasonic intensity, beam size and frequency on the dissolved clot volume. In order to achieve sufficient penetration through the skull the frequency of 0.5 MHz and 1 MHz was used. Focused ultrasound targeting the clot at the focal point or slighter off the focus is used with temporal average *in situ* intensities ranging from 2.8 W/cm² to 36.8 W/cm². Various pulse protocols were investigated having as a

goal that the temperature change at the clot does not exceed 1°C (called safe temperature). Safe temperature was set to 1⁰C in order to avoid tissue damage resulting from the long duration (around 60 min) that each treatment requires to dissolve the thrombus. The current study will give us a good indication regarding the optimum protocol to be used using the proposed MRgFUS.

9.2 HIFU SYSTEM

Figure 9.1 shows the block diagram of the HIFU system which includes the following subsystems: a) Focused ultrasound system b) Artery/tissue/clot model, c) Positioning device and d) Temperature measurement. A description of each of the subsystems follows below.

9.2.1 FOCUSED ULTRASOUND SYSTEM

The ultrasound system consists of a radio frequency (RF) generator/amplifier (100 W, JJ&A Instruments, Duvall, WA, USA), and a spherically shaped transducer made from piezoelectric ceramic of low magnetic susceptibility (Piezotechnologies, Etalon, Lebanon, IN, USA). Two transducers were used operating either at 0.5 MHz or 1 MHz. Both transducers have focal length of 10cm and a diameter of 5cm. The transducers were navigated by a 3D positioning device (MEDSONIC, Limassol, Cyprus). The 3D positioning device and the transducer were utilized inside an MRI scanner (Signa 1.5 T, by General Electric, Fairfield, CT, USA).

9.2.2 ARTERY/TISSUE/CLOT MODEL

The artery is modelled by a clear silicone tube (United States Plastic Corporation, Lima OH, USA), the tissue is modelled by a polyacrylimide gel (ONDA Corporation, Sunnyvale CA, USA) and the clot is modelled by using coagulated blood.

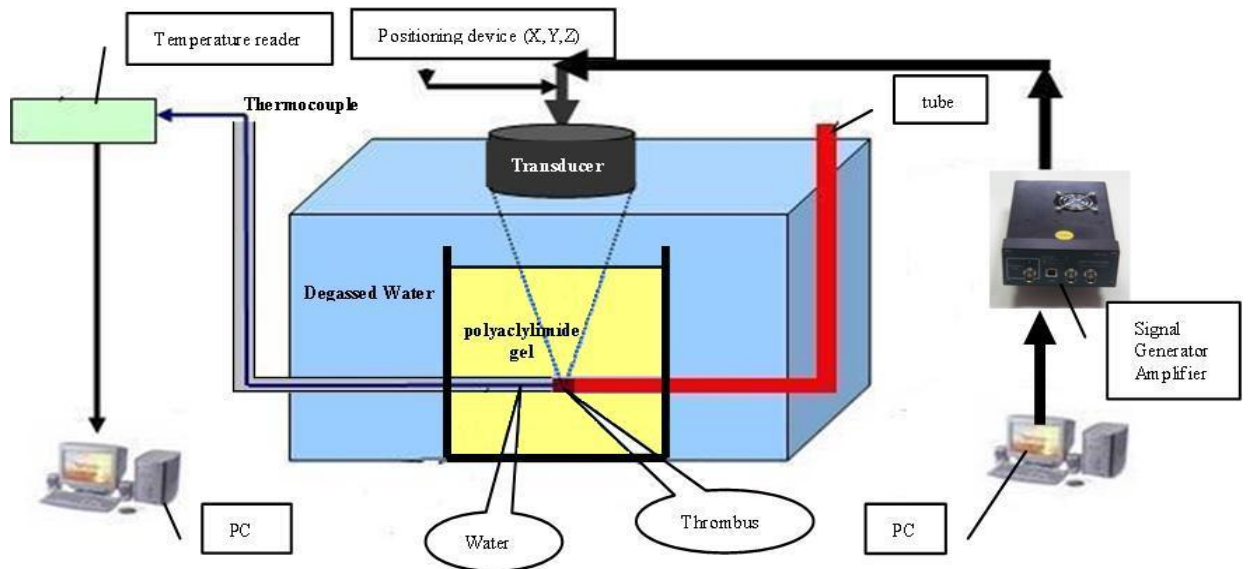


Figure 9.1 HIFU system for *in vitro* sonothrombolysis

Production of sample clots

Blood clots were obtained by natural coagulation of animal blood samples from healthy cows. Blood was drawn into small containers and placed in a 37° C water bath for 3 h and then stored in a refrigerator at a temperature of 5° C for at least 72 h before use in the experiments to allow complete clot retraction [173]. At the end, a decision was made based on observation on which clots to be kept for the experiments. Theoretically, good clots appear in dark colour. In addition, clots were evaluated based on the test results.

Preparation of rt-PA

The rt-PA was obtained as a lyophilized powder (rt-PA, Activase, Genentech, San Francisco, CA, USA) mixed with sterile water as per manufacturer's instructions. A dose of 1mg/mL was administered.

9.2.3 POSITIONING DEVICE

A manual positioning device (Velmex inc., Bloomfield NY, USA) was used in order to navigate the ultrasound transducer. The transducer was mounted on the arm of the 3D positioning device. Figure 9.2 shows the photo of the positioning device.



Figure 9.2 The positioning device

9.2.4 TEMPERATURE MEASUREMENT

A data acquisition board (6251 DAQ, National Instruments, Texas, USA) was used in order to measure the temperature in the clot. An analogue input of the board is used to capture the temperature. An Omega (M2813-1205, OMEGA Engineering, INC. Stamford, Connecticut, USA) voltage to temperature converter was used to measure temperature using a software written in MatLab (The Mathworks Inc., Natick, MA). Figure 9.3 shows a photo of the temperature measurement system. A thermocouple (Omega engineering) was placed in the clot to locate the focal point of the transducer during the experiments and to measure temperature elevation at the focal point.



Figure 9.3 Photo of the temperature measurement system, the omega thermocouple-to-analogue connector, National Instruments data acquisition board, and the custom made software

9.3 IN VITRO EXPERIMENTS

Various *in vitro* experiments were carried out to create thrombolysis. A silicon tube was placed 1cm deep inside the polyacetylimide gel and into the container filled with degassed water (figure 9.4). The clot was placed inside the silicon tube which is 1 cm deep in the mimicking tissue. Transducer of 0.5 MHz and US exposure alone (US) was used. Thereafter, a thermocouple was inserted, and placed exactly at the middle of the clot to monitor temperature elevation. During the experiments, temperature was recorded in steps of 0.2s. To locate the focal point of the transducer and place it exactly at the centre of the clot, the following steps were taken: a) Using the 3D positioning device and by moving it in all three directions (X, Y, and Z) the transducer was placed on top of the tube (observed by eye). Then, a ruler was used to measure the distance from the centre of the transducers concave surface to the middle of the tube (10 cm). b) Then, the signal generator was set to a low power continuous wave. At the same time using the positioning device, the transducer was moved in all directions and the temperature was monitored. c) During ultrasound exposure, if temperature was maximized at a certain point indicated that the focus was aimed at the thermocouple.

The transducer was placed on the arm of the positioning device and was immersed in the water tank, thus providing good acoustical coupling between thrombus and transducer. Any bubbles that may have collected under the face of the transducer were removed in order to eliminate any reflections.

The same experiments were performed but without the polyacetylimide gel for better observation on the thrombus condition. The transducer operating at 1 MHz was used. Ultrasound exposure alone (US), rt-PA alone and ultrasound exposure combined with rt-PA (US + rt-PA) were used.

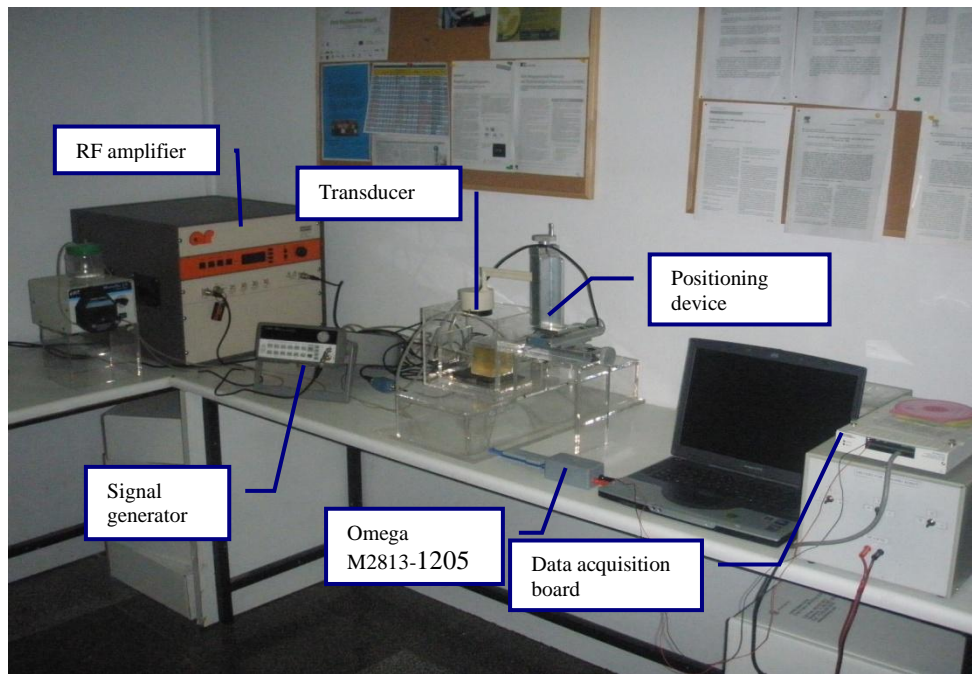


Figure 9.4 Photo of the HIFU system setup in the Lab

Coagulated blood (2 ml) was inserted from one side of the tube and 1 ml of rt-PA from the other side. A thin rod was used in order to push the rt-PA towards the clot. The artery/clot/tissue was then placed in the container filled with degassed water. The transducer was placed at the bottom of a water container. The transducer is energized using low intensity and therefore the disturbance of the water (jet) indicates the beam. Then the clot was placed accurately on the focal beam. Figure 9.5 shows a photo of the above system. This technique provides a very fast and accurate placement of the clot in the focal beam. The ultrasound temporal average *in situ* intensity ranged between 2.8 W/cm^2 and 36.8 W/cm^2 , with a duty factor (DF) of 10% and pulse repetition frequency (PRF) of 1 Hz. The ultrasound energy was applied for 60 minutes.



Figure 9.5 Photo of the artery/clot system

9.4 RESULTS

The goal in this study was to control temperature elevation and to have maximum ΔT not to exceed the 1°C limit. In order to achieve that various pulsed protocols were investigated (table 9.1). Figure 9.6 shows how temperature behaves at the centre of the clot under the sonication parameters used in table 9.2. Keeping the same power (5W) but tripled the duty factor, the maximum ΔT is also tripled (see figure 9.6A and 9.6B). Changing the power from 5W (figure 9.6A) to 10W (figure 9.6C) and leave the duty factor the same (10%) the maximum ΔT is also doubled its value. Using the same power (10W) but decreasing the duty factor to half, the maximum ΔT drops from 5°C to 3°C . ΔT is dropped only by 2°C (and not 2.5°C as in previous case) because PRP was increased from 1 ms to 1 s. Also, by doubled the power and keeping duty factor (5%) and PRP (1s) the same (figure 9.6D-9.6E), then the maximum ΔT was increased from 3°C to 5°C . Figure 9.7 summarizes the changes in temperature elevation (ΔT) with respect to power, duty factor, and PRP.

Table 9.2 Various sonication parameters

Case	Acoustical Power (W)	Duty Factor (DF)	Pulse Repetition Period (PRP)	Count	Temperature elevation (ΔT)
1	5	10%	1 ms	100	$<3^{\circ}\text{C}$
2	5	30%	1 ms	300	$>3^{\circ}\text{C}$
3	10	10%	1 ms	100	$>3^{\circ}\text{C}$
4	10	5%	1 s	50000	$<3^{\circ}\text{C}$
5	20	5%	1 s	50000	$>3^{\circ}\text{C}$

Ultrasound alone did not manage to liquefy the thrombus. Even though the acoustic power was increased from 5W to 30W and duty factor from 5% to 50%, the size of the thrombus remained unchanged. No alterations occurred regarding the size of the thrombus. The same experiment was repeated for different values of acoustic power and duty factor. Table 9.3 shows the sonication parameters used in the experiments. Because of the very high duty factor used, temperature elevation was always above 1°C.

Table 9.3 Sonication parameters (without rt-PA)

Power (W)	Acoustical Power (W)	Duty Factor (DF)	Pulse Repetition Period (PRP)	Thrombus size
10	5	30%	1 ms	unchanged
10	5	50%	1 ms	unchanged
20	10	40%	1 ms	unchanged
40	20	30%	1 s	unchanged
60	30	20%	1 s	unchanged

Figure 9.8 shows the silicone tube, which includes the clot (left), rt-PA (right) and dissolved clot (red colour). This was the effect of applying focused ultrasound for 60 minutes using frequency of 1 MHz, PRF of 1 Hz and duty factor of 10%. Approximately 6 mm of the clot was dissolved. The volume of the dissolved clot was 95.3 mm³. There was no generation of large amounts of clot fragments, which are undesirable therapeutically, because they could obstruct distal small arteries if used in humans.

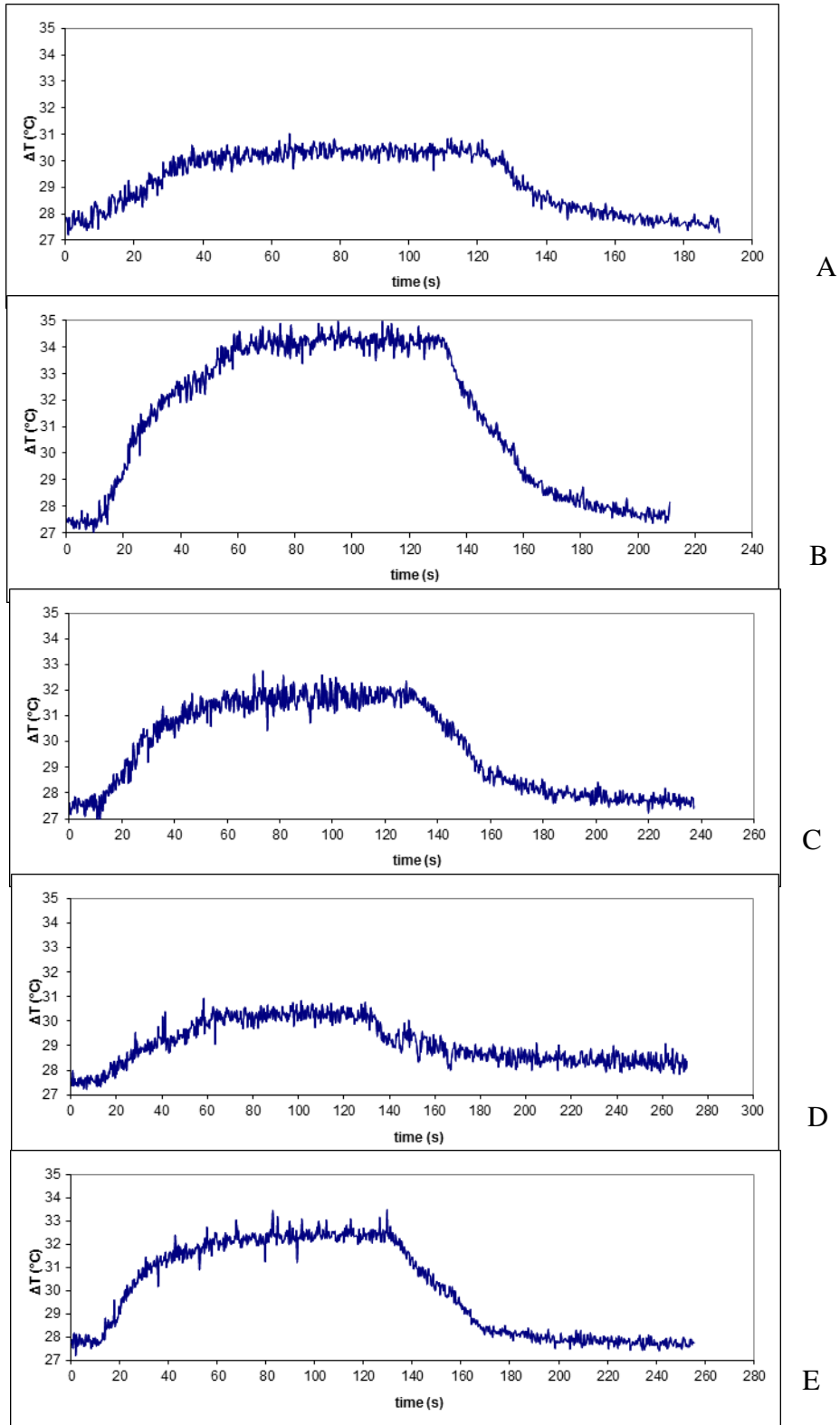


Figure 9.6 D; A $P=5$ W, $DF=10\%$, $PRP=1$ ms; B. $P=5$ W, $DF=30\%$, $PRP=1$ ms; C. $P=10$ W, $DF=10\%$, $PRP=1$ ms; D. $P=10$ W, $DF=5\%$, $PRP=1$ s; E. $P=20$ W, $DF=5\%$, $PRP=1$ s.

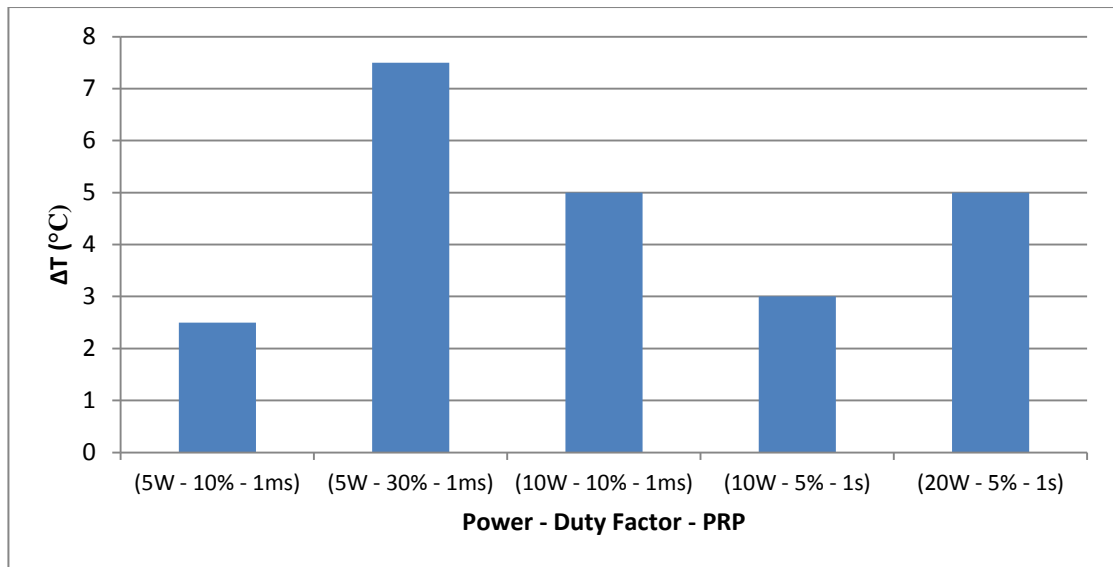


Figure 9.7 Temperature elevation vs power, duty factor, and PRP

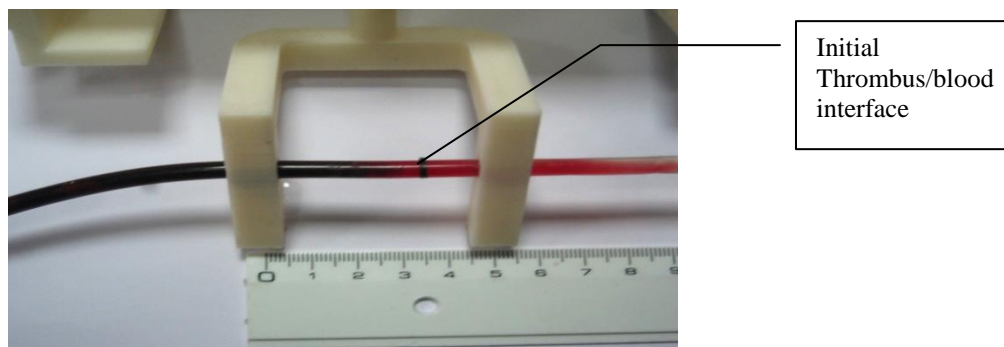
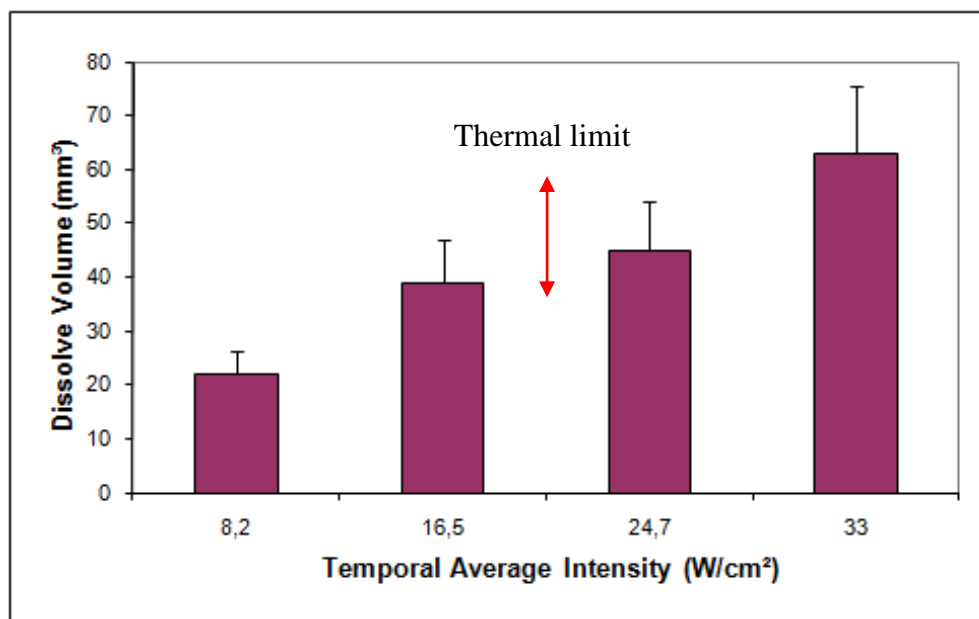


Figure 9.8 Silicone tube showing the clot (left), the rt-PA (right). The dissolved clot which is between the inserted clot and rt-PA appears in red colour.

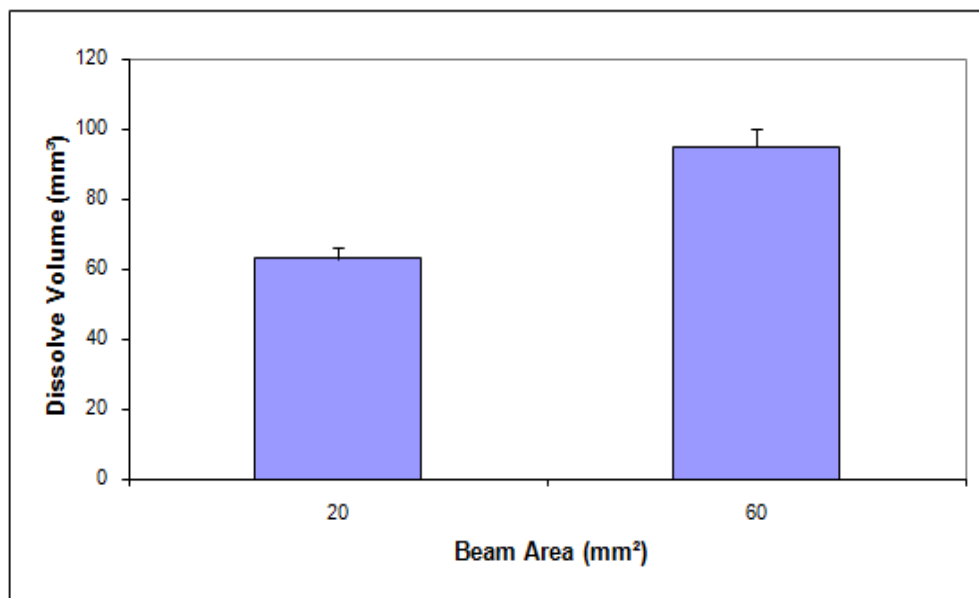
Figure 9.9A shows the effect of spatial average temporal average (SATA) *in situ* intensity on the volume of the dissolved clot with frequency of 1 MHz, duty factor of 10%, and PRF of 1 Hz. As the intensity increases the volume of the dissolved clot increases. Going to higher intensities, there is a risk of heating the clot (thermal ultrasound). For this specific experiment, using intensity below 20 W/cm² achieves a safe temperature (below 1° C) according to the thermocouple measurement. Figure 9.9B shows the effect of transducer beam area on the volume of the dissolved clot with frequency of 1 MHz, duty factor of 10%, and pulse repetition frequency of 1 Hz. The beam area of 20 mm² represents the case when the clot was placed on the focal beam. To achieve the 60 mm² beam area (derived from simulations), the clot was placed 1cm off the focus, thus achieving this large area. In both cases, the same *in situ* intensity (SATA) was used in the

target. Figure 9.9C shows the effect of the frequency on the volume of the dissolved clot using intensity of 36.8 W/cm^2 , duty factor of 10%, and PRF of 1 Hz. A higher frequency (1 MHz) transducer has a narrow beam (around 1–2 mm) and therefore achieves less thrombolysis than a lower frequency (0.5 MHz) transducer.

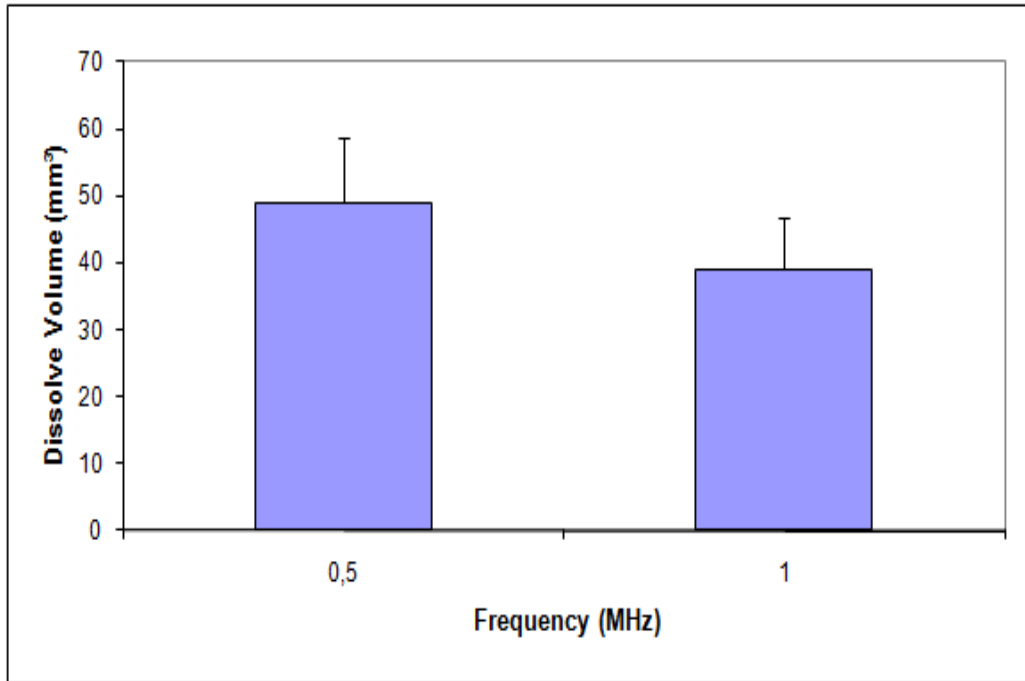
When rt-PA was used alone, under the same parameters used in US+rt-PA, the total amount of the dissolved thrombus was around 40%. Figure 9.9D compares the two types of treatment after 60 min exposure and under different intensities.



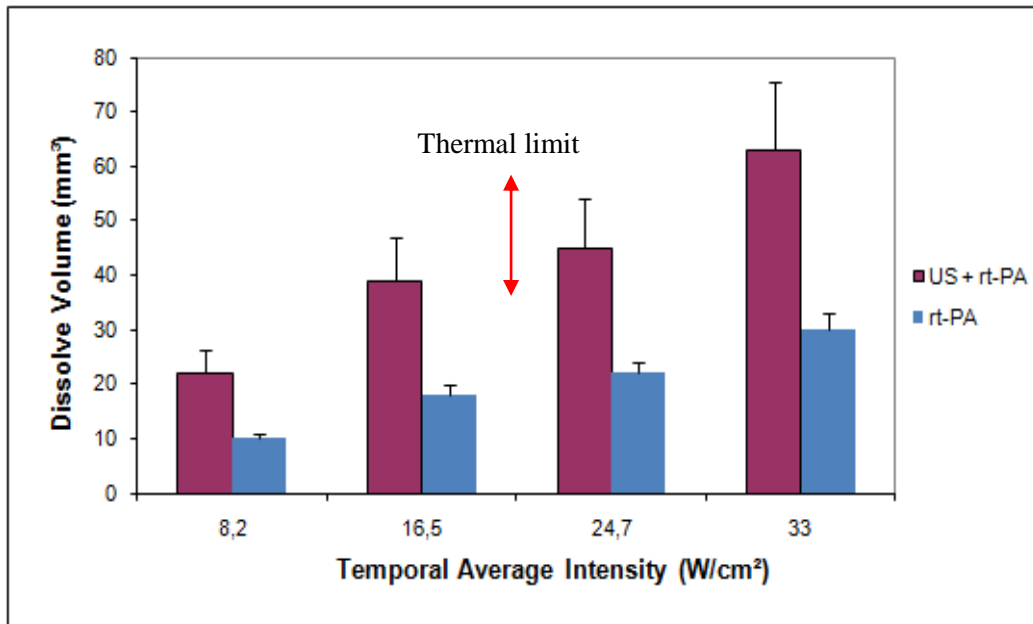
A



B



C



D

Figure 9.9 A. The effect of temporal average *in situ* intensity (SATA) on the volume of the dissolved clot with frequency of 1 MHz, duty factor of 10%, and PRF of 1 Hz.; B. The effect of transducer beam area on the volume of the dissolved clot with frequency of 1 MHz, duty factor of 10%, and PRF of 1 Hz. For both beam areas the same temporal average *in situ* intensity was used; C. The effect of frequency on the volume of the dissolved clot using temporal average *in situ* intensity of 36.8 W/cm², duty factor of 10%, and PRF of 1 Hz; D. Comparison between US+rt-PA and rt-PA on the total dissolved clot volume after 60 min exposure.

9.5 DISCUSSION

The results in this study demonstrate the ability of the HIFU system to dissolve clots in combination with rt-PA. The main task in this parametric study is to evaluate the effect of intensity, beam area and frequency on the volume of the dissolved clot, while maintaining temperature change at the clot below 1°C.

In this study, we have shown that higher intensity results to higher volume of dissolved clot, but there is a limit of the intensity to be used in order to avoid heating of the clot and the surrounding tissue. The goal in this study was to achieve temperature elevation not exceeding 1°C. With lower intensity, the volume of the dissolved clot is lower which means longer treatment time. This is a limiting factor since for the potential use of this system (treatment of ischaemic stroke), time is limited to around 3 hours. With the parameters used in the experiment of figure 9.9A it was found that the maximum temporal average *in situ* intensity to use is around 20 W/cm². It was found that the larger the beam area the larger the dissolved clot volume. Finally, the lower the frequency, the larger the volume of the dissolved clot (figure 9.9C). High frequencies have poor skull penetration and a small beam size at the focus, while low frequencies have better skull penetration but with the risk of reaching the unpredictable effect of cavitation.

The importance of minimizing the thermal effects by monitoring and controlling the temperature is cited in many papers. For example in the study by Ishibashi et al. [47] a temperature of 3°C is reported for a 60 min sonication. In another study by Kornowski et al. [174] a temperature of 7° C is reported for a sonication of 60 minutes which could possibly produce thermal heating if the same protocol was applied in humans. In the study by Francis et al. [185], the effect of intensity on temperature was demonstrated. By using ultrasound to dissolve clots with intensity of 8 W/cm² the temperature produced was 3° C, whereas by decreasing the intensity to 2 W/cm² the resulting temperature was 1° C.

The effect of increased fibrinolysis due to increased intensity was shown by several studies using unfocused ultrasound. Also, in the study by Suchkova et al.

[186] it was shown that fibrinolysis increases dramatically with intensity and above 1 W/cm² no more significant increase is observed. In the study by Suchkova et al. [186] increased fibrinolysis with ultrasound was achieved with minimal mechanical disruption of the clot, indicating that enhancement of clot dissolution is due primarily to accelerated enzymatic action. The same trend of fibrinolysis due to increased intensity was also seen by Francis et al. [185], Suchkova et al. [187] and Nedelmann et al. [188], which were demonstrated that fibrinolysis is dependent on the applied ultrasound intensity and on the exposure time. The effect of rt-PA dose, repetition frequency and duty factor was already shown by Suchkova et al. [187] and therefore not explored in the present study. The study by Suchkova et al. [187] and Holland et al. [173] have shown that statistically significant enhancement of the fibrinolysis rate was achieved even with a 1% duty cycle. The ultrasound efficacy with duty cycles of 10% or less tell us that ultrasound quickly produces a change in the clot that persists for a significant time after the sound is turned OFF.

In the present study we have used ultrasound and rt-PA alone. Significant improvement in the efficacy of this technology could be achieved by using microbubbles as it was recently shown by Datta et al. [189] provided that uncontrolled cavitation effects are avoided. Even though the ultrasound intensities used to achieve a significant thrombolytic effect were relatively low, the safety and efficacy of ultrasound thrombolysis requires a careful evaluation in animal models, regarding the biological side effects of ultrasound in brain tissue, especially if cavitation exists.

For therapeutic applications in the brain, noninvasive external application of ultrasound compared to endovascular use of ultrasound [190] has greater potential, because it requires neither angiography nor selective catheterization [186]. It eliminates the risk of vessel wall damage by the catheter, and it could be used for small vessels or vessels that are inaccessible for catheterization.

The results presented in this study correspond to targets that are 1 cm deep. If this technology is applied to humans with target ranging from 3-8 cm [188], then to get the same intensity (or pressure) as in the 1 cm case (covered by this chapter),

one has to increase the power, which might cause excess tissue heating. Therefore, the only controlling parameter to reduce the heating is to lower the duty factor. Thus, the application of this technology in humans requires extensive parametric studies (including intensity, frequency, duty factor, pulse repetition frequency, and exposure time) in order to avoid thermal heating. The successful application of FUS to improve fibrinolytic therapy in clinical settings will depend critically on the choice of ultrasound parameters to maximize fibrinolytic enhancement, while limiting unwanted adverse effects such as heating and cavitation. The results reported here point to the use of frequency around 0.5 MHz and pulsing to optimize thrombolysis and skull penetration and at the same time avoiding unwanted heating. Table 9.4 presents a summary of the parameters used for the recommended HIFU system.

Table 9.4 Summary of the recommended HIFU system

Frequency (MHz)	Intensity (W/cm ²)	Pulse Duration (min)	Transducer Beam	Duty Factor (DF)	ΔT
1	2.8 - 20	60	At the focus	10%	$\leq 1^{\circ}\text{C}$
0.5	36.8	60	At the focus	10%	$\leq 1^{\circ}\text{C}$
1	20	60	1 cm off the focus	10%	$\leq 1^{\circ}\text{C}$

The following chapter presents experiments *in vivo*. The thrombus model was tested in the rabbit carotid and in the ear artery *in vivo*. Also, the effect of HIFU was examined in cooperation with rt-PA to liquefy thrombus which was placed in the ear artery of the rabbit *in vivo*.

CHAPTER 10: APPLICATION OF MR-GUIDED FOCUSED PULSED ULTRASOUND FOR DESTROYING CLOTS *IN VIVO* USING THROMBOLYTIC DRUGS

10.1 INTRODUCTION

Stroke is the third cause of death after heart diseases and cancer (see table 2.1). Stroke is the number one cause leading to disability. Rt-PA is the only FDA approved drug for the treatment of stroke. The therapeutic result of rt-PA is due to the opening of canals and the bypassing of the blocked artery and is function only to selected patients. However, the success of the method is not yet significant. Intracerebral haemorrhages occur within 36 hours in 6.4% of the patients who received thrombolytic therapy [192].

Ischaemic stroke is by far the most common kind of stroke, accounting for about 88% of all strokes. The brain depends on its arteries to bring fresh blood from the heart and lungs. When an artery to the brain is blocked then ischaemic stroke occurs. If the artery remains blocked for more than a few minutes, the brain cells may die. This is why immediate medical treatment is critical. Ischaemic stroke can be divided into two main types: thrombotic and embolic. A thrombotic stroke occurs when diseased or damaged cerebral arteries become blocked by the formation of a blood clot within the brain. In an embolic stroke, a blood clot forms somewhere in the body and travels via the arteries to the brain until it reaches a vessel small enough to block its passage.

In previous studies, unfocused ultrasound has been proven to accelerate fibrolysis and to significantly reduce the size of the thrombus or to restore recanalization (table 10.2). In addition, the range of intensity used ranged from 0.2–1.3 W/cm² (spatial peak temporal average intensities) and the frequency ranged from 25 kHz to 2 MHz using unfocused ultrasound. Table 10.1 summarizes some of the characteristics of ultrasound and thrombolysis derived from experiments *in vivo*.

In this chapter, the thrombus model was tested in the rabbit carotid and ear artery *in vivo*. Also, the effect of therapeutic ultrasound was examined in cooperation with rt-PA to liquefy thrombus which was placed in the ear artery of the rabbit *in*

vivo. For the first time, HIFU targeting the thrombus at the focal point was used with acoustic power of 50W and a frequency of 1 MHz. The goal in this study was to investigate the ability of the thrombus to block the artery and to investigate the proposed protocol for its capability to destroy the thrombus.

10.2 FOCUSED ULTRASOUND SYSTEM/ULTRASONIC DOPPLER SYSTEM

The ultrasound system consists of a radio frequency (RF) generator/amplifier (100 W, JJ&A Instruments, Duvall, WA, USA), and a spherically shaped transducer made from piezoelectric ceramic of low magnetic susceptibility (Piezotechnologies, Etalon, Lebanon, IN, USA). The transducer used operates at 1 MHz and has focal length of 10 cm and a diameter of 5 cm. An ultrasonic Doppler system (Philips HD7 series Ultrasound Systems, Philips and Neusoft Medical Systems Co. Ltd, Shenyang, China) was used to observe the blood flow.

Table 10.1: Characteristics of Ultrasound and Thrombolysis (Protocol: *in vivo*)

Subject	Frequency	Intensity	Mode	Duty Factor	Sonication Time (min)	Focused / Unfocused	rt-PA Dose	Results	First Author
Humans	2 MHz	415 mW/cm ²	CW		25m to 24H	TCCD	None – aspirin 250mg	1 person complete recanalization, 83% the rest.	Cintas et al. 2002 [217]
	1.8 MHz	179 mW/cm ²	PW	transcranial pulsed wave	60	diagnostic ultrasound	0.9 mg/kg	Recanalization: With US=57.9% Without US: 22.2%	Eggers et al. 2008 [169]
Rats	185 KHz	1.27 W/cm ²	CW		90	unfocused	1mL/100mg/mL	185KHz is superior to 1 MHz diagnostic US.	Behrens et al. 2001 [216]
	25.570 Hz	0.6 W/cm ²	PW	20%	60	unfocused	10mg/kg	Reduction of infract volume by 68%. Bleeding effects: 9.3%.	Daffertshofer et al. 2004 [54]
	490 KHz	0.8 W/cm ²	CW		60	unfocused	1.2 mg/animal	Thrombolysis: TUS: 76.2 % t-PA: 45 % Death: TUS: 4.55 % t-PA: 4.76 %	Saguchi et al. 2008 [168]
Rabbits	1 MHz	6 W/cm ²	PW	10%	60	HIFU	1.0 mg/ml	Complete Recanalization	Hadjisavvas et al. 2012

10.3 ARTERY/TISSUE/CLOT MODEL

Coagulated blood (thrombus) was inserted through the carotid artery and through the ear artery. Blood flow was observed in the brain and in the ear artery before and after the insertion of coagulated blood. To observe the blood flow, a Philips Ultrasonic Doppler system was used.

Production of sample clots

Blood clots were obtained by natural coagulation of animal blood samples from healthy cows. Blood was drawn into small containers and placed in a 37° C water bath for 3 h and then stored in a refrigerator at a temperature of 5° C for at least 72 h before use in the experiments to allow complete clot formation [173].

Preparation of rt-PA

The rt-PA was obtained as a lyophilized powder (rt-PA, Activase, Genentech, San Francisco, CA, USA) mixed with sterile water as per manufacturer's instructions. A dose of 1mg/mL/kg was administered.

10.4 TESTING THE THROMBUS FUNCTIONALITY *IN VIVO*

To test the quality of thrombus, New Zealand adult rabbits were used weighting approximately 3.5-4 kg. Three rabbits were used in the experiments. The rabbits were anaesthetized using a mixture of 500 mg of ketamine (100 mg/mL, Aveco, Ford Dodge, IA), 160 mg of xylazine (20 mg/mL, Loyd Laboratories, Shenandoah, IA), and 20 mg of acepromazine (10 mg/mL, Aveco, Ford Dodge, IA) at a dose of 1 mL/kg. The animal experiments protocol was approved by the national body in Cyprus responsible for animal studies (Ministry of Agriculture, Animal Services).

The presence of the skull in the ultrasonic path distorts the ultrasonic field by reflection and distortion. Therefore, a craniotomy was necessary in order to permit unimpeded passage of the sound. The craniotomy should be large enough to reveal the whole brain (top view). Figure 10.1 shows the craniotomy and the top view of the rabbit brain. For better understanding the structure and location of the main brain arteries, CT and MRA images are shown. Figure 10.2 shows a CT image of the rabbit's brain and pointing out the basilar and vertebral arteries

[193]. Middle Cerebral Arteries (MCA) were imaged successfully using Magnetic Resonance Angiography (MRA). Figure 10.3 shows an MRA image of the rabbit MCA.

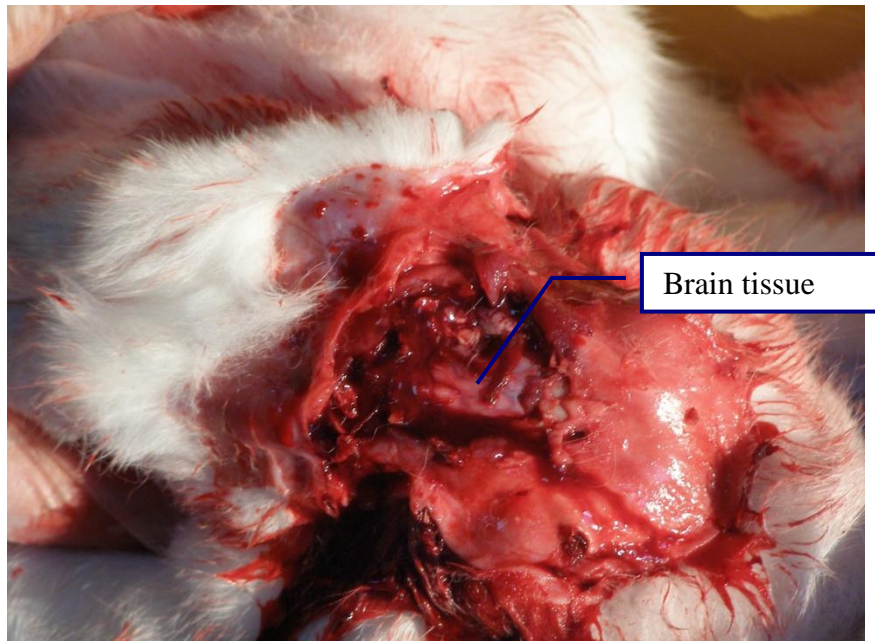


Figure 10.1 A top view of a rabbit brain after a craniotomy was performed.

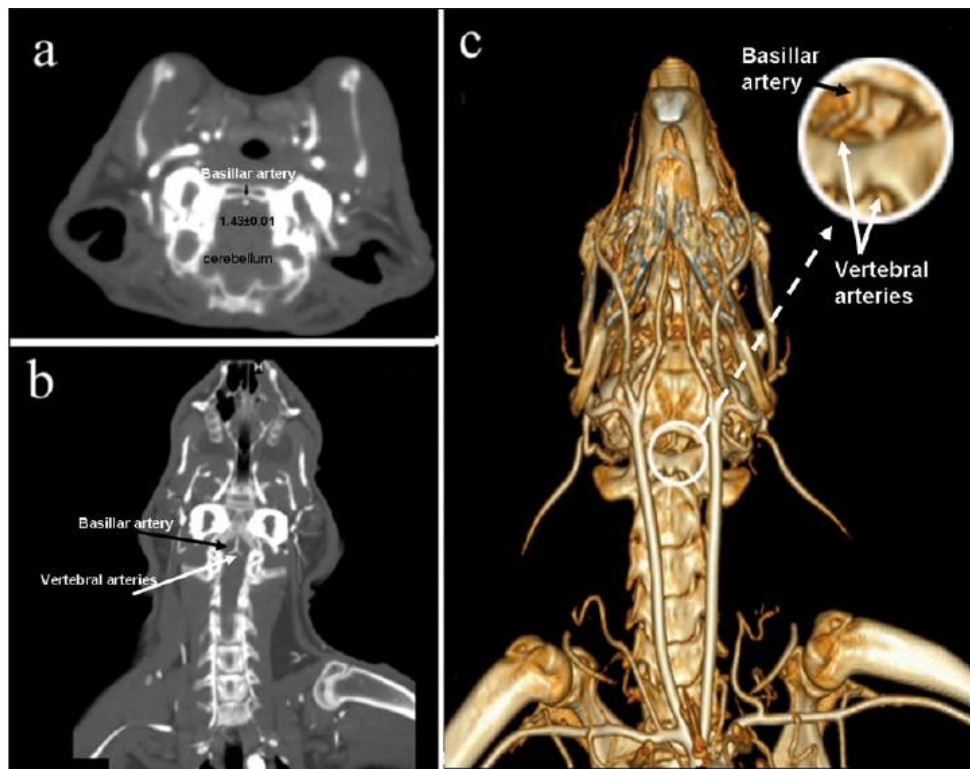


Figure 10.2 a) MRI axial, b) MRI coronal, c) three-dimensional cranial CT of basilar and vertebral arteries in rabbit[193]



Figure 10.3 MRA image of a rabbit MCA

A cut was made at the side of the rabbit neck to extract the carotid (figure 10.4). Figure 10.5 shows a photo how the ultrasonic probe is used to scan the blood flow on top of the brain and the carotid artery. Figure 10.6 shows the displacement of the catheter into the carotid. A 24 G over the needle standard intravenous catheter was used. Through the catheter the thrombus (clot) was inserted into the carotid and the blood flow was observed in the brain using a Doppler ultrasound.

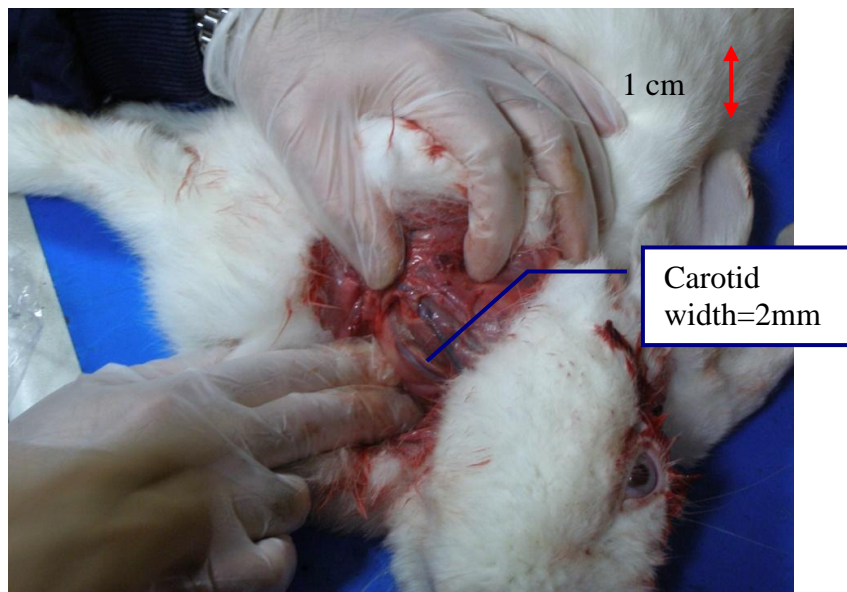


Figure 10.4 Extracting the carotid.

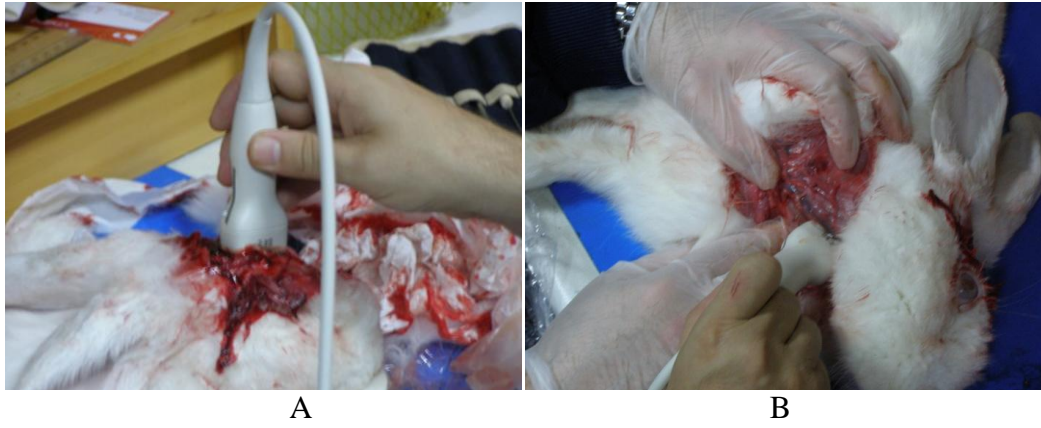


Figure 10.5 A. Ultrasonic imaging probe placed on top of the brain; B. Ultrasonic imaging probe placed on the exposed carotid.

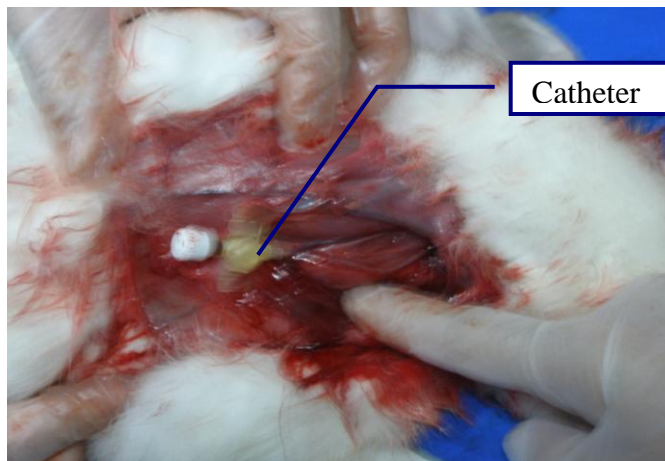


Figure 10.6 The displacement of the catheter into the carotid.

The ultrasonic probe was placed on top of the brain and continuously monitored the blood flow from the moment that the thrombus was injected through the catheter until the rabbit died (stroke was the cause of death).

10.5 DETECTION OF THROMBUS USING MRI

MRI contrast between blood and clot (thrombus) has been tested. Figure 10.7A shows a picture of the container made by ABS. The ABS material is MRI compatible. Figure 10.7B shows the container before it was placed in the MRI scanner (Signa 1.5 T, by General Electric, Fairfield, CT, USA). In the middle of the container, there was a canal of 3 mm width simulating an artery. On the same path, there was another trunk where the thrombus was placed. On the left and on the right of the canal two lamb brains were placed. The general idea was to have an artery drawn inside the brain and to investigate the potential of the MRI to

distinguish between blood and thrombus. To image the thrombus, T1 and T2 W FSE MRI sequence were used (T1-W FSE: TR=500 ms, TE=9 ms and T2-W FSE: TR=2500 ms, TE=60 ms).

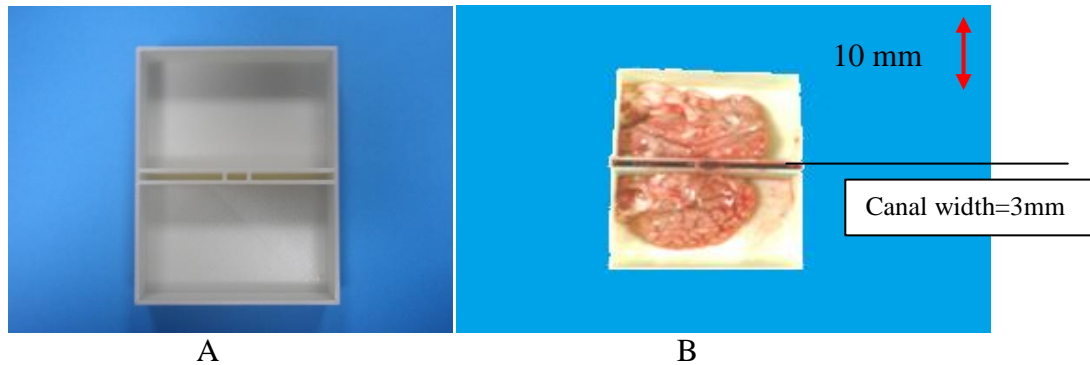


Figure 10.7 A. MRI compatible container; B. Artery/thrombus/brain tissue model.

10.6 THROMBOLYSIS *IN VIVO*

10.6.1 COUPLING METHOD

A new coupling method was used for the *in vivo* experiments. A long transducer holder (figure 10.8) was developed for better accuracy and control when focusing the beam. The transducer was mounted on a metallic stand and water was injected through one of the 2 holes at the top of the holder (figure 10.9). As the water was injected from one hole, air escaped from the other hole. Caution was taken to avoid any bubbles inside the holder. A thin membrane was placed at the bottom of the holder. For localization, a thermocouple was used. A plastic circular cover with a hole in the centre was placed above the thermocouple (figure 10.10). The transducer was aligned with the circular cover and then the cover was removed. Localization was accurate within 1 mm (figure 10.10).



Figure 10.8 Long transducer holder.

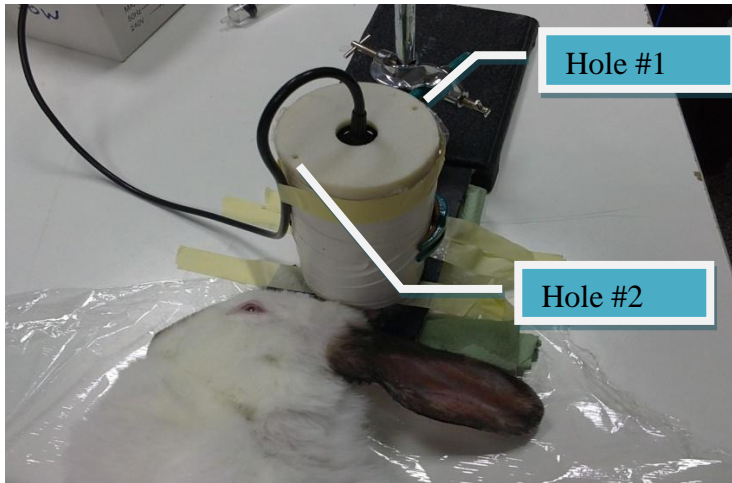


Figure 10.9 Transducer setup showing the two holes on top of the holder.



Figure 10.10 Transducer localization.

10.6.2 THROMBUS MODEL

For the following experiments, both ears of the rabbit had to be shaved (figure 10.11).



Figure 10.11 Shaving rabbit ears.

There are many ways by which the middle cerebral artery (MCA), the external/internal carotid, or any other artery can be blocked in order to provoke thrombosis or a stroke in experimental animal models. Some of the methods used are: injection of a foreign or autologous thrombus, microemboli, electrocoagulation, microvascular clips, etc. Table 10.2 summarizes the most popular thrombus models used in animals.

Two different methods of experiments were performed; first to investigate the functionality of the thrombus (method A) and second to destroy thrombus using focus ultrasound and rt-PA (method B).

Method A: through the ear artery, 1 ml of thrombus [10] was injected (figure 10.12) and the blood flow was monitored by a Doppler ultrasound. As soon as the thrombus was injected degradation of the blood flow was noticed. A few minutes later there was no flow at all (figure 10.20B). The thrombus has totally blocked the ear artery. With this method neither ultrasound nor a thrombolytic drug were applied.

Method B: The ear artery was punctured very carefully using a small hammer (figure 10.13A). When the artery was damaged (injured), the clot started to construct (figure 10.13B). At the same time, the blood flow was monitored using the Doppler ultrasound. Eventually, after 20 minutes, the ear artery was 100% blocked. No blood flow was observed (figure 10.21B).

Table 10.2: Thrombus model in animals

Thrombosis Models	Animal	Model of injection / Method(Area)	Thrombus formation	Ref.
Ferric chloride-induced thrombosis	Rats	carotid-artery	thrombus formation by chemical damage to the vessel wall via topical administration of FeCl ₃	Heran et al [194]
Venous	Rats	inferior vena cava	induce stasis of blood in the inferior vena cava	Sato et al [195]
Arteriovenous Shunt Model	Rats, Rabbits	placed in-line between the carotid artery and the jugular vein	formation of a “mixed” thrombus (platelet and fibrin-dependent)	Wiley et al [196], Wong et al [197]
Disseminated Intravascular Coagulation	Rats, Mice		Systemic thrombosis or disseminated intravascular coagulation (DIC)	Yamazaki et al [198]
Wessler Rabbit Model	Rabbits	jugular vein	a stasis is produced in the jugular vein and a thrombogenic substance, such as thrombin, is placed in the stasis “pouch”	Wessler et al [199]
Thrombin-Induced Rabbit Femoral-Artery Thrombosis	Rabbits	A clot is introduced into an isolated segment of femoral artery	by injection of thrombin, calcium chloride, and fresh blood via a side branch	Shebuski et al [200]
Folts Coronary Thrombosis Model.	Dogs, Rabbits	stenosed coronary arteries of open-chest femoral or carotid artery	Partial obstruction of the coronary artery with a plastic Lexan cylinder results in episodic cyclical reductions in coronary blood flow that are caused by platelet-dependent thrombus formation	Folts et al [201]
Copper Coil-Induced Canine Arterial Thrombosis	Dogs	The spiral was inserted through the coronary-vessel wall in open-chest dogs. Insertion of the thrombogenic coils via the left carotid artery under fluoroscopic guidance in closed-chest dogs	spiral wires constructed of aluminum-magnesium alloy inserted into the coronary circulation of dogs to produce slowly developing occlusive thrombi	Blair et al [202], Kordenat et al [203]
Canine femoral arterial	Dogs, Rabbits	uses the same thrombogenic coils, but does not require fluoroscopy		Bush et al [204]
Thrombin-Induced Clot Formation in the Canine Coronary Artery	Canine	coronary-artery thrombosis	The vessel was intentionally de-endothelialized by external compression with blunt forceps	Gold et al [205]
Injury-Induced (Electrolytic) Arterial Thrombosis in the Canine	Dogs	electrode was placed directly into the coronary artery of an open-chest, anesthetized dog	anodal current was delivered to the intravascular lumen of a coronary artery in the dog via a stainless-steel electrode	Romson et al [206]
Arteriovenous Shunt Model in Baboons	Baboons	exteriorized chronic arteriovenous shunt	a thrombogenic segment is placed in an exteriorized chronic arteriovenous shunt	Todd et al [207]
Venous Thrombosis	Cats, Baboons		rely primarily on stasis in which blood flow is interrupted for varying periods of time to induce clot formation	Eppheimer et al [208], Wakefield et al [209]
Rabbit Auricular artery	Rabbits	Direct injection of 1 ml of thrombus Artery was carefully injured	Thrombus was injected into the auricular artery Thrombus formation after 20min	Hadjisavvas et al. 2012



Figure 10.12 injection of the thrombus.



Figure 10.13 A. Creation of clot (thrombus) using a hammer; B. Clot formation.

Once the blockage of the ear artery was confirmed using the Doppler ultrasound (no blood flow was observed), then the ultrasound and rt-PA (US + rt-PA) therapy was applied. Figure 10.14 demonstrates the localization method used on the rabbits ear. The thermocouple was only used to find the focal point. The focal point was found when temperature rose fast during continuous ultrasound exposure and dropped fast when the ultrasound exposure was turned off. A 1mg/ml/kg rt-PA was injected in the ear artery (figure 10.15A). Then, a 60 min ultrasound exposure using 50W of acoustic power, pulse rate of 10 Hz, frequency of 1 MHz and duty factor of 10% was applied. Figure 10.15B shows the setup of the ultrasonic system.



Figure 10.14 A. Thermocouple placements on clot for localization; B. Transducer target for quick localization



Figure 10.15 A. injection of rt-PA; B. Ultrasonic system setup.

10.7 RESULTS

Currently available MRI methods to determine arterial occlusion are depended on different parameters such as blood flow, blood longitudinal relaxation time and sequence parameters [210]. Signal intensity, which is based on these parameters, may make analysis of thrombolysis complicated. Even though different publications by Johnstone et al [211], Corti et al [212] and Schmitz et al [213] have demonstrate the ability of the MRI to point out the location of a thrombus, some others such as Johansson et al [214] and Peter et al [215] have shown the difficulty of differentiating between the blood and thrombus. Corti et al. [204] have demonstrated that MRI sequences (T1-W and T2-W) have the potential to image thrombus at the carotid. Thrombotic and normal carotid arteries were identified correctly in the axial images using black-blood technique. Figure 10.16 shows the axial black-blood T2-W MRI image of a 24-hour-old thrombus.

The potential of the MRI to distinguish between blood and clot in a custom-made system using MRI T1 W FSE and T2 W FSE, values of blood and clot are similar and therefore contrast is very poor. Figure 10.17 demonstrates that the contrast between blood and clot is the same.

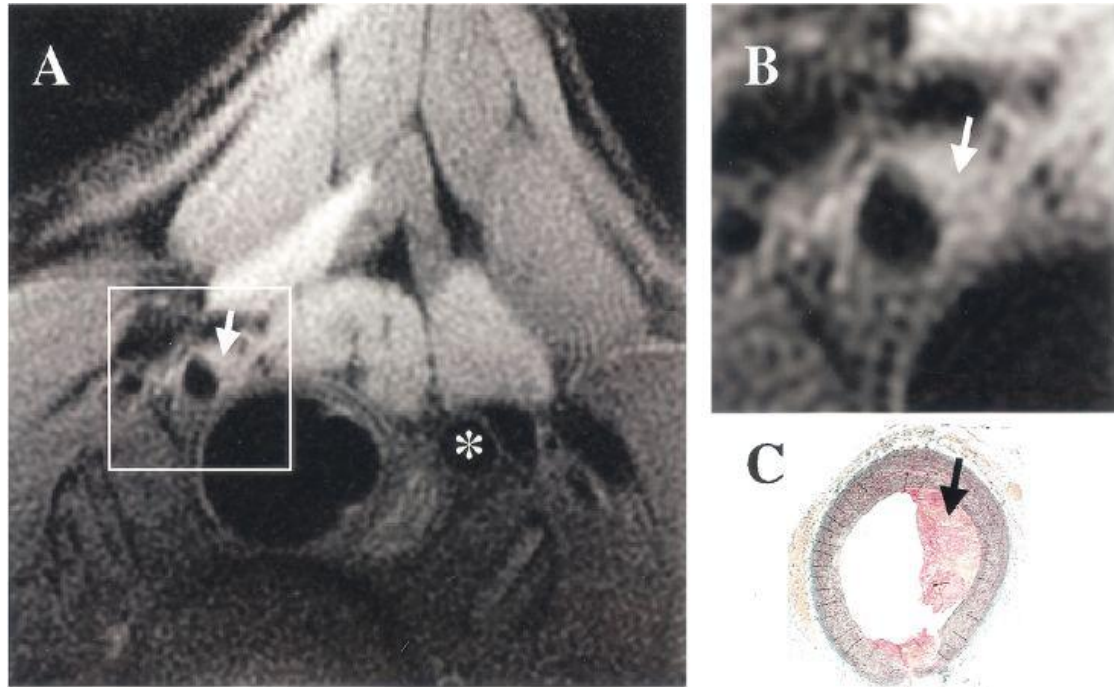


Figure 10.16 A. axial black-blood T2-weighted magnetic resonance images showing a 24-h old thrombus; B. the arrows indicate the thrombus in the injured right carotid artery, and the asterisk indicates the non injured left carotid artery; C. the appearance of the thrombus on the magnetic resonance image correlates closely with the matched histologic section shown in C (Corti et al. [212]).

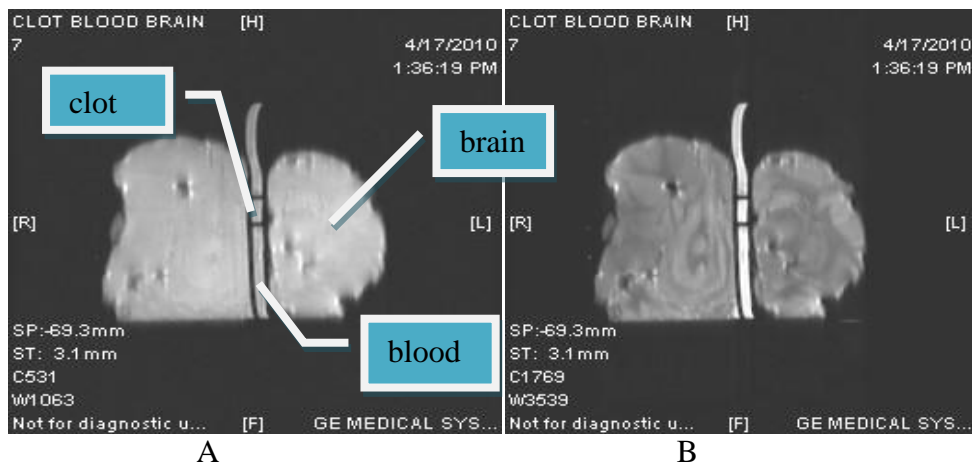


Figure 10.17 MRI images A. using T1 FSE; B. using T2 FSE.

Using Doppler ultrasound, images of the blood flow at the brain tissue and at the carotid were captured. Figure 10.18A demonstrates scan images of the blood flow

at the carotid and figure 10.18B demonstrates scan images of the blood flow at the top of the brain, both before the thrombus injection.

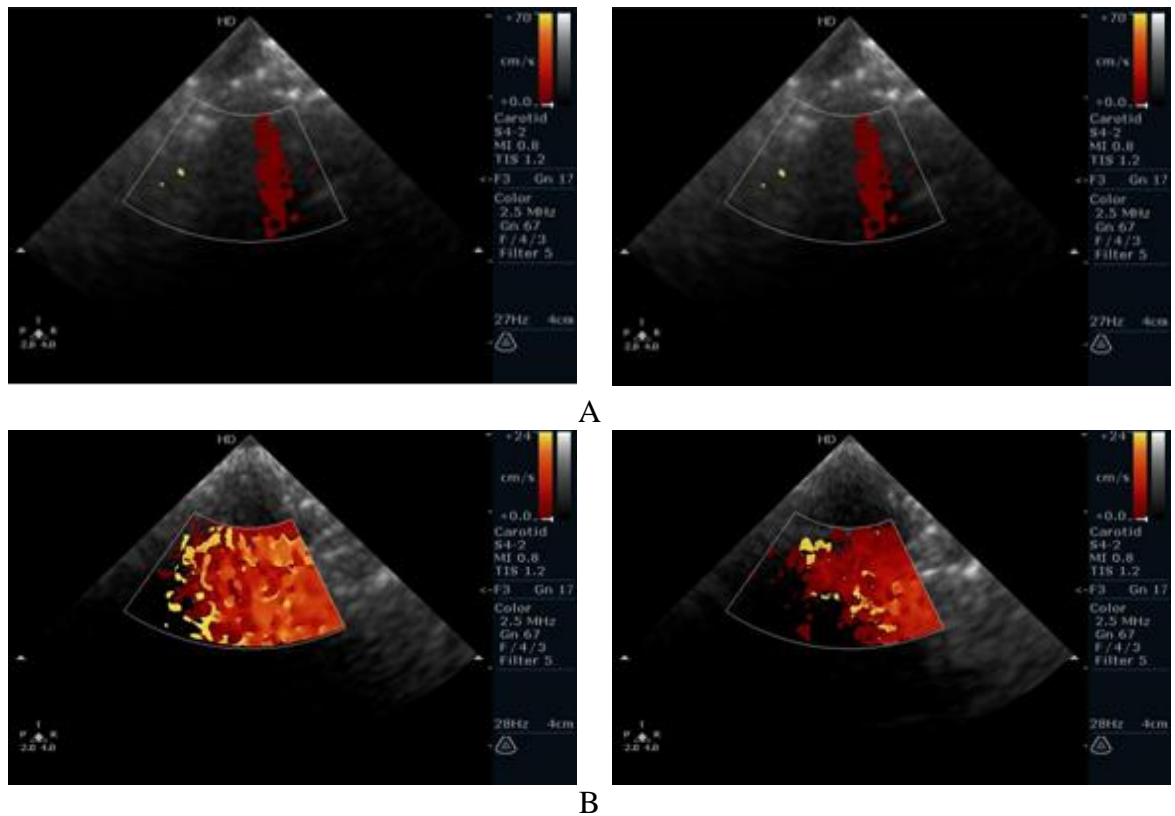


Figure 10.18 Blood flow using Doppler ultrasound; A. At the carotid; B. At the top of the brain.

Figure 10.19 show scan images of the blood flow in the brain after the thrombus was injected into the carotid via a catheter. It was observed that the blood flow was decreasing with respect to time and in approximately 2 ½ minutes there was no flow at all causing death.

Using method A, when 1 ml of thrombus was injected in the ear artery, a similar behaviour occurred as when it was placed in the carotid. The Doppler ultrasound was placed on the ear artery before and after the thrombus to monitor the blood flow. Ten minutes after the injection of the thrombus, the ear artery was totally blocked. Figure 10.20 show scan images of the blood flow at the ear artery before and after the injection of the thrombus.

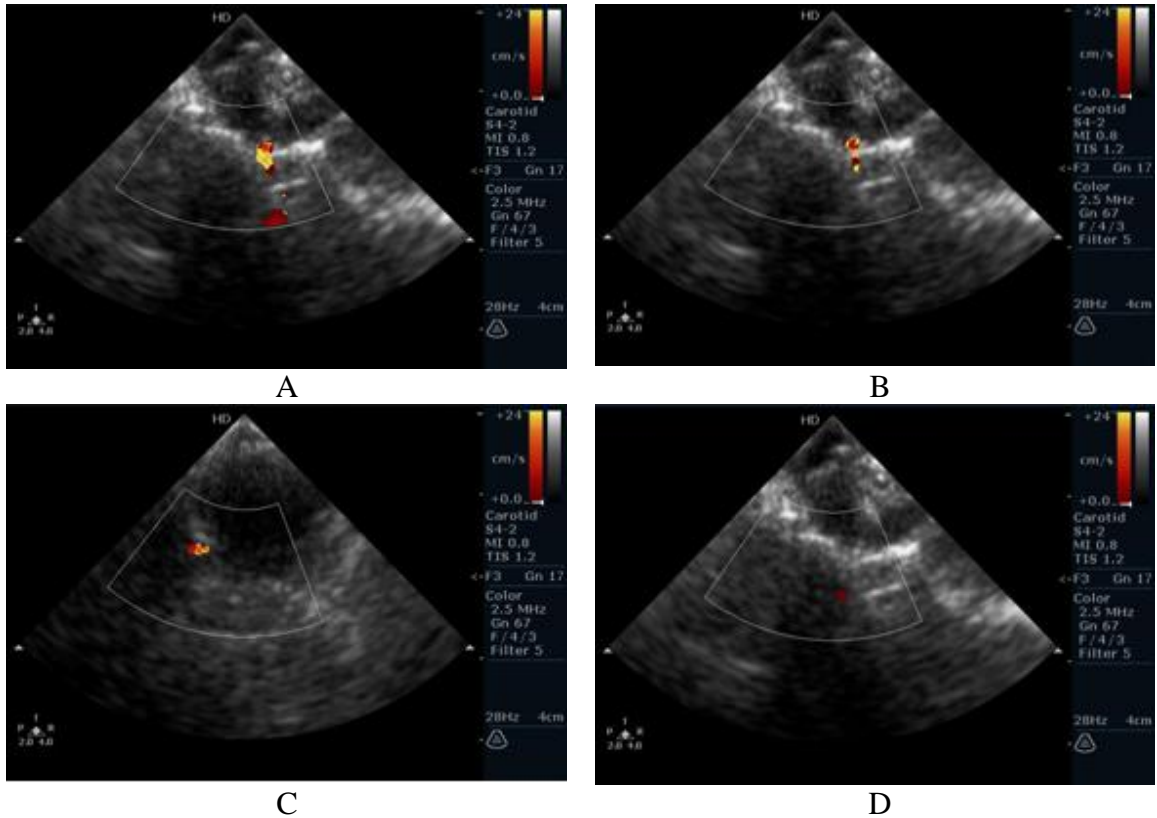


Figure 10.19 Blood flow after the injection of a thrombus using a Doppler ultrasound; A. after 1 min; B. after 1½ min; C. after 2 min; D. after 2½ min

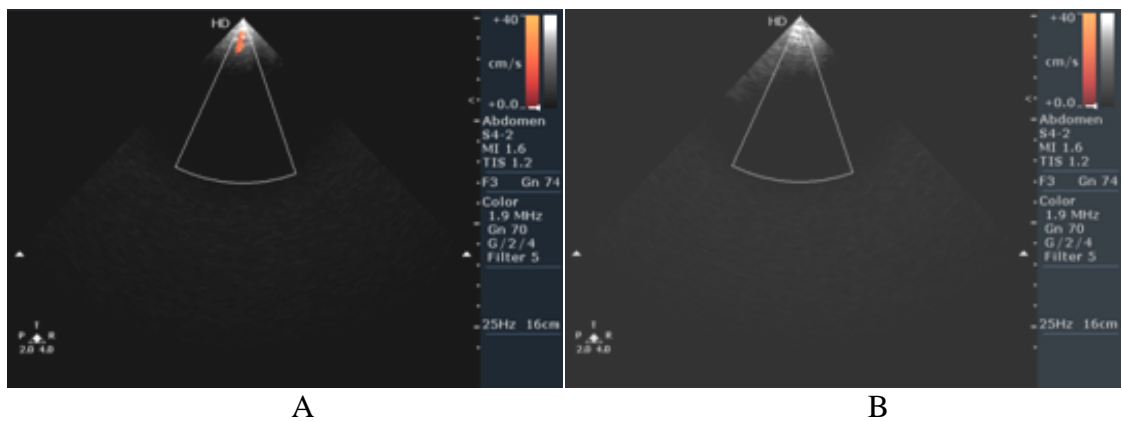


Figure 10.20 Blood flow; A. before the thrombus injection; B. after the thrombus injection.

Using method B, as soon as the artery was totally blocked the thrombolytic drug (rt-PA) was injected and ultrasound exposure (US) was initiated. Figure 10.21A shows a scan image of the blood flow at the ear artery before the creation of the thrombus, figure 10.21B shows the blood flow after the obstruction of the artery from the thrombus, and figure 10.21C shows the blood flow after sonothrombolysis (US + rt-PA) was applied.

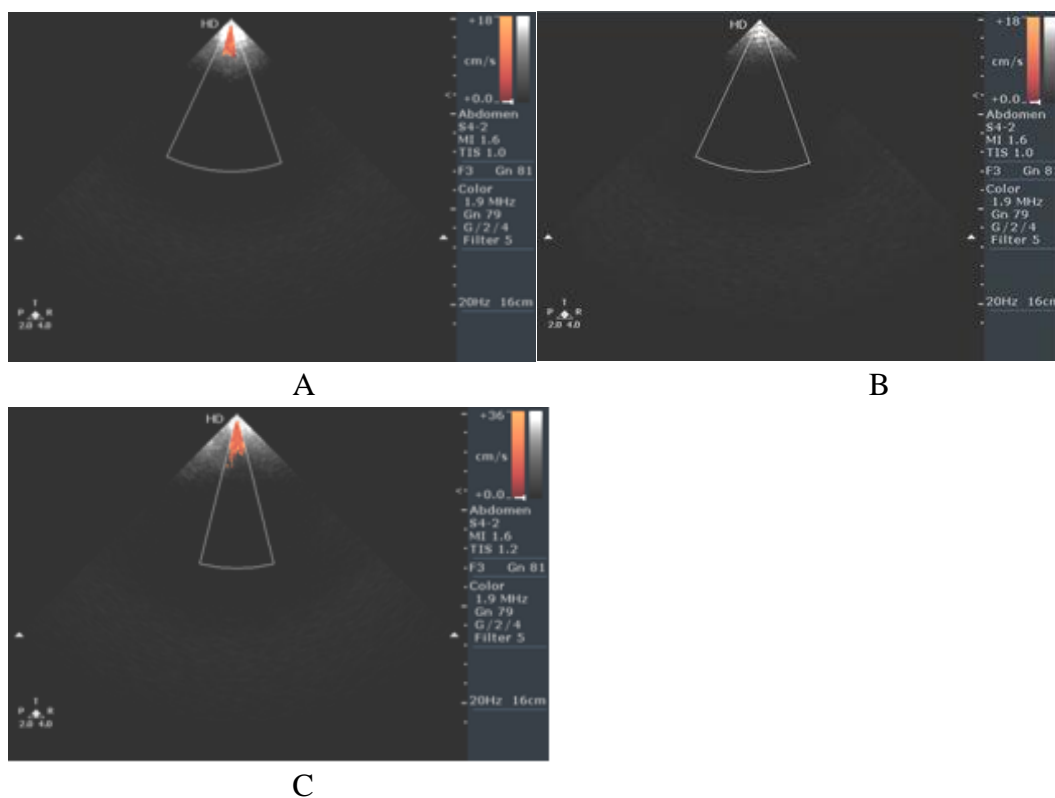


Figure 10.21 Blood flow; A. before thrombus creation; B. after artery occlusion; C. after sonothrombolysis.

10.8 DISCUSSION

The results in this study demonstrate the ability of the ultrasonic system to evaluate the quality of the thrombus and to dissolve the thrombus in combination with rt-PA. It was shown that when a thrombus (coagulated blood) was inserted via catheter in the exposed carotid artery (figure 10.6) the blood flow was blocked in the brain and within 2 to 3 mins the rabbit died due to a stroke. In order to test the functionality of the thrombus on a different artery (ear artery), the same but smaller amount of thrombus was used. The thrombus was injected in the ear artery (figure 10.12) and the blood flow was observed using a Doppler ultrasound. After 10 mins, there was no indication of blood flow at the ear artery. Therefore, coagulated blood is a good model for clot since it can cause a stroke.

To create a clot model, a different technique was also used (see method B). The ear artery was injured using a small hammer. Monitoring the blood flow at all times, it was noticed that in approximately 20 mins after the creation of the

trauma, there was no blood flow at all. Therefore, both methods proved to be sufficient for creating a clot model.

MRI T1 W FSE and T2 W FSE sequence were used to image the thrombus in an *in vitro* experiment. The values of blood and clot are very similar and therefore contrast is poor. This is a limiting factor since the potential use of the MRI system towards the treatment of ischaemic stroke is inadequate.

The new coupling technique was proven easy and functional. The transducer could be easily rearranged either manually or automatically (placed on control by a computer robot) anywhere on the animal. Coupling was excellent in avoiding air bubbles to stand between the transducer and the tissue. Focusing the beam sometimes it was time consuming. With this simple method, focusing was done fast and accurately.

The main goal in this study was to dissolve the thrombus using sonothrombolysis. Ultrasound and rt-PA (US + rt-PA) were used alone. With the parameters used in the experiment of figure 10.15 it was found that the thrombus was completely dissolved. Blood flow was resumed as it was before the creation of the thrombus. Table 10.3 presents a summary of the parameters used for the recommended HIFU system.

Table 10.3 Summary of the recommended HIFU system

Frequency (MHz)	Intensity (W/cm ²)	Pulse Duration (min)	Duty Factor (DF)	Mode	Pulse Rate
1	6	60	10%	PW	10 H

CHAPTER 11: CONCLUSION AND FUTURE WORK

11.1 CONCLUSION

The aim of this thesis was to develop a HIFU system that is guided with MRI imaging for two brain applications (cancer and stroke) and to perform *in vitro* (freshly excised lamb brain) *and in vivo* (rabbit brain) studies in order to investigate thermal protocols created by HIFU, or mechanical protocols (thrombolysis) using HIFU in combination with thrombolytic drugs. Such research will shed more light in how we can utilise HIFU in the treatment of brain tumours and in the treatment of stroke.

In this study, it was found that for low temperatures the change in attenuation was insignificant. The attenuation vs. temperature study alone does not give a sound physical explanation of the effect of heating. The time the temperature was maintained (estimated using the thermal dose) gives more information on the physical changes in tissue. The attenuation vs. thermal dose trend shows that the attenuation starts to increase in soft tissues for doses in the range of 100-1000 min (thermal dose referenced to 43 °C). This proves that when the thermal dose threshold of necrosis was reached the tissue attenuation starts to increase. In lamb brain, temperature and thermal dose showed similar behaviour with those seen in the attenuation study. Thus, the change of attenuation with temperature was dominated primarily by the absorption. During the application of short pulse ultrasound the temperature elevation depends primarily on the ultrasonic source parameters (intensity and pulse duration), and on the absorption of the tissue. The ultrasonic source parameters are accurately determined and controlled. Thus, the tissue absorption remains the key factor for determining the tissue temperature. Moreover, for high intensity applications where the tissue temperature is typically 50-100°C, the change in absorption with temperature can be the dominant factor for understanding temperature trends.

The simulated temperature was in good agreement with the experimental temperature during HIFU exposures. During the decaying part, the experimental one was higher than the simulated. When the power was off, conduction was the dominant factor for the temperature change, therefore the difference between the

experimental and simulated temperature was attributed to uncertainty in conductivity. By calculating attenuation and absorption, it was possible to calculate the temperature elevation at the focal point inside the tissue. The prediction of lesion size requires the knowledge of the thermal dose that causes necrosis. The aim was to predict the lesion size based on the intensity used on the resulting tissue temperature at the focal point. This quantity allowed us to execute a theoretical study to investigate the effect of various physical parameters on the size and shape of the lesions for brain tissue.

The simulation results gave us a good indication regarding lesion size (length and width) and temperature elevation in brain tissue. Based on the simulation results the transducers were developed. The simulation results suggested that the lesion size could be controlled by adjusting the duration of the sonication and by adjusting the amount of the acoustic power. Also, depending on the focal depth (5 cm and 1 cm deep into the tissue), the lesions size could be increased or decreased. When the focal point was closer to the skin, then the lesion width was increased and the lesion length was decreased.

This is the first study, demonstrating creation of large lesions both *in vitro* and *in vivo* in brain formed by scanning the transducer in grid formation. Both thermal and bubbly lesions were monitored successfully using all three MRI sequences (T1-W FSE, T2-W FSE and FLAIR) with excellent contrast, proving the potential of HIFU to treat reliably tumours in the brain in the future. The proposed system effectively creates large lesions in brain and at the same time, these lesions are effectively monitored using MRI enabling the accurate determination of the margins of these lesions, especially when using T1-W FSE. The length of the lesions created in *in vivo*, measured parallel to the ultrasonic beam (i.e. deep in the brain), was much higher than the length in *in vitro*, proving that the penetration in the *in vitro* brain is limited by reflection due to trapped bubbles in the blood vessels.

Previous literature demonstrated that lesions can be monitored with excellent contrast in rabbit brain (*in vivo*) using T1-W FSE with TR=500 ms. The lesions imaged in the previous studies and also in this study appeared bright with T1-W

FSE, whereas brain tissue appeared gray. However, in the previous studies only thermal lesions were shown. In this study, the use of MRI was explored extensively to image both lesions created under thermal mechanisms and mechanisms that create bubbly lesions (cavitation or boiling). The contrast between lesion and brain tissue out of the three pulse sequences used was found to be best with T1-W FSE. The signal intensity of the brain tissue is homogeneous when using this method, and therefore the contrast with thermal lesions or with bubbly lesions is excellent. Best contrast is observed for TR above 500 ms. This was proved by plotting the CNR vs. TR. The relaxation time T1 of thermal lesions increases, and therefore lesions appear brighter than brain tissue.

The three MRI pulse sequences T1-W FSE and T2-W FSE and FLAIR were all able to detect lesions. This advantage was attributed to the significant difference in signal intensity between the thermal or bubbly lesions and brain tissue. It was observed that bubbly lesions appeared darker than thermal lesions. Bubbly lesions appear dark, due to the air spaces resulting from cavities. This study has demonstrated that non-degassed excised tissue is a good model for easily initiating cavitation. This model of cavitation might not be of any significance for clinical use since the cavitation threshold in live tissue was very different from the threshold in the *in vitro* tissue. However, this model of initiating cavitation was very useful for studying the MRI appearance of bubbly lesions. Cavitation was initiated if a blood vessel (which might include trapped bubbles) was targeted. Thus, the nature of lesion (thermal or cavitation) in brain *in vitro* primarily depends on the nature of the target and secondarily to the level of intensity. Therefore, in conclusion, it has been demonstrated that tumours could respond to HIFU and MRI could monitor these changes.

In addition, the simulation results provide a good indicator of temperature elevation at the focal point during the treatment of a stroke using pulsed focused ultrasound. The temperature increases as a function of applied power with the rate of increase dependent upon the duty factor and frequency. The temperature elevation was simulated for different power and duty factor. It was found that the temperature increased linearly with duty factor. The higher the power the lower the duty factor needed to keep the temperature change within the safe limit of 1°C.

Also, the higher the frequency the lower the duty factor needed to keep the temperature change to the safe limit of 1°C. This simulation model has provide us with the values needed for the acoustic parameters such as frequency, power, duty factor and pulse repetition frequency during the application of pulse ultrasound at various depths in tissue so that safe temperature (1°C) is maintained during the treatment.

The ability of this HIFU system to dissolve clots in combination with rt-PA in an *in vitro* model was also demonstrated. The main task in this parametric study was to evaluate the effect of intensity, beam area and frequency on the volume of the dissolved clot, while maintaining temperature change at the clot below 1°C. It was shown that higher intensity results to higher volume of dissolved clot. However, there was a limit of the intensity to be used in order to avoid heating of the clot and the surrounding tissue and to achieve temperature elevation not exceeding 1°C. With lower intensity the volume of the dissolved clot was lower which meant longer treatment time. This is a limiting factor since for the potential use of this system (treatment of ischaemic stroke), time is limited to around 3 hours. It was also found that the maximum temporal average *in situ* intensity (SATA) to use is around 20 W/cm². It was also found that the larger the beam area the larger the dissolved clot volume. Finally, the lower the frequency, the larger the volume of the dissolved clot. The ultrasound efficacy with duty cycles of 10% or less tell us that ultrasound quickly produces a change in the clot that persists for a significant time after the sound was turned OFF. In the present study, ultrasound and rt-PA alone was used. Even though the ultrasound intensities used to achieve a significant thrombolytic effect were relatively low, the safety and efficacy of ultrasound thrombolysis requires a careful evaluation in animal models, regarding the biological side effects of ultrasound in brain tissue, especially if cavitation exists.

The ability of this HIFU system to dissolve clots in combination with rt-PA in an *in vivo* model was also proven. In this study, the ability of the ultrasonic system to evaluate the quality of the thrombus and to dissolve the thrombus in combination with rt-PA was demonstrated. The thrombus was injected in the ear artery and the blood flow was observed using a Doppler ultrasound. After 10 mins there was no

indication of a blood flow at the ear artery. A different technique was also used to create thrombus. The ear artery was injured using a small hammer and the blood flow was monitored. It was noticed that in approximately 20 mins after the creation of the trauma, there was no blood flow at all. Therefore, both methods provided, are very good for creating a thrombus.

The main aim was to dissolve the thrombus using sonothrombolysis. Ultrasound and rt-PA were used alone. For 60 min ultrasound exposure using 50W of acoustic power, frequency of 1 MHz, pulse rate of 10 Hz, and duty factor of 10% thrombus was completely dissolved. Blood flow was resumed as it was before the creation of the thrombus.

Finally, the ability of a single element HIFU to penetrate through a human skull was tested. The goal was to provide preliminary evidence as for the trust of the mechanism that was used, first to monitor the temperature at the focal point with and without the skull and second to investigate the ultrasound propagation through a skull phantom. It was proven that higher frequency has poor skull penetration and a small beam size at the focus, while low frequencies have better skull penetration but with the risk of reaching the unpredictable effect of cavitation. It was demonstrated that using a frequency of 0.5 MHz versus 1 MHz, ultrasound propagation through the phantom skull was higher. With these low changes of temperature, the conduction effect was small and therefore this temperature change was related to intensity. Therefore, with 0.5 MHz approximately 60% of the ultrasonic intensity propagates. Finally, it was found experimentally using MRI (detection of temperature using FSPGR) that this system has the ability to penetrate the skull especially if the frequency is around 0.5 MHz.

11.2 FUTURE WORK

The proposed system in this research successfully creates large lesions in the brain and at the same time, these lesions are successfully monitored with excellent contrast using MRI (T1-W FSE) enabling the accurate determination of the margins of these lesions. In addition, the successful application of FUS to improve fibrinolytic therapy in clinical settings will depend critically on the choice of ultrasound parameters to maximize fibrinolytic enhancement, while limiting unwanted adverse effects such as heating and cavitation. The results reported in this study point to the use of frequency around 0.5 MHz and pulsing to optimize thrombolysis and skull penetration and at the same time avoiding unwanted heating. For treating tumours located deep in the brain and for dissolving thrombus causing an acute ischaemic stroke, further extensive clinical studies will be needed before this technology is applied to humans.

There is a scope for future work utilizing this HIFU technology such as:

- The investigation of the capability of HIFU in destroying tumours located deep in the brain. This can be accomplished by conducting experiments in animals with larger brains than the ones used in this research such as pigs or lambs.
- The determination if tumours are totally destroyed after a HIFU therapy is still uncertain. Adding MR spectroscopy (MRS) to the present system (HIFU and MRI) will make it more trustworthy. MRS has the potential to provide metabolic evidence of tumour activity that may be an important guide for therapeutic decisions. MRS can distinguish cancerous tissue from healthy tissue. Eventually, MRS will replace the more invasive needle biopsy. Even though the existing systems are quite mature as far as therapeutic ultrasound is concerned, they present the disadvantage that even with the use of MRI there is an uncertainty that all the cancerous cells are destroyed. The proposed ultrasonic system will make use of an MRS in order to distinguish what substances of tissue are damaged by thermal ablation.

- The efficiency of therapeutic ultrasound in cooperation with rt-PA to liquefy thrombus *in vivo* was examined only in the ear artery of the rabbit. Further studies are required in order to examine when thrombus is injected or formed at different arteries such as the carotid or the femoral artery and to investigate the potential of the current system to effectively dissolve the thrombus. To avoid removing a piece of the skull, a phased array system will be also utilised combined with rt-PA to investigate its ability of dissolving the thrombus when a brain artery such as MCA or basillar or vertebral artery is blocked.
- The success of a HIFU system combined with rt-PA to dissolve thrombus demonstrated in this research by protecting the structure of the artery must be confirmed with histological analysis during which the absence of internal wall rupture will be verified. Histology on the rabbit's ear artery will be performed to investigate the structure of the artery after HIFU exposures. The macroscopic study will verify whether any of the samples has any evidence of tissue rupture after a HIFU treatment.

REFERENCES

- [1] John G. Lynn, Raymond L. Zwemer, Arthur J. Chick, and August E. Miller. “A New Method For The Generation And Use Of Focused Ultrasound In Experimental Biology”. *The Journal of General Physiology*. 1942; 26, 179-193.
- [2] Fry FJ: “Precision high intensity focusing ultrasonic machines for surgery” *AmJ Phys Med*. 1958; 37:152–156.
- [3] Fry WJ, Mosberg WH Jr, Barnard JW, Fry FJ. “Production of focal destructive lesions in the central nervous system with ultrasound”. *J Neurosurg*. 1954; 11:471–478.
- [4] Jolesz FA, Hynynen K. “Magnetic resonance image-guided focused ultrasound surgery”. *Cancer J* 8 [Suppl 1]:S100–S112, 2002.
- [5] Jolesz FA, Hynynen K, McDannold N, Tempany C. “MR imaging-controlled focused ultrasound ablation: A noninvasive image-guided surgery”. *Magn Reson Imaging Clin N Am*. 2005; 13:545–560.
- [6] *Human Anatomy and Physiology, Fifth Edition*. Elaine N. Marieb, Benjamin/Cummings, 2000.
- [7] *The Human Brain: An Introduction to Its Functional Anatomy, Fifth Edition*. John Nolte, Mosby, 2002.
- [8] <http://www.rightdiagnosis.com/>
- [9] <http://www.abta.org> (World Health organization (WHO), The World Health report 2002)
- [10] Woydt M, Krone A, Soerensen N, Roosen K. Ultrasound-guided neuronavigation of deep-seated cavernous haemangiomas: clinical results and navigation techniques. *Br J Neurosurg*. 2001; 15(6):485-95.
- [11] Julow J, Viola A, Major T, Mangel L, Bajzik G, Repa I, Sagi S, Valalik I, Emri M, Tron L, Nemeth G. Volumetric changes following 125I interstitial brachytherapy of gliomas, *Ideggyogy Sz*. 2005; 58(3-4):120-32.
- [12] Boisserie G, Cornu P, Dormont D, Sahel M, Hardiman C, Tep B, Mandin AM, Barret C, Faillot T, Delattre JY, Monjour A, Poisson M, Marsault C, Philippon J, Simon JM, Baillet F, Mazon JJ. Iridium 192 brachytherapy of supra-tentorial high grade glioma recurring in irradiated areas: technique and preliminary results of the Pitie-Salpetriere hospital group, *Bull Cancer Radiother*. 1996; 83(3):144-52.

- [13] Kobayashi T, Mori Y, Uchiyama Y, Kida Y, Fujitani S. Long-term results of gamma knife surgery for growth hormone-producing pituitary adenoma: is the disease difficult to cure? *J Neurosurg.* 2005; 102:119-23.
- [14] Gralla J, Nimsky C, Buchfelder M, Fahlbusch R, Ganslandt O. Frameless stereotactic brain biopsy procedures using the Stealth Station: indications, accuracy and results. *Zentralbl Neurochir.* 2003; 64(4):166-70.
- [15] Chang EL, Hassenbusch SJ 3rd, Shiu AS, Lang FF, Allen PK, Sawaya R, Maor MH. The role of tumour size in the radiosurgical management of patients with ambiguous brain metastases. *Neurosurgery* 2003; 53(2):272-80; discussion 280-1.
- [16] Paleologos TS, Dorward NL, Wadley JP, Thomas DG. Clinical validation of true frameless stereotactic biopsy: analysis of the first 125 consecutive cases. *Neurosurgery* 2001; 49(4):830-5.
- [17] Yokoi K, Kamiya N, Matsuguma H, Machida S, Hirose T, Mori K, Tominaga K. Detection of brain metastasis in potentially operable non-small cell lung cancer: a comparison of CT and MRI. *Chest.* 1999; 115(3):714-9.
- [18] Furie DM, Provenzale JM. Supratentorial ependymomas and subependymomas: CT and MR appearance. *J Comput Assist Tomogr.* 1995; 19(4):518-26.
- [19] Buatti JM, Friedman WA, Bova FJ, Mendenhall WM. Linac radiosurgery for high-grade gliomas: the University of Florida experience. *Int J Radiat Oncol Biol Phys.* 1995 Apr 30; 32(1):205-10.
- [20] Tanaka T, Kobayashi T, Kida Y, Oyama H, Niwa M. The results of gamma knife radiosurgery for malignant skull base tumours. *No Shinkei Geka.* 1996; 24(3):235-9.
- [21] Hou Y, Tang J, Ma Z, Qiu B, Liu Y. Therapy for intracranial lesions by gamma knife. *Hunan Yi Ke Da Xue Xue Bao.* 1997; 22(4):347-50.
- [22] Simon JM, Cornu P, Boisserie G, Hasboun D, Tep B, Hardiman C, Valery CA, Delattre JY, Dormont D, Baillet F, Mazon JJ. Brachytherapy of glioblastoma recurring in previously irradiated territory: predictive value of tumour volume. *Int J Radiat Oncol Biol Phys.* 2002; 53(1):67-74.
- [23] Kida Y, Kobayashi T, Mori Y. Gamma knife radiosurgery for low-grade astrocytomas: results of long-term follow up. *J Neurosurg.* 2000; 93: 3:42-6.

- [24] Landy HJ, Schwade JG, Houdek PV, Markoe AM, Feun L. Long-term follow-up of gliomas treated with fractionated stereotactic irradiation. *Acta Neurochir Suppl.* 1994; 62:67-71.
- [25] Taratuto AL, Monges J, Lylyk P, Leiguarda R. Superficial cerebral astrocytoma attached to dura. Report of six cases in infants. *Cancer* 1984; 54(11):2505-12.
- [26] <http://www.emedicine.com> or <http://www.cancercompass.com>
- [27] <http://www.strokecenter.org/patients/stats.htm>
- [28] Truelsen T, Ekman M, Boysen G. Cost of stroke in Europe. *Eur J Neurol.* 2005; 12:78-84
- [29] Lloyd-Jones D, Adams R, Carnethon M. Heart disease and stroke statistics–2009 update: a report from the American Heart Association Statistics Committee and Stroke Statistics Subcommittee. *Circulation* 2009; 119:e21-181
- [30] Orso F, Baldasseroni S, Maggioni AP. The role of thrombolysis in acute ischaemic stroke. *Herz.* 2008; 33:498-506
- [31] The National Institute of Neurological Disorders and Stroke rt-PA Stroke Study Group. Tissue plasminogen activator for acute ischaemic stroke. *N Engl J Med.* 1995; 333:1581-8
- [32] Derex L, Nighoghossian N. Intracerebral haemorrhage after thrombolysis for acute ischaemic stroke: an update. *J Neurol Neurosurg Psychiatry.* 2008; 79:1093-9
- [33] Gonzalez ER. Intracoronary thrombolysis to abort heart attacks: wave of the future? *JAMA.* 1981; 245:11-3
- [34] Multicentre Acute Stroke Trial–Italy G. Randomised controlled trial of streptokinase, aspirin, and combination of both in treatment of acute ischaemic stroke. *Lancet.* 1995; 346:1509-14
- [35] The Multicenter Acute Stroke Trial – Europe Study G. Thrombolytic therapy with streptokinase in acute ischaemic stroke. *N Engl J Med.* 1996; 335:145-50
- [36] Donnan G, Davis S, Chambers B, et al. Streptokinase for acute ischaemic stroke with relationship to time of administration: Australian Streptokinase (ASK) Trial Study Group. *JAMA.* 1996; 276:961-6
- [37] Wahlgren N, Ahmed N, D valos A, et al. Thrombolysis with alteplase for acute ischaemic stroke in the Safe Implementation of Thrombolysis in Stroke-Monitoring Study (SITS-MOST): an observational study. *Lancet.* 2008;369:275-282

- [38] Hacke W, Kaste M, Fieschi C. Intravenous thrombolysis with recombinant tissue plasminogen activator for acute hemispheric stroke. The European Cooperative Acute Stroke Study (ECASS). JAMA 1995; 274:1017-25
- [39] Hacke W, Kaste M, Fieschi C. Randomised double-blind placebo-controlled trial of thrombolytic therapy with intravenous alteplase in acute ischaemic stroke (ECASS II). Lancet. 1998; 352:1245-51
- [40] Clark WM, Wissman S, Albers GW. Recombinant tissue-type plasminogen activator (Alteplase) for ischaemic stroke 3 to 5 hours after symptom onset: the ATLANTIS Study: a Randomized Controlled Trial. JAMA 1999; 282:2019-26
- [41] Association of outcome with early stroke treatment: pooled analysis of ATLANTIS, ECASS, and NINDS rt-PA stroke trials. Lancet 2004; 363:768-74
- [42] Hacke W, Kaste M, Bluhmki E. Thrombolysis with alteplase 3 to 4.5 hours after acute ischaemic stroke. N Engl J Med. 2008; 359:1317-29
- [43] Major Ongoing Stroke Trials. Stroke 2008; 39:e154-62
- [44] R. Trubestein, H.R. Bernard, F. Etzel, A. Sobbe, A. Cremer, U. Stumpff. Thrombolysis by ultrasound, Clin. Sci. Mol. Med. 1976; 51: 697–698.
- [45] K. Tachibana, S. Tachibana. Ultrasonic vibration for boosting fibrinolytic effects of urokinase *in vivo*, Thromb. Haemost. 1981; 46: 211.
- [46] Mahon BR, Nesbit GM, Barnwell SL. North American clinical experience with the EKOS MicroLysUS infusion catheter for the treatment of embolic stroke. AJNR Am J Neuroradiol. 2003; 24(3): 534-538.
- [47] Ishibashi T, Akiyama M, Onoue H, Abe T, Furuhashi H. Can transcranial ultrasonication increase recanalization flow with tissue plasminogen activator? Stroke 2002; 33(5): 1399-1404.
- [48] Alexandrov AV, Molina CA, Grotta JC. Ultrasound-enhanced systemic thrombolysis for acute ischaemic stroke. N Engl J Med. 2004; 351(21): 2170-2178.
- [49] M. Kimura, S. Iijima, K. Kobayashi, H. Furuhashi. Evaluation of the thrombolytic effect of tissue-type plasminogen activator with ultrasound irradiation: *in vitro* experiment involving assay of the fibrin degradation products from the clot. Biol. Pharm. Bull. 1994; 17: 126–130.
- [50] M. Akiyama, T. Ishibashi, T. Yamada, H. Furuhashi. Low-frequency ultrasound penetrates the cranium and enhances thrombolysis *in vitro*. Neurosurgery 1998; 43: 828–832.

- [51] M. Daffertshoffer, M. Hennerici. Ultrasound in the treatment of ischaemic stroke. *Lancet Neurol.* 2003; 2: 283–290.
- [52] S. Behrens, K. Spengos, M. Daffertshofer, S. Wirth, M. Hennerici. Potential use of therapeutic ultrasound in ischaemic stroke treatment. *Echocardiography* 2001; 18: 259–263.
- [53] M. Daffertshofer, M. Hennerici. Sonothrombolysis: experimental evidence. *Front Neurol. Neurosci.* 2006; 21: 140–149.
- [54] M. Daffertshofer, Z. Huang, M. Fatar, M. Popolo, H. Schroeck, W. Kuschinsky. Efficacy of sonothrombolysis in a rat model of embolic ischaemic stroke. *Neurosci. Lett.* 2004; 361: 115–119.
- [55] M. Daffertshofer, A. Gass, P. Ringleb. Transcranial low frequency ultrasound-mediated thrombolysis in brain ischemia: increased risk of hemorrhage with combined ultrasound and tissue plasminogen activator. *Stroke.* 2005; 36: 1441–1446.
- [56] Barreto A, Sharma V, Lao A, Schellinger P, Amarenco P, Sierzenski P, Alexandrov A, Molina C. Safety and dose-escalation study design of Transcranial Ultrasound in Clinical SONolysis for acute ischaemic stroke: the TUCSON Trial. *Int J Stroke.* 2009; 4: 42-48.
- [57] Eggers J, König I R, Koch B, Händler G, Seidel G. Sonothrombolysis With Transcranial Color-Coded Sonography and Recombinant Tissue-Type Plasminogen Activator in Acute Middle Cerebral Artery Main Stem Occlusion: Results From a Randomized Study. *Stroke* 2008; 39:1470-1475;
- [58] Ram Z, Cohen ZR, Harnof S, Tal S, Faibel M, Nass D, Maier SE, Hadani M, Mardor Y. “Magnetic resonance imaging-guided, high-intensity focused ultrasound for brain tumour therapy”. *Neurosurgery* 2006; 59:949–956.
- [59] Zderic V, Keshavarzi A, Noble ML, Paun M, Sharar SR, Crum LA, Martin RW, Vaezy S. Hemorrhage control in arteries using high-intensity focused ultrasound: A survival study. *Ultrasonics* 2006; 44:46–53.
- [60] Stewart EA, Rabinovici J, Tempany CM, Inbar Y, Regan L, Gostout B, Hesley G, Kim HS, Hengst S, Gedroyc WM. Clinical outcomes of focused ultrasound surgery for the treatment of uterine fibroids. *Fertil Steril.* 2006; 85(1):22-9.
- [61] Kinoshita M, McDannold N, Jolesz FA, Hynynen K. Noninvasive localized delivery of Herceptin to the mouse brain by MRI-guided focused

- ultrasound-induced blood-brain barrier disruption. Proc Natl Acad Sci U S A. 2006; 103:11719–11723.
- [62] Hynynen K, Clement GT, McDannold N, Vykhodtseva N, King R, White PJ, Vitek S, Jolesz FA. 500-element ultrasound phased array system for noninvasive focal surgery of the brain: A preliminary rabbit study with *in vitro* human skulls. Magn Reson Med. 2004; 52: 100–107.
- [63] Pernot M, Aubry JF, Tanter M, Thomas JL, Fink M. High power transcranial beam steering for ultrasonic brain therapy. Phys Med Biol. 2003; 48(16):2577-89.
- [64] Jacques and Pierre Curie,
http://www.pccontrol.co.uk/piezoelectric_effect.htm
- [65] Lee De Forest, <http://people.clarkson.edu/~ekatz/scientists/deforest.htm>
- [66] Paul Langévin, <http://www.ob-ultrasound.net/langevin.html>
- [67] Ronald V. Christie MB, Ch.B. and Alfred L. Loomis. “The Relation Of Frequency To The Physiological Effects Of Ultra-High Frequency Currents”, The Journal of Experimental Medicine. The Rockefeller Institute for Medical Research New York 1929; 49: 303-321
- [68] Fry WJ, Meyers R. “Ultrasonic method of modifying brain structures”. Confin Neurol. 1962; 22: 315–327.
- [69] Cosman BJ, Hueter TF. “Instrumentation for ultrasonic neurosurgery”. Electronics 1959; 5:53–57.
- [70] Leksell L. “Echoencephalography. II. Midline echo from the pineal body as an index of pineal displacement”. Acta Chir Scand. 1958; 115:255–259.
- [71] Fry FJ, Goss SA. “Further studies of the transkull transmission of an intense focused ultrasonic beam: Lesion production at 500 kHz”. Ultrasound Med Biol. 1980; 6: 33–38.
- [72] Fry FJ, Goss SA, Patrick JT. Transkull focal lesions in cat brain produced by ultrasound. J Neurosurg. 1981; 54: 659–663.
- [73] Heimburger RF. Ultrasound augmentation of central nervous system tumour therapy. Indiana Med. 1985; 78: 469–476.
- [74] Jolesz F A and Zientara G P. “MRI-guided laser-induced thermotherapy: basic principles Laser Induced”, Interstitial Thermotherapy ed G M`uller and A Roggan. Washington, DC: SPIE Opt. Eng. Press. 1995; 294–324

- [75] History of MR guided Focused Ultrasound: A literature review, ExAblate® 2000, Vol. 1, No. 1, Insightec.
- [76] Lynn JG, Zwemer RL, Chick AJ, Miller AG. A new method for the generation and use of focused US in experimental biology. *Gen Physiol.* 1942; 26: 179-193.
- [77] Fry WJ, Barnard JW, Fry FJ, Krumins RF, Brennan JF. Ultrasonic lesions in the mammalian central nervous system. *Science.* 1955; 122: 517-518.
- [78] Lizzi FL. High-precision thermotherapy for small lesions. *Eur Urol.* 1993; 23: 23-28.
- [79] Coleman DJ, Lizzi FL, Driller J, Rosado AL, Chang S, Iwamoto T, Rosenthal D. Therapeutic ultrasound in the treatment of glaucoma. I. Experimental model. *Ophthalmology.* 1985; 92: 339-336.
- [80] Coleman DJ, Silverman RH, Iwamoto T, Lizzi FL, Rondeau MJ, Driller J, Rosado A, Abramson DH, Ellsworth RM. Treatment of glaucoma with highintensity focused ultrasound. *Ophthalmology.* 1986; 93: 831-833.
- [81] Vallancien G, Harouni M, Veillon B, Mombet A, Brisset J, Bougaran J. Focused extracorporeal pyrotherapy. *Eur Urol.* 1993; 23: 48-52.
- [82] Vallancien G, Harouni M, Guillonneau B, Veillon B, Bougaran J. Ablation of superficial bladder tumours with focused extracorporeal pyrotherapy. *Urology.* 1996; 47:204-207.
- [83] Gail Ter Haar GR, Clarke RL, Vaughan MG, Hill CR. Trackless surgery using focused ultrasound: Technique and case report. *Min Inv Ther.* 1991; 1: 13-15.
- [84] Visioli AG, Rivens IH, ter Haar GR, Horwich A, Huddart RA, Moskovic E, Padhani A, Glees J. Preliminary results of a phase I dose escalation clinical trial using focused ultrasound in the treatment of localized tumours. *Eur J Ultrasound.* 1999; 9: 11-18.
- [85] Wu F, Wang ZB, Chen WZ, Wang W, Gui YZ, Zhang M, Zheng GQ, Zhou YJ, Xu GL, Li M, Zhang CW, Ye HY, Feng R. Extracorporeal high intensity focused ultrasound ablation in the treatment of 1038 patients with solid carcinomas in China: An overview. *Ultrasonics Sonochem.* 2004; 11: 149-154.
- [86] Bo Xie, Jiajun Ling, Weiming Zhang, Xueqin Huang, Jihua Zhen and Yanzhe Huang. The efficacy of high-intensity focused ultrasound (HIFU) in

- advanced pancreatic cancer. *Chinese Journal of Clinical Oncology*. 2008; 5: 183-186.
- [87] Kennedy JE, terHaarGR, Wu F, Gleeson FV, Roberts IS, Middleton MR, Cranston D. Contrast-enhanced ultrasound assessment of tissue response to high-intensity focused ultrasound. *Ultrasound Med Biol*. 2004; 30: 851-854.
- [88] Kennedy JE, Wu F, ter Haar GR, Gleeson FV, Phillips RR, Middleton MR, Cranston D. High-intensity focused ultrasound for the treatment of liver tumours. *Ultrasonics*. 2004; 42: 931-935.
- [89] Okuno T, Ganaha F, Lee CO, Shimizu T, Osako K, Oka S, Lee KH, Chen WZ, Zhu H, Park SH, Qi Z, Shi D, Song HS. Feasibility of extracorporeal HIFU using Chongqing Haifu-knife as an adjunct to the endovascular therapy for breast conservation particularly in patients with recurrent breast carcinoma, 4th International Symposium on Therapeutic Ultrasound, Tachibana K, ter Haar GR (eds.), ISTU, Kyoto. 2004; pp. 66.
- [90] Hynynen K, Darkazanli A, Unger E, Schenck JF. MRI-guided noninvasive ultrasound surgery. *Med Phys*. 1993; 20: 107-115.
- [91] Hynynen K, Pomeroy O, Smith DN, Huber PE, McDannold NJ, Kettenbach J, Baum J, Singer S, Jolesz FA. MR imaging-guided focused ultrasound surgery of fibroadenomas in the breast: A feasibility study. *Radiology*. 2001; 219: 176-185.
- [92] Tempany CMC, Stewart EA, McDannold N, Quade BJ, Jolesz FA, Hynynen K. MR imaging-guided focused ultrasound surgery of uterine leiomyomas: A feasibility study. *Radiology*. 2003; 226: 897-905.
- [93] Madersbacher S, Kratzik C, Szabo N, Susani M, Vingers L, Marberger M. Tissue ablation in benign prostatic hyperplasia with high-intensity focused ultrasound. *Eur Urol*. 1993; 23: 39-43.
- [94] Chaussy C, Thuroff S. High-intensity focused ultrasound: Complications and adverse effects. *Molec Urol*. 2000; 4: 183-187.
- [95] Thuroff S, Chaussy C, Vallancien G, Wieland W, Kiel HJ, Le Due A, Desgrandchamps F, De La Rosette J, Gelet A. High-intensity focused ultrasound and localized prostate cancer: Efficacy results from the European multicentric study. *J Endourol* (2003) 17: 673-677.

- [96] Daum DR, Smith NB, King R, Hynynen K. *In vivo* demonstration of noninvasive thermal surgery of the liver and kidney using an ultrasonic phased array. *Ultrasound Med Biol* 25:1087–1098, 1999.
- [97] White PJ, Clement GT, Hynynen K. Longitudinal and shear mode ultrasound propagation in human skull bone. *Ultrasound Med Biol* 32:1085–1096, 2006.
- [98] Hynynen K. The threshold for thermally significant cavitation in dog's thigh muscle *in vivo*. *Ultrasound Med Biol*. 1991; 17:157–169.
- [99] Samir Mitragotri. Healing sound: the use of ultrasound in drug delivery and other therapeutic applications. *American Institute of Ultrasound in Medicine*. 2005, 4(3): 255-260.
- [100] Miller DL, Song J. Tumour growth reduction and DNA transfer by cavitation-enhanced high intensity focused ultrasound *in vivo*. *Ultrasound Med Biol* 2003; 29:887–93.
- [101] Nightingale K, Soo MS, Nightingale R. Acoustic radiation force impulse imaging: *in vivo* demonstration of clinical feasibility. *Ultrasound Med Biol*. 2002; 28:227–35.
- [102] Lizzi FL, Muratore R, Deng CX. Radiation-force technique to monitor lesions during ultrasonic therapy. *Ultrasound Med Biol*. 2003; 29: 1593–605.
- [103] Frenkel V, Li KCP. Potential role of pulsed-high intensity focused ultrasound in gene therapy. *Oncol* 2006; 2: 111–9.
- [104] Cohen ZR, Zaubermann J, Harnof S, Mardor Y, Nass D, Zadicario E, Hananel A, Castel D, Faibel M, Ram Z. Magnetic resonance imaging-guided focused ultrasound for thermal ablation in the brain: A feasibility study in a swine model. *Neurosurgery* 2007; 60:593–600.
- [105] Hynynen K, Colucci V, Chung A, Jolesz F. Noninvasive arterial occlusion using MRI-guided focused ultrasound. *Ultrasound Med Biol*. 1996; 22:1071–1077.
- [106] Treat LH, McDannold N, Vykhodtseva N, Zhang Y, Tam K, Hynynen K. Targeted delivery of doxorubicin to the rat brain at therapeutic levels using MRI-guided focused ultrasound. *Int J Cancer* 2007; 121:901–907.
- [107] Frenkel V, Etherington A, Greene M, Quijano J, Xie J, Hunter F, Dromi S, Li KC. Delivery of liposomal doxorubicin (Doxil) in a breast cancer tumour

- model: Investigation of potential enhancement by pulsed-high intensity focused ultrasound exposure. *Acad Radiol.* 2006; 13:469–479.
- [108] Stone MJ, Frenkel V, Dromi S, Thomas P, Lewis RP, Li KC, Horne M 3rd, Wood BJ. Pulsed-high intensity focused ultrasound enhanced tPA mediated thrombolysis in a novel *in vivo* clot model, a pilot study. *Thromb Res.* 2007; 121:193–202.
- [109] Lindstrom PA. Prefrontal ultrasonic irradiation—A substitute for lobotomy. *AMA Arch Neurol Psychiatry.* 1954; 72:399–425.
- [110] Lele PP. Concurrent detection of the production of ultrasonic lesions. *Med Biol Eng.* 1966; 4:451–456.
- [111] Lele PP. Production of deep focal lesions by focused ultrasound—Current status. *Ultrasonics* 1967; 5:105–112.
- [112] J. C, Bamber, C. R. Hill. Ultrasonic Attenuation And Propagation Speed In Mammalian Tissues As A Function Of Temperature. *Ultrasound In Med. & Biol.* 1979; 5: 149-157.
- [113] S. A. Ooss, L. A. Frizzell, F. Dunn. Ultrasonic Absorption And Attenuation In Mammalian Tissues. *Ultrasound In Med. & Biol.* 1979; 5: 181-186
- [114] O'Neil, H. Theory of focussing radiators. *J. Acoust. Soc. Am.* 1949; 21:516-526.
- [115] Swindell W, Roemer RB, Clegg ST. Temperature distributions caused by dynamic scanning of focused ultrasound transducers. *IEEE ultrasonic Symp.* 1982; 745-749
- [116] Fan X, and Hynynen K. "The effect of wave reflection and refraction at soft tissue interfaces during ultrasound hyperthermia treatments," *J. Acoust. Soc. Am.* 1992; 91 (3), 1727-1736.
- [117] Pennes, M. Analysis of tissue and arterial blood temperature in the resting human forearm. *J. Appl. Physiol.* 1948; 1:93-122.
- [118] AH Goodman, R Einstein and HJ Granger. Effect of changing metabolic rate on local blood flow control in the canine hindlimb. *Circulation Research* 1978; 43: 769-776.
- [119] Dewey W C, Hopwood L E, Sapareto S A, Gerweck L. E. Cellular responses to combinations of hyperthermia and radiation. *Radiology.* 1977; 123, 463-474.

- [120] Sapareto S, Dewey W. "Thermal dose determination in cancer therapy." *Int. J. radiation oncology Biol. Phys.* 1984; 10: 787-800.
- [121] Damianou C, and Hynynen K. "The effects of various physical parameters on the size and shape of necrosed tissue volume during ultrasound surgery," *J. Acoust. Soc. Am.* 1994; 95 (3), 1641-1649.
- [122] Christakis Damianou, M. Pavlou, O. Velez, K. Kyriakou, M. Trimikliniotis. High intensity focused ultrasound ablation of kidney guided by MRI. *Journal of Ultrasound Med Biol.* 2004; 30 (3): 397-404.
- [123] Damianou C. *In vitro* and *in vivo* ablation of porcine renal tissues using High Intensity focused Ultrasound. *Journal of Ultrasound in Medicine and Biology.* 2003; 29 (9):1321-1330.
- [124] Vykhodtseva N, Sorrentino V, Jolesz FA, Bronson RT, Hynynen K. MRI detection of the thermal effects of focused ultrasound on the brain. *Ultrasound Med Biol.* 2000; 26(5):871–880.
- [125] Dunn F. "Temperature and amplitude dependence of acoustic absorption in tissue", *J. Acoust. Soc. Am.* 1962; 34 (10), 1545-1547.
- [126] Dunn F. and Brady J. "Temperature and frequency dependence of ultrasonic absorption in tissue". in *Proceedings of 8 th International Congress on Acoustics.* 1974; 366c.
- [127] Gammell P, Le Croisette D, Heyser R. "Temperature and frequency dependence of ultrasonic attenuation in selected tissues". *Ultrasound in Med & Biol.* 1979; 5, 269-277.
- [128] Fry F, Reiley C, Dines K, Etchison M, Trauner E. "Absorption in liver at the focus of an ultrasonic shock wave field". *Ultrasound in Med. & Biol.* 1991; 17 (1), 65-69.
- [129] Robinson T, and Lele P. "An analysis of lesion development in the brain and in plastics by high-intensity focused ultrasound at low-megahertz frequencies". *J. Acoust Soc. Am.* 1969; 51 (2), 133-1351.
- [130] Bamber J, and Hill C. "Ultrasonic attenuation and propagation speed in mammalian tissues as a function of temperature". *Ultrasound in Med. & Biol.* 1979; 5, 149-157.
- [131] Kossoff G, Kelly-Fry E, Jellins J. "Average velocity of ultrasound in the human female breast". *J. Acoust. Soc. Am.* 1973; 53 (6), 1730-1736.

- [132] Fry W, and Fry R. "Determination of absolute sound levels and acoustic absorption coefficients by thermocouple probes-theory". J. Acoust. Soc. Am. 1954; 26 (3), 294-310.
- [133] Bamber J, and Nassiri D. "Effect of gaseous inclusions on the frequency dependence of ultrasonic attenuation in liver". Ultrasound in Med. & Biology. 1985 11 (2), 293-298.
- [134] Frizzell L, Carstensen E, Davis D. "Ultrasonic absorption in liver tissue". J. Acoust. Soc. Am. 1979; 65 (5), 1309-1312.
- [135] Lele PP. A simple method for production of trackless focal lesions with focused ultrasound. J. Physiol. 1962; 160:494-512.
- [136] Fry F. and Johnson LK., (1978) Tumour irradiation with intense ultrasound. Ultrasound Med. Biol. 4(4):337-41.
- [137] Britt RH, Lyons BE, Pounds DW, Prionas SD. Feasibility of ultrasound hyperthermia in the treatment of malignant brain tumours. Med Instrum. 1983; 7(2):172-7.
- [138] Guthkelch AN, Carter LP, Cassady JR, Hynynen KH, Iacono RP, Johnson PC, Obbens EA, Roemer RB, Seeger JF, Shimm DS. Treatment of malignant brain tumours with focused ultrasound hyperthermia and radiation: results of a phase I trial. J Neurooncol. 1991; 10(3):271-84.
- [139] <http://clinicaltrials.gov/ct2/show/NCT01473485>. ExAblate (Magnetic Resonance-guided Focused Ultrasound Surgery) Treatment of Brain Tumors, November 2011.
- [140] Vykhodtseva NI, Hynynen K, Damianou C. Pulse duration and peak intensity during focused ultrasound surgery: theoretical and experimental effects in rabbit brain *in vivo*. Ultrasound Med Biol. 1994; 20(9): 987-1000.
- [141] Hynynen K, Vykhodtseva NI, Chung AH, Sorrentino V, Colucci V, Jolesz FA. Thermal effects of focused ultrasound on the brain: determination with MR imaging. Radiology 1997; 204(1): 247-53.
- [142] Hynynen K. McDannold N. Vykhodtseva N. Jolesz F. Noninvasive MR Imaging-guided Focal Opening of the Blood-Brain-Barrier in Rabbits. Radiology 2001; 230:640-646.
- [143] Hynynen K, McDannold N, Martin H, Jolesz F, Vykhodtseva N. The threshold for brain damage in rabbits induced by bursts of ultrasound in the presence of

- an ultrasound contrast agent (optison). *Ultrasound in Med. & Biol.* 2003; 29 (3): 473–481.
- [144] Hynynen K, McDannold N, Sheikov N, Jolesz F, Vykhodtseva N. Local and reversible blood–brain barrier disruption by noninvasive focused ultrasound at frequencies suitable for trans-skull sonications. *NeuroImage* 2005; 24: 12–20.
- [145] Damianou C, Ioannides K, Milonas N. ‘Positioning device for MRI-guided high intensity focused ultrasound system’. *Computer-Assisted Radiology and Surgery.* 2008; 2 (6): 335-345.
- [146] Hynynen K, Darkazanli A, Damianou DC, Unger E, Schenck JF. (1992) MRI-guided ultrasonic hyperthermia, RSNA meeting.
- [147] Hynynen K, Damianou CA, Colucci V, Unger E, Cline HH, Jolesz FA. MR monitoring of focused ultrasonic surgery of renal cortex: experimental and simulation studies. *Journal of Magnetic Resonance Imaging.* 1995; 5(3): 259-266.
- [148] Christakis Damianou, M. Pavlou, O. Velez, K. Kyriakou, M. Trimikliniotis. High intensity focused ultrasound ablation of kidney guided by MRI. *Journal of Ultrasound Med Biol.* 2004; 30 (3): 397-404.
- [149] Rowland IJ, Rivens I, Chen L, Lebozer CH, Collins DJ, ter Haar GR, Leach MO. MRI study of hepatic tumours following high intensity focused ultrasound surgery. *British Journal of Radiology.* 1997; 70: 144-53.
- [150] Rouviere O, Souchon R, Salomir R, Gelet A, Chapelon JY, Lyonnet D. Transrectal high-intensity focused ultrasound ablation of prostate cancer: Effective treatment requiring accurate imaging. *Eur J Radiol.* 2007; 63(3): 317-327.
- [151] Pisani L, Ross A, Diederich C, Nau W, Sommer F, Glover G, Butts K. Effects of spatial and temporal resolution for MR image-guided thermal ablation of prostate with transurethral ultrasound. *J Magn Reson Imaging.* 2005; 22(1): 109-18.
- [152] Damianou C. *In vitro* and *in vivo* ablation of porcine renal tissues using High Intensity focused Ultrasound *Journal of Ultrasound in Medicine and Biology.* 2003; 29 (9): 1321-1330.
- [153] Chen L, Bouley D, Yuh E, D;Arceuil H, Butts K. Study of focused ultrasound tissue damage using MRI and histology. *J Magn Reson Imaging.* 1999; 10(2): 146-53.

- [154] Dickinson RJ, Hall AS, Hind AJ, Young IR. Measurement of changes in tissue temperature using MR imaging. *J Comput Assist Tomogr.* 1986; 10: 468–472.
- [155] Fry FJ, Sanghvi NT, Morris RF, Clendenon JL, Dines KA, Patrick JT, Goss SA. Ultrasonic diagnostic system for interactive interrogation of adult brain through intact skull. *Invest Radiol.* 1982; 7(5): 463-9.
- [156] Maxwell AD, Owens G, Gurm HS, Ives K, Myers DD Jr, Xu Z. Noninvasive Treatment of Deep Venous Thrombosis Using Pulsed Ultrasound Cavitation Therapy (Histotripsy) in a Porcine Model. *J Vasc Interv Radiol.* 2010 Dec 29.
- [157] Maxwell AD, Cain CA, Duryea AP, Yuan L, Gurm HS, Xu Z. Noninvasive thrombolysis using pulsed ultrasound cavitation therapy - histotripsy. *Ultrasound Med Biol.* 2009; 35(12): 1982-94.
- [158] K. Spengos, S. Behrens, M. Daffertshofer, Carl E. Dempfle And M. Hennerici. Acceleration Of Thrombolysis With Ultrasound Through The Cranium In A Flow Model. *Ultrasound In Med. & Biol.* 2000; 26(5): 889–895.
- [159] J. Eggers, Inke R. König, B. Koch, G. Händler and G. Seidel. Sonothrombolysis With Transcranial Color-Coded Sonography and Recombinant Tissue-Type Plasminogen Activator in Acute Middle Cerebral Artery Main Stem Occlusion: Results From a Randomized Study. *Stroke* 2008; 39; 1470-1475.
- [160] G.T. Clement. Perspectives in clinical uses of high-intensity focused ultrasound. *Ultrasonics* 2004; 42: 1087–1093.
- [161] Chuan-Xing Li, Guo-Liang Xu, Zhen-You Jiang, Jian-Jun Li, Guang-Yu Luo, Hong-Bo Shan, Rong Zhang, Yin Li. Analysis of clinical effect of high-intensity focused ultrasound on liver cancer. *World J Gastroenterol* 2004; 10(15): 2201-2204.
- [162] C. Damianou, Ioannides K., Hadjisavvas V., Milonas N., Couppis A, Iosif D. ‘*In vitro* and *in vivo* brain ablation created by high intensity focused ultrasound and monitored by MRI’. *IEEE Transaction on Ultrasonics, Ferroelectrics and Frequency Control*, 2009; 56(6): 1189-1198.
- [163] Kennedy JE. High-intensity focused ultrasound n treatment of solid tumours. *Nat Rev Cancer* 2005; 5:321–7.

- [164] Zenitani T, Suzuki R, Maruyama K, Furuhashi H. Accelerating effects of ultrasonic thrombolysis with bubble liposomes. *J Med Ultrasonics* 2008; 35:5-10.
- [165] Soltani A, Prokop A, Vaezy S. Stability of alteplase in presence of cavitation. *Ultrasonics* 2008; 48:109-116.
- [166] Eggers J, Ossadnik S, Seidel G. Enhanced clot dissolution *in vitro* by 1.8-mhz pulsed ultrasound. *Ultrasound in Med. & Biol.* 2009; 35(3): 523–526.
- [167] Shaw G, Meunier J, Lindsell C, Holland C. Tissue plasminogen activator concentration dependence of 120 khz ultrasound-enhanced thrombolysis. *Ultrasound in Med. & Biol.* 2008; 34(11): 1783–1792.
- [168] Saguchi T, Onoue H, Urashima M, Ishibashi T, Abe T, Furuhashi H. Effective and safe conditions of low-frequency transcranial ultrasonic thrombolysis for acute ischaemic stroke: neurologic and histologic evaluation in a rat middle cerebral artery stroke model. *Stroke*. 2008; 39: 1007-1011.
- [169] Jürgen Eggers, Inke R. König, Björn Koch, Götz Händler, Günter Seidel. Sonothrombolysis With Transcranial Color-Coded Sonography and Recombinant Tissue-Type Plasminogen Activator in Acute Middle Cerebral Artery Main Stem Occlusion: Results From a Randomized Study. *Stroke* 2008; 39; 1470-1475.
- [170] Kim YS, Rhim H, Choi MJ, Lim HK, Choi D. High-intensity focused ultrasound therapy: an overview for radiologists. *Korean J Radiol.* 2008; 9(4): 291-302.
- [171] Frenkel V, Oberoi J, Stone MJ, Park M, Deng C, Wood BJ, Neeman Z, Horne M 3rd, Li KC. Pulsed high-intensity focused ultrasound enhances thrombolysis in an *in vitro* model. *Radiology* 2006; 239(1):86-93.
- [172] Joshua E. Sonesson, Matthew R. Myers. Gaussian representation of high-intensity focused ultrasound beams *J. Acoust. Soc. Am.* 2007; 122(5): 2526-2531.
- [173] Holland CK, Vaidya SS, Datta S, Coussios C-C, Shaw GJ. Ultrasound enhanced tissue plasminogen activator thrombolysis in an *in vitro* porcine clot model. *Thromb Res* 2008; 121: 663-673.

- [174] R. Kornowski, R. S. Meltzer, A. Chernine, Z. Vered, A. Battler. Does External Ultrasound Accelerate Thrombolysis? Results From a Rabbit Model. *American Heart Ass.* 1994; 89: 339-344.
- [175] M. Nedelmann, P. Reuter, M. Walberer, C. Sommer, B. Alessandri, D. Schiel, N. Ritschel, O. Kempfski, M. Kaps, C. Mueller, G. Bachmann, T. Gerriets. Detrimental Effects Of 60 Khz Sonothrombolysis In Rats With Middle Cerebral Artery Occlusion. *Ultrasound in Med. & Biol.* 2008; 34(12): 2019–2027.
- [176] Francis CW, Blinc A, Lee S, Cox C. Ultrasound accelerates transport of recombinant tissue plasminogen activator into clots. *Ultrasound Med. Biol.* 1995; 21: 419–424.
- [177] Blinc A, Francis CW, Trudnowski JL, Carstensen EL. Characterization of ultrasound-potentiated fibrinolysis *in vitro*. *Blood.* 1993; 81:2636–2643.
- [178] Polak JF. Ultrasound energy and the dissolution of thrombus. *New Engl. J. Med.* 2004; 351:2154–2155.
- [179] Birnbaum Y, Luo H, Nagai T, Fishbein MC, Peterson TM, Li S, Kricsfeld D, Porter TR, Siegel RJ. Noninvasive *in vivo* clot dissolution without a thrombolytic drug: recanalization of thrombosed iliofemoral arteries by transcutaneous ultrasound combined with intravenous infusion of microbubbles. *Circulation.* 1998; 97: 130–134.
- [180] Culp WC, Erdem E, Roberson PK, Husain MM. Microbubblepotentiated ultrasound as a method of stroke therapy in a pig model: preliminary findings. *J. Vasc. Interv. Radiol.* 2003; 14: 1433–1436.
- [181] Holland CK, Apfel RE. Thresholds for transient cavitation produced by pulsed ultrasound in a controlled nuclei environment. *J. Acoust. Soc. Am.* 1990; 88: 2059–2069.
- [182] Schumann PA, Christiansen JP, Quigley RM, McCreery TP, Sweitzer RH, Unger EC. Targeted-microbubble binding selectively to GPIIb IIIa receptors of platelet thrombi. *Invest. Radiol.* 2002; 37: 587–593.
- [183] The IMS Study Investigators Combined intravenous and intraarterial recanalization for acute ischaemic stroke: the interventional management of stroke study. *Stroke* 2004; 35: 904–912.

- [184] Alexandrov AV, Wojner AW, Grotta JC. CLOTBUST Investigators
CLOTBUST: design of a randomized trial of ultrasound-enhanced
thrombolysis for acute ischaemic stroke. *J Neuroimaging*. 2004; 14:108-12.
- [185] Francis CW, Onundarson PT, Carstensen EL, Blinc A, Meltzer RS, Schwarz
K, Marder VJ. Enhancement of Fibrinolysis *In Vitro* by Ultrasound. *J. Clin.
Invest.* Volume 1992; 90: 2063-2068.
- [186] Suchkova V, Siddiqi, Carstensen EL, Dalecki D, Child S, Francis CW.
Enhancement of Fibrinolysis With 40-kHz Ultrasound. *Circulation* 1998;
98: 1030-1035.
- [187] Suchkova V, Carstensen EL, Francis CW. Ultrasound Enhancement Of
Fibrinolysis At Frequencies OF 27 TO 100 kHz. *Ultrasound in Med. &
Biol.* 2002; 28: 377–382.
- [188] Nedelmann M, Martin B, Lierke EG, Heimann A, Kempfski O, Hopf HC.
Low-Frequency Ultrasound Induces Nonenzymatic Thrombolysis *In Vitro*.
J Ultrasound Med. 2002; 21:649–656.
- [189] Datta S, Coussios C, Ammi A, Mast TD, De Courten-Myers G, Holland C.
Ultrasound-Enhanced Thrombolysis Using Definity® As A Cavitation
Nucleation Agent. *Ultrasound in Med. & Biol.* 2008; 34: 1421–1433.
- [190] Shlansky-Goldberg RD, Cines DB, Sehgal CM. Catheter-delivered
ultrasound potentiates *in vitro* thrombolysis. *J Vasc Interv Radiol.* 1996; 7:
313–320.
- [191] American Stroke Association, Stroke Statistics 2006.
- [192] Schellinger P, Jansen O, Fiebich J, Heiland S, Steiner T, Schwab S, Pohlers
O, Ryssel H, Sartor K, Hacke W. Monitoring Intravenous Recombinant
Tissue Plasminogen Activator Thrombolysis for Acute Ischaemic Stroke
With Diffusion and Perfusion MRI. *Stroke* 2000; 31(6): 1318-1328.
- [193] <http://www.surgicalneurologyint.com/article.asp?issn=2152-7806%3Byear=2011%3Bvolume=2%3Bissue=1%3Bspage=29%3Bepage=29%3Baulast=Sasani>.
- [194] Heran C, Morgan S, Kasiewski C, Bostwick J, Bentley R, Klein S.
Antithrombotic efficacy of RPR208566, a novel factor Xa inhibitor, in a rat
model of carotid artery thrombosis. *Eur. J. Pharmacol.* 2000; 389, 201–207.
- [195] Sato K, Kawasaki T, Hisamichi N, Taniuchi Y, Hirayama F, Koshio H.
Antithrombotic effects of YM-60828, a newly synthesized factor Xa

- inhibitor, in rat thrombosis models and its effects on bleeding time. *Br. J. Pharmacol.* 1998; 123, 92–96.
- [196] Wiley MR, Weir LC, Briggs S, Bryan NA, Buben J, Campbell C. Structure-based design of potent, amidine-derived inhibitors of factor Xa: evaluation of selectivity, anticoagulant activity, and antithrombotic activity. *J. Med. Chem.* 2000; 43, 883–899.
- [197] Wong AG, Gunn AC, Ku P, Hollenbach SJ, and Sinha U. Relative efficacy of active site-blocked factors IXa, Xa in models of rabbit venous and arterio-venous thrombosis. *Thromb. Haemostasis.* 1997; 77(6): 1143–1147.
- [198] Yamazaki M, Asakura H, Aoshima K, Saito M, Jokaji H, Uotani, C. Effects of DX-9065a, an orally active, newly synthesized and specific inhibitor of factor Xa, against experimental disseminated intravascular coagulation in rats. *Thromb. Haemostasis.* 1994; 72: 393–396.
- [199] Wessler S. Studies in intravascular coagulation. I. Coagulation changes in isolated venous segments. *J. Clin. Invest.* 1952; 31: 1011–1014.
- [200] Shebuski RJ, Storer BL, and Fujita T. Effect of thromboxane synthetase inhibition on the thrombolytic action of tissue-type plasminogen activator in a rabbit model of peripheral arterial thrombosis. *Thromb. Res.* 1988; 52: 381–392.
- [201] Folts JD, Crowell EB, and Rowe GG. Platelet aggregation in partially obstructed vessels and its elimination with aspirin. *Circulation* 1976; 54: 365–370.
- [202] Blair E, Nygren E, and Cowley RA. A spiral wire technique for producing gradually occlusive coronary thrombosis. *J. Thorac. Cardiovasc. Surg.* 1964; 48: 476–485.
- [203] Kordenat R. K. and Kezdi P. Experimental intracoronary thrombosis and selective in situ lysis by catheter technique. *Am. J. Heart.* 1972; 83: 360–364.
- [204] Bush LR, Mellott MJ, Kanovsky SM, Holahan MA, and Patrick DH. A model of femoral artery thrombolysis in dogs. *Fibrinolysis.* 1989; 3: 107–114.
- [205] Gold HK, Fallon JT, Yasuda T, Leinbach RC, Khaw BA, Newell JB. Coronary thrombolysis with recombinant human tissue-type plasminogen activator. *Circulation.* 1984; 70: 700–707.

- [206] Romson JL, Haack DW, and Lucchesi BR. Electrical induction of coronary artery thrombosis in the ambulatory canine: a model for *in vivo* evaluation of antithrombotic agents. *Thromb. Res.* 1980; 17: 841–853.
- [207] Todd ME, McDevitt EL, and Goldsmith EI. Blood-clotting mechanisms of nonhuman primates: choice of the baboon model to simulate man. *J. Med. Primatol.* 1972; 1: 132–141.
- [208] Eppehimer MJ. and Schaub RG. P-selectin-dependent inhibition of thrombosis during venous stasis. *Arterioscler. Thromb. Vasc. Biol.* 2000; 20(11): 2483–2488.
- [209] Wakefield TW, Strieter RM, Schaub R, Myers DD, Prince MR, Wroblewski SK. Venous thrombosis prophylaxis by inflammatory inhibition without anticoagulation therapy. *J. Vasc. Surg.* 2000; 31(2): 309–324.
- [210] Reese T, Bochelen D, Sauter A, Beckmann N, Rudin M. Magnetic resonance angiography of the rat cerebrovascular system without the use of contrast agents. *NMR Biomed.* 1999; 12: 189–196.
- [211] Johnstone MT, Botnar RM, Perez AS, Stewart R, Quist WC, Hamilton JA, Manning WJ. *In vivo* magnetic resonance imaging of experimental thrombosis in a rabbit model. *Arterioscler Thromb Vasc Biol.* 2001; 21: 1556–1560.
- [212] Corti R, Osende JI, Fayad ZA, Fallon JT, Fuster V, Mizsei G, Dickstein E, Drayer B, Badimon JJ. *In vivo* non-invasive detection and age definition of arterial thrombus by MRI. *J Am Coll Cardiol.* 2002; 39: 1366–1373.
- [213] Schmitz SA, Winterhalter S, Schiffler S, Gust R, Wagner S, Kresse M, Coupland SE, Semmler W, Wolf KJ. USPIO-enhanced direct MR imaging of thrombus: preclinical evaluation in rabbits. *Radiology* 2001; 221: 237–243.
- [214] Johansson LO, Bjornerud A, Ahlstrom HK, Ladd DL, Fujii DK. A targeted contrast agent for magnetic resonance imaging of thrombus: implications of spatial resolution. *J Magn Reson Imaging.* 2001; 13: 615–618.
- [215] Peter D. Schellinger, Olav Jansen, Jochen B. Fiebach, Sabine Heiland, Thorsten Steiner, Stefan Schwab, Olivia Pohlert; Henning Rysse, Klaus Sartor, Werner Hacke. Monitoring Intravenous Recombinant Tissue Plasminogen Activator Thrombolysis for Acute Ischaemic Stroke With Diffusion and Perfusion MRI. *Stroke.* 2000; 1318-1328.

- [216] Behrens S, Spengos K, Daffertshofer M, Schroeck H and Dempfle C E. Transcranial ultrasound-improved thrombolysis: diagnostic vs. therapeutic ultrasound. *Ultrasound Med. Biol.* 2001; 27: 1683–9.
- [217] Cintas P, Pavy Le Taron A, Larrue V. High rate of recanalization of middle cerebral artery occlusion during 2-MHz transcranial color-coded Doppler continuous monitor without thrombolytic drug. *Stroke.* 2002; 33: 626-628.

APPENDIX

JOURNALS

1. C Damianou, K Ioannides, V HadjiSavvas, N Milonas, A Couppis, D Iosif, M Komodromos, F Vrionides. 'Thermal ablation system using high intensity focused ultrasound (HIFU) and guided by MRI'. Therapeutic Ultrasound 2007; 6: 123-128.
2. C Damianou, Ioannides K, Hadjisavvas V, Milonas N, Couppis A, Iosif D. 'In vitro and in vivo brain ablation created by high intensity focused ultrasound and monitored by MRI'. IEEE Transaction on Ultrasonics, Ferroelectrics and Frequency Control 2009; 56(6): 1189-1198.
3. Mylonas N, Ioannides K, Hadjisavvas V, Iosif D, Kyriacou P, Damianou C. 'Evaluation of fast spin echo MRI sequence for an MRI guided high intensity focused ultrasound system for in vivo rabbit liver ablation'. J. Biomedical Science and Engineering, 2010; 3: 241-246.
4. Christakis Damianou, Kleanthis Ioannides, Venediktos Hadjisavvas, Nikos Mylonas, Andreas Couppis, Demetris Iosif, Panayiotis A. Kyriacou. MRI monitoring of lesions created at temperature below the boiling point and of lesions created above the boiling point using high intensity focused ultrasound. J. Biomedical Science and Engineering, 2010; 8: 763-775.
5. Venediktos Hadjisavvas, Kleanthis Ioannides, Michalis Komodromos, Nikos Mylonas, Christakis Damianou. Evaluation of the contrast between tissues and thermal lesions in rabbit *in vivo* produced by high intensity focused ultrasound using fast spin echo MRI sequences. J. Biomedical Science and Engineering. 2011; 4: 51-61.
6. Venediktos Hadjisavvas, Christakis Damianou. Temperature estimation of focused ultrasound exposures for stroke treatment. J. Biomedical Science and Engineering 2011; 4(5):410-417

CONFERENCES

1. C. Damianou, N. Milonas, V. HadjiSavvas, A. Couppis, D. Iosif, K. Ioannides, 'Thermal ablation system using High Intensity Focused Ultrasound (HIFU) and guided by MRI' CARS 2008 Computer Assisted Radiology and Surgery, June 25-28, Barcelona, Spain ,2008 (Abstract).
2. C. Damianou, K. Ioannides, V. HadjiSavvas, N. Milonas, A. Couppis, D. Iosif, M. Komodromos F. Vrionides, 'Thermal ablation system using high intensity focused ultrasound (HIFU) and guided by MRI', International Society of Therapeutic Ultrasound, Minneapolis, 10-13 September, 2008 Ultrasound in Medicine & Biology, 1438, 35(8):218.

3. C.Damianou, K. Ioannides, V. HadjiSavvas, N. Milonas, A. Couppis, D. Iosif, M. Komodromos, F. Vrionides, 'High intensity focused ultrasound (HIFU) system guided by MRI'. 12th World Congress of the World Federation for Ultrasound in Medicine and Biology, 30 August – 3 September 2009, Sydney Convention & Exhibition Centre, Sydney, Australia Ultrasound in Medicine & Biology, 35(8):367.
4. C.Damianou, N. Milonas, V. HadjiSavvas, A. Couppis, D. Iosif, K. Ioannides, Evaluation of the contrast between tissues in rabbit *in vivo* and thermal lesions produced by HIFU using fast spin echo MRI sequences in liver, kidney, heart, brain and pancreas. International Society of Therapeutic Ultrasound, Aux En Provence, France, 23-26 September, 2009 AIP Conf. Proc. 1215, pp. 44-48.
5. C. Damianou, K. Ioannides, N. Mylonas, V. HadjiSavvas, A. Couppis, D. Iosif 'Liver ablation using a high intensity focused ultrasound system and MRI guidance', 9th International Conference on Information Technology and Applications in Biomedicine, November 5-7, 2009, Larnaca, Cyprus (4 Pages).
6. V. HadjiSavvas, C. Damianou, K. Ioannides, N. Mylonas, , A. Couppis, P. Kyriakou, D. Iosif, , T. Hadji Charambous, G. Parea, 'Penetration of high intensity focused ultrasound *in vitro* and *in vivo* rabbit brain using MR imaging', 9th International Conference on Information Technology and Applications in Biomedicine, November 5-7, 2009, Larnaca, Cyprus (4 Pages).
7. C. Damianou, V. Hadjisavvas, K. Ioannides, G. Parea, 'Therapeutic system for brain cancer and stroke using high intensity focused ultrasound (HIFU) under MRI guidance'. 14th Conference on Biomedical Engineering (ICBME), Singapore 1-6 Aug, 2010 (Abstract).
8. C. Damianou, V. Hadjisavvas, K. Ioannides, G. Parea, 'Brain diseases therapy using high intensity focused ultrasound (HIFU) under MRI guidance. EUROSON, August 22-25, Denmark 2010 (Abstract).
9. N. Mylonas, V. Hadjisavvas, C. Damianou, An MR compatible positioning device for treating brain cancer and stroke using high intensity focused ultrasound (HIFU) under MRI guidance, 10th meeting of the International Society of Therapeutic Ultrasound, ISTU10, Tokyo, Japan, June 9-12, 2010 (Poster).
10. V. Hadjisavvas, K. Ioannides, C. Damianou, Application of MR-guided focused pulsed ultrasound for destroying clots *in vitro* using thrombolytic drugs. 10th meeting of the International Society of Therapeutic Ultrasound, ISTU10, Tokyo, Japan, June 9-12, 2010; pp 126-131.
11. V. Hadjisavvas, C. Damianou, A simulation model for predicting temperature during the application of MR-guided focused ultrasound for stroke treatment

using pulsed ultrasound, 10th meeting of the International Society of Therapeutic Ultrasound, ISTU10, Tokyo, Japan, June 9-12, 2010; pp 253-258.

12. V. Hadjisavvas, N. Mylonas, K. Ioannides, C. Damianou, An MR-compatible phantom for evaluating the propagation of high intensity focused ultrasound through the skull, 11th meeting of the International Society of Therapeutic Ultrasound, ISTU11, New York, USA, April 11-13, 2011 (Poster).
13. C. Damianou, V. Hadjisavvas, K. Ioannides, An MR-Compatible Plastic Phantom for Evaluating the Propagation of High Intensity Focused Ultrasound Through the Skull, 13th World Congress of Ultrasound in Medicine and Biology, WFUMB 2011, Vienna, Austria, August 26-29, 2011 (Abstract).
14. Yiallouras C, Marinos I, Alexis A, HadjiSavvas V, Milonas N, Damianou C. A software platform controlling an MRI guided focused ultrasound system for cancer therapy. 12th IEEE International Conference on BioInformatics and BioEngineering, November 11-13, 2012, Larnaca, Cyprus (4 Pages).